64-2

ML-TDR-64-43
Volume I

IMPROVED FILAMENT-WOUND CONSTRUCTION FOR CYLINDRICAL PRESSURE VESSELS

Volume I - Structural Analysis and Materials and Processes

TECHNICAL DOCUMENTARY REPORT NO. ML-TDR-64-43, VOLUME I

March 1964

Nonmetallic Materials Division
Air Force Materials Laboratory
Research and Technology Division
Wright-Patterson Air Force Base, Ohio

Project No. 7340, Task No. 734003
Project No. 7381, Task No. 738101

(Prepared under Contract No. AF 33(616)-8442 by the Aerojet-General Corporation, Von Karman Center, Azusa, California; F. J. Darms, R. Molho, and B. E. Chester, authors)

323

NOTICE

When Government drawings, specifications, or other data are used for any purpose other than in connection with a definitely related Government procurement operation, the United States Government thereby incurs no responsibility nor any obligation whatsoever; and the fact that the Government may have formulated, furnished, or in any way supplied the said drawings, specifications, or other data, is not to be regarded by implication or otherwise as in any manner licensing the holder or any other person or corporation, or conveying any rights or permission to manufacture, use, or sell any patented invention that may in any way be related thereto.

This report is releasable to OTS.

Qualified requesters may obtain copies of this report from the Defense Documentation Center (DDC), (formerly ASTIA), Cameron Station, Bldg. 5, 5010 Duke Street, Alexandria 4, Virginia.

Copies of this report should not be returned to the Research and Technology Division unless return is required by security considerations, contractual obligations, or notice on a specific document.

FOREWORD

This report was prepared by the Structural Materials Division of Aerojet-General Corporation at Aerojet's Von Karman Center under USAF Contract No. AF 33(616)-8442. This contract was initiated under Project No. 7340, "Nonmetallic and Composite Materials," Task No. 734003, "Structural Plastics and Composite Materials," and Project No. 7381, "Materials Application," Task No. 738101, "Exploratory Design and Prototype Development." The work was administered under the direction of the Nonmetallic Materials Division of the Air Force Materials Laboratory, with Mr. Sidney Litvak acting as project engineer.

The report covers work conducted from 1 July 1961 through 31 January 1964 and incorporates all data presented in the ASD-TDR-62-878 summary report. It is submitted in fulfillment of the contract and is catalogued by Aerojet-General as Report No. 2784.

W. T. Cox, Chief Engineer of the Structural Materials Division, provided technical direction. The program was conducted by personnel from the Design Engineering Department; it was initiated under A. M. Cecka and concluded under S. B. Fabeck and F. J. Darms, department heads. Those assisting were D. Pollman, Program Manager; R. Molho and B. E. Chester, Project Engineers; G. A. Lunde, Stress Analyst; and R. J. Barry and L. P. DuBois, Development Engineers.

D. Pollman, Head
Structural Programs Section
Design Engineering Department

F. J. Darms, Manager
Design Engineering Department
Structural Materials Division

W. T. Cox, Chief Engineer
Structural Materials Division

ABSTRACT

A design-optimization program was conducted that included stress analyses and the determination of design parameters, winding patterns, and fabrication techniques for filament-wound, cylindrical, pressure vessels. An investigation of the materials, processes, and structural analyses required to efficiently utilize the improved mechanical properties of new glass fibers was also conducted, with the aim of improving filament-wound composite structures.

Analytical studies preceded the selection of various design and fabrication concepts for optimum filament-wound pressure vessels with typical rocket-motor-case port openings. These selections were validated by a series of tests on model and full-scale chambers. The test results indicated that no specific head contour or wrap pattern will yield the highest performance for all variations in dimensional criteria, and that ranges exist in which each design exhibits the better performance. Definite improvement in the composite structure was demonstrated by the use of new glass fibers. Data are provided for use in the design and fabrication of optimum-weight, filament-wound cases. Recommendations are presented for additional research to enhance the future of the filament-wound structures.

This technical documentary report has been reviewed and is approved.

H. S. Schwartz

H. S. SCHWARTZ, Chief
Plastics and Composites Branch
Nonmetallic Materials Division
AF Materials Laboratory

TABLE OF CONTENTS, VOL. I

ILLUSTRATIONS

ILLUSTRATIONS (cont.)

ILLUSTRATIONS (cont.)

ILLUSTRATIONS (cont.)

TABLES

TABLES (cont.)

I. INTRODUCTION

This final report covers the work of the Structural Materials Division of Aerojet-General Corporation under Contract AF 33(616)-8442 during a six-phase, 30-month period ending 31 January 1964. Design parameters, winding patterns, fabrication techniques, and buckling and stiffness criteria were determined for optimum filament-wound cylindrical pressure vessels, and stress analyses were performed. In addition, new and improved glass fibers were evaluated for use in the construction of such vessels.

The initial objective was definition of the approach and method of analysis required to produce the optimum filament-wound rocket-motor case. Toward this end, Aerojet conducted a three-phase, 13-month program that was subsequently extended by 17 months to permit application of the improved physical properties of new glass fibers to the defined approaches and demonstration of further optimization.

Phase I was directed toward the selection of design and fabrication concepts required to produce the optimum filament-wound pressure vessel. Phase II was devoted to two specific tasks: validation of the design criteria determined in Phase I, and establishment of data suitable for the planning and design of future rocket cases. The work in Phase III was undertaken to evaluate the scale-up factors and to verify the data obtained from the model pressure vessels tested in Phase II.

In Phase IV a laboratory and subscale-case test program was undertaken for evaluation of the physical properties of the specific lots of glass roving from which the large-scale chambers were to be constructed. Phase V covered evaluation of the performance of S994 glass fiber as a material of construction by the design, fabrication, and testing of a large-scale chamber (similar to those fabricated during Phase III). Phase VI was directed toward subjecting a large-scale chamber (identical, within practical limitations, to the Phase V chamber) to axial-compression and bending-moment loads and obtaining additional information about applications in which buckling and stiffness are critical considerations.

This report presents a detailed summary of all work performed during Phases I through VI, in addition to conclusions and recommendations related to program results and their implications for future work in the field of filament winding. Design details and structural analyses for the large-scale (44.3-in.-dia) chambers fabricated during this program are presented in Appendixes I through VII of Volume I. Information pertinent to the design and analysis of filament-wound pressure vessels in general is presented in Appendixes I through VII of Volume II.

Manuscript released by authors March 1964 for publication as an ML Technical Documentary Report.

II. PROGRAM PLAN

A. PHASE I - ANALYSIS

This phase of the program was directed toward the selection of design and fabrication concepts required to produce the optimum filament-wound pressure vessel. The effort was divided into three basic portions: analytical studies, empirical studies, and the selection of optimum designs.

1. Analytical Studies

The analytical studies were planned to include review, verification, and optimization of design and fabrication concepts developed in other filament-winding programs. They were to encompass the establishment of equations necessary for evaluation of a filament-wound structure incorporating off-center ports in the heads and ports in the cylinder. To be included were investigations of head contours and their complementary wrap patterns, in addition to such variables as the chamber-length-to-diameter (L/D_c) ratio, boss-diameter to chamber-diameter ratio (D_b/D_c), effects of thickness, and port reinforcements for cut filaments. The analyses were to be facilitated by the use of an IBM 7094 digital computer. In addition, design concepts, construction materials, and fabrication techniques for cases and mandrels developed by Aerojet in other filament-winding programs were to be reviewed.

2. Empirical Studies

The empirical studies were to incorporate data from 6-in.-dia tubes, obtained from another program, in order to separate the effects caused by filament crossovers from the other factors that reduce the efficiency of the fabricated case below the theoretical optimum. It was planned to confirm the general analyses and the predicted effects of filament deviation from the true geodesic path by reviewing data obtained from tests of 18-in.-dia model chambers in Phase II.

3. Selection of Optimum Design

The specific designs for further study in the model phase of the program were to be selected on the basis of a theoretical-performance factor, defined as burst pressure times internal volume divided by weight of glass-resin composite (pV/W), which relates the basic pressure-vessel parameters. The designs exhibiting the highest performance factor were to be considered as optimum.

B. PHASE II - CONSTRUCTION AND TESTING OF MODELS

Phase II was to be devoted to the following specific tasks: (1) validation of the design criteria determined in Phase I, and (2) establishment of data suitable for the planning and design of optimum filament-wound rocket cases. These tasks were to be accomplished by means of tests performed on models fabricated to the specifications determined in Phase I. The test plan was to be designed to permit sufficient information for a statistical evaluation to be obtained with a minimum number of chambers.

In accordance with suggestions from the Air Force, the original plan for Phase II was modified to provide for concentration on validation of the Phase I analyses by submitting each model chamber to a short hydroburst test rather than to pressure-time cycling tests or to fatigue and stress-rupture tests.

Eighteen, 18-in.-dia, model chambers with various L/D_c ratios were to be fabricated from high-strength glass filaments. These chambers were to have integrally wound end closures and complementing wrap patterns, and were to include center bosses with specific D_b/D_c ratios. Concentration on the validation of design parameters eliminated the tests on model chambers with off-center ports from the program as initially proposed. The model chambers were to be subjected to proof and burst tests, and the performance of each case was to be rated on the basis of its actual performance factor (pV/W).

C. PHASE III - INVESTIGATION OF SCALE FACTORS

Phase III was to be directed toward evaluation of scale factors and verification of the data obtained from the model-pressure-vessel tests in Phase II.

The contractual requirements for Phase III included the fabrication and evaluation of scaled-up chambers for use in verifying the Phase II results. The program plan initially required the fabrication of three units simulating the size and the porting requirements of the third-stage Minuteman case (approximately 37.5 in. in diameter and 76 in. long). Subsequent discussion with Air Force representatives resulted in a program redirection requiring application of the scaling factor to two larger units simulating the size and including the multiple nozzle porting and interstage attachment skirts of the second-stage Minuteman case (approximately 44.3 in. in diameter by 127 in. long). The designs for the two chambers were to be based solely on internal-pressure considerations. The first chamber (Serial No. 1) was to be fabricated to the established state of the art with regard to fabrication techniques, materials, and design concepts. The second chamber (Serial No. 2) was to be fabricated to a design that incorporated the results of Phase I analyses and Phase II tests.

After fabrication, each chamber was to be subjected to a two-cycle hydrostatic test. A proof pressure of 587 psi was to be applied for 90 sec while instruments continuously recorded the internal pressure, volumetric expansion, radial and longitudinal expansion, and strains developed in the case. The second cycle was the simple application of internal pressure until bursting occurred. These two designs and their test results were to be compared to determine the design improvements achieved through the use of the data developed during Phases I and II.

D. PHASE IV - TESTING AND EVALUATION OF MATERIALS

Phase IV was to provide an accurate evaluation of the properties of the specific lots of S994 glass roving* that were to be used to fabricate 44.3-in. dia chambers in Phases V and VI.** This evaluation, to be accomplished by means of laboratory testing and 18-in.-dia-chamber burst tests, was to be directed toward the definition of exact physical properties of the materials from which the larger chambers were to be constructed. This information subsequently was to be used for chamber designing in Phases V and VI.

The S994 glass was to be laboratory-tested to determine the tensile properties of the glass and the characteristics of the glass resin system.

The material was to be further evaluated for glass tensile strength by fabricating two 18-in. chambers containing axial bosses and wrapped with a balanced pattern (i.e., failure could occur in either hoop or longitudinal filaments). These chambers, fabricated from the same lots of glass roving that would be used to fabricate the 44.3-in. chambers were then to be pressurized to the burst point.

The data obtained from these chambers were to be compared with data available from similar chambers previously fabricated with "E" glass. This information, to be used in conjunction with the data obtained from the tests of the 44.3- and 18-in. "E" glass chambers fabricated in Phases II and III, was then to form the basis for determination of the final design allowables of the Phase V and VI, 44.3-in. chambers.

E. PHASE V - DESIGN, FABRICATION, AND TESTING OF 44.3-INCH-DIAMETER S994 CHAMBER

The objective of this phase was to evaluate the performance of S994 glass roving as a material of construction for large-scale structures. The chamber-design criteria were to be based on data obtained in Phase IV. For purposes of comparison, a 44.3-in. chamber of the same configuration as the Phase III, Serial No. 2, 44.3-in. chamber was to be fabricated.

After fabrication, the chamber was to be subjected to a two-cycle hydrostatic test. A proof pressure of 587 psi was to be applied for 90 sec while the internal pressure, volumetric expansion, radial and longitudinal expansion, and strains developed in the case were continuously recorded. Sequence-camera

---

*Experimental lots of Owens-Corning Fiberglas Corporation high-strength glass roving were designated X994; this type of material was used to fabricate the Serial No. 3, 18-in. chamber and the Serial No. 3, 44.3-in. chamber. The manufacturer subsequently designated production-run quantities as S994 glass roving; this type of material was used to fabricate the Serial No. 4, 18-in. chamber and the Serial No. 4, 44.3-in. chamber. In this report, both types are referred to as S994 glass roving.

**YM31A glass roving was originally required contractually for Phase VI use but was subsequently deleted, as discussed in paragraph IV,D,1,b.

coverage was to indicate the occurrence of the resin-craze threshold in terms of chamber pressure. The second cycle was to feature the simple application of internal pressure until bursting occurred.

The overall efficiencies of the Serial No. 1, 2, and 3, 44.3-in. chambers were to be compared by means of the performance factor (pV/W) and strength-to-density ratios. Finally, performance data for the glass cases were to be tabulated and compared with data for similar homogeneous steel and titanium cases fabricated and tested by Aerojet in the Minuteman program.

F. PHASE VI - AXIAL-COMPRESSION AND BENDING TESTS OF 44.3-INCH-DIAMETER S994 CHAMBER

The basic objectives of Phase VI were (1) to provide additional information for the designing of optimum-weight, filament-wound, rocket-motor cases in applications where buckling and stiffness criteria are critical considerations, and (2) demonstration of the feasibility of subjecting large-scale structures made with S994 roving to axial-compression and bending-moment loads.

These objectives were to be accomplished by testing a chamber fabricated as nearly identical as possible to the Phase V, Serial No. 3, 44.3-in. chamber. This would provide the best possible correlation of data for determining the actual effect of axial-compression and bending-moment loads on a case of this type.

The completed chamber was to be hydrostatically tested to a proof pressure of 587 psi, and held for 90 sec while the internal pressure, volumetric expansion, radial and longitudinal expansion, and strains in the case were continuously recorded. Sequence-camera coverage was to indicate the craze threshold of the resin in terms of chamber pressure.

The chamber was then to be assembled to a test fixture designed to induce axial-compression loads and bending moments. Axial compression was to be applied to the forward skirt of the case by means of hydraulic jacks attached to a ring designed to transfer the load uniformly around the circumference of the skirt. The axial force was to be approximately 60% of the force calculated as that required to buckle the chamber. Case deflection was to be measured with linear-motion transducers. The data recorded were to be used to calculate the compressive modulus of the case (E_c) and its compressive rigidity (E_cA).

A bending moment representing 60% of the calculated critical-bending moment was then to be applied to the case. The bending modulus of the case (E_b) and its flexural rigidity (E_bI) were to be determined from data recorded by linear-motion transducers and the actual case thickness and diameter that had previously been recorded.

In order to evaluate the interaction between E_c and E_b, a simultaneous axial-compression force and bending moment was to be applied to the case. The axial force was to be approximately 30% of the force calculated as that required to buckle the chamber, and the bending moment was to be approximately 30% of the calculated critical-bending moment. This combined loading was to be evaluated on the basis of instrumental data. The linear-motion transducers

were to be removed, and the chamber was to be pressurized until it burst. The pressurization rate during the burst cycle and the proof-pressure cycle was to be maintained at a strain rate of 1%/min, as in all previous tests.

III. SUMMARY

The major objectives of this program were met and the work accomplished, summarized below, represents significant advances in the field of filament winding.

A. PHASE I - ANALYSIS

1. Design concepts, construction materials, fabrication techniques, and other miscellaneous Structural Materials Division data in such areas as closure contours, wrap patterns, resin binders, glass roving, and test methods were reviewed.

2. A method was established for judging the efficiency of any pressure vessel on the basis of a performance factor that relates the basic parameters of pressure, volume, and weight (pV/W).

3. Two basic concepts with the highest theoretical-performance factors were selected for further study in Phase II. They included balanced-design head contours with in-plane wrapping and isotensoid contours wrapped with filaments following a geodesic path.

4. A method of analysis was developed for cut-filament reinforcements for off-center ports in the head and for ports in the cylindrical section of filament-wound composite structures.

5. Data were obtained for the purpose of establishing a standard rate of loading during laboratory testing of materials and hydrostatic testing of pressure vessels. The aims were to minimize possible variations in test results and to permit more meaningful comparisons of filament-winding vendors. The results indicated that a substantial increase in tensile properties occurred as the strain rate was increased from 1%/min.

B. PHASE II - CONSTRUCTION AND TESTING OF MODELS

1. Tests were performed on 18 model chambers fabricated to specific design variables. The evaluated variables included chamber-length to chamber-diameter (L/D_c) and boss-diameter to chamber-diameter (D_b/D_c) ratios for balanced and isotensoid head contours wrapped with in-plane and geodesic patterns, respectively.

2. The test data were evaluated, and the performance factor was plotted as a function of D_b/D_c ratios for equal- and unequal-boss configurations. The results indicated that no specific head contour or wrap pattern will produce the highest performance for all variations in dimensional criteria and that ranges exist in which each design exhibits the better performance. The results also indicated that little variation in performance factor exists for the ranges of model-chamber lengths considered.

C. PHASE III - INVESTIGATION OF SCALE FACTORS

1. Two cases the size of the second-stage Minuteman chamber (approximately 44.3 in. in diameter by 127 in. long) were fabricated with "E" glass roving and were hydrostatically tested to destruction. The first unit (Serial No. 1) had a hoop-composite stress of 86,000 psi at the proof pressure and an ultimate hoop-filament stress of 317,000 psi at the burst. The second unit (Serial No. 2) was lighter in weight than the first and had a modified forward-head contour. It had a hoop-composite stress at the proof pressure of 95,100 psi, and it burst within 0.5% of the theoretical design burst pressure of 734 psi.

2. A structural analysis was developed that includes equations for the designing of filament-wound chambers in a proper sequence, thereby permitting design engineers to arrive at a complete chamber design methodically.

D. PHASE IV - TESTING AND EVALUATION OF MATERIALS

1. Comprehensive laboratory tests were conducted on four separate lots of glass roving: (a) S994 roving used in the construction of the Serial No. 3, 44.3-in. chamber, (b) YM31A roving rejected because of unsatisfactory physical characteristics, (c) S994 roving that was substituted for the YM31A glass as a result of program redirection, but was rejected on the basis of low fiber strength, and (d) S994 roving used in the fabrication of the Serial No. 4, 44.3-in. chamber.

2. Tests were performed on two 18-in. chambers (designated as the Serial No. 3 and 4 subscale chambers) that were fabricated from material taken from the lots of roving used on the corresponding 44.3-in. chambers. The Serial No. 3 subscale chamber attained ultimate-tensile-stress levels of 388,000 and 375,000 psi in the hoop and longitudinal directions, respectively; the corresponding values for the Serial No. 4 subscale chamber were 403,600 and 376,700 psi.

E. PHASE V - DESIGN, FABRICATION, AND TESTING OF 44.3-INCH-DIAMETER S994 CHAMBER

1. One second-stage Minuteman-size case was fabricated with S994 glass roving to the same configuration as the Phase III chamber (Serial No. 2) and was hydrostatically tested to destruction. This unit (Serial No. 3), the lightest fabricated during the program, had a hoop-composite stress level of 155,700 psi when it burst at a pressure of 728 psi, which was within 1% of the theoretical design burst pressure of 734 psi.

2. The performance data for the Type "E" and S994 glass chambers were compared with data for similar homogeneous steel and titanium second-stage Minuteman chambers fabricated by Aerojet-General. These comparisons indicated the S994 glass chamber is superior to the other cases on the basis of strength-to-density ratios and the performance factor (pV/W).

F. PHASE VI - AXIAL-COMPRESSION AND BENDING TESTS OF 44.3-INCH-DIAMETER S994 CHAMBER

1. One second-stage Minuteman-size case was fabricated to the identical configuration used for the Phase V chamber (within practical limitations), was subjected to structural end loads, and was then hydrostatically tested to destruction. This case (Serial No. 4) was subjected to an axial-compression load, a combined axial-compression and bending load, and two bending loads (applied at 1 and 5% strain rates), and was then pressurized to destruction. The case burst within 5% of the design burst pressure;* it had a hoop-filament stress level of 346,000 psi and a hoop-composite stress level of 138,900 psi.

2. Using data recorded during the structural tests, the compressive modulus of elasticity of the case (E_c) was calculated to be 3.22×10^6 psi and the compressive rigidity of the case (E_cA) was found to be 4.95×10^7 lb.

3. The modulus of elasticity in bending (E_b) was determined to be 4.31×10^6 psi, while the flexural rigidity of the case in bending (E_bI) was calculated to be 1.62×10^{10} lb-sq in.

IV. TECHNICAL DISCUSSION

Advances in glass-reinforced plastic structures utilizing the filament-winding process have resulted from (a) improvements in the properties of the glass and resin that form the basic case, (b) improvements in tooling and fabrication techniques, and (c) efficient designing of the composite structure. Phases I, II, and III of this program were concerned with the problem of developing design data in an effort to analyze, validate, and optimize various design parameters peculiar to filament-wound pressure vessels. Phases IV, V, and VI dealt with the application of these design parameters to the newer glass fibers to obtain further improvement. The work performed is discussed below. Design details and structural analyses for the 44.3-in.-dia chambers fabricated during this program are presented in Appendixes I through VII of Volume I.

A. PHASE I - ANALYSIS

1 1. Analytical Studies

a. Methods of Rating Designs

The three standard methods used to judge the efficiency of pressure vessels are the performance factor, strength-to-density ratio, and burst pressure.

(1) Performance Factor

The performance or efficiency of any pressure vessel may be best judged by a factor that relates the basic parameters of the chamber. This factor, defined as pressure times volume divided by weight (pV/W), is theoretically equal to a "shape factor" times the strength-to-density ratio of the materials of construction:

*The actual burst pressure was within 5% of the predicted burst pressure for the internal-pressurization-only condition.

$$\frac{pV}{W} = K\left(\frac{\sigma}{\rho}\right) \qquad (1)$$

For homogeneous chambers, it can be shown that the shape factor (K) is dependent on the configuration of the case. On the other hand, for filament-wound pressure vessels, this factor remains constant for all shapes, provided that the stresses within the structure are exactly met in all directions, and that σ/ρ is the strength-to-density ratio of the unidirectional composite. A sphere, which represents the optimum configuration for homogeneous pressure vessels, is theoretically no more efficient for filament-wound rocket-motor cases than any other shape, and certain practical considerations actually relegate it to an efficiency level below that of several other configurations.

To attain the theoretical optimum performance, the filament-wound pressure vessel must exactly meet all stresses within the structure and thus provide equal margins of safety in all directions. This basic criterion of equal margins of safety is usually modified in practice because of three practical and highly important considerations: filament continuity, fabricational limitations, and stress concentrations. These result in an actual performance factor that may be written as

$$\frac{pV}{W} = \left|\alpha_1\alpha_2\alpha_3 \ldots\ldots\alpha_n\right| K\left(\frac{\sigma}{\rho}\right) \qquad (2)$$

where α_1, α_2, α_3, etc. represent coefficients for chamber continuity, placement, stress concentrations, etc. Although many variations in design are required to separate the α terms, Equation (2) is extremely valuable in that it combines all factors to produce a complete evaluation of one material or design relative to another.

(2) Strength-to-Density Ratio

The strength-to-density-ratio method of judging the performance of pressure vessels is primarily used for material evaluation. For homogeneous materials, consideration must be given to the particular area of reference on the chamber; this is because the degree of performance increase, caused by the biaxial force fields on the pressure-vessel shell, is not as high in the heads as in the cylinder. The increase in strength of a homogeneous cylinder, for example, will be approximately 15% over that of a unidirectional test specimen, when the cylinder is subjected to the 2-to-1 force field from internal pressure, whereas no increase is apparent in a spherical dome because of the 1-to-1 force field. The strength-to-density ratios of heads and cylinders for composite structures differ to an even greater degree for another reason. With filament-wound composite structures, the strength-to-density ratio is an inverse function of the summation of the two forces on the structure. In a 2-to-1 force field, as found in a cylindrical section, the summation of the forces is represented by 2 + 1, or 3. For this case, therefore, the strength-to-density ratio would be one-third of that for the unidirectional composite. Again, in a spherical configuration with a 1-to-1 biaxial force field, the strength-to-density ratio would be one-half the unidirectional value. Statements about strength-to-density ratios must therefore be qualified with regard to the force field and/or the area of the pressure vessel. If an average ratio for the entire pressure

vessel is given, the shape of the heads and the ratio of head weight to total chamber weight must be given.

(3) Burst Pressure

The burst-pressure method of evaluating pressure-vessel performance is applicable only when the two other basic parameters (volume and weight) are maintained constant for all units in the comparison.

One important factor that must be included in evaluating any filament-wound pressure vessel is related to the strain-rate, ultimate-strength relationship. This factor is overlooked by many pressure-vessel designers familiar only with homogeneous materials, but it plays an exacting role in the strengths demonstrated in the hydrobursting of any filament-wound chamber. Data previously gathered at Aerojet indicate (a) that the tensile properties of composite structures increase substantially as the strain rate increases above 1%/min, and (b) that for rates below 1%/min, the results approach those for a steady-state condition, with a lower variation in tensile strength. Results obtained by testing roving in accordance with Aerojet's strand-test procedures at various rates of loading are presented in Appendix I of Volume II.

The filament is the primary structural material in a filament-wound composite. To provide a proper and complete index for the comparison of data from pressure-vessel tests, it is necessary to determine the resin content of the structure. Resin content and its application in terms of weight and volume are discussed in detail in Appendix II of Volume II.

b. Design of Cylinders

The unidirectional filaments in a cylindrical section of a pressure vessel are oriented to meet the biaxial force field. The approaches to this orientation include a single helical pattern, a combination of helical and circumferential patterns, and a combination of longitudinal and circumferential patterns.

All winding patterns are theoretically capable of producing cylinders of the same weight and strength, provided that the same ratio of equivalent strengths is maintained in the two principal directions. However, a review of the patterns for the cylinder revealed that, although the theoretical weights would be the same, a construction placing the fibers in the principal force directions would produce a more dense and more efficient structure, primarily because of the elimination of excess resin and the reduction of filament crossovers.

Resin stresses play an important part in the selection of any pattern for the cylindrical section of a pressure vessel. The previous statement that any combination of patterns could be balanced to produce an optimum cylindrical section is based primarily on the filament stress and does not consider stresses within the resin system. Resin stresses in a given layer can only be reduced by ensuring that the stresses and strains in the system are equally balanced in all directions so that the filament direction

does not change when the cylinder is pressurized. It may therefore be expected that a combination of hoop and helical patterns would not be as efficient as the straight helical or the hoop-and-longitudinal patterns. Practical considerations indicate that a cylindrical section with the filaments placed in layers with no crossovers would result in the optimum design from the standpoint of stress concentrations in the fibers and minimization of resin volume. Aerojet experience indicates that pure hoop and pure longitudinal patterns approximate this condition.

Two primary layer-orientation alternatives exist for designs that include circumferential wraps. These alternatives, which are related to the location of the circumferential wraps within the layers of the composite structure, are (1) to place all the circumferential wraps on the outer surface of the cylinder, and (2) to intersperse these wraps with layers of another pattern. The designs in this program incorporated the former pattern and did not establish the better method; however, some comments are presented below.

(1) Interspersion permits the attainment of a higher shear rigidity with the composite cylinder, although both designs provide sufficient rigidity for most rocket-motor chambers.

(2) Interspersion also provides a more intimate bond bebetween the circumferential layer and the lower layers of the composite.

(3) The design with the circumferential filaments on the outside of the case permits the grouping of all filaments that are to extend onto the head, so that no filament discontinuity or bridging exists at the head-to-cylinder juncture.

(4) The configurations with the types of patterns grouped together permit the designing of skirts that attach to the cylindrical section of the chamber and do not induce stress concentrations in the heads.

The stress distribution in thick-walled homogeneous cylinders subjected to internal pressure can be calculated by equations developed by Lamé. According to these equations, higher tangential stresses are developed at the inner surface than at the outer surface. Constant filament stresses can be achieved in thick-walled, filament-wound, pressure vessels by applying Lamé's equations to determine the amount of tension required in each layer in order that equal filament stresses exist throughout the wall at the working pressure.

A second factor must be considered in calculating the stress distribution in the cylindrical section of a pressure vessel. It concerns the relative rigidity of the mandrel to the filaments. As each successive wrap is added, additional external pressure is applied to the mandrel. This pressure results in radial deflection of the mandrel and reduction of the tensions in the prior wraps. Pre-tensioning of the layers, to compensate for this effect and to produce equal stresses in all filaments, requires that higher tensions be applied to the inner layers, rather than to the outer layers as dictated by Lamé's equations.

The typical rocket-motor case may be considered to be a thin-walled pressure vessel, because the thickness is less than 10% of the radius. The effect of stress variation caused by thickness, as predicted by Lame's equations, may therefore be neglected, and the tensioning becomes only a function of the relative rigidities of the mandrel and filaments.

Curves used by Aerojet in selecting the proper mandrel materials for typical filament-wound rocket-motor cases are presented in Figure 1. With these selected mandrel materials, chambers with equivalent efficiencies can be produced by employing a step calculation in which the pressure supplied by each suceeding wrap and the relative radial deflection of the mandrel must be added to establish the preload of the preceding layers of filaments. The equation used to accomplish this for hoop wraps is

$$T_q = \frac{(1 + K)\, T_1}{1 + q\, K} \tag{3}$$

where

$$K = \frac{E_f\, t_f}{E_m\, t_m} \tag{4}$$

T_q = tension of layer in question, lb

T_1 = tension of first layer, lb

q = layer number (the first layer is the one nearest the mandrel)

E_f = modulus of filaments, psi

E_m = modulus of mandrel, psi

t_f = equivalent thickness of filament layer, in.

t_m = mandrel-wall thickness, in.

c. Head Contours and Winding Patterns

The principal forces on all types of closures are in the meridional and circumferential directions. The placement of filaments and their orientation are much more critical for shapes with double curvatures than for cylinders, because of (1) the tendency of the filaments to slip when they are not placed properly on the surface, (2) filament buildup as the axis of the chamber is approached, and (3) change in the biaxial force field. In the construction of pressure vessels with a cylinder and integral closure, the closure contour must therefore complement the wrap pattern. Closure contours that have been prepared to fit specific wrap patterns are discussed below.

(1) Geodesic-Isotensoid Contour

The term "geodesic" describes the shortest path between any two points on a surface, and "isotensoid" refers to uniform filament tension. Consequently, "geodesic-isotensoid" head contours are designed

specifically so that the filaments will be placed on geodesic paths and, under pressure loading, will exhibit uniform tensions in all fibers throughout their length.

The geodesic-isotensoid is one of the primary head contours currently used in the filament-winding industry for pressure vessels and rocket-motor cases. Contours of this type are established by assuming that the filaments follow a specific geodesic path on the head, and by determining the head geometry at a particular point. The geodesic path used is the one that passes tangentially to the axial boss in the head. The head geometry is determined by placing the resultant stress at each point along the path in the direction of the path. As determined from Ref. 1, the principal membrane forces in a shell of revolution are

$$N_{\phi} = \frac{p\, r_2}{2} \tag{5}$$

and

$$N_{\theta} = \frac{p\, r_2}{2}\left(2 - \frac{r_2}{r_1}\right) \tag{6}$$

where

N_{ϕ} = meridional force per unit of width

N_{θ} = circumferential force per unit of width

p = pressure

and r_1 and r_2 are the meridional and circumferential radii of curvature, respectively (see Figure 2). The geometric identities may be established by noting the octant of the surface of revolution, as shown in Figure 2. The principal radii of curvature at any point may be expressed in terms of the x,y coordinate system by the following equations (derived from Ref. 2):

$$r_1 = \frac{-\left[1 + (y')^2\right]^{3/2}}{y''} \tag{7}$$

and

$$r_2 = \frac{-x\left[1 + (y')^2\right]^{1/2}}{y'} \tag{8}$$

where y' and y" are the first- and second-order derivatives of y with respect to x. The filament strengths in the two principal directions are given by

$$N_{\phi,f} = \sigma_f\, t_f \cos^2 \alpha \tag{9}$$

and

$$N_{\theta,f} = \sigma_f\, t_f \sin^2 \alpha \tag{10}$$

where

$N_{\phi,f}$ = meridional force in filament per unit of width

$N_{\theta,f}$ = circumferential force in filament per unit of width

σ_f = filament stress

t_f = equivalent filament thickness

α = angle between meridian and filament

A balance between the available filament strength and the forces in the shell caused by pressure may be obtained by equating N_ϕ to $N_{\phi,f}$ and N_θ to $N_{\theta,f}$. These identities, plus Equations (5) through (10), produce the equation that ensures equal margins of safety in all directions at any given point:

$$\frac{r_2}{r_1} = 2 - \tan^2 \alpha$$

or

$$\frac{xy''}{y'\left[1 + (y')^2\right]} = 2 - \tan^2 \alpha \qquad (11)$$

The head contour is established by combining Equation (11) with the following equation of the geodesic path (Ref. 3):

$$x \sin \alpha = \text{constant} \qquad (12)$$

The boundary condition at the edge of the center boss ($x = x_o$) may be used to determine the constant of this equation. Noting that the filaments at this point have $\alpha = 90^\circ$, Equation (12) reduces to

$$\sin \alpha = \frac{x_o}{x} \qquad (12a)$$

Equations (11) and (12) are sufficient for determination of the contour, provided two boundary conditions are known. This requirement is satisfied by noting that $y = 0$ at $x = a$ = radius of cylinder, and $y' = -\infty$ at $x = a$.

The solution of the equations with appropriate boundary conditions is a difficult and tedious process requring a step integration. Aerojet's Computing Sciences Division has developed a program for the IBM 7094 computer that determines the x,y coordinates of the head by a step-integration technique known as the Runge-Kutta method. Equation (11) has an inflection point when $\tan^2 \alpha = 2$, which makes the curve unusable for any value of x less than $x_o \sqrt{3/2}$. Therefore, to provide a solution to $x = x_o$, a spherical section was assumed for the distance from the inflection point to $x = x_o$. Using this program, geodesic-isotensoid contours for different sizes of center bosses were calculated; they are shown in Figure 3.

The foregoing approach to the solution for the contour has not limited the solution to one demanding a constant filament stress at all points on the filament path. However, verification that the contour is an isotensoid can be made by a point-by-point analysis of filament stresses.

Because the filament path (and thus the helix angle of the cylindrical section) is determined by the boss diameter, the axially located openings at each end of the chamber incorporating geodesic-isotensoid heads must be equal in size. Several design modifications may be made when these sizes are not equal, but they usually reduce the efficiency of the head, either because the filaments must be cut or because the continuity of the filament paths is destroyed.

(2) Zero-Hoop-Stress Contour

The zero-hoop-stress contour is primarily a geodesic-isotensoid in which the center boss has been reduced to zero and the geodesic path lies on the meridian; thus the angle between the meridian and the filament (α) equals zero for all points on the filament path. Because

$$N_{\theta,f} = N_{\theta} = \sigma_f \, t_f \, \sin^2 \alpha$$

as shown in the geodesic-isotensoid solution, it may be seen that the hoop stresses are reduced to zero.

Equation (11) is used to generate the contour. However, with $\alpha = 0$, the equation can be integrated easily. This integration reduces Equation (11) to

$$y = \pm a \sqrt{2} \left[\frac{-F(\sqrt{2}/2,\mu)}{2} + E(\sqrt{2}/2,\mu) \right] \tag{13}$$

where

$$\mu = \sin^{-1} \left[1 - \left(\frac{x}{a} \right)^2 \right]^{1/2} \tag{14}$$

$$a = \text{radius of equator} \tag{14}$$

and $F(\sqrt{2}/2,\mu)$ and $E(\sqrt{2}/2,\mu)$ are common elliptical functions.

It is impractical to wrap the head of a pressure vessel with the filaments on a meridional path, because all filaments must go through the longitudinal axis at the same point. Such wrapping would result in excessive thickness at that point; furthermore, most designs require a center boss for mandrel shafting.

In practice, the zero-hoop-stress contour has also been used with a center boss. The filament is wrapped on a plane established by the boss diameter at each end and by the length of the chamber. This technique produces a chamber that is neither geodesic nor isotensoid; however, high performances have been achieved for chambers with small center bosses or with a significant L/D_c ratio (3 to 1).

The geometry of a head with an in-plane wrap pattern is shown in Figure 4. With reference to that figure, the equation of the plane of wrap is

$$x \cos \theta = B + Ay \tag{15}$$

The filament angle at any point (p) is given by

$$\tan \alpha = \frac{A \sin \phi + \cos \phi \cos \theta}{\sin \theta} \tag{16}$$

where

$$\tan \phi = -y' \tag{17}$$

The zero-hoop-stress contour may be calculated on a computer, using the equations for the geodesic-isotensoid contour. With the calculation of the contour, the filament path and its parameters can be obtained as an additional function of the computer program. Figure 5 shows the zero-hoop-stress contour.

(3) Balanced-in-Plane Contour

The "balanced-in-plane" head contour is one in which the filaments are oriented within a plane. The filament path is described by the intersection of the plane and the head. The stresses along the filaments are balanced with the pressure loading by adjusting the radii of curvature. The balanced-in-plane contour therefore combines the desirable qualities of both the geodesic-isotensoid contour and the in-plane wrapping method by providing a head contour designed to meet the filament orientation while incorporating simple wrap patterns. The force and geometry equations for this contour are the same as for the geodesic-isotensoid contour. New equations, however, are used to develop the filament path.

Equation (11) is used in conjunction with Equations (15), (16), and (17) to establish the contour and the filament path. These equations differ from those for the zero-hoop-stress in-plane wrap in that Equations (15), (10), and (11) are used to establish the contour as well as the filament path. Solution of the equations indicates that, as for the geodesic-isotensoid, there is an inflection point on the curve at $\tan^2 \alpha = 2$. Also, as for the other contour, a spherical segment has been used to complete the contour from $x_o \sqrt{3/2} \leq x \geq x_o$. It should be noted that the plane of wrap is a function of the chamber length as well as of the boss diameters; the head contour is therefore a function of both parameters. Figures 6 through 8 show balanced-in-plane contours for various center-boss openings and L/D_c ratios.

(4) Redundant-Isotensoid Contour

The "redundant-isotensoid" head contour incorporates two or more different geodesic wrap patterns. It presents interesting features that may be desirable when the design incorporates unequal bosses. When two geodesic patterns are used, the first is established by ignoring the desired boss diameter and wrapping the filaments to a diameter approaching that of the mandrel shaft, and the second is then wrapped to the desired boss

diameter. After the chamber is cured, the filaments of the first pattern are cut to produce the required opening. Among the advantages of this pattern, as compared with the single geodesic-isotensoid pattern, is the fact that the crown height of the head approaches the smaller crown height of the zero-hoop-stress contour, thus permitting a greater chamber volume within a given missile envelope.

d. Cut-Filament Ports and Reinforcements

(1) Off-Center Ports

The two major design categories for off-center ports are (a) designs that require the cutting of filaments and incorporation of localized reinforcements, and (b) designs in which filaments are wrapped around the local openings and are not required to be cut.

The filament-winding industry primarily employs the first technique. Variations in methods of accomplishment are usually related to the reinforcements around the opening. Some designs incorporate spiral-wound disks that provide the strength tangential to the opening. These disks are usually used in conjunction with other reinforcements to provide the complete structural requirements in the vicinity of the off-center bosses. Another method of providing reinforcements for cut filaments utilizes filaments placed tangentially to the opening to provide a pattern similar to the pattern for axially located ports. For both concepts, proper reinforcement width must be maintained in order to provide sufficient shear transfer of the loads within cut filaments to the reinforcements.

In any design for cut-filament, off-center-port reinforcement, the following three specific factors must be controlled: (a) the structural integrity of the chamber, (b) the continuity of the head in a circumferential path, and (c) the smoothness of the contour (in order to avoid bridging that would be detrimental to the shear transfer of the forces to reinforcements).

The use of off-center ports when the filaments are wrapped around the port to avoid the requirement that they be cut is usually associated with small-diameter openings, primarily because of the disturbances to the desired filament path in other sections of the chamber.

(2) Reinforcements

Placing openings off-center from the axis of a filament-wound chamber, although it utilizes a head contour of a given geometry, reduces the efficiency of the chamber. Reinforcement must be placed locally around the opening in order to realize the maximum strength of the chamber. The cut-filament and reinforcement concept of construction is considered in this analysis because it is possible to produce thereby a more symmetrical chamber than can be produced by using wrapped-in designs.

A method of analysis has been developed for determining the required amount of reinforcement around off-center ports. It applies to zero-hoop-stress, balanced-in-plane, geodesic-isotensoid, and other head contours. No restriction is imposed on the location of the openings in the heads.

To minimize the required reinforcement at any opening, the strength of every filament must be considered when cut-filament designs are analyzed. A method has been established for determining the stiffness at any point and in any direction. This stiffness is particularly important in the direction of the principal curvatures of the head. The three parameters required to determine stiffness in any direction are the modulus of elasticity, thickness, and radius of curvature. The modulus of elasticity is that of the composite in the specified direction. It can be computed from the physical properties of the filament and resin, filament orientation, and relative quantities of filament and resin. By means of the basic anisotropic formula, the modulus can thus be determined along each of the principal curvatures. Because the thickness and the curvature of the given shell are known, the stiffness in the direction of the principal curvatures can be established at any point on the head by multiplying the modulus of elasticity by the thickness divided by the radius of curvature squared.

For an opening of specific size and position, the removed stiffness is placed vectorially with respect to the cut filaments along the perimeter of the hole. The vectorial equalization of removed stiffness to required reinforcement stiffness constitutes the minimum reinforcement. The two principal methods of supplying reinforcement to the hole involve tangentially placed unidirectional tapes and spirally wound disks.

(a) Tangentially Placed Unidirectional Tapes

Preimpregnated, unidirectional, glass tapes are placed tangentially and equiangularly along the perimeter of the opening. The stiffness of each tape reinforcement, at a particular point and in the direction of the tape, is calculated as the product of modulus of elasticity and cross-sectional area divided by radius of curvature squared. Because the principal radii of curvature are known, the radius of curvature may be calculated in any direction between the principal radii by applying Euler's relationship (see Appendix III of Volume II).

The total stiffness of an array of tapes is the summation of the stiffness of all tapes intersecting a radial line from the axis of the opening at any point on the periphery of the opening. The angle between any tape and the tangent to the opening determines the relative stiffness of that tape with respect to the point under consideration. A tape tangent to the opening at the point under consideration is fully effective, whereas the tapes with an angle have reduced the stiffness. There is thus a point at which the angle between the tangent and the tapes is so large that no stiffness is gained from the tape; this may be considered a cutoff point. Because a very short distance is required to develop the full bond strength of filaments and tapes, this cutoff point determines the required tape lengths.

(b) Spirally Wound Reinforcement Disks

The analysis for spirally wound reinforcement disks is basically the same as that for tangentially placed unidirectional tapes; the modifications are slight.

Only circular ports employing cut-filament designs were analyzed in this program. A review of typical off-center-port

requirements for rocket-motor cases indicates that the size of the openings required prohibits designs employing wrapped-in concepts. Although Aerojet has successfully hydrotested designs with wrapped-in, off-center ports in chambers as large as the Polaris second-stage motor, the disturbances to filament-winding patterns in adjacent head and cylindrical sections, plus the structural requirements in areas not covered by filaments, result in considerably less efficiency than that attained with the cut-filament concept.

Although there is some evidence that openings with other than circular shapes might exhibit high efficiencies, a review of rocket-motor-case requirements indicates that shape changes would complicate both the machining and sealing problems to a point at which such designs would have questionable utility and would be extremely difficult to justify. This subject was not investigated further, because of time limitations and the questionable merit of the concept.

(3) .Ports in Cylindrical Sections

A modification of the analysis of off-center ports and cut-filament reinforcements for heads (Appendix III of Volume II) was adapted to the designing of ports in cylindrical sections of filament-wound structures; it is presented in Appendix IV of Volume II. The principal difference is that, for cylindrical ports, the magnitude of the forces in the biaxial stress field within the shell remains constant at all points, whereas the magnitude of the force field in the head varies as a function of the distance from the chamber axis.

2. Empirical Studies

The Phase I work outlined in Section II,A was completed except for the reporting of empirical data that were to be obtained from another program in which 6-in.-dia tubes were to be tested during the same period of performance as the work under AF 33(616)-8442. The purpose of that 6-in.-dia-tube program was to establish relationships between the stresses in the materials of the composite and the biaxial forces occurring in chamber membranes. That task was to be accomplished by wrapping several helical patterns on 6-in.-dia tubes and then obtaining both crazing-threshold data and rupture data for various ratios of force fields. The biaxial force ratio was to be controlled by pressurizing the cylinder and applying pure axial forces. These data were to be compared with the results of a theoretical cylindrical analysis to determine the biaxial forces required to produce the most efficient composite structure for a particular wrap angle and resin modulus. Glass-filament crossover factors were also to be derived from the study. These factors were to be related to the longitudinal-filament winding angle on heads of pressure vessels to produce new head contours and winding patterns. The fabrication and testing of these tubes were initiated in the early phases of that program as scheduled, but the results were inconclusive because of failures in areas other than the composite structure.

The original 6-in.-dia tube design was modified in order to develop a suitable test vehicle. A test specimen having a pure longitudinal wrap and axially loaded in tension failed in the bond of the composite to the metal hardware at an axial load of 41,000 lb. This total load is equivalent to 2252 lb per inch of circumference and a longitudinal-filament stress of 199.5 ksi. The low filament stress indicated that a 50% improvement in the bond

strength would have to be achieved before the composite structure could be expected to fail and the effect of filament crossover could be determined. This 50% improvement was considered beyond the technology at that time, and the effort was therefore discontinued. Although the information sought in that program is considered to be of value, no further fabrication or testing of the 6-in.-dia specimens is planned. It should be noted that the data to have been obtained from that program would in no way have altered the conclusions based on the work conducted for this program, because the tube data were intended for use in assigning portions of the general performance factors to specific characteristics of the filament-wound composite, particularly filament crossovers. The general performance of wrap patterns and head contours can therefore be defined on the basis of the information presented in this report.

3. Selection of Optimum Designs

The selection of specific designs for further study and evaluation in Phase II was based primarily on the theoretical-performance factors of specific head contours (see Section IV,A,1, foregoing). Performance factors were calculated for all contours considered.

To facilitate performance-factor calculations, the computer program was extended to determine the internal volume, filament length, and filament stress for each contour. A maximum allowable stress was assumed for this purpose, and the surface equidistant from the inner and outer surfaces of the glass-resin composite was selected as the desired contour. The volume used to determine the performance factor was the volume contained within the inner surface of the composite. The weights were determined by the length of filament path, thickness of composite, resin content, and densities of materials used.

Composite thickness was determined by iteration. It was first calculated at the equator, on the basis of the assumed maximum allowable stress, and was then readjusted to limit the maximum stress to the amount required. The method used to calculate the filament stress did not cover the effect of the center boss; at the boss, therefore, the calculated stress was infinite. It is known that the center boss reduces the stress in the adjacent filament to the stress imposed by the hoop load only, and that this effect damps out rapidly a short distance from the boss. To include the effect of the center boss, the location of maximum stress was selected at the point where ϕ, the angle between the circumferential radius of curvature and the longitudinal axis of revolution, was 5° greater than the angle ϕ at the center boss.

Figures 9 through 11 were prepared to show the performance factors for the three contour types, with variations in the D_b/D_c and L/D_c ratios. For these curves, the assumed filament stress was 310,000 psi, the resin content was 19 wt%, the glass density was 0.092 lb/cu in., and the resin density was 0.042 lb/cu in. On the basis of the theoretical-performance factors, the geodesic-isotensoid and balanced-in-plane head contours were selected for further study in Phase II. Equation (2), which gives the actual performance factor for filament-wound pressure vessels (Section IV,A,1), shows that many factors govern the overall efficiency of the chamber. For certain design parameters, therefore, specific head contours will be more efficient than others. It is not expected that one class of head contours will serve as the optimum for all variations in chamber-dimension parameters. The Phase II

model chambers were planned for use in defining the range within which each of the two selected designs would result in the most efficient chamber.

B. PHASE II - CONSTRUCTION AND TESTING OF MODELS

1. Test Plan

A definitive test plan was adopted so that the maximum amount of information would be obtained from a minimum number of chambers. Tests were performed on 18 model chambers fabricated to specifications and design parameters determined on the basis of the Phase I analyses. The variables under study were chosen so that analysis of the results would assure reliable and valid conclusions. These evaluated variables included L/D_c and D_b/D_c ratios for both balanced-in-plane and geodesic-isotensoid head contours. Each model was subjected to a two-cycle hydrostatic test: (a) a 1-min proof test, followed by (b) a burst test. Pressures were applied in both cycles at a strain rate of approximately 1%/min in the circumferential direction, in accordance with standard Aerojet practice. This strain rate (see Appendix I of Volume II for a detailed discussion) was selected in order to produce a failure approximating that occurring in a steady-state condition, and to minimize the amount of scatter caused by the time-rate sensitivity of the materials being used.

Twelve of these chambers were fabricated by Aerojet with balanced contours and the in-plane wrapping pattern. The remaining six units had isotensoid contours, and were wrapped on the geodesic path. They were filament-wound by Rohr Aircraft Corporation in Riverside, California.

2. Design and Fabrication

The model chambers were 18 in. in diameter, with center-boss diameter equal to either 20, 50, or 70% of the chamber diameter. Chamber lengths were selected so that the L/D_c ratios were approximately 0.6 (back-to-back heads), 2, or 4. Table 1 summarizes the important data acquired during this portion of the program. It presents the basic parameters, the test results, and the performance factors (pV/W values) used to judge the efficiency of those units.

The basic pressure vessels were fabricated from 20-end "E" glass roving with Owens-Corning HTS sizing. The roving was preimpregnated with E-787 epoxy resin, formulated by U.S. Polymeric Chemicals, Inc. Aerojet's specified minimum requirement for the "E" HTS 20-end roving is an ultimate tensile strength of 280,000 psi.

Center bosses were fabricated from 7075-T6 aluminum alloy. Aluminum is preferred because of its light weight and its relatively low elastic modulus, which makes it more compatible with the glass-resin composite. (The unidirectional modulus of elasticity for the composite is approximately 7.0×10^6 psi, as compared with 10.3×10^6 psi for 7075-T6 aluminum alloy.) The 20% bosses incorporated standard 2.500-12 UN-3B (AND 10050-32) gasket-seal threads in accordance with Military Specification MIL-S-7742. The 50 and 70% center bosses were designed to incorporate a bolt-type joint.

The models were wrapped on mandrels fabricated entirely from Hydrocal plaster cast on steel shafts. Dimensional control of the outside contour was accomplished by accurately sweeping a final Kerr DMM plaster layer over the Hydrocal with metal templates. The cases were sealed with an impervious elastomeric liner of neoprene rubber. Two layers of the uncured rubber, each 0.060 in. thick, were added in orange-peel segments directly over the plaster mandrel. The integrity of the seal was assured by staggering the butt joints of the layers. In addition to material familiarity and ease of fabrication, this type of liner has proved to be highly reliable and has demonstrated excellent impermeability in many glass-filament-wound chambers previously fabricated and hydrostatically tested by Aerojet. The neoprene liners were vacuum-bagged and oven-cured directly on the mandrels, thus eliminating costly metal molds. In addition, neoprene required lower curing temperatures than other elastomeric materials, which minimized the possible degradation of the plaster mandrel.

3. Test Results

The detailed discussions below present design factors, fabrication problems, and other specific data considered significant with regard to each of the 18 model chambers fabricated and tested during Phase II. Table 1 presents a comprehensive summary of the design and test results for each model. All units were tested at a pressurization rate in the range from 200 to 250 psig/min.

a. Chamber 176435

This chamber incorporated back-to-back heads, geodesic-isotensoid contours, and 20% bosses on both ends (i.e., $D_b/D_c = 0.2$). The measured internal volume was 1990 cu in., and the weight of the glass-resin composite was 1.49 lb. The chamber was successfully proof-tested to 480 psig with a 1-min hold in the first cycle. In the burst cycle, the chamber failed at a test pressure of 530 psig; failure originated in the filaments in the area around the boss where filament crossovers were particularly predominant. Figure 12 shows the chamber after fabrication; Figure 13 shows the hydroburst case and, in particular, the area of failure. The longitudinal-filament stress at the burst pressure was 245,400 psi. Hoop filaments were not required because of the back-to-back heads. The performance factor (pV/W) for this unit was 0.71×10^6 in., and the strength-to-density ratio was 2.07×10^6 in.

b. Chamber 176436

This chamber incorporated back-to-back heads, balanced-in-plane contours, and 20% bosses on both ends. The measured internal volume was 2030 cu in., and the glass-resin-composite weight was 2.10 lb. As with Chambers 176435, 176437, and 176438, this unit did not require hoop filaments because of the back-to-back heads. Figures 14 through 18 illustrate typical back-to-back head-contour units during various stages of fabrication. The chamber was successfully proof-tested to 600 psig with a 1-min hold time at pressure. In the burst cycle, it failed at 893 psig; failure originated in the knuckle or equator. The longitudinal-filament stress at the burst pressure was 327,000 psi. The strength-to-density ratio of this unit was 2.93×10^6 in. The hydroburst chamber is shown in Figure 19.

c. Chamber 176437

This chamber incorporated back-to-back heads, balanced-in-plane head contours, and 50% bosses at both ends. The internal volume was 2373 cu in., and the weight of the glass-resin composite was 2.70 lb. The completed chamber is shown in Figure 20. The chamber was successfully proof-tested to 600 psig with a 1-min hold. (In the burst cycle, it failed at 943 psig; this failure originated in the knuckle or equator and was almost identical to the failure of Chamber 176436. The longitudinal-filament stress at the burst pressure was 318,500 psi. The strength-to-density ratio of the unit was 2.86×10^6 in.

d. Chamber 176438

Back-to-back heads, balanced-in-plane head contours, and 20 and 50% bosses were incorporated in this chamber. The internal volume was 2180 cu in., and the weight of the glass-resin composite was 2.26 lb. The completed chamber is shown in Figure 21. It was successfully proof-tested to 600 psig for a 1-min duration. In the burst cycle, the chamber failed at 690 psig; failure originated in, and was confined to, a small section in the knuckle or equator. The longitudinal-filament stress at the burst pressure was 243,900 psi. Because of the lower ultimate filament stress of this unit, as compared with the two previous cases, a review was initiated to establish the possible cause. Examination of the fabrication records revealed that filament slippage occurred during curing. To correct this, all future chambers were vacuum-bagged immediately after winding.

e. Chamber 176439

This chamber incorporated geodesic-isotensoid head contours, with $L/D_c = 2$. Typical views of units with this L/D_c ratio are shown in Figures 22 and 23 before and after liner application on the plaster mandrel. Both heads had 20% bosses. The internal volume was 8218 cu in., and the weight of the glass-resin composite was 6.57 lb. The fabricated unit is shown in Figure 24. The chamber was successfully proof-tested at 480 psig for a 1-min duration. In the burst cycle, it failed at 580 psig; failure originated in the hoop filaments. The longitudinal-filament stress at the burst pressure was 264,200 psi, and the hoop-filament stress was 267,400 psi. The performance factor was 0.76×10^6 in. The strength-to-density ratio of the heads was 2.10×10^6 in.; in the cylinder section, this ratio was 1.49×10^6 in. The hydroburst chamber is shown in Figure 25.

f. Chamber 176440

This chamber incorporated geodesic-isotensoid head contours, with $L/D_c = 2$; both heads had 50% bosses. The internal volume was 8265 cu in., and the weight of the glass-resin composite was 11.24 lb. The chamber was successfully proof-tested to 680 psig for a 1-min duration. In the burst cycle, it failed at 1140 psig; failure originated in the hoop filaments of the cylinder. The longitudinal-filament and hoop-filament stresses were 275,000 and 330,900 psi, respectively. The performance factor was 0.83×10^6 in., and the strength-to-density ratios for the head and cylinder were 1.82×10^6 and 1.79×10^6 in., respectively. The chamber after hydrotesting is shown in Figure 26.

g. Chamber 176441

This chamber incorporated geodesic-isotensoid head contours, with $L/D_c = 2$; identical 70% bosses were on both heads. Figure 27 shows the chamber during fabrication, prior to the application of the hoop wraps. The completed chamber is shown in Figure 28. The internal volume was 8338 cu in.; the weight of the glass-resin composite was 9.00 lb. The unit underwent a successful 570-psig proof test for a 1-min duration. It failed in the hoop filaments at 1080 psig in the burst cycle. The longitudinal-filament and hoop-filament stresses were 295,100 and 347,100 psi, respectively. The performance factor was 0.79×10^6 in., and the strength-to-density ratios for the head and cylinder were 1.27×10^6 in., and 1.77×10^6 in., respectively. The chamber after hydroburst is shown in Figure 29.

h. Chamber 176442

This chamber incorporated balanced-in-plane head contours, with $L/D_c = 2$; both heads had 20% bosses. The internal volume was 8226 cu in., and the weight of the glass-resin composite was 7.69 lb. The chamber was successfully proof-tested at 600 psig for a 1-min duration. In the burst cycle, it failed at 700 psig; failure originated in the hoop filaments. The longitudinal-filament stress at the burst pressure was 252,300 psi; the hoop-filament stress was 262,400 psi. The strength-to-density ratios for the heads and cylinder were 2.22×10^6 and 1.5×10^6 in., respectively.

i. Chamber 176443

This chamber incorporated balanced-in-plane head contours, with $L/D_c = 2$; both heads had 50% bosses. The internal volume was 8265 cu in., and the weight of the glass-resin composite was 8.15 lb. The chamber was successfully proof-tested to 600 psig for a 1-min duration. In the burst cycle, it failed at 850 psig; failure originated in the hoop filaments. The longitudinal-filament and hoop-filament stresses were 261,000 and 319,100 psi, respectively. The strength-to-density ratios for the head and cylinder were 2.30×10^6 and 1.70×10^6 in., respectively.

j. Chamber 176444

This chamber incorporated balanced-in-plane head contours, with $L/D_c = 2$. Both heads had 70% bosses. The case design required two revolutions of longitudinal wraps (i.e., four layers of longitudinal filaments). The relatively large boss diameter, combined with the in-plane wrapping pattern, created excessive filament slippage on the second revolution and prevented fabrication to the original design. It was decided to utilize only one revolution of longitudinal filaments and to decrease the number of hoop layers; the burst pressure was lowered accordingly. No further fabrication problems were encountered. The completed chamber is shown in Figure 30. It was successfully hydrotested to a revised 300 psig proof pressure for a 1-min duration. In the burst cycle, the chamber failed at 360 psig; failure occurred in the longitudinal filaments of one head. The performance factor was 0.63×10^6 in. The longitudinal-filament stress at the burst pressure was 176,400 psi, and the hoop-filament stress was 285,300 psi. The strength-to-density ratio of the heads was 1.67×10^6 in.; in the cylinder, this ratio was 1.39×10^6 in. The hydroburst chamber is shown in Figure 31.

k. Chamber 176445

This chamber incorporated geodesic-isotensoid head contours, with $L/D_c = 2$. The heads utilized unequal bosses - a 20% boss on one end and a 50% boss on the other. Because of the unequal-boss design and the use of a geodesic winding pattern, the pattern was wrapped to the smaller boss diameter. Glass-tape reinforcing disks were placed between winding layers of the larger-boss head, and the basic filaments in this head were cut to the larger diameter. Figures 32 and 33 respectively show the larger-boss head prior to and after the cutting of the filaments. The internal volume of the case was 8203 cu in., and the glass-resin-composite weight was 7.33 lb, including the reinforcing disks. The chamber failed at 410 psig in the first cycle prior to reaching the proof pressure of 480 psig. Failure was attributed to inadequate resin shear strength between longitudinal layers on the large boss, which in turn caused separation between the boss and the case, as shown in Figure 34. The performance factor was 0.46×10^6 in. The longitudinal-filament stress at the burst pressure was 184,500 psi, and the hoop-filament stress was 179,600 psi. The strength-to-density ratios for the head and cylindrical section were 1.53×10^6 and 1.04×10^6 in., respectively.

l. Chamber 176446

Balanced-in-plane head contours, with $L/D_c = 2$ and with 20 and 50% bosses on opposite heads, were incorporated in this chamber. The internal volume was 8240 cu in., and the glass-resin-composite weight was 8.10 lb. The chamber successfully underwent a hydrostatic-proof-pressure test at 600 psig with a 1-min hold. In the burst cycle, failure occurred in the filaments around the large boss at 760 psig. As shown in Figure 35, separation occurred between the large boss and the composite structure. The performance factor was 0.79×10^6 in.; the longitudinal-filament and hoop-filament stresses were 248,200 and 296,800 psi, respectively; and the strength-to-density ratios for the head and cylinder were 2.15×10^6 and 1.60×10^6 in., respectively.

m. Chamber 176447

This geodesic-isotensoid chamber was essentially the same as Chamber 196445, except that a 70% boss was used on one end rather than a 50% boss. Reinforcing glass-tape disks were also used between the geodesic-pattern layer on the larger-boss head. The internal volume was 8113 cu in., and the glass-resin-composite weight was 7.62 lb, including the reinforcing disks. The failure was similar to that of Chamber 176445 and occurred at 395 psig, when the large boss separated from the case. The longitudinal-filament stress at the burst pressure was 180,800 psi, and the hoop-filament stress was 169,100 psi. The strength-to-density ratios for the heads and cylinder were 1.50×10^6 and 0.99×10^6 in., respectively.

n. Chamber 176448

This chamber incorporated balanced-in-plane head contours, with $L/D_c = 2$. One head had a 20% boss; the opposite axial-boss diameter was 70% of the chamber diameter. The internal volume was 8358 cu in., and the weight of the glass-resin composite was 8.78 lb. Excessive filament slippage was encountered during application of the longitudinal wraps, and special care and additional time were required to complete the wrapping. Chamber failure

during hydrotesting occurred in the first cycle at 515 psig. Again, as was true for all balanced-in-plane chambers with 70% bosses, the failure was attributed to separation between the large boss and the longitudinal filaments in the head. At the burst pressure, the longitudinal-filament and hoop-filament stresses were 152,700 and 192,300 psi, respectively. The strength-to-density ratios at failure were 1.30×10^6 in. for the head and 0.98×10^6 in. for the cylinder.

o. Chamber 176449

This chamber incorporated balanced-in-plane head contours, with $L/D_c = 4$; both heads had 50% bosses. The completed chamber is shown in Figure 36. The internal volume was 17,274 cu in., and the glass-resin-composite weight was 17.26 lb. The unit underwent a successful 600-psig proof-pressure test for a 1-min duration. It failed in the burst cycle at 830 psig because of separation between the boss and longitudinal filaments on one of the heads. The performance factor was 0.84×10^6 in. The longitudinal-filament stress was 242,700 psi, and the hoop-filament stress was 315,700 psi. The strength-to-density ratios for the head and cylinder were 2.12×10^6 and 1.72×10^6 in., respectively. The chamber after hydroburst is shown in Figure 37.

p. Chamber 176450

This chamber utilized balanced-in-plane head contours, 70% bosses on both ends, and $L/D_c = 4$. The internal volume was 17,507 cu in., and the weight of the glass-resin composite was 18.55 lb. The chamber successfully underwent a proof-pressure test to 600 psig for a 1-min duration. In the burst cycle, failure occurred (as with all 70% bosses) in the area of the head and was caused by separation between the boss and the glass filaments (see Figure 38). The burst pressure was 610 psig. The longitudinal-filament stress at the burst pressure was 150,800 psi, and there was a 247,900-psi stress in the hoop filaments. The strength-to-density ratios were 1.30×10^6 in. at the head and 1.15×10^6 in. in the cylinder.

q. Chamber 176451

This chamber incorporated balanced-in-plane head contours, with $L/D_c = 4$. The heads had unequal bosses - one of 20% and the other 50%. The internal volume was 17,242 cu in., and the glass-resin-composite weight was 16.82 lb. Figure 39 shows the completed chamber. After filament wrapping and curing, the chamber was damaged during removal from the oven when the head with the 20% boss was accidentally dropped onto the center shaft of the handling cart. A localized area was depressed near the equator of the head contour, although supported internally by the plaster mandrel, and the filaments became separated. Damage caused by cutting of the filaments was not apparent. In the hope of salvaging the chamber it was decided to recure the localized area after injecting resin. The hydroburst on the first cycle, at a pressure of 125 psig, proved that this repair procedure was of no value. Failure occurred in the damaged area of the head as shown in Figure 40. Limited funds prevented the fabrication of an additional unit.

r. Chamber 176452

This chamber incorporated balanced-in-plane head contours, with $L/D_c = 4$ and unequal center-boss ratios (20 and 70%). The internal volume was 17,362 cu in., and the glass-resin-composite weight was 17.14 lb. The unit failed at 540 psig in the first cycle as the result of separation between the glass filaments and the 70% boss. The performance factor was 0.54×10^6 in. The longitudinal-filament stress was 166,500 psi, and the hoop-filament stress was 202,700 psi. The strength-to-density ratios of the head and cylinder were 1.45×10^6 and 1.09×10^6 in., respectively. The burst chamber is shown in Figure 41.

4. Evaluation of Test Data

The Phase II tests performed on the 18-in. model chambers were limited in number, but led to several findings of value for the planning, designing, and investigation of future glass-filament-wound rocket-motor cases and pressure vessels. The actual-performance-factor results obtained are summarized in Table 1; they were plotted graphically and are presented as a function of D_b/D_c ratios in Figures 42 and 43 for chambers incorporating equal- and unequal-boss configurations on opposite heads. The results indicate that little variation exists for the ranges of model-chamber lengths considered in this program. Therefore, only one curve was drawn for the various chamber lengths.

The curves show that no specific head contour or wrap pattern will yield the highest performance for all variations in dimensional criteria. Figure 42 indicates that end-for-end wrap patterns with complementing balanced-in-plane head contours produced the more efficient pressure vessels in D_b/D_c-ratio ranges up to 52%. Chambers having ratios from 52 to 72% would be more efficient with the geodesic-isotensoid head contour. Beyond the 72% ratio, it can be surmised that the helix angle resulting from the large bosses produces a ratio of hoop to longitudinal strength in the cylindrical section that would be greater than the required 2-to-1 force-field ratio created by the pressure. It is believed that, at 72%, the maximum performance will be achieved by winding to a geometry created by a small boss, inserting reinforcements, and cutting to the required diameters. A comparison between the balanced-in-plane and geodesic-isotensoid contours in large-boss-diameter ranges indicates that the former contour, with cut filaments and reinforcements, will result in the higher-performance case.

One advantage of end-for-end wrap patterns is their ability to comply with unequal-axial-boss criteria without the cutting of filaments. This advantage is maintained up to a specific D_b/D_c value at which fabrication problems reduce the effectiveness of the structure. Figure 43 indicates that, with a D_b/D_c ratio of 20% in one end of the filament-wound chamber, the maximum chamber performance is maintained by the balanced-in-plane contour up to the opposite boss ratio of 42%. It is believed that configurations utilizing reinforcements are required for the best results beyond this range.

C. PHASE III - INVESTIGATION OF SCALE FACTORS

1. Design

Scaling factors were evaluated by means of two chambers the size of the second-stage Minuteman case (approximately 44.3 in. in diameter by 127 in. long) fabricated with "E" glass roving. The overall configuration was based on the Wing II titanium-alloy case. Both glass-filament-reinforced cases were designed to withstand a hydrostatic proof pressure of 587 psi (in accordance with Aerojet Minuteman specifications) and a design ultimate pressure of 734 psi (25% above the proof pressure as generally required for glass-filament-wound rocket-motor cases). Appendix V of Volume II describes the general design approach for filament-wound pressure vessels. Appendix VI of Volume II analyzes the application of scale factors.

The skirt-to-skirt length of the two scaled-up chambers was 108.9 in., in accordance with the latest available Wing II drawings. Four nozzle ports, of the size required by second-stage Minuteman homogeneous-rocket-motor cases, were located at the radial distance and the station specified for the homogeneous chambers. In addition, one axially located boss was placed in each head - the one in the forward head because of the igniter and for fabricational reasons, and the other in the aft head for purely fabricational reasons.

The design of the first 44.3-in.-dia chamber (Serial No. 1) was based on concepts proven in the manufacture, testing, and evaluation of Polaris A-3 first- and second-stage rocket-motor cases at Aerojet. These concepts, which were considered as representing the most advanced state of the art at the inception of the program, resulted in a composite design-allowable stress of 80,000 psi in the hoop direction of the cylindrical section of the chamber at the proof pressure. The design stresses in the hoop and longitudinal filaments at the proof pressure were 208,000 and 152,000 psi, respectively. Design details are shown in Figure 44, and a structural analysis is presented in Appendix I of Volume I.

In previous tests of 18-in.-dia cases for the Polaris program, the hoop strength achieved ranged from 84 to 105% of the Aerojet-strand-test strength for cases using the same processes. The first 44.3-in. case was within this range, having demonstrated a hoop-filament tensile strength that was 97.5% of the material strength of 326,000 psi. The design ultimate tensile strength of hoop filaments for the second case was based on the demonstration of a value that was approximately 84% of the strand strength (324,000 psi) at a burst pressure (734 psi) 25% above the required proof pressure (587 psi). This criterion resulted in a design strength of 294,000 psi at a pressure of 734 psi; it was hoped that this value would be exceeded and that the case would achieve the same ultimate tensile strength (317,000 psi) in the hoop direction as the first unit. In the interest of meeting pressure requirements, however, a design level equal to that predicted by the lower value in the range of case-strength to strand-strength ratios was required. At the design burst pressure, the hoop strength of the composite in the cylindrical section of the second case was 119,000 psi, based on the expected resin content (19 wt%) and filament strengths (294,000 psi in the hoop direction). Stresses in the case at the proof pressure were not set at the design criteria, but were established by applying a specific factor (80%) to the design burst strengths. This technique permitted demonstration of the higher operating

performances, based on the standard parameters of pressure vessels (i.e., pressure, volume, and weight). The selection of an arbitrary design level for the proof pressure (such as a composite hoop stress of 80,000 psi) would merely result in a factor of safety greater than 25% and in a proportionately heavier case.

The second 44.3-in.-dia chamber (Serial No. 2) was to be used in demonstrating the improvements in design technology produced during this program. This demonstration was to be accomplished by comparing test data obtained with (a) a chamber incorporating these design improvements, and (b) another representing the state of the art at the inception of the program (the Serial No. 1 chamber). The improvements were to be limited to those of design by using identical materials and processes for both chambers. A design analysis of the Serial No. 2 chamber is presented in Appendix II of Volume I and a structural analysis in Appendix III of Volume I.

Specifically, the second chamber (shown in Figure 45) was intended to display improvement over the first by more effective use of longitudinal filaments through modification of the forward contour and adjustment of the design burst pressure to 25% above the proof pressure. A balanced-in-plane contour was selected because (a) the theoretical performances of balanced-in-plane and geodesic-isotensoid head contours are approximately equal for bosses having diameters less than 20% of the chamber diameter, (b) the pattern is considered more efficient when there are unequal bosses at each end of the chamber, because primary filaments will not have to be cut, and (c) fabrication could be more easily accomplished at Aerojet by means of slight modifications in the winding patterns selected for the first chamber. Actual performance factors (outlined in the data presented for 18-in. model chambers in Section IV,B) confirmed this selection.

The lead time for the 7075-T6 aluminum-alloy aft-closure plate (Figure 46) required that fabrication be initiated before the selection of specific contours. The criteria for the aft head were therefore the same as those for the first chamber (i.e., basically a zero-hoop-stress head with modifications produced by the buildup of nozzle-port reinforcements). The forward boss (Figure 47) was made from 7075-T6 aluminum alloy and was identical for both chambers.

The design of the off-center ports for the aft head of both chambers was based on the cut-filament concept, using preimpregnated, unidirectional, glass tapes for localized reinforcement. This concept is consistent with that employed by Aerojet in the successful reinforcement of off-center aft-closure ports for both stages of the Polaris. The tapes, fabricated on a male layup mold into the reinforcements, were placed in a precise pattern tangentially to simulated port openings. Proper reinforcement width was maintained in order to provide sufficient shear transfer of the loads from the cut filaments to the reinforcements. When required during chamber winding, the reinforcements were removed from the layup mold and were spaced between the layers of longitudinal wraps. Specifically, seven layers of reinforcement were required in the first chamber (alternating with the eight longitudinal layers), and five layers were required in the second (alternating with the six longitudinal layers).

In the designing of skirts for filament-wound rocket-motor cases, special consideration must be given to the shear-plane transition area through which loads are transferred from the skirt to the chamber. The design factors include (a) limiting the hoop strains of the chamber in this area to the strain associated with the skirt material, (b) establishing proper skirt-adhesive thicknesses and bond lengths, and (c) minimizing temperature effects on the bond joint. Current skirt configurations are either of all glass-cloth-resin composite or of a combination aluminum-alloy and glass-cloth-resin composite. The glass composite extends into the cylindrical section, and is selected to be compatible with the strains in the case during pressurization. In addition, the lower thermal conductivity of the composite reduces the amount of heat flow into the bond area, and the thermal coefficient of expansion of the skirt is compatible with that of the chamber. The aluminum alloy is generally used as a flange for interstage attachment purposes.

Although it was realized that the aforementioned configuration would provide an improved design for a firing unit, it was believed that the main Phase III effort should be concerned with the chamber. The skirts were therefore designed principally for handling purposes. As a result, and in order to expedite fabrication, the forward and aft skirts for both chambers were fabricated from 6061-T6 aluminum alloy. The forward- and aft-skirt drawing are presented in Figures 48 and 49, respectively. The skirts extended 2.00 in. from the datum plane onto the cylindrical section, although modification of the forward contour on the second chamber reduced this extension to 1.60 in. The ends extending over the cylindrical section were slit approximately every 2 in. to eliminate any stress concentrations that might have occurred because of radial restraint offered by the skirts. This design had been used successfully for previous chambers, including the first- and second-stage Polaris.

2. Fabrication

a. Mandrel

An all-plaster mandrel was used in the fabrication of both 44.3-in. chambers. It was selected not only for economy reasons, which included the limited number of chambers to be made, but also for the dimensional stability, load-deflection characteristics, and adequate strength demonstrated with previous mandrels of this type.

In the strict sense, the all-plaster version is not a mandrel fabricated entirely from plaster, but is so called to contrast it to a segmented mandrel made either from accurately machined metal segments or by sweeping a thin plaster coating over the machined metal segments. These latter techniques, although initially costlier, are used when higher production rates are required, in order to eliminate the need for repeated fabrication of a support cage for the plaster. Additional advantages of the all-plaster mandrel include (1) simple construction, with no special tooling required, (2) use of readily available and inexpensive raw materials, (3) ease of modification to conform to design changes, (4) ease of sweeping to desired dimensions and adequate retention of these dimensions, (5) good strength characteristics, sufficient to withstand filament-winding stress, and (6) ease of removal in reasonable fashion, both by mechanical means and by dissolving.

The all-plaster winding mandrels were made by fabricating a series of longitudinal plaster ribs reinforced with steel rods. These ribs were supported by parallel plaster disks attached to a machined-steel winding shaft (Figure 50). A Hydrocal B-11 plaster and wet-hemp mixture was built up in successive layers over a reinforced wire screen placed around the ribbed framework. During mandrel fabrication, a chain and a wire cable were incorporated in a spiral pattern at various levels in the plaster layers to facilitate mandrel removal. Unwinding of the chain after chamber fabrication broke out the major portion of the plaster. A final layer of Kerr DMM plaster was applied over the Hydrocal-hemp mixture, and the entire mandrel was then accurately swept to the required dimensions by positioning the shaft on centers and rotating it past contoured sweep templates. The mandrel was then oven-dried to remove excess moisture. Figure 51 shows the plaster mandrel prior to the lining operation.

b. Liner

Synthetic rubber (neoprene) was selected as the liner material to perform the task of sealing the internal surfaces of both scale-up chambers. Extensive experience at Aerojet has demonstrated the ability of neoprene to meet this requirement, and the cost is considerably lower than that of other elastomeric materials. The superior impermeability of neoprene has been proved on the basis of Aerojet tests conducted on many subscale and Polaris, first- and second-stage, glass-filament-wound chambers. In addition, neoprene can be cured at a temperature below that required for other sealants and its use is therefore less detrimental to the plaster materials employed in mandrel fabrication.

Two layers of the uncured rubber, each 0.060 in. thick, were added in orange-peel segments directly over the plaster mandrel, which had been coated with liquid neoprene to provide a tacky surface for ease of rubber layup. Although redundant, this thickness was selected because it permitted easier handling of the material during layup. A sealed case was assured by staggering the butt joints of the two layers. The forward boss and aft closure were cleaned, etched, primed, covered with a 0.030-in.-thick layer of neoprene, and placed between the two 0.060-in.-thick layers to ensure a proper seal. The assembly (Figure 52) was then vacuum-bagged with a polyethylene bag and oven-cured at 225°F for 8 hours. The bag was removed after the cure, and the liner was cleaned with a dry cloth.

c. Winding

Owens-Corning ECG-140 Fiberglas roving was the basic material employed in the winding of the case structure of the first two 44.3-in. chambers. It was supplied as 20-end roving and had an HTS (high-tensile-strand) type of finish. All glass-filament-wound chambers that were being produced at Aerojet during 44.3-in.-case fabrication used this particular glass and surface treatment. The material has consistently demonstrated higher average tensile strengths than the 280,000 psi required in Aerojet specifications.

Fabricational-processing techniques required the use of preimpregnated roving (prepreg) for the longitudinal windings of the 44.3-in. cases. The advantages of prepregs for filament winding are (1) high-speed winding equipment can be used, (2) precise resin content under controlled conditions

can be achieved, (3) more-accurate control of filament or tape orientation is possible, (4) in-process damage to the load-carrying glass fibers during fabrication is reduced, because the glass is protected by "B" staged resin, and (5) closer quality control can be maintained by evaluating the material in composite form prior to chamber fabrication. The most suitable prepreg system evaluated to date, and the one selected at Aerojet for both cases, is produced by U.S. Polymeric from its E-787 resin system.

The 44.3-in.-dia chambers were wound by positioning the mandrel in the machine, adjusting the tension and width of the glass filaments to form the desired tape, and placing the tape on the mandrel in the required winding patterns. The pattern selected for both units utilized end-for-end wraps (longitudinal) and hoop wraps (circumferential).

The first operation in the winding of each case was the placement of 3.0-in.-wide bands at each end of the cylindrical portion of the chamber near the tangent (Figure 53). The case was designed to provide a uniform OD and to permit the skirts to be integrally wrapped directly over the longitudinal structure. As a result, it was necessary to add a portion of the hoop wraps inside the longitudinal layers to compensate for the hoop filaments not applied in the cylindrical section of the chamber because of the presence of skirts. The continuity of longitudinal structure was maintained by providing grooves for the hoop bands in the lined mandrel so that when the required outer hoop layers were applied, the OD of the cylindrical section of the chamber became uniform. A single strand of preimpregnated 20-end roving was used for this operation; a 10-lb tension was applied at the spool.

The second winding operation consisted of applying the longitudinal roving (see Figure 54). Nine 20-end strands of roving were used, with a 10-lb tension supplied at each of the nine spools; the tension was checked on each strand between the final payoff head of the machine and the mandrel. The pattern was designed so that each tape would lie adjacent to the prior one, and no overlaps or gaps would exist. The thicknesses of individual layers and total longitudinal composite were thus controlled by the tape width, owing to the fact that the cross section of the tape was constant because of a constant number of strands.

One basic concept in the designing of all filament-wound rocket-motor cases, whether they employ the helical or end-for-end wrap patterns, is that an even number of longitudinal layers is required in order to provide balance between right- and left-hand patterns. The nozzle-port reinforcements (Figure 55) were designed so that one reinforcement was positioned between each pair of longitudinal layers. Each reinforcement layer was made up of four quadrants (one reinforcement for each port). Reinforcements were fabricated by placing Scotchply 1009-26 (Minnesota-Mining and Manufacturing Company), unidirectional, glass-filament, preimpregnated tape tangentially to the perimeter of the port and equiangularly around it. To expedite fabrication and to ensure that the reinforcement would have the proper drape, the quadrants were prefabricated on a male layup form that duplicated the contour of the aft head of the chamber. All reinforcements were stored on a form in a 0°F storage box until required for case fabrication.

After the combined longitudinal wrapping and reinforcement placement, two layers of dry-roving hoop wraps (to be removed in a later

operation) were placed over the longitudinal layers in the cylindrical section to compress the glass-resin composite before the skirts were applied. By "squeezing" the longitudinal wraps, a more rigid mandrel (composed of the original mandrel and the longitudinal composite) was obtained for maximum hoop-filament efficiency. In addition, this procedure also prevented movement of the longitudinal filaments until preparations were completed for the application of skirts and hoop filaments. Dry roving was used for economy. When the squeeze wrap was removed, the forward and aft skirts were assembled to the case by means of positioning fixtures. Accurate locations were obtained by positioning the fixtures from the axial bosses and the mandrel shaft.

The final winding operation consisted of positioning the skirts and wrapping the cylindrical portion of the chamber with hoop filaments (Figure 56). The number of spools, tensioning techniques, and bandwidth were the same as described for longitudinal wraps. Individual strand tensions were varied from 16 to 12 lb (four layers at 16 lb, four layers at 14 lb, and the remaining layers at 12 lb) in accordance with standard design practices aimed at maintaining constant filament stresses throughout the chamber wall and compensating for compression of the mandrel because of pressure imposed by wrap tensions.

Upon completion of hoop winding, the case was cured in a vertical oven. The cycle included preliminary curing at 120 to 130°F for 4 to 5 hours, during which the excess resin bled from the aft-head reinforcements and was removed by careful wiping with a clean cloth. This excess resin was particularly evident on the aft head, because the reinforcement disks had a higher resin content than the glass roving (26 wt%, as compared with 19 wt% for the glass roving). The chamber subsequently underwent a gelling cycle at 200°F for 4 hours, and a curing cycle at 300°F for 9 hours. The oven temperature was increased and decreased at the rate of 25°F/hour to control thermal expansions between the mandrel, metal hardware, and composite structure.

A hoop-bleeder-wrap technique was used to obtain a surface finish compatible with current production chambers, to secure a dense composite wall structure, and to absorb the excess resin of the cylindrical section. This technique, which is standard practice for first-stage Polaris chambers, included the following procedures: (1) The entire cylindrical section was covered with one layer of No. 2353 Dacron cloth, to facilitate release after curing, and one layer of No. 181 glass cloth, to absorb excess resin; (2) stainless-steel sheets, each 0.018 in. thick and 2.0 ft wide, were applied to the full length of the cylindrical section and acted as an outer curing mold for the glass-resin composite; and (3) a hoop layer of glass was applied over the steel sheets. The hoop layer, wound over the entire cylindrical section, held the metal sheets in position and provided a pressure of approximately 15 psi to the chamber during the cure. The roving, steel sheets, glass cloth, and Dacron cloth were removed after the curing cycle.

Visual examination of the completed chamber revealed that the hoop-bleeder-wrap technique produced a chamber whose cylindrical surface was greatly improved and whose irregularities (normal in chambers fabricated with all hoop layers outside the longitudinal structure) were minimized. In addition, the glass cloth had absorbed excess resin, which normally flows to the surface of the composite during the cure and remains there.

After oven curing, the chamber was placed in a pit with its aft end up, to facilitate nozzle-port cutting. The center of each aft nozzle port to be cut was located with respect to a suitable reference point, and a hole was made with a circular hole saw. A router was positioned by an arm attached to a port-locating fixture within the mandrel, and both rough and finish cuts were made (Figure 57). This rapid, reliable, and reproducible technique produced ports to the required dimensions and tolerances without damaging the composite structure in the area adjacent to the hole.

The final step in fabrication was removal of the all-plaster mandrel. A chamber harness was first assembled around the cylindrical section, and the shaft was freed by removing the shaft adapters and carefully chipping the plaster away from the shaft. The chamber was then removed from the pit, leaving the shaft. By unwinding the chain previously imbedded in the plaster during mandrel fabrication, the mandrel was mechanically broken into pieces small enough to permit removal through the forward- and aft-boss openings. The internal surfaces of the chamber were thoroughly cleaned with a water and detergent solution, and dimensional checks were made (see Figure 58). Table 2 summarizes the basic design and fabrication parameters for the Serial No. 1 and 2, 44.3-in. chambers, as well as for the Serial No. 3 and 4 chambers fabricated later in the program.

3. Testing

The Serial No. 1, 44.3-in. case was hydrotested on 15 March 1962, and the Serial No. 2 on 25 May 1962. The Serial No. 1 is shown in the test stand in Figure 59. Each chamber was instrumented with strain gages; after it was placed on the test stand, linear-motion transducers were attached in accordance with Figure 60 for use in measuring deflections during the proof cycle. Additional data obtained during the tests included internal volume, volumetric expansion at the proof and burst pressures, and permanent volumetric expansion after the proof cycle.

The Serial No. 1 and 2 chambers were proof-tested at 587 psi for 90 sec, in accordance with Minuteman test procedures. This pressure is 10% above the estimated operating pressure of the chamber (534 psi). The design burst pressure for the chamber (734 psi) was 25% above the proof pressure. It should be noted that the current homogeneous-metal-case design burst pressure (668 psi) is 25% above the estimated operating pressure.

The test sequence for the Serial No. 1 chamber was as follows: (a) The chamber was subjected to the proof pressure at the rate of 286 psig/min; (b) the chamber pressure was reduced to zero to permit visual inspection of the case and disassembly of the linear-motion transducers; (c) the chamber was pressurized to 610 psi when the limit switch, set for the proof cycle, stopped the pumps, and the pressure was reduced to zero after a 10- to 20-sec hold; and (d) the chamber was pressurized at the rate of 339 psig/min to the burst pressure (855 psi).

The Serial No. 2 test sequence was as follows: (a) The chamber was subjected to the proof pressure at an average rate of 140 psig/min; (b) the chamber pressure was reduced to zero to permit visual inspection of the case and disassembly of the linear-motion transducers; and (c) the chamber was pressurized at the rate of 272 psig/min to the burst pressure (730 psi).

After the successful proof tests, both chambers were visually examined for indication of possible areas of eventual failure. No such areas were found, nor was there any evidence of stress crazing of the resin in the heads or in the cylindrical section of either chamber.

4. Evaluation of Test Data

Figure 61 indicates that the hoop filaments and the igniter boss of the Serial No. 1 chamber burst essentially simultaneously. Analysis of the boss indicated that stresses in its flange were within a few percent of the ultimate tensile strength of the material; this fact and the high filament stresses exhibited at the time of bursting indicate that both areas were near failure. Rather than attempt to determine which failed first, it is believed sufficient to state that apparently a simultaneous failure occurred.

The Serial No. 2 chamber burst as a result of hoop-filament failure between the center and the aft end of the cylindrical section. Figure 62 shows that the destructive burst in the hoop wraps occurred so uniformly that the shock disintegrated the hoop cylindrical section in this area. Longitudinal filaments remained intact, thereby indicating a degree of redundancy, although it may be seen that the sudden burst caused collapse of the forward head as well as separation of the forward and aft skirts.

The structural data obtained from the tests are presented in Table 3. The actual burst pressure of the second chamber was within 0.5% of the design burst pressure. The performance factors used to evaluate chamber efficiencies were calculated using measured burst pressures, volumes, and weights (see Table 4).

As previously stated, the second case was intended to display improvement over the first by a more efficient use of longitudinal filaments through design modification of the forward contour. In addition, by adjusting burst pressures for the Serial No. 2 to a specific value (25%) above the required proof pressure, the weight would be reduced and the result would therefore be a higher hoop-composite stress in the cylinder at the proof pressure. This would be accomplished if the basic fabrication methods, materials, and test methods were identical for both chambers. These improvements, coupled with attainment of the same ultimate hoop-filament strength (317,000 psi), would have resulted in the achievement of a higher performance factor (pV/W) with the Serial No. 2. Although the improvements were successfully accomplished, and the demonstrated burst pressure of the Serial No. 2 was 24.5% above the proof pressure (25% is generally required for glass-filament-wound, rocket-motor cases), the ultimate hoop-filament strength of the Serial No. 2 did not meet the value achieved with the Serial No. 1.

For further evaluation of the data in Table 3, special attention is directed to the results of Aerojet strand tests of incoming lots of material. For all practical purposes, the strengths of the composite material used in both cases were equal. The hoop strength achieved in 18-in. chambers for the Polaris program ranged from 84 to 105% of the Aerojet-strand-test strength. Identical fabrication processes were specified for all these 18-in. chambers. The observed scatter is believed to result from errors in the strand data and from chamber-to-chamber processing variations. It is of interest to note that the demonstrated hoop-filament-strength to strand-strength ratios for the

first and second chambers were 0.975 and 0.90, respectively. Because the processing was identical for both, and because there was no design variation from one chamber to another that would affect the achieved ultimate tensile strength of the hoop filaments, it must be assumed that the hoop strength is a more accurate measure of the relative merits of the materials of one chamber as compared with another. On this basis, the adjusted performance factor for the Serial No. 2 would be (317/293) $0.63 \times 10^6 = 0.68 \times 10^6$ in.

The strain values shown in Table 3 were obtained from transducer readings taken in the center of the cylinder (hoop growth) and at the end of one skirt with reference to the other skirt (longitudinal growth). The modulus of elasticity was obtained by dividing the composite stress by the strain.

A typical calculation for the flexural rigidity (EI) of the case is presented below, using the measured tensile modulus of the chamber as the bending modulus; the example cited is for the Serial No. 1 chamber.

$$EI = E \pi R^3 t = (3.30 \times 10^6)(\pi)(22.1)^3 (0.150)$$

$$= 1.68 \times 10^{10} \text{ lb-sq in.}$$

With regard to hydroburst data for filament-wound chamber, the importance of the dependence of strength on strain rate must be emphasized. All chambers and materials tested at Aerojet are strained at a rate of approximately 1%/min. A review presented in Appendix I of Volume II reveals that increases in chamber strength of approximately 10% would be realized if this strain rate were increased to 5%/min. Typical Serial No. 2 chamber strengths at the burst pressure for these higher strain rates would thus increase to the following values:

	Increase, psi
Hoop-composite strength	From 118,300 to 130,000
Hoop-filament strength	From 293,000 to 320,000
Longitudinal-filament strength	From 229,400 to 252,000

Although the higher strain rates appear more impressive, they do not supply realistic values for the rocket-motor-case evaluation. In a rocket-motor case, the high rate of pressurization at ignition is accompanied by an equally high increase in filament strength. The increase compensates for the ignition peak occurring in the pressure-time curve for the unit. The more critical period of operation is the period of relatively static pressure when the motor is in normal operation. The duration of current typical rocket motors is from 60 to 90 sec, during which a specific margin of safety must be maintained. The only way to ensure that a design has the specified margin of safety is to establish "static" burst pressures. Data provided in Appendix I of Volume II indicate that the strain rate of 1%/min selected by Aerojet approaches the static burst pressure to a reasonable degree. Any evaluation of filament-wound-chamber data for rocket-motor-case application must take the foregoing facts into account.

D. PHASE IV - TESTING AND EVALUATION OF MATERIALS*

1. Laboratory Testing

a. S994 Glass Roving (Lot F-1053)

Thirty rolls of S994 20-end HTS glass roving weighing a total of approximately 423 lb were purchased from Owens-Corning Fiberglas for use in material evaluation and fabrication of the Serial No. 3, 44.3-in.-dia chamber for Phase V of the program. Laboratory tests were conducted on the as-received glass roving by both Owens-Corning and U.S. Polymeric; they covered the ultimate tensile strength, weight per linear yard, and ignition loss (%). The test results are presented in Table 5.

The S994 roving was then preimpregnated with the U.S. Polymeric E-787 epoxy-resin system. The E-787 system was selected because (1) it had previously been qualified for the Polaris program, and (2) its use would facilitate comparison with results obtained in Phase III since the Serial No. 1 and 2, 44.3-in. chambers utilized the identical resin system with "E" glass.

Table 6 presents physical-property data from tests performed by U.S. Polymeric and Aerojet on the preimpregnated material. Comparison of the data, as well as data from Table 5, indicates reasonable correlation between the test results of the three companies. This correlation is particularly apparent in the results for weight per linear yard, horizontal shear, volatile content, and resin content.

Although all three companies followed the required qualification-acceptance procedures, wide deviation is apparent in the ultimate-tensile-strength results, particularly for the as-received and preimpregnated roving. The differences in the average ultimate tensile strengths for the as-received roving tested by Owens-Corning and U.S. Polymeric were minor; similarly, the differences in the average ultimate tensile strengths after impregnation as tested by U.S. Polymeric and Aerojet were not overly large. The difference between these two average values before and after impregnation was significant, however, amounting to more than 10% of the tensile strength.

Differences in tensile-strength results before and after impregnation have been noted previously for "E" glass roving tested in the Polaris program (Ref. 4). Filament ultimate tensile strengths for as-received roving lots averaging 350.0 ksi by the Aerojet strand test dropped to an average of 296.0 ksi after resin impregnation. Additional tests were conducted

---

*Experimental lots of the Owens-Corning Fiberglas high-strength glass roving were designated X994; this type of material was used to fabricate the Serial No. 3, 18-in. chamber and the Serial No. 3, 44.3-in. chamber. Subsequently, production-run quantities of this roving were designated S994 glass roving by the manufacturer; this type of material was used to fabricate the Serial No. 4, 18-in. chamber and the Serial No. 4, 44.3-in. chamber. In this report, both types are referred to as S994 glass roving.

on the glass after acetone extraction of the epoxy resin and vinyl coating of the strand. The strength-test results approximated the original 350.0 ksi (actually 346.0 ksi), which indicated that detrimental effects from impregnation processing were negligible and that differences before and after impregnation were due to the type of resin used. The mechanism of these variations has not been completely defined. It may be noted that rolls of ECG-140/HTS glass roving obtained for the Polaris program were exhibiting 350.0 ksi in U.S. Polymeric strand tests, while the S994 specimens prepared and tested by the same vendor averaged 442.6 ksi, or 26% greater in strength than the preimpregnated "E" glass fibers.

An apparent anomaly was noted in the material-property values obtained for Roll No. 10. Material from this roll was used in fabricating the S994 Serial No. 3 subscale chamber and was also extensively tested at various intervals. For the as-received roving, U.S. Polymeric reported strengths higher than those originally reported by Owens-Corning. In addition, U.S. Polymeric reported a still higher strength after the material was impregnated; the data and other material-property parameters for Roll No. 10 are presented in Table 7. Aerojet also conducted NOL-ring tests on three rolls; Table 8 gives the results. The fiber stresses calculated for specimens from the tested rolls were comparable with or slightly superior to the strengths determined by the Aerojet-strand-test method.

b. YM31A Glass Roving (End Use: Serial No. 4, 44.3-Inch Chamber, Longitudinal Wrap)

Several developments occurred that resulted in cancellation of the Phase IV and VI work utilizing beryllia-containing high-modulus YM31A glass roving, and redirection to the use of S994 glass roving. Because of the possible toxicity of the YM31A material, various negotiations were conducted to resolve questions of indemnification. Although Aerojet had purchased approximately 160 lb of YM31A from Owens-Corning for use in Phases IV and VI, final negotiations for impregnation with a resin system were delayed because of increased impregnation costs and vendor apprehension with regard to toxicity. Arrangements were finally made with Owens-Corning to impregnate the glass with the Shell 58-68R resin system rather than the U.S. Polymeric E-787 used on previous glass. Among the several factors leading to this approach were Owens-Corning (1) acceptance of the 18 ±2% resin-content requirements, (2) guarantee of a minimum return of 147 lb of preimpregnated roving, and (3) willingness to perform 100% testing and certification of the material.

In contrast, because of unfamiliarity with the YM31A material, the vendor originally considered for roving impregnation was reluctant to guarantee the resin content and the minimum weight to be returned, and would accept the program only on a best-efforts basis. Impregnation with the Shell 58-68R resin was decided upon because of recent evaluations made in the Polaris program which indicated that the composite tension and horizontal-shear-strength properties of Shell 58-68R preimpregnated specimens were equivalent to those of U.S. Polymeric E-787 preimpregnated specimens, and in some cases were superior (Ref. 5). The impregnation order to Owens-Corning was subsequently canceled at the direction of the Air Force, because of a belief that this approach would introduce a new variable that might jeopardize the

attainment of target goals and the comparison of data and results with those for similar units tested in Phases III and V.

The roving was tested in the Structural Materials Division laboratory to determine physical properties prior to delivery of the high-modulus YM31A glass for impregnation.

Visual examination of all 11 rolls of the roving indicated low-quality material in comparison with previous lots (see Ref. 6). Although the purchase order specified 20-end roving, which is the standard used by Aerojet for all filament-winding programs, it was found that the material delivered was actually 80-end roving. It is believed that the filaments on the deliverable glass total 51 per end, in contrast to the normal 204 filaments per end for 20-end roving.

The roving also had a relatively high electrostatic charge, had a high degree of fuzziness, and was somewhat brittle. This brittleness, often characteristic of higher-modulus materials, contributed to difficulties in threading the roving around pulleys prior to vinyl coating of the glass for tensile-strand testing.

The material that could be tested proved to be nonuniform in ignition loss and weight per linear yard. The average tensile strength of four strand specimens on the roll that tested highest was 286 ksi. The strength is not considered to be an improvement over the strengths of sample lots determined by Aerojet several years ago. Complete test results are presented in Table 9.

c. S994 Glass Roving (Lot F-1226)

Representatives of the Air Force, Owens-Corning Fiberglas, and Aerojet-General met on 12 March 1963, at the Space Systems Division, and agreed to replacement of the high-modulus YM31A beryllia glass with high-strength S994 glass roving. This redirection was due in part to the inconsistent and wide variations in physical properties encountered in the preliminary laboratory testing of the YM31A glass and in part to difficulties anticipated in scaling up and correlating the laboratory-test results with the test results from the 44.3-in. chamber. It was agreed that the higher-modulus YM31A material had negligible advantages over the S994 glass roving, and the added cost of application on the 44.3-in. case was not warranted. This was particularly true in view of the experimental nature of the 160-lb batch of YM31A glass roving already procured, and there were no assurances that future batches would be improved. In contrast, the S994 glass roving would be procured from a production run indicating a proven reliability. Owens-Corning agreed to furnish 370 lb of S994 glass and also physical-property data for all rolls of the newly furnished material. The S994 glass-fiber material strength was to be equivalent to that used in the first 44.3-in. S994 chamber.

After receipt from Owens-Corning, the 370-lb S994 lot was shipped to U.S. Polymeric for impregnation with the E-787 resin system. After preimpregnation and delivery to Aerojet, the material was again tested. Test

results for the glass in the as-received and preimpregnated conditions, respectively, are presented in Tables 10 and 11. NOL-ring-specimen tests were made on five rolls from this lot and the results are given in Table 12.

This lot of roving had an average ultimate tensile strength of 440.1 ksi as opposed to the average of 488.8 ksi for the lot used on the Serial No. 3, 44.3-in. chamber. The Air Force ruled against the use of this lot of material and requested procurement of glass with a lot-average ultimate tensile strength equal to or exceeding 488.8 ksi; Aerojet therefore procured additional S994 glass roving in an effort to meet these requirements.

d. S994 Glass Roving (Lots F-1333 and F-1379)

Negotiations with Owens-Corning brought out that a lot-average ultimate tensile strength of 488.8 ksi was not feasible on a commercial run. The vendor agreed, however, to supply material having a lot average of 480 ksi, with a minimum ultimate tensile strength of 450 ksi for any single roll.

Upon receipt of Air Force approval to procure material with these strength values, a purchase order was issued to Owens-Corning authorizing shipment of 360 lb of S994 to Aerojet. This roving (Lot F-1333) was received in a shipment of 28 rolls; the results of vendor tests of its ultimate tensile strength are presented in Table 13.

This material was delivered to U.S. Polymeric for impregnation with E-787 resin. That firm re-tested it in the as-received condition prior to impregnation, and 13 rolls of roving were rejected for excessive catenary. Table 13 presents the results of these tests.

Owens-Corning agreed to replace these rolls with new S994 material, which was delivered directly to U.S. Polymeric for testing and processing. The Owens-Corning and U.S. Polymeric test results for these new rolls are presented in Table 14.

The acceptable material was then impregnated with the E-787 resin system and delivered to Aerojet. The tests performed on this roving by both U.S. Polymeric and Aerojet-General are summarized in Tables 15 and 16.

These two lots of preimpregnated S994 roving were reviewed and the most suitable material was selected for use on the Serial No. 4, 44.3-in. chamber; Table 17 presents the properties of the glass roving used for that chamber.

Roll No. 4 of Lot F-1333 was selected for the fabrication of Serial No. 4 subscale chamber. Physical test data for this roll are presented in Table 18.

2. Subscale-Chamber Testing (18-Inch Diameter)

a. Serial No. 3

An 18-in. S994 chamber with axial bosses was designed (Figure 63), fabricated, and tested under conditions identical to those employed for

the standard control chambers in the Polaris subscale program. The chamber structure was subjected to biaxial force fields, and the results were used for the final evaluation of material properties. Material from Roll No. 10 was used in fabricating this chamber. The case was wound on a lined plaster mandrel, with two revolutions (four layers of glass) in the longitudinal direction having an average of 552 turns per revolution, and six glass layers in the hoop direction having an average of 167 turns per layer. A 10-lb tension was applied on the preimpregnated roving for both the longitudinal and hoop windings. No particular material-handling problem was encountered, except that the glass-roving width, after application on the mandrel, was narrower than expected. As a consequence, slight gapping was noticed after the winding of the chamber was completed.

The chamber was cured in an oven at atmospheric pressure for 2 hours at 200°F. In general, it had a uniform appearance that was considered consistent with the appearance of previous chambers. After curing and removal of the plaster mandrel, it was placed on a stand for testing at ambient-temperature conditions (Figure 64). It was first subjected to a proof test at 400 psig, with the pressure held for 1 min. After a return to 0 psig, the chamber was subsequently pressurized to the hydroburst point, at an average rate of 148 psig/min. Failure occurred in the hoop filaments at 1313 psig. Almost-complete disintegration of the hoop filaments occurred (Figure 65), while the liner and longitudinal wrap remained intact; this is indicative of very uniform winding tension and pressure loading on the filaments. The chamber was examined for signs of stress crazing and any damage after the proof-test cycle and after failure occurred. The stress crazing was considered no greater than previously found on units with "E" glass HTS roving and the identical E-787 resin system.

The test results for the Serial No. 3, 18-in. chamber are summarized in Table 19; they were considered very satisfactory, and the slight gapping of the filaments noticed after winding was apparently not detrimental. The values of 375.0 ksi for the longitudinal-filament stress and 388.0 ksi for the hoop-filament stress were the highest that had been achieved to that date by Aerojet on a standard, 18-in., filament-wound chamber under biaxial loading conditions. Table 19 also presents data obtained on the latest 18-in., standard, control unit fabricated and tested in the Polaris program to that date. Comparable longitudinal- and hoop-filament stresses for the "E" glass chamber were 295.0 and 307.0 ksi, respectively, or a strength difference of approximately 26 to 27% as compared with the subscale S994 chamber.

b. Serial No. 4

A standard 18-in. chamber fabricated and tested identically to the Serial No. 3 subscale chamber was used to evaluate the properties of the S994 material to be used for the Serial No. 4, 44.3-in. chamber in accordance with the original test plan. Roll No. 4 of Lot F-1333 was used to wind this chamber.

This chamber failed in the hoop direction at 1385 psig. The longitudinal- and hoop-filament stress levels at the time of failure were 376.7 and 403.6 ksi, respectively. The hoop-composite stress level at burst was 170.4 ksi. These test results, summarized in Table 20, were considered very satisfactory. The chamber is shown before and after bursting in Figures 66 and 67, respectively.

E. PHASE V - DESIGN, FABRICATION, AND TESTING OF 44.3-INCH-DIAMETER S994 CHAMBER (SERIAL NO. 3)

1. Design

The Serial No. 3, 44.3-in. chamber was designed to the same configuration as the "E" glass, Phase III, Serial No. 2 chamber except that S994 glass was used in the composite structure. The overall design features of the large-scale cases are described in detail in Section IV,C,1. Basically, these include (a) a forward closure with a balanced-in-plane contour, (b) a 7075-T6 aluminum-alloy plate in the aft closure, with a zero-hoop-stress contour and four off-center ports, (c) a 7075-T6 aluminum-alloy forward igniter boss, (d) 6061-T6 aluminum-alloy forward and aft skirts, and (e) preimpregnated, unidirectional, glass tapes in a precise configuration for localizing reinforcement of the cut-filament, off-center, aft-closure ports. These features were combined with the high-strength S994 glass fibers in the Serial No. 3 chamber, for which an engineering drawing is presented in Figure 68. The design analysis for this chamber is presented in Appendix IV of Volume I, and a structural analysis, based on the laboratory results and winding data, is presented in Appendix V of Volume I.

2. Fabrication

To minimize the introduction of new processing variables, the many operations required in the fabrication of the Serial No. 3 chamber were kept the same as those utilized for the two previous large-scale chambers. These operations (described in detail in Section IV,C,2) involved the use of an all-plaster winding mandrel that was made by sweeping plaster over a framework of steel-rod-reinforced longitudinal plaster ribs and parallel plaster disks attached to a machined-steel winding shaft. The case was sealed by applying two neoprene-rubber layers directly over the plaster mandrel, and curing it to form an impervious liner. The winding operations are identical with those previously performed, except for the winding pattern of layers and turns. The pattern and other pertinent case parameters are given in Table 2.

Various views of the completed case after resin curing and removal of the internal winding mandrel are presented in Figures 69 through 76.

3. Testing

The Serial No. 3, 44.3-in. chamber was hydrotested on 7 February 1963. Strain gages were first applied to the chamber; the unit was then placed in the test stand and linear-motion transducers were located for deflection measurement during the proof-pressure test (Figure 77). Figure 78 presents an overall view of the test setup. The chamber was first proof-tested to 558 psi, held for 90 sec. As outlined in Appendix V of Volume I, a composite wall hoop stress of 119,000 psi (25% above the proof-pressure stress level of the Serial No. 2 chamber) was selected as the level to be attained by the Serial No. 3 in order to minimize the possible detrimental stress crazing that might prevent attainment of the design burst pressure (734 psi). For this reason, the case had been fabricated with additional filaments, but examination of the winding records indicated that still more filaments were necessary. The only other alternative (if the 119,000-psi stress level was not to be exceeded) was to

lower the proof pressure accordingly. The chamber was successfully proof-tested in this manner. Sequence-photo coverage of the forward head was secured at 50-psig intervals to establish whether the level of initial stress carzing could be observed. No crazing threshold was apparent in the photographs (Figure 79); visual examination of the forward head after the proof cycle also revealed no predominant craze lines or areas of possible failure.

The chamber burst at 728 psi as a result of a hoop-filament failure in the cylindrical section between the center of the case and the aft end (Figure 80). This failure simulated that of the Serial No. 2 chamber. Failure occurred so uniformly that the hoop cylindrical section in this area disintegrated. Longitudinal filaments remained intact, indicating some redundancy. It was noted, however, that the burst caused separation of the forward and aft skirts (Figure 81).

4. Evaluation of Test Data

The structural data obtained are presented in Table 3, along with test results for the Serial No. 1, 2, and 4 chambers. The principal findings were that the ultimate hoop-composite stress in the cylinder was 155,700 psi; the hoop-filament stress was 367,000 psi; the ultimate strength-to-density ratios for the composite structure in the cylinder and heads were 2.1×10^6 and 2.68×10^6 in., respectively; and the performance factor was 0.76×10^6 in.

Weight comparisons for the glass cases fabricated in this program are presented in Table 4. Although the Serial No. 2 and 3 chambers failed within 2 psi of each other (730 and 728 psi, respectively), and within 1% of the 734-psi design burst pressure, a weight reduction of 17.5% was obtained in the composite structure of the Serial No. 3. Table 4 indicates that, had the weight of the nozzle reinforcements of the Serial No. 3 been 25% less than that of the Serial No. 2 reinforcements, the overall composite-structure weight reduction for the Serial No. 3 would have approached 25%. Such a weight reduction would correspond to the 25% greater strength displayed by S994 glass fibers in comparison with the "E" glass fibers.

F. PHASE VI - AXIAL-COMPRESSION AND BENDING TESTS OF 44.3-INCH-DIAMETER S994 CHAMBER (SERIAL NO. 4)

1. Design

The Serial No. 4, 44.3-in. chamber was designed to exactly the same configuration as the Phase V Serial No. 3 chamber to provide good correlation of the test results for determining the effect of axial-compression and bending loads. The design features (described in detail in Section IV,C,1 and shown in Figure 68) included (a) a forward closure with a balanced-in-plane contour, (b) an aft closure with a zero-hoop-stress contour, (c) four off-center ports and a 7075-T6 aluminum-alloy plate in the aft closure, (d) a 7075-T6 aluminum-alloy forward igniter boss, (e) 6061-T6 aluminum-alloy forward and aft skirts, and (f) preimpregnated, unidirectional, glass tapes in a precise configuration for localized reinforcement of the cut-filament, off-center, aft-closure ports. These features were combined with high-strength S994 glass fibers for the Serial No. 4 chamber. The design analysis is presented in Appendix VI of

Volume I, and a structural analysis, based on the laboratory results and winding data, is presented in Appendix VII of Volume I.

2. Fabrication

To minimize the introduction of variables, the Serial No. 4 chamber was fabricated in the same manner as the Serial No. 3. These operations (described in detail in Section IV,C,2) involved the use of the all-plaster winding mandrel. The case was sealed by applying two layers of neoprene rubber directly over the plaster mandrel and curing them to form an impervious liner. The winding operations and winding patterns were identical with those used for the Serial No. 3. The winding pattern and other pertinent case parameters are given in Table 2.

3. Test Setups and Testing

This chamber was structurally tested on 13 December 1963 in accordance with the program plan (see Section II,F).

The basic objectives of this test were (a) to provide additional information for the design of optimum-weight, filament-wound, rocket-motor cases in applications where buckling and stiffness are critical considerations, and (b) to demonstrate the feasibility of subjecting large-scale structures made with S994 glass fibers to axial-compression and bending-moment loads (see Appendix VII of Volume II). These objectives were successfully accomplished. The results are discussed below.

a. Hydrostatic Proof-Pressure Test

The chamber was filled with water, was pressurized to 558 psig, and was proof-tested at that pressure for 90 sec. Nine linear-motion transducers continuously recorded chamber-growth characteristics during this cycle; volumetric expansion was also recorded. Post-test examination revealed no visible damage to, or crazing of, the chamber; however, slight delamination was observed in the skirt area.

Because this chamber was to simulate the condition of the Serial No. 3 chamber prior to burst, a decision was made to proof-test it at 558 psig instead of 587 psig. This decision was based on the following considerations:

(1) Actual fabrication data and Aerojet-strand-test data indicated that failure would occur at 730 psig in the longitudinal filaments, due to the lower strength of the glass available for this chamber (see paragraph IV,D,1,d). A pressure of 558 psig preloaded the longitudinal filaments to a stress level of 224,000 psi, which was identical to that induced in the Serial No. 3 chamber at the proof pressure.

(2) The Serial No. 3 chamber had also been tested at 558 psi.

b. Assembly of Test Fixture and Skirt-Case Joint Reinforcement

The test-fixture loading ring was assembled to the forward skirt of the chamber, and further delamination in the skirt-attachment area was noted

at that time. It was decided to strengthen both the forward and the aft skirt-to-case joints prior to testing, to prevent possible joint failure during the application of axial-compression and bending loads. These areas were strengthened as follows:

(1) Three layers of dry S994 glass roving were applied over a 4-in.-wide area, centered on the tangent plane, and were then impregnated with room-temperature-curing EPON 828 resin mixed with 10% DTA catalyst.

(2) Three layers of Type 181 glass cloth impregnated with the same resin system were applied over the joint, also centered on the tangent plane.

(3) A steel strip (0.004 in. thick by 4 in. wide) was wrapped around the case, over the glass-resin reinforcement; it was held in place with a layer of S994 glass roving impregnated with the EPON 828 and 10% DTA resin system.

These reinforcements were instrumental in preventing possible joint failure during the test sequence; it is believed that they did not affect the test results, because the nearest instrumentation was 10 in. from the reinforced area, a satisfactory distance to allow the cylindrical section to act freely in buckling. The delamination that occurred was not unanticipated, because the skirts had been designed principally for handling purposes. The overall test setup is shown in Figure 82.

c. Instrumentation

The instruments used to record the growth characteristics of the chamber under bending and axial-compression loading consisted of 24 linear-motion transducers and 18 strain gages.

d. Axial-Compression Loading

An axial-compression load of 41,982 lb was applied to the forward skirt through four hydraulic jacks. Loading was applied at a 1% strain rate in 100-psi increments (hydraulic-pressure-gage reading). Intermittent instrument readings were taken at these intervals. The maximum load of 41,982 lb was held for 60 sec. After the load was released, the case was visually examined; no signs of damage or crazing were observed.

e. Combined Axial-Compression and Bending Load

A combined axial-compression and bending load was next applied to the case to permit investigation of the interaction between compression and bending loads. It was induced by putting a compressive load of 2800 lb on each of two adjacent jacks, and a load of 7696 lb on each of the remaining two adjacent jacks. This induced a simultaneous combination of a compressive stress of 3210 psi and a tensile stress of 415 psi in the chamber. The loads were applied in 50-psi increments to all four jacks until a hydraulic pressure of 227 psi was reached, at which time two jacks were locked off (load = 2800 lb each). The remaining two jacks were loaded in 75-psi increments until the full load of 7696 lb per jack was reached. This combined load was held for 60 sec and was

then released to zero. Several popping sounds were heard, on the tension side of the case in the area of the aft tangent plane, at about 50% loading during this cycle. Examination of the chamber revealed no visible indications of damage.

f. Bending-Load Test (1% Strain Rate)

For determination of the effect of pure bending on this chamber, the loading jacks were divided into two pairs, one on either side of the neutral axis. Each pair was then loaded in equal but opposite directions until 4897 lb had been applied to each jack; this induced the required bending moment of 603,815 in.-lb. The load was applied in increments of 100 psi (hydraulic pressure) at a strain rate of 1%/min, to allow intermittent instrument readings to be taken. The maximum load was held for 60 sec and was then released to zero. Loud popping sounds were heard on the lower section of the tension side of the case, as in the combined-load cycle. They were noted at 300 psi and continued through approximately 600 psi. The case was examined visually, and again showed no signs of structural damage.

g. Bending-Load Test (5% Strain Rate)

When examination revealed no case damage due to the previous bending load, it was decided to again apply a bending load using a strain rate of 5%/min (i.e., maximum load to be applied in 25 sec) to establish whether the bending modulus might be related to the rate of strain application. (This task, outside of the scope of contract requirements, was performed as a service at no additional cost.) The load was applied at a continuous rate of 15,000 lb/min rather than in step intervals. This precluded the use of the selector-switch-controlled recording instruments (ten strain gages). The load was applied and maintained at this rate until the attachment-bolts tore out of the 6061-T6 sheet-aluminum skirt, allowing the load to relax. This failure occurred at about 50% of the maximum load. The skirt-to-case joint did not fail; however, due to relaxation of the load, the data recorded in this cycle were insufficient to allow determination of the effect of the 5% strain rate on the flexural characteristics of the chamber.

h. Hydroburst Cycle

The chamber was pressurized at a rate of 280 psi/min (i.e., 1% strain rate) until failure occurred, at 696 psi, in the cylindrical section approximately 20 in. forward of the aft tangent plane (approximately 24 in. above the base plate). Sequence-photo coverage is presented in Figure 83. Prior to cylinder failure, the forward skirt joint failed, the skirt separated from the case, and a few hoop filaments burst in the cylindrical section.

4. Evaluation of Test Data

The structural data obtained from this test are presented in Table 3. The significant findings included the following: The compressive modulus of elasticity (E_c) in the cylinder was 3.22×10^6 psi, the compressive rigidity of the chamber (E_cA) was 4.95×10^7 lb, the modulus of elasticity in bending (E_b) was 4.31×10^6 psi, and the flexural rigidity of the chamber (E_bI) was

1.62×10^{10} lb-sq in. None of the strain values recorded during structural loading exceeded 750 microinches per inch, and the stress levels at the hydroburst pressure were within 5% of the calculated design values. A satisfactory correlation exists between the actual and the calculated values for the compressive modulus (E_c) - 3.22×10^6 and 3.07×10^6 psi, respectively - and the compressive rigidity (E_cA) - 4.95×10^7 and 4.62×10^7 lb, respectively.

The performance of this chamber was only slightly below that of the Serial No. 3 ($pV/W = 0.66 \times 10^6$ and 0.76×10^6 in., respectively). This is considered satisfactory because the case had been subjected to four structural-load cycles and one proof-pressure cycle before being pressurized to the burst point.

G. COMPARISON WITH MINUTEMAN ROCKET-MOTOR CASES

The weights of the filament-wound chambers fabricated and tested in this program are compared with the weights of the insulated steel (Wing I) and titanium (Wing II) chambers currently in use as second-stage cases for the Minuteman missile in Table 21. Insulation weights for the filament-wound chambers were based on the weight of insulation for the Wing II design. Table 21 indicates that the Serial No. 2 chamber weighed 31.4 lb (or 8.6%) less than the titanium case and that the Serial No. 3 chamber weighed 78.8 lb (or 21.6%) less than the titanium case.

Four modifications of filament-wound test cases are also shown in Table 21. The Mod I and Mod III show the weight reduction (30 lb) that could be accomplished with an aft-closure-plate design duplicating that employed for Polaris cases, rather than with a design based on simplicity of fabrication. The Mod II and Mod IV are basically of the same design as the Mod I and Mod III, except that additional longitudinal filaments have been applied to meet the flight-load design criteria shown below for the second-stage Minuteman rocket-motor case.

	Value
Expected operating pressure	534 psi
Maximum expected operating pressure	587 psi
Proof pressure	587 psi
Burst pressure	
Homogeneous chamber	668 psi
Filament-wound chamber	734 psi
Flight loads	
Maximum bending moment	980,000 in.-lb
Maximum axial force	178,000 lb

Because of the lower modulus of the composite structure, the flexural stiffness of a filament-wound chamber designed to meet only pressure forces is lower than that of either a titanium or a steel case, based on the same criteria. To meet specific flexural-rigidity (EI) requirements beyond the rigidities produced by these pressure vessels requires the addition of longitudinal filaments to the cylindrical section. Figure 84 compares filament-wound chambers with the existing homogeneous chambers by showing the weights of all chambers listed in Table 21 as a function of desired flexural rigidity.

It is apparent that the use of filament-wound chambers meeting the second-stage Minuteman flight criteria will permit a weight reduction of as much as 63.8 lb in comparison with the current Wing II case.

Figures 85 and 86 compare the Serial No. 2 and 3, 44.3-in., filament-wound chambers with the Wing I and II chambers fabricated for the Minuteman program on the basis of performance factor (pV/W) as a function of proof and burst pressures, respectively. Figure 87 compares the same chambers on the basis of strength-to-density ratios. The weights are in accordance with those in Table 21. The design burst pressure used for the metal case was 668 psi, the burst pressure used for the filament-wound case was 734 psi, and the design proof pressures were the same for all designs (587 psi).

The comparisons shown in Figures 85 through 87 and Table 21 were based on ultimate design allowables of 200,000 and 160,000 psi for steel and titanium, respectively. These allowables were established at the inception of the design work on the basis of values that were readily obtainable at the time. Improved materials and processes have resulted in the attainment of steel and titanium strengths in the vicinity of 300,000 and 180,000 psi, respectively. One titanium case, tested in the second-stage Minuteman program, demonstrated an ultimate stress of 205,000 psi in the biaxial-stress field of the cylinder. Advanced titanium-case designs are expected to be based on an ultimate strength of 180,000 psi in the cylindrical section, or 12% above the current allowables. The design allowables for the filament-wound composite structure used for the comparisons presented in this report were based on the ultimate tensile strength of commercially available material - i.e., Owens-Corning ECG-140, 20-end HTS (which averages 350,000 psi) and Owens-Corning S994, 20-end HTS (which averages 437,000 psi).

The basic concept of chamber fabrication (i.e., use of the mandrel and insulation as the form for filament winding) permits the immediate use of new materials, thereby increasing margins of safety or reducing chamber weight without requiring the modification of tooling processes. Test-weight chambers with high margins of safety utilized for nozzle and propellant evaluations may be procured merely by increasing the amount of composite material placed on the mandrel. Developments involving the optimization of insulation thickness may also be accomplished by employing mandrel designs that incorporate a thin layer of plaster between the structural components of the mandrel and the insulation. New insulation profiles will require only minor changes in tooling, with a minimum of lead time. The delivery of a development chamber can be accomplished with a short period after the insulation is received.

A filament-wound chamber can be produced that meets all the structural requirements of the Minuteman missile system but this does not mean that it can be loaded and fired in the same manner as the metal Minuteman missile. The second-stage Minuteman motor employs a bipropellant grain. Current casting techniques for this system utilize the larger-diameter opening of the homogeneous design. The filament-wound design employs the concept of integral heads. Some modifications of propellant-casting techniques would be required to produce a chamber that could be loaded and fired. These modifications probably would not offer any real difficulty, but different tooling and casting techniques will be required.

V. CONCLUSIONS AND RECOMMENDATIONS

The major objectives of this program were met and the work accomplished represents significant advances in the field of filament winding. Recommendations are included below for the application of the knowledge gained in this program, and for work aimed at the acquisition of additional data to enhance the utility of filament winding for future applications. Strong consideration should be given to pursuing the work recommended under subscale and full-scale chamber research (Sections V,B,1 and 3 below). It is believed that these tasks are of particular significance to the future of the filament-wound structure.

A. CONCLUSIONS

1. Phase I

a. Theoretical analysis revealed the geodesic-isotensoid and balanced-in-plane contours as the most efficient for filament-wound chambers. The efficiencies of these designs were determined on the basis of a theoretical-performance factor (pV/W), which relates the basic parameters of the pressure vessel and was developed during this program.

b. It was also determined that the most satisfactory rate of loading of filament-wound pressure vessels is at a strain rate of 1%/min; this allows a minimal change in tensile properties for a variation in loading rate, thus minimizing variation in the test results.

2. Phase II

Model-test results in Phase II showed that

a. Pressure vessels fabricated to the back-to-back head design (L/D_c approximately 0.6) exhibited the most desirable structural properties and highest performance factors of any configurations, and additionally offered fabrication simplicity. The unit with balanced-in-plane head contours proved superior to the comparable case with geodesic-isotensoid contours. Units with equal bosses on the opposite heads, and particularly those with the smaller boss-diameter to chamber-diameter ratios, had superior performance ratings and fewer fabrication problems than those with unequal bosses. These oblate-spheroid cases present a configuration worthy of serious consideration for many applications in which the envelope requirements permit their use.

b. The structural properties of, and performances achieved by, pressure vessels with either balanced-in-plane or geodesic-isotensoid head contours were comparable for units having equal bosses and boss-diameter to chamber-diameter ratios up to and including 50%. Greater filament-winding simplicity was noted for the balanced-in-plane units.

c. For the units having equal bosses, with boss-diameter to chamber-diameter ratios greater than 50%, the geodesic-isotensoid cases were superior in structural properties and simpler to fabricate (because filament-slippage problems resulted from in-plane wrapping with large-diameter bosses).

d. The method selected for cutting filaments on the unequal-boss design for the geodesic-isotensoid units did not prove satisfactory, and the development of a feasible technique will require further study and design effort. Adequate interlaminar shear strengths were not developed on the tested units

because of inadequate coverage of the reinforcement disks between the glass-filament layers. A redundant-isotensoid type (two geodesic wrap patterns) may exhibit a satisfactory approach; limited time and funds prevented further development effort. The 20 and 50% unequal-boss design for the balanced-in-plane chamber was considered satisfactory, although other design concepts (particularly those involving the addition of reinforcement disks between glass layers around the larger boss) may prove superior beyond the 50%-boss-diameter range, if properly designed.

e. As compared with balanced-in-plane contours, the setup and programing were costlier for chambers with geodesic-isotensoid contours, and far more complex fabrication procedures were required.

3. Phase III

a. On the basis of tests performed in other programs and verified by data from Phases II and III, individual factors were assigned to each of the material, dimensional, and environmental variables associated with the design of filament-wound pressure vessels. These are presented in Appendix V of Volume II. Of particular importance in this program was the influence of scale-up, and a design factor representing the effect of chamber diameter on design allowable stress is also presented there. These factors are based on the results of tests performed on chambers up to 54 in. in diameter. The application of scale factors to establish design allowables for filament-wound rocket-motor cases up to 300 in. in diameter is presented in Appendix VI of Volume II, along with a predicted curve on design factors for chambers up to this size.

b. The significance of the analytical methods developed is emphasized by the performance of the Serial No. 2, 44.3-in.-dia chamber, which was designed using the structural analysis based on data obtained during Phases I and II. The Serial No. 2 reflected a 24-lb weight reduction as compared with the Serial No. 1 and still met the design requirements.

4. Phase IV

The Phase IV testing and analysis of high-strength S994 glass filaments and high-modulus YM31A glass filaments indicated that

a. The YM31A is currently too brittle to be handled and processed for use as a filament-winding material.

b. The tensile strength of the vendor's production-run S994 glass filaments was at least 10% below that of his experimental-run X994 filaments.

c. The tensile properties of glass filament are much more accurately evaluated by the fabrication and testing of a filament-wound pressure vessel than by the strand-test method.

5. Phase V

a. The Serial No. 3, 44.3-in. chamber fabricated from S994 glass filament demonstrated weight improvements of 47.4 lb as compared with the Serial No. 2 "E" glass filament chamber, and 78.8 lb as compared with the

existing second-stage, titanium, Minuteman chamber while still meeting the design requirements imposed on the previous glass chamber.

b. This chamber successfully demonstrated the adaptability of the S994 system for use on large chambers under conditions of internal pressure only.

6. Phase VI

a. Structural loading tests performed on the Serial No. 4, 44.3-in. chamber apparently had negligible effects on the chamber, because (1) the chamber burst within 5% of the design burst pressure after four previous structural loads had been applied, and (2) the maximum strain-gage readings at any location during any load cycle were less than 800 microinches, indicating the presence of very low stress levels.

b. Values derived from test data for the compressive modulus of elasticity (E_c), compressive rigidity (E_cA), modulus of elasticity in bending (E_b), and flexural rigidity (E_bI) correlated well with those previously used for chamber-design calculations. The compressive modulus of elasticity of 3.22×10^6 psi was 5% higher than the theoretically calculated value of 3.07×10^6 psi. The measured compressive rigidity of 4.95×10^7 lb was also comparable to the previously assumed value of 4.62×10^7 lb. The modulus of elasticity in bending (not previously calculated) was determined to be 4.31×10^6 psi, and the flexural rigidity was calculated to be 1.62×10^{10} lb-sq in.

B. RECOMMENDATIONS

Development efforts directed toward the three major task areas outlined below are recommended on the basis of the essential first step provided by this program in the selection of optimum designs with specific envelope and design parameters.

1. Subscale Pressure Vessels

Work is recommended in the following areas:

a. Cut-filament center-port designs for balanced-in-plane and geodesic-isotensoid chambers

b. Redundant-isotensoid chambers with and without cut-filament center ports

c. A statistically designed test program to support the data of Figures 42 and 43 at parameters that were not included in the Phase II model-chamber test program

d. A statistically designed test program on identical chambers for study and evaluation of the effect of pressurization rate on filament-wound pressure vessels

e. A test program on identical chambers for study and evaluation of the effect of stress repetition on filament-wound pressure vessels

f. A program to determine the optimum rate of strain application in compressive-loading tests for the accurate determination of moduli of elasticity in compression and bending.

2. Materials Development and Evaluation

The following work is recommended in the field of materials:

a. A program for the development of a high-modulus, high-tensile-strength material with improved handling and processing properties

b. A study program to develop improved laboratory-test methods for glass-filament, tensile-strength determinations

c. A resin-impregnation-method study to improve the relationship between the wetting of the filaments and the degree of ribbonization obtained.

3. Full-Scale Chambers

Data obtained from the testing of 44.3-in. chambers indicate the need for a greater number of specimens of the same design so that a proper evaluation can be made. It is recommended that additional units of this design be fabricated and tested to confirm the data obtained under various loading conditions, particularly in axial compression and bending.

The comparisons presented in Table 21 and Figure 87 are based on second-stage Minuteman cases containing four nozzle ports. The filament-wound chamber-design concept used to meet these porting requirements necessitates the insertion of a reinforcement in the aft head and the cutting of the basic filament structure at the ports. Some reduction in the efficiency of a filament-wound structure results from this discontinuity of the basic filaments.

The present indications are, however, that the future porting of rocket-motor cases will be tailored to single-nozzle designs. As a consequence, unequal-boss designs (particularly those in which the nozzle-boss-diameter to case-diameter ratio is 40 to 80% and the igniter-boss ratio is 20% or less) will dominate future configurations.

Any design incorporating this single-nozzle-port concept would eliminate the loss in efficiency in the filament-wound composite, and would yield a lighter-weight, higher-performance chamber.

It is therefore strongly recommended that a program be initiated to determine the actual efficiency improvement as compared with the existing S994 four-nozzle-port design. Such a program would not only provide data specifically for the second-stage Minuteman but would also provide good scaling data for large-solid-rocket programs (120-in., 260-in., etc.).

GLOSSARY

Balanced-in-plane contour	A head contour in which the filaments are oriented within a plane and the radii of curvature are adjusted to balance the stresses along the filaments with the pressure loading.
End	A strand of roving consisting of a given number of filaments gathered together. The group of filaments is considered an end or strand before twisting, and a yarn after the twist is applied (see Ref. 7).
Fiber (filament)	An individual filament made by attenuating molten glass. A continuous filament is a glass fiber of great or indefinite length. A staple fiber is a relatively short glass fiber (generally less than 17 in.) (see Ref. 8).
Finish	Any after-treatment performed on fibrous-glass products prior to their end use (see Ref. 9).
Fuzz	A measure of broken filaments in a strand or roving (see Ref. 7).
Geodesic-isotensoid contour	A head contour in which the filaments are placed on geodesic paths (the shortest distance between any two points on a curved surface) so that the filaments will exhibit uniform tensions throughout their length under pressure loading.
Lot	A specific amount of glass roving produced at one time and offered for sale as a unit quantity (see Ref. 7).
Prepreg roving	Roving containing a specified quantity of resin in a partially cured condition.
Ribbonization	Describes the degree of bonding together of the strands of roving that make up the roving band (see Ref. 7).
Roving	Groups of continuous-filament strands in a cylindrically wound package (see Ref. 9).
Size (sizing)	Any coating applied to fibers in the forming operation (see Ref. 8).
Strand	The continuous bundle of continuous filaments gathered together in the forming operation (see Ref. 9).
D_b	Boss diameter, in.
D_c	Chamber diameter, in.
E	Modulus of elasticity, psi
E_f	Modulus of elasticity of filaments, psi

E_m	Modulus of elasticity of mandrel, psi
I	Area moment of inertia, $in.^4$
K	Shape factor
L	Chamber length, in.
N_Θ	Circumferential force per unit of width, lb/in.
$N_{\Theta,f}$	Circumferential force in filament per unit of width, lb/in.
N_ϕ	Meridional force per unit of width, lb/in.
$N_{\phi,f}$	Meridional force in filament per unit of width, lb/in.
p	Chamber pressure, psi
r_1	Meridional radius of curvature, in.
r_2	Circumferential radius of curvature, in.
T_1	Winding tension of first layer, lb
T_q	Winding tension of specific layer, lb
t_f	Equivalent thickness of filament layer, in.
t_m	Mandrel-wall thickness, in.
V	Internal volume of chamber, cu in.
W	Weight of chamber composite, lb
α	Angle between meridian and filament, degrees
Θ	Angle between meridional plane and a reference axial plane, degrees
ρ	Density of chamber composite, lb/cu in.
σ	Stress, psi
σ_f	Filament stress, psi
ϕ	Angle between meridional radius of curvature and vertical axis, degrees

REFERENCES

1. R. J. Roark, Formulas for Stress and Strain, New York, McGraw-Hill, 1954, p. 269.

2. L. L. Smail, Analytical Geometry and Calculus, New York, Appleton-Century-Crofts, 1954, p. 361.

3. The Geodesic Line in Filament Winding, Aerojet-General Solid Rocket Plant Technical Memorandum 171, 14 December 1961.

4. J. P. McNally, Final Report - Development of Materials and Process Specifications, Phase II, Increment VI, Aerojet-General Report 327-R62-62, 24 August 1962, p. 4.

5. M. Segimoto, Final Report - Prepreg Evaluation, Phase III, Increment VI, Aerojet-General Report 327-R62-71, 18 September 1962, p. 1.

6. Engineering Properties of High Modulus Reinforced Plastics, ASD-TDR-62-65, May 1962, Table 7.

7. Glossary of Terms for Filament Winding, Aerospace Division, Owens-Corning Fiberglas Corporation.

8. E. B. Shand, Glass Engineering Handbook, New York, McGraw-Hill, 1958.

9. R. H. Sonneborn, Fiberglass Reinforced Plastics, New York, Reinhold, 1954.

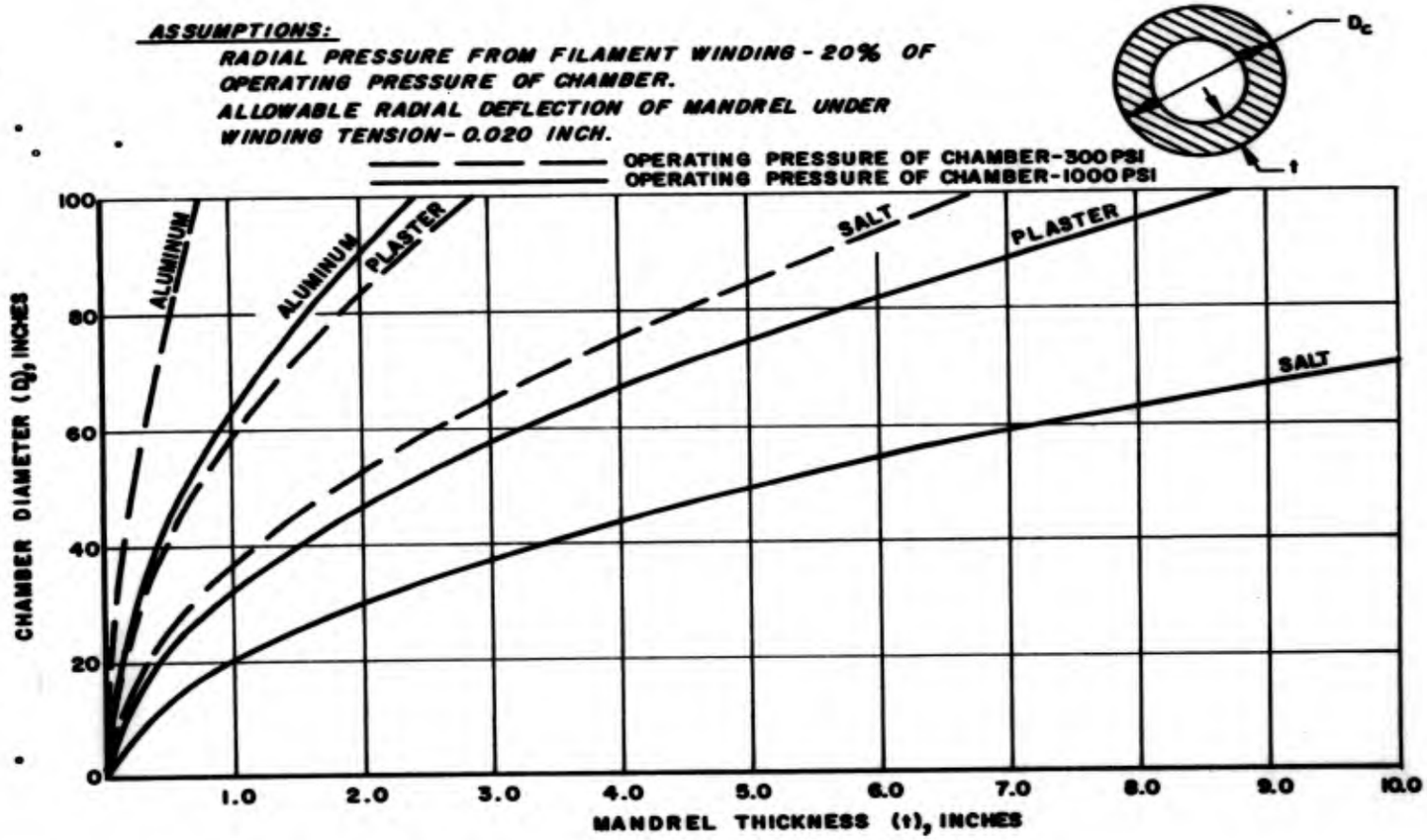

Figure 1. Diameter vs Thickness for Various Materials Used for Mandrels in Filament-Wound Cylinders

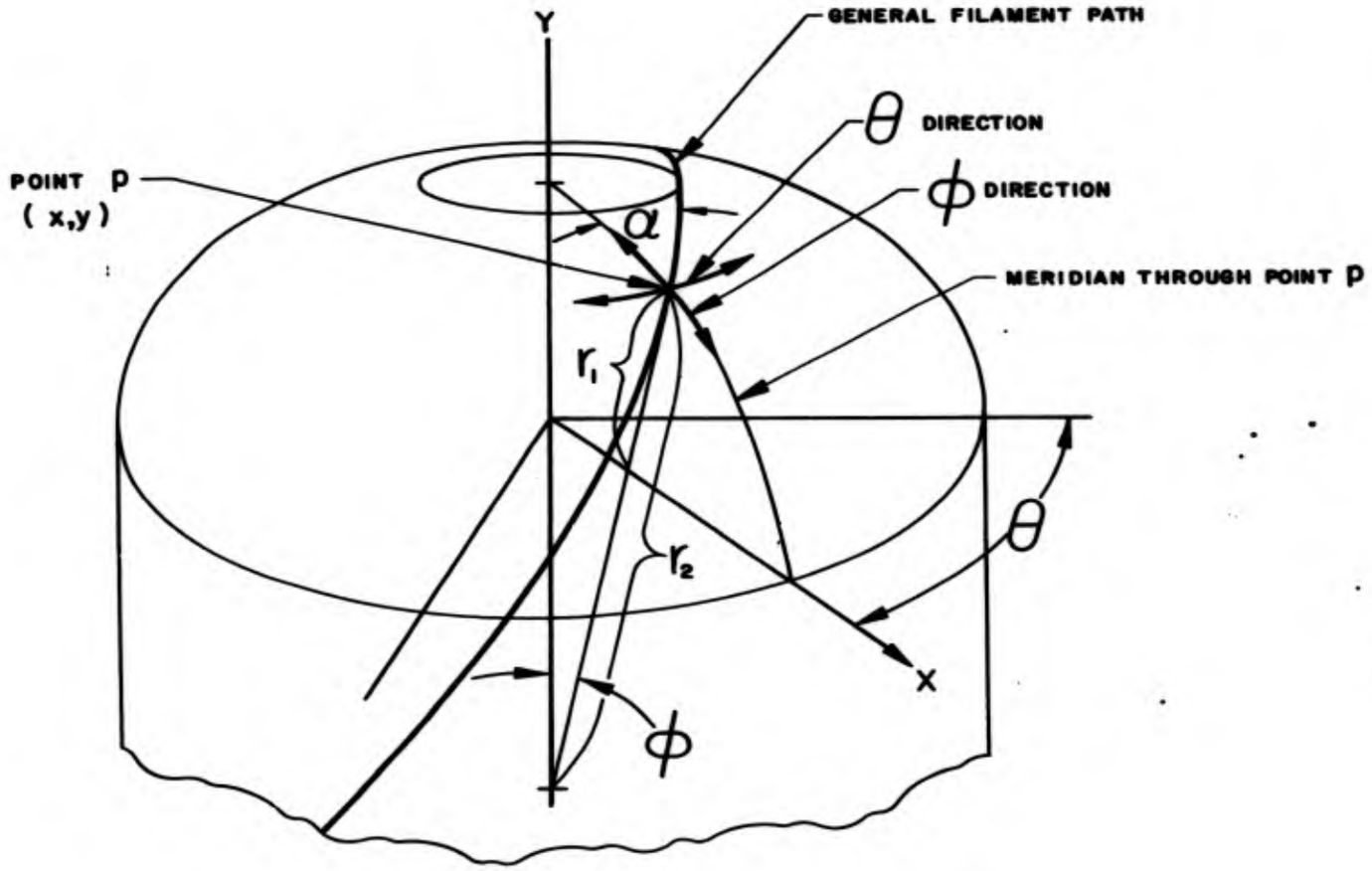

Figure 2. Geometry of General Winding Pattern

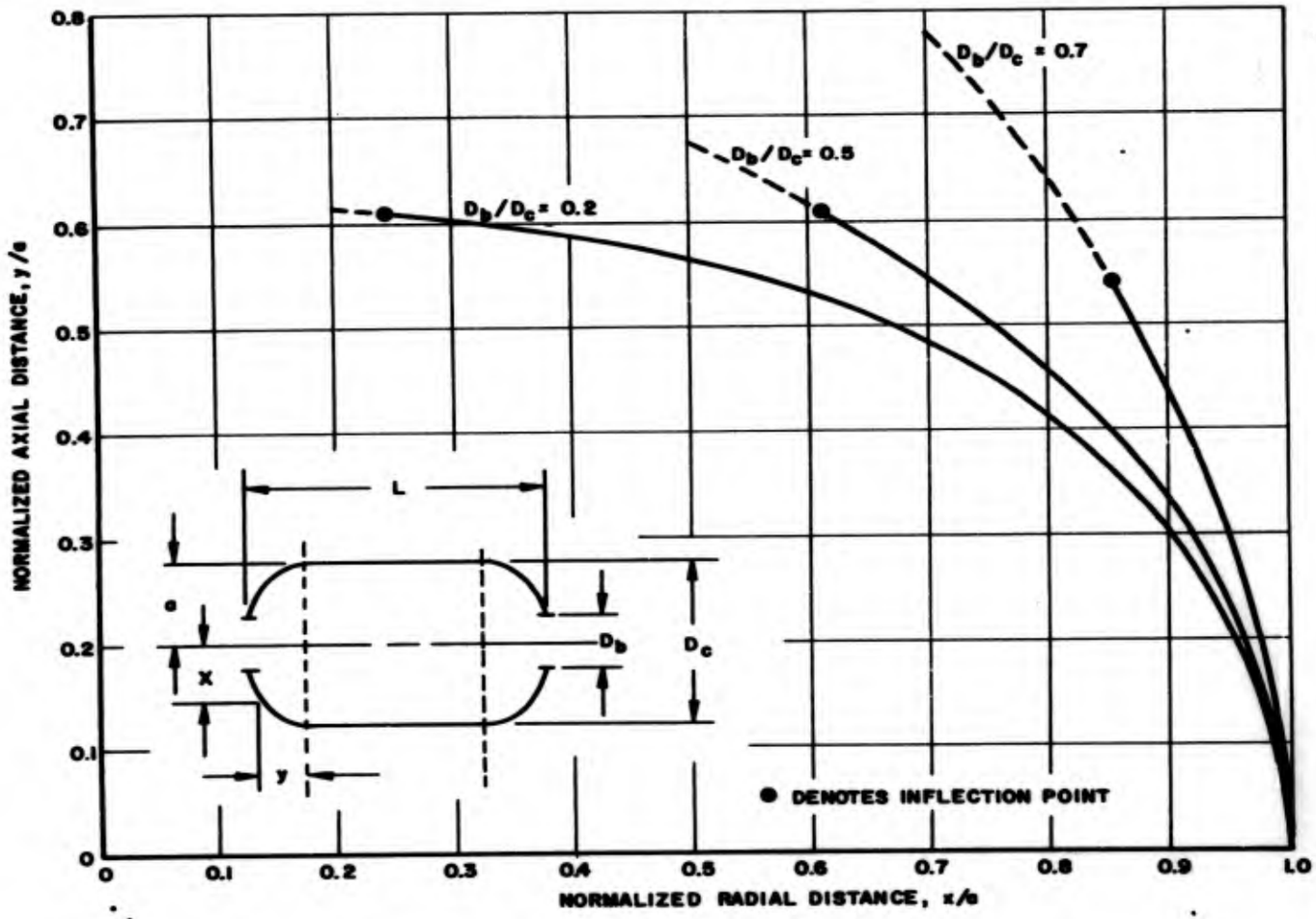

Figure 3. Geodesic-Isotensoid Head Contours, Filament-Wound Chambers

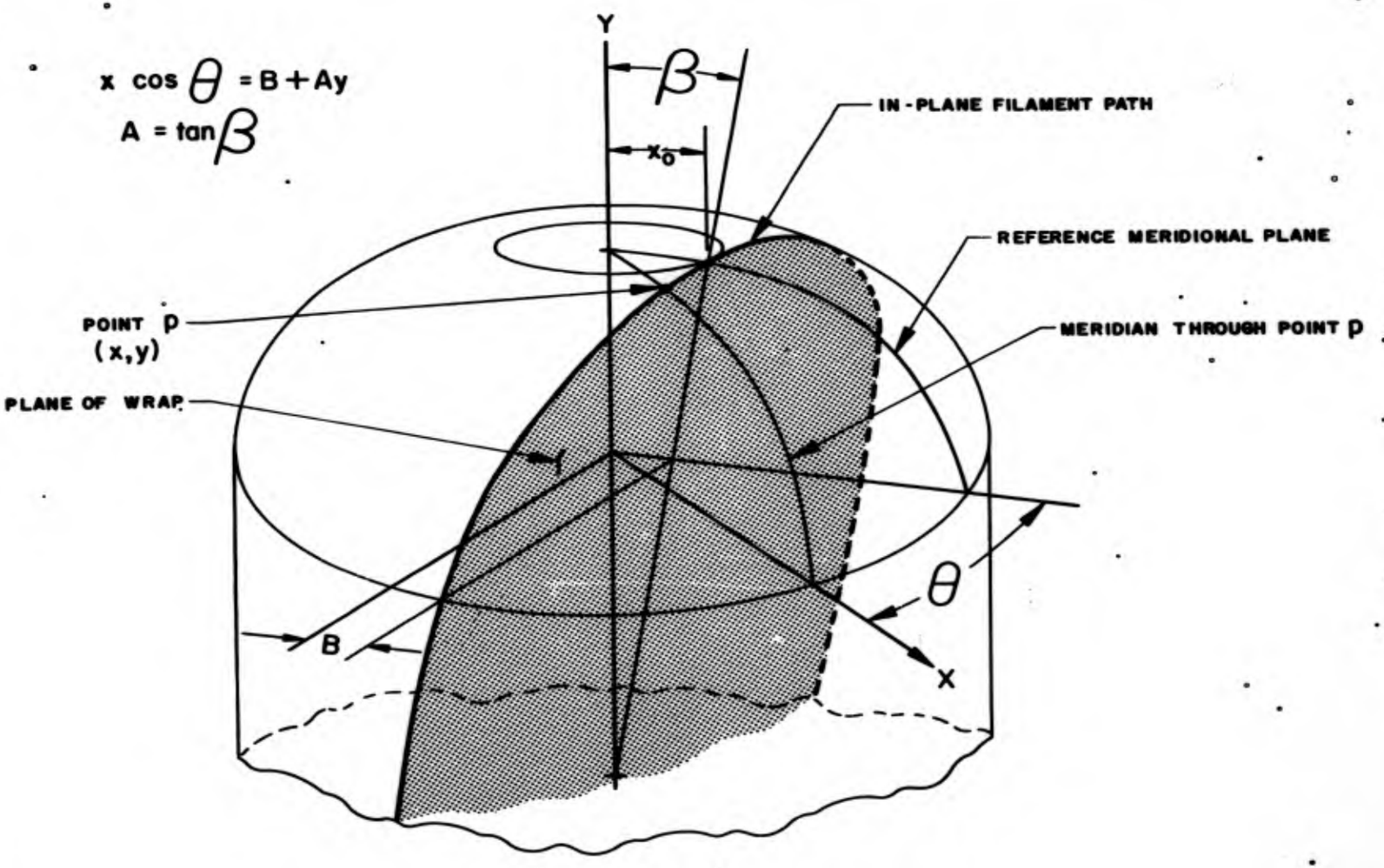

Figure 4. Geometry of In-Plane Winding Pattern

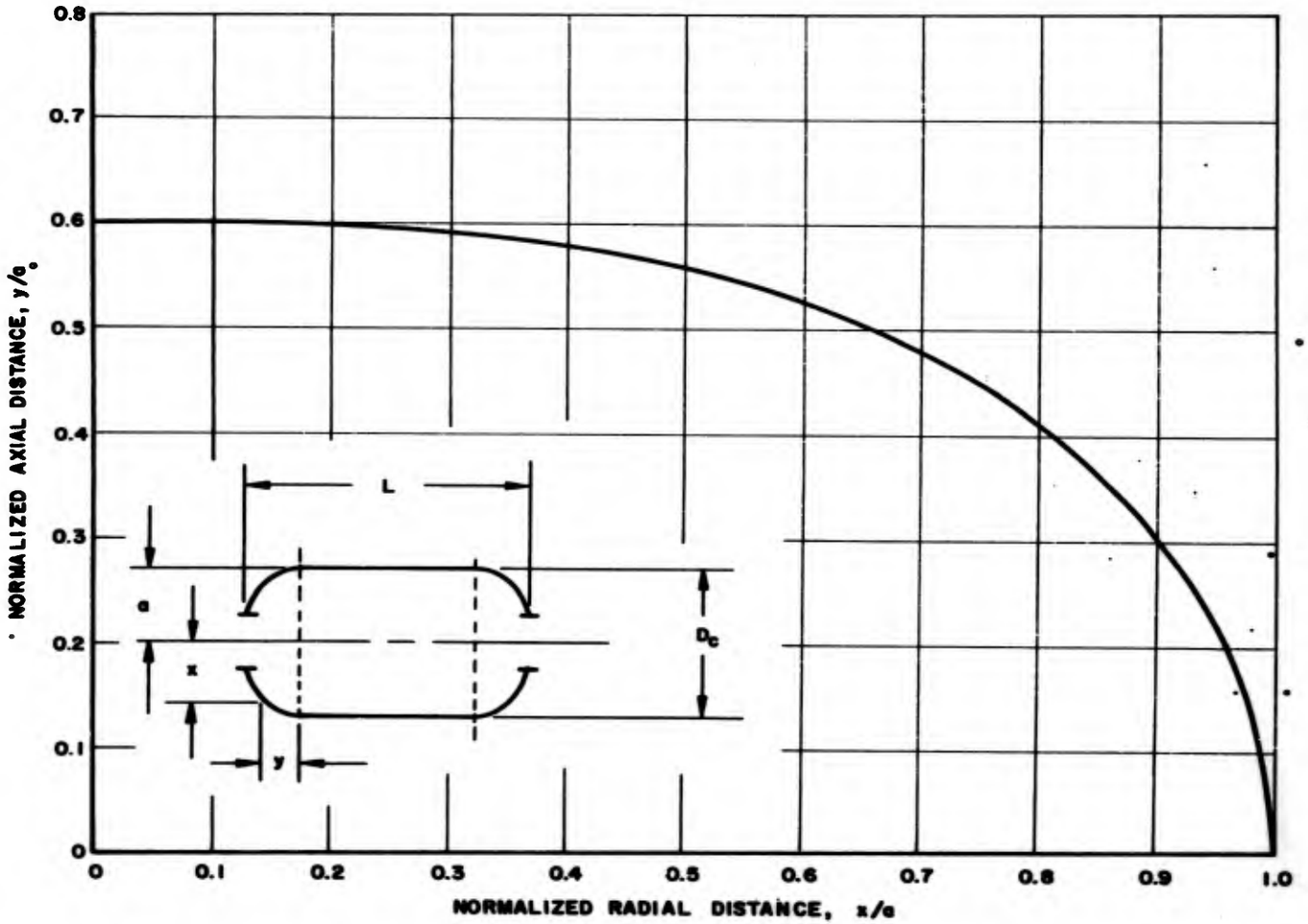

Figure 5. Zero-Hoop-Stress Head Contour for Filament-Wound Chambers

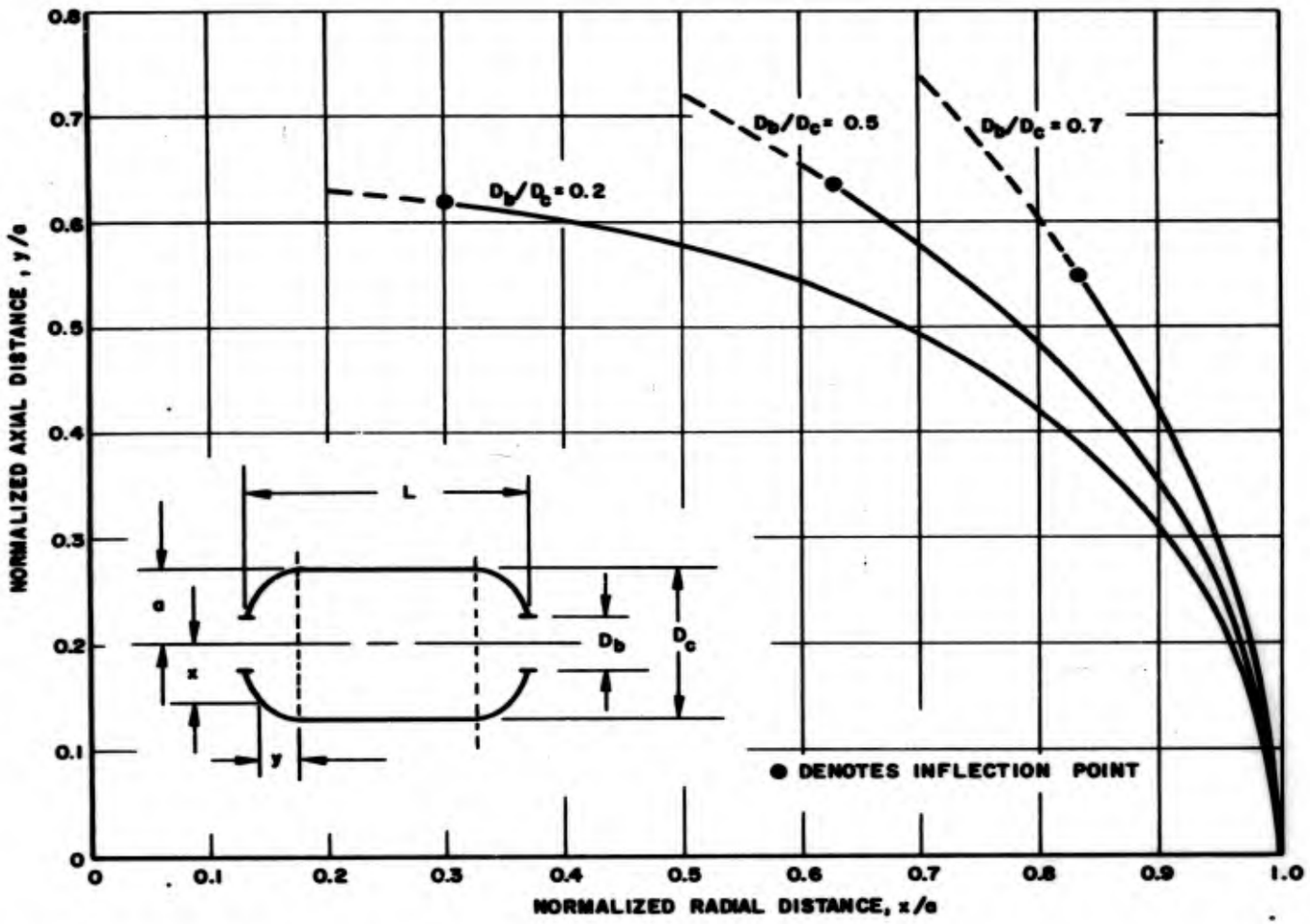

Figure 6. Balanced-in-Plane-Wrap Head Contours for Filament-Wound Chambers, Back-to-Back Heads

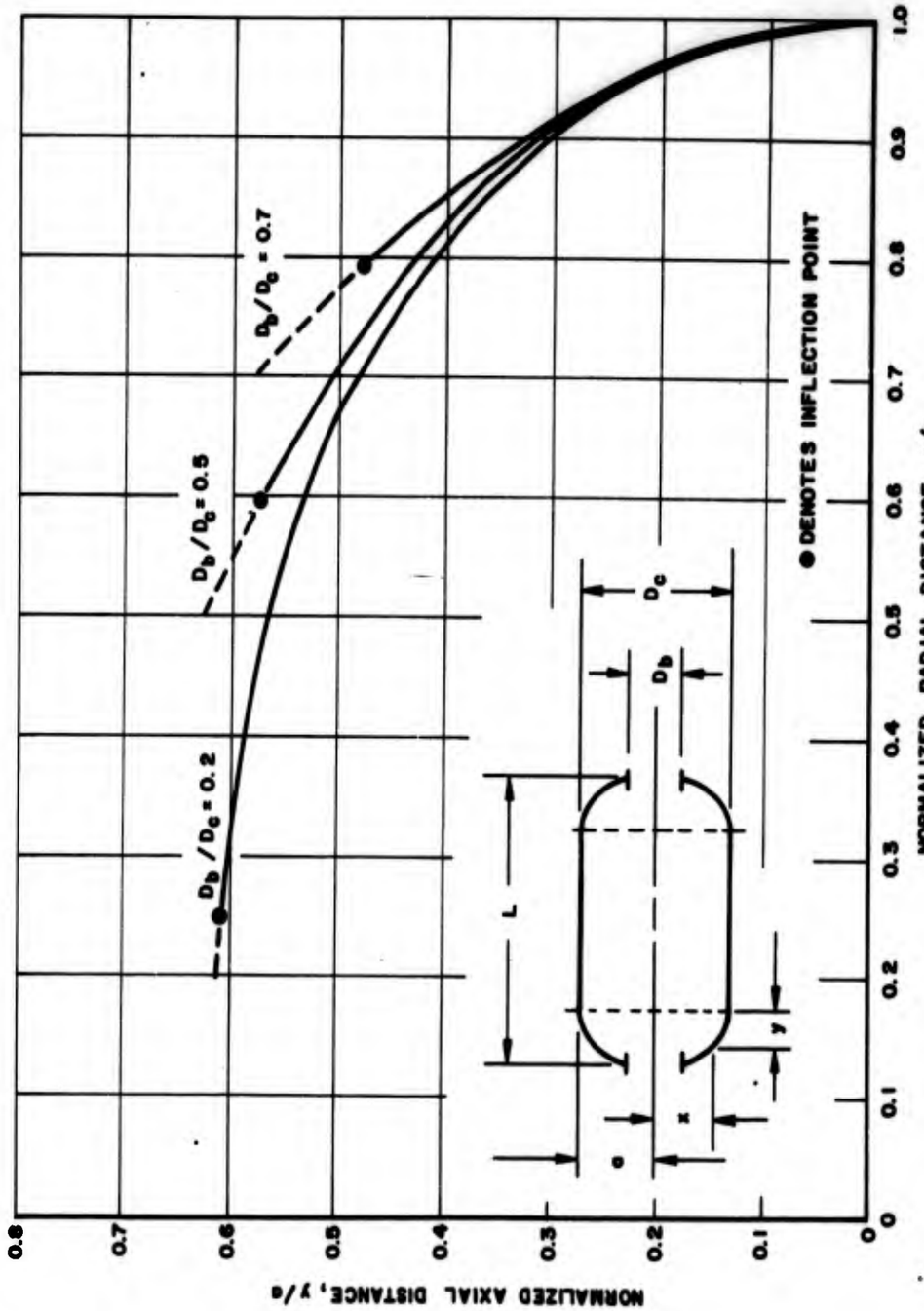

Figure 7. Balanced-in-Plane-Wrap Head Contours for Filament-Wound Chambers, $L/D_c = 2$

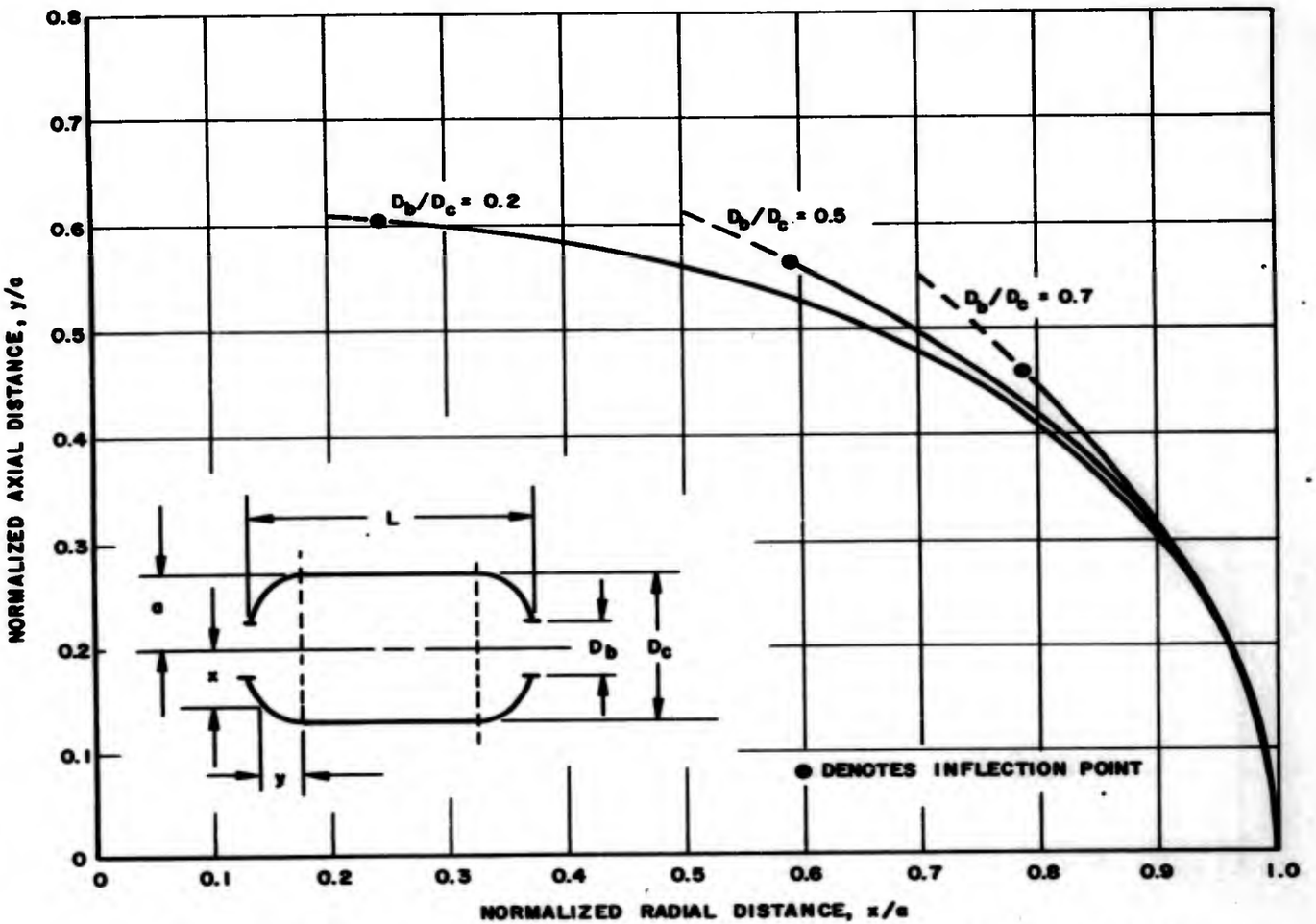

Figure 8. Balanced-in-Plane-Wrap Head Contours for Filament-Wound Chambers, $L/D_c = 4$

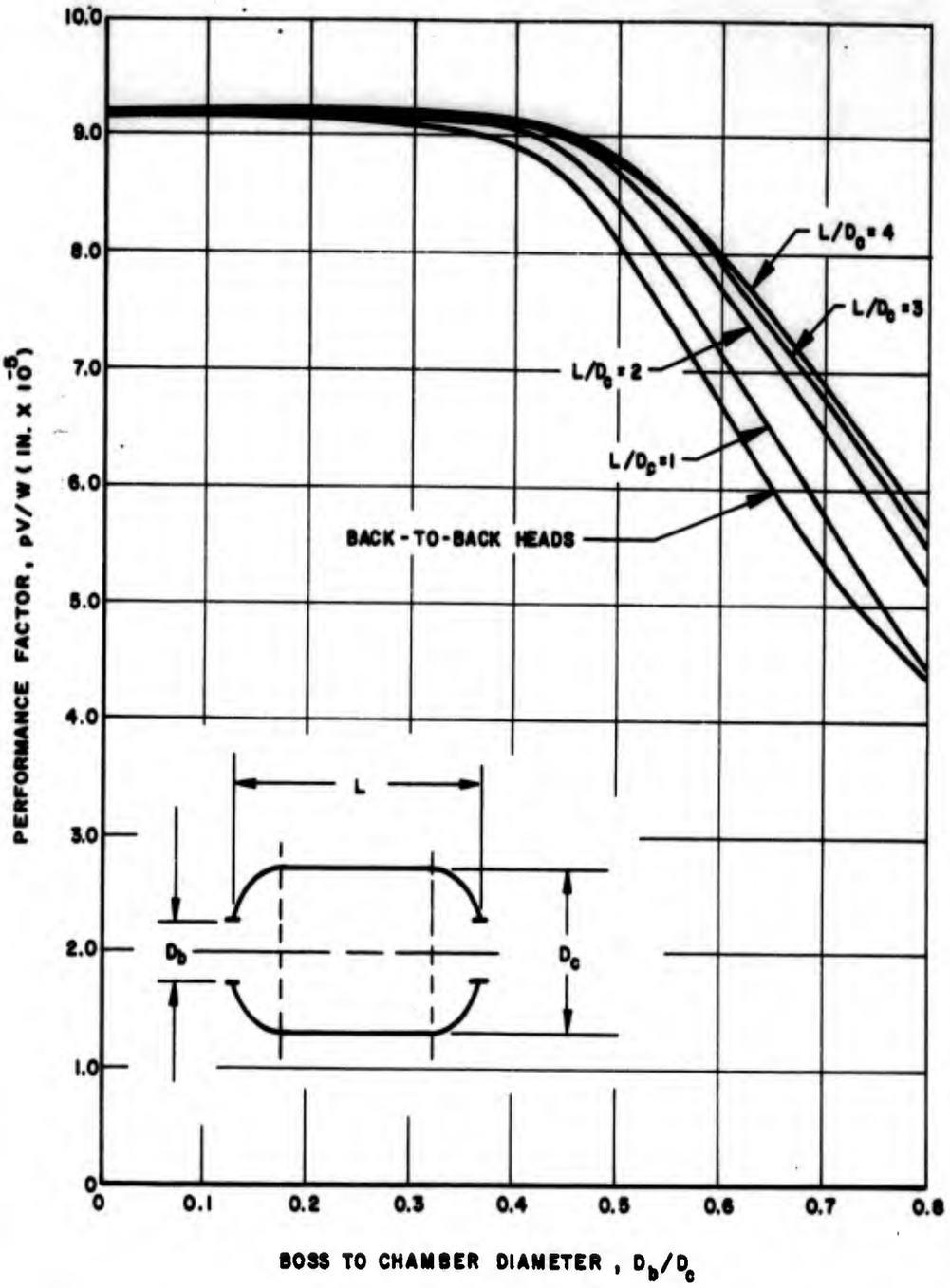

Figure 9. Theoretical Performance Factor vs Dimensional Parameters, Geodesic-Isotensoid Contour

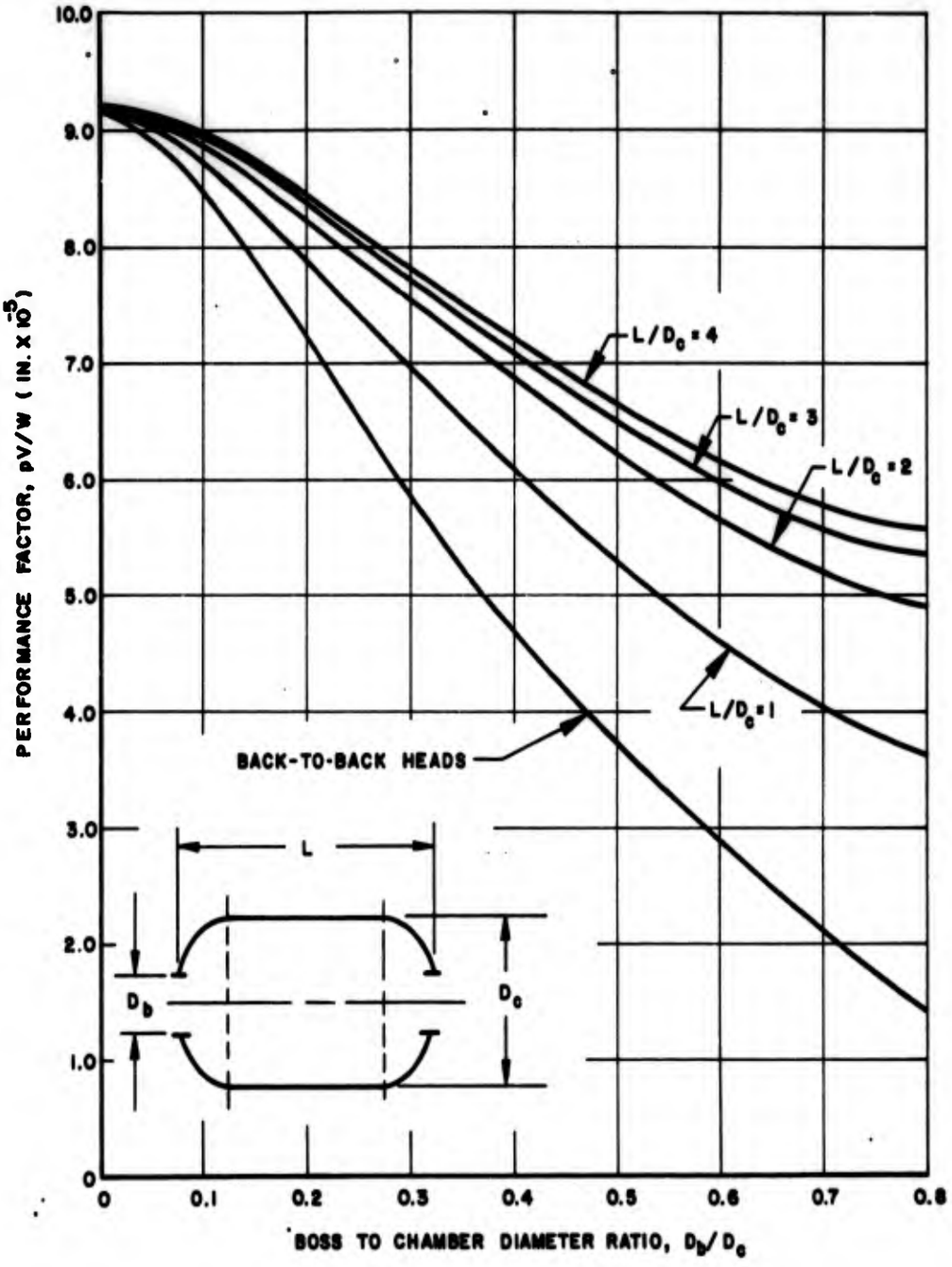

Figure 10. Theoretical Performance Factor vs Dimensional Parameters, Zero-Hoop-Stress Contour

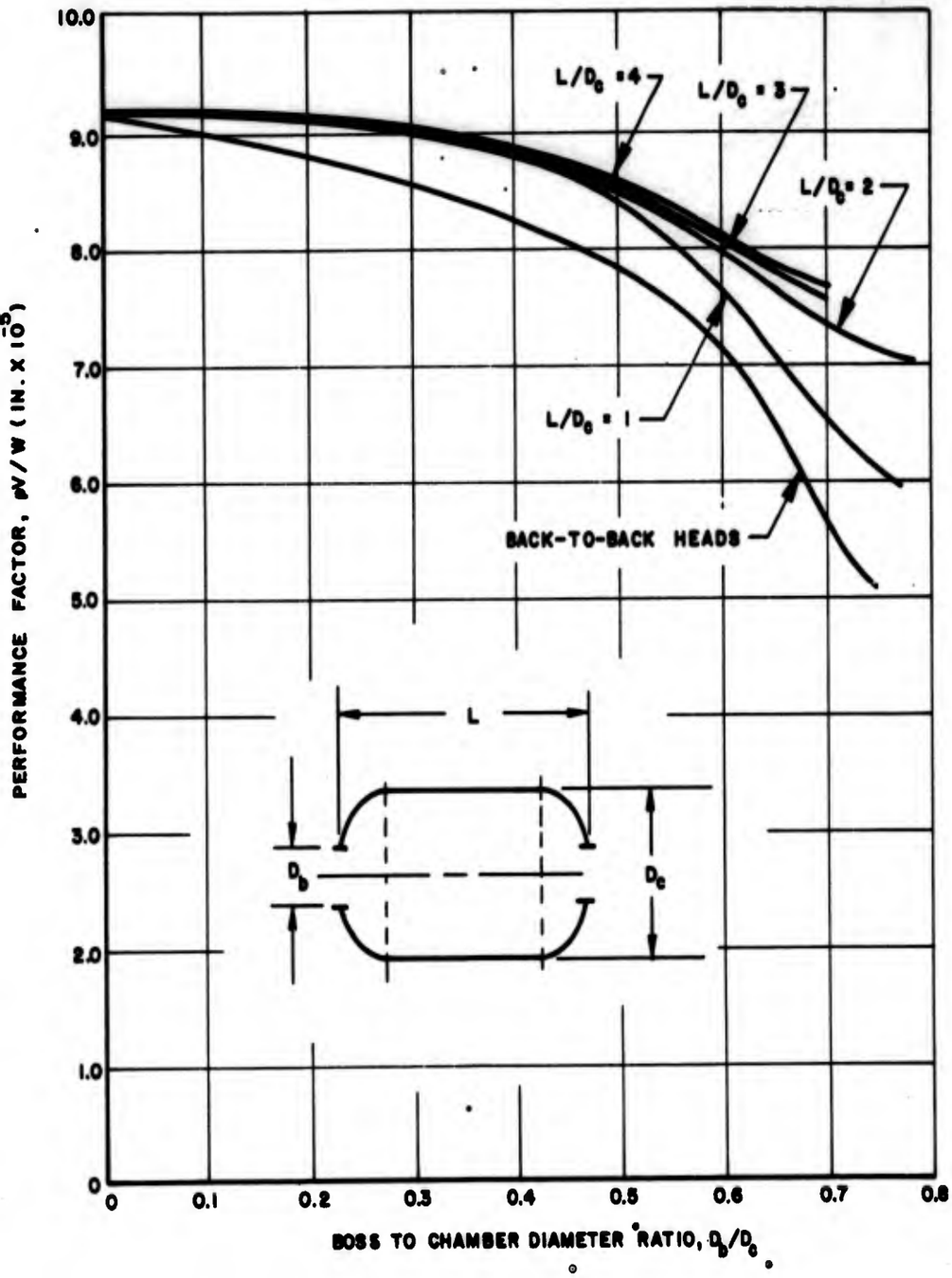

Figure 11. Theoretical Performance Factor vs Dimensional Parameters, Balanced-in-Plane-Wrap Contour.

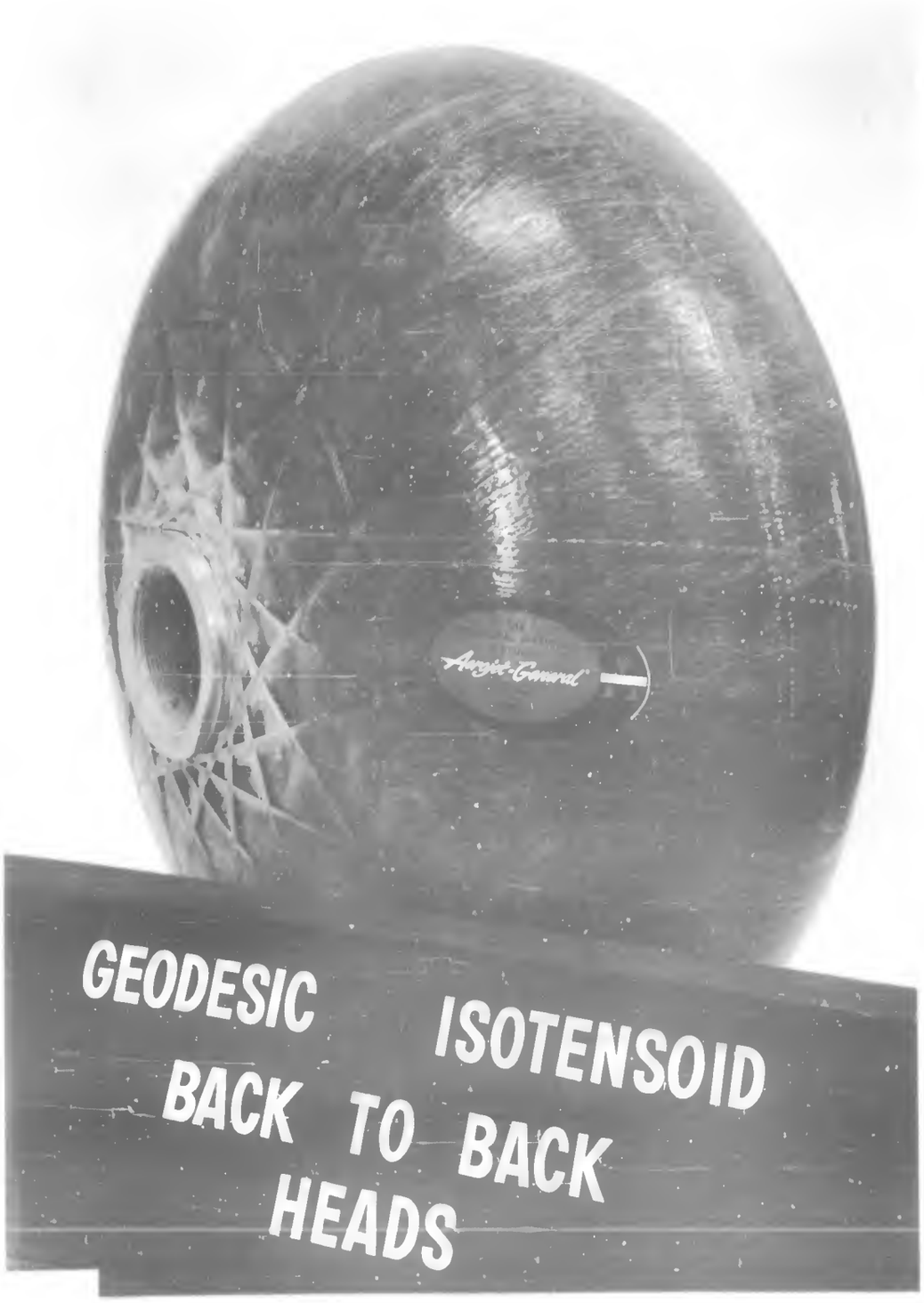

Figure 12. Chamber 176435, Overall View

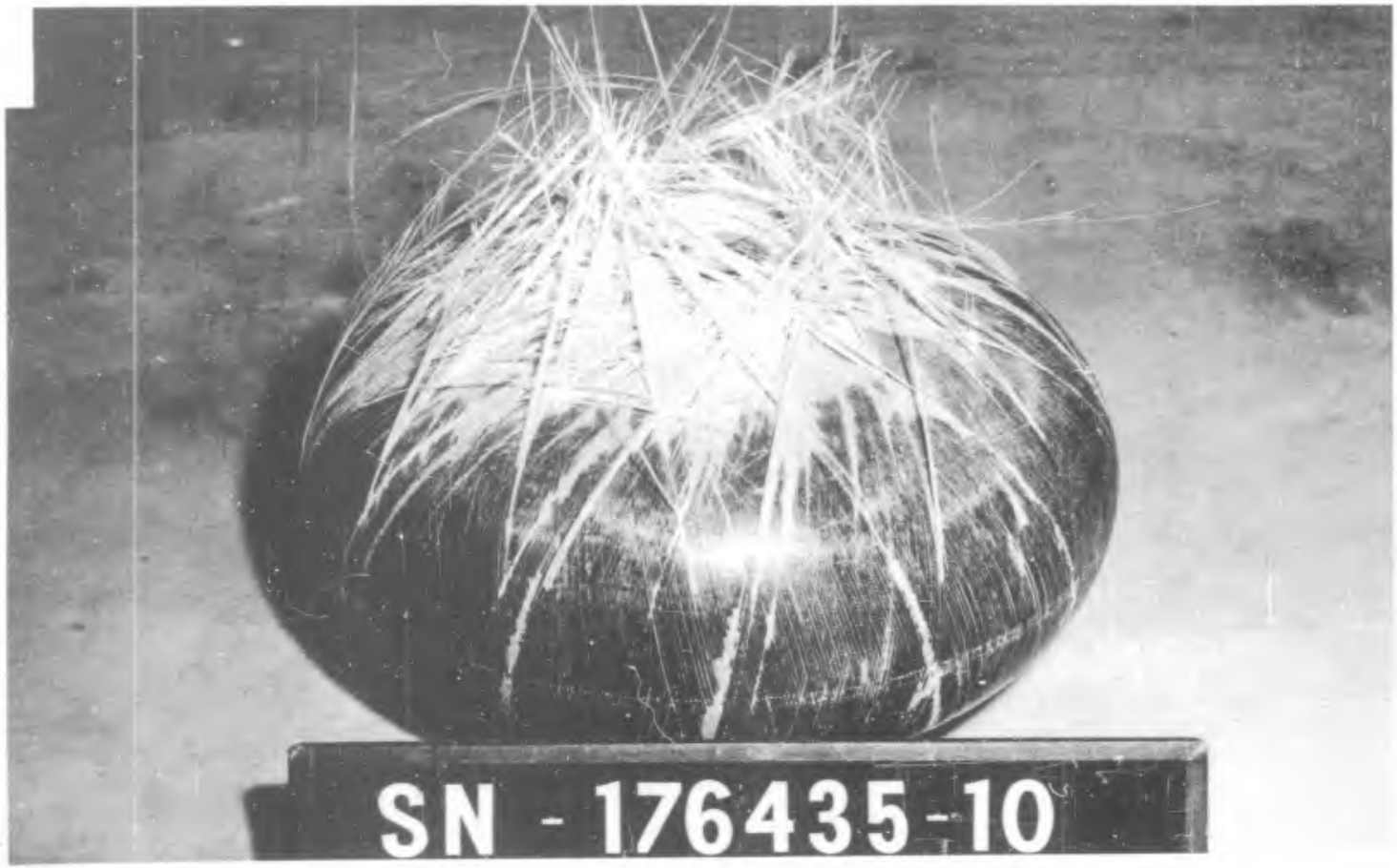

Figure 13. Chamber 176435, After Hydrotest

Figure 14. Back-to-Back Model Chamber, Mandrel Being Lined

Figure 15. Back-to-Back Model, Lined Mandrel After Cure

Figure 16. Back-to-Back Model, During Winding

Figure 17. Back-to-Back Model, After Cure

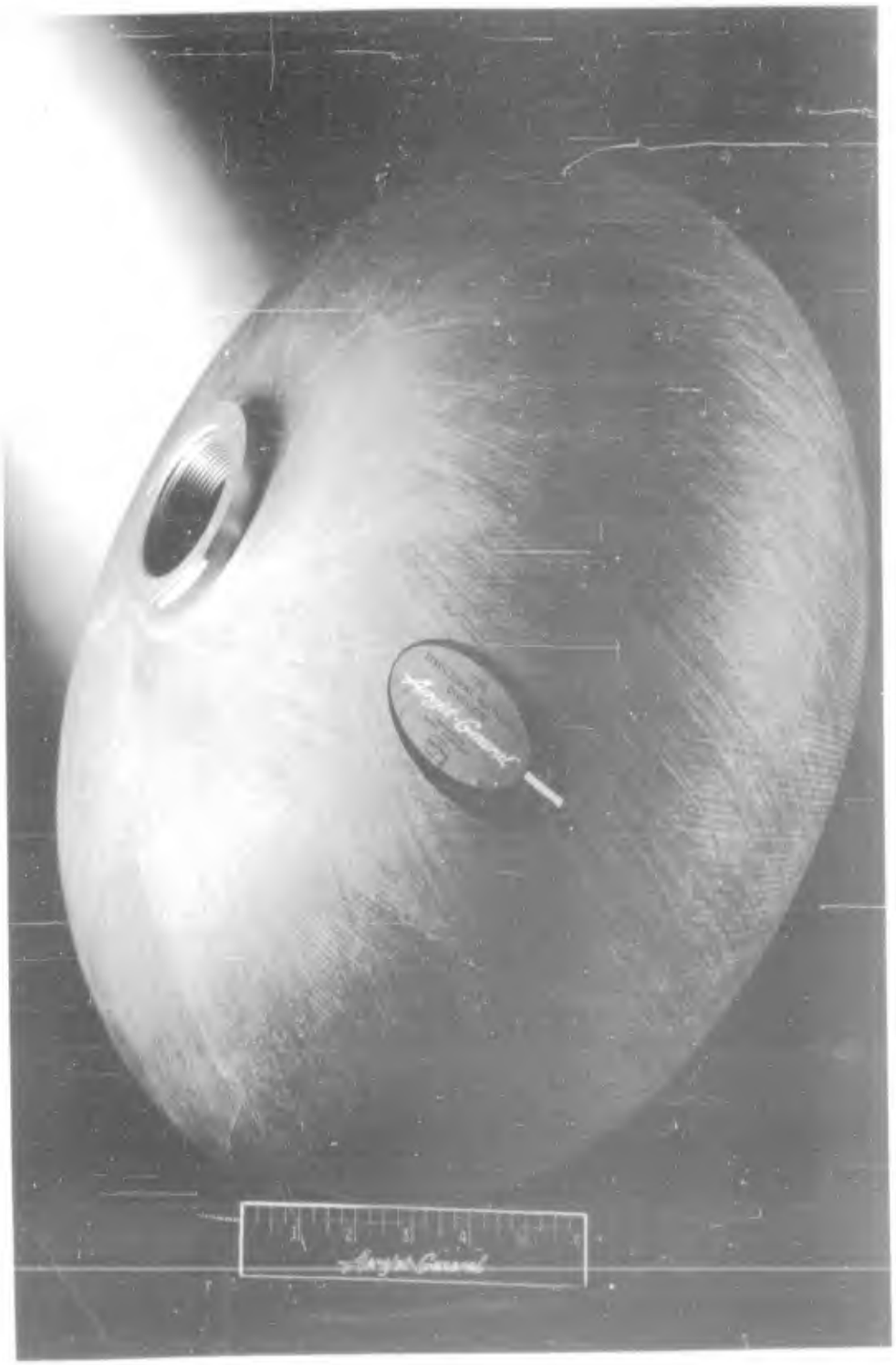

Figure 18. Back-to-Back Model, Finished Chamber

Figure 19. Chamber 176436, After Hydrotest

Figure 20. Chamber 176437, Overall View

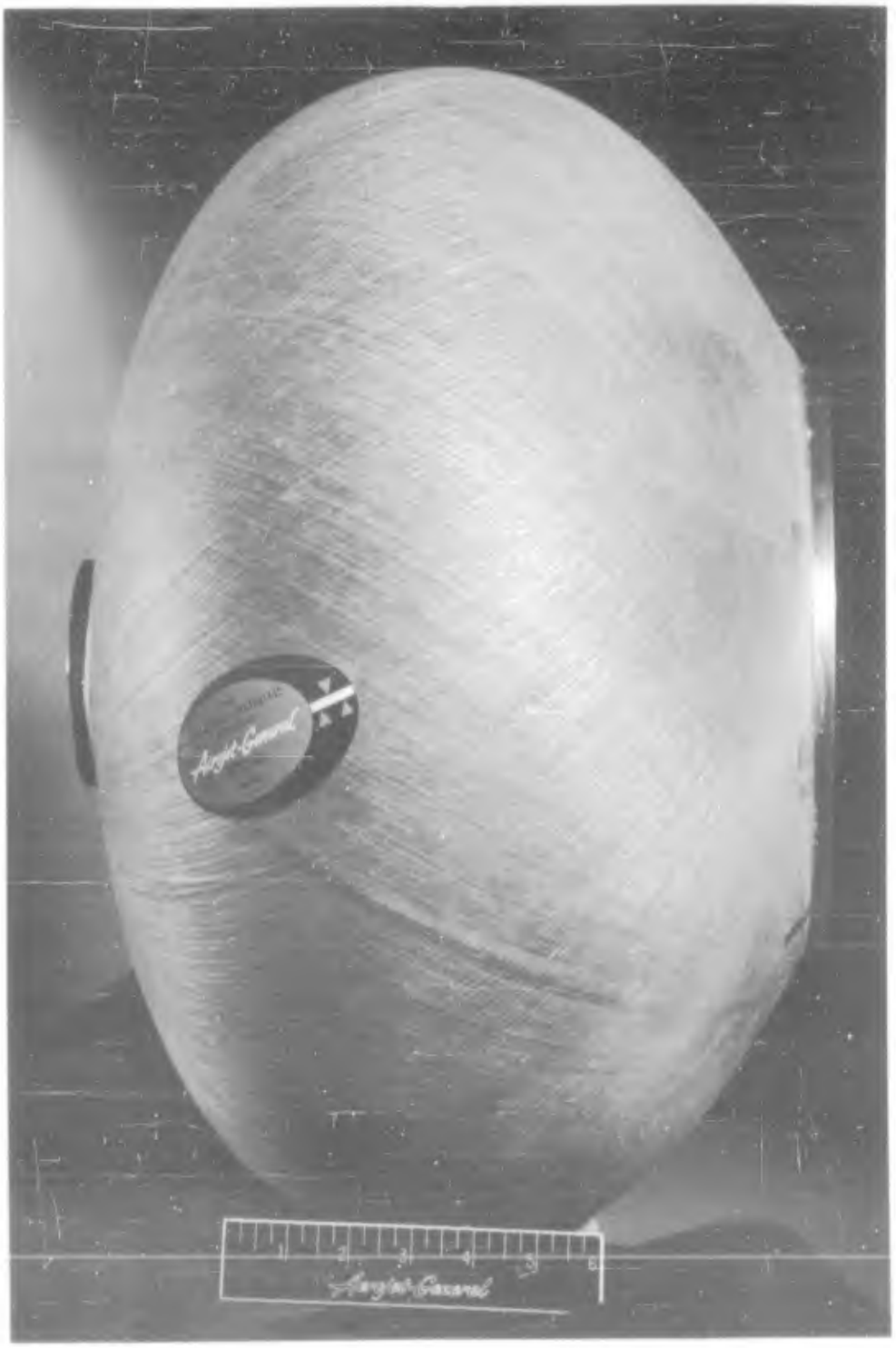

Figure 21. Chamber 176438, Side View

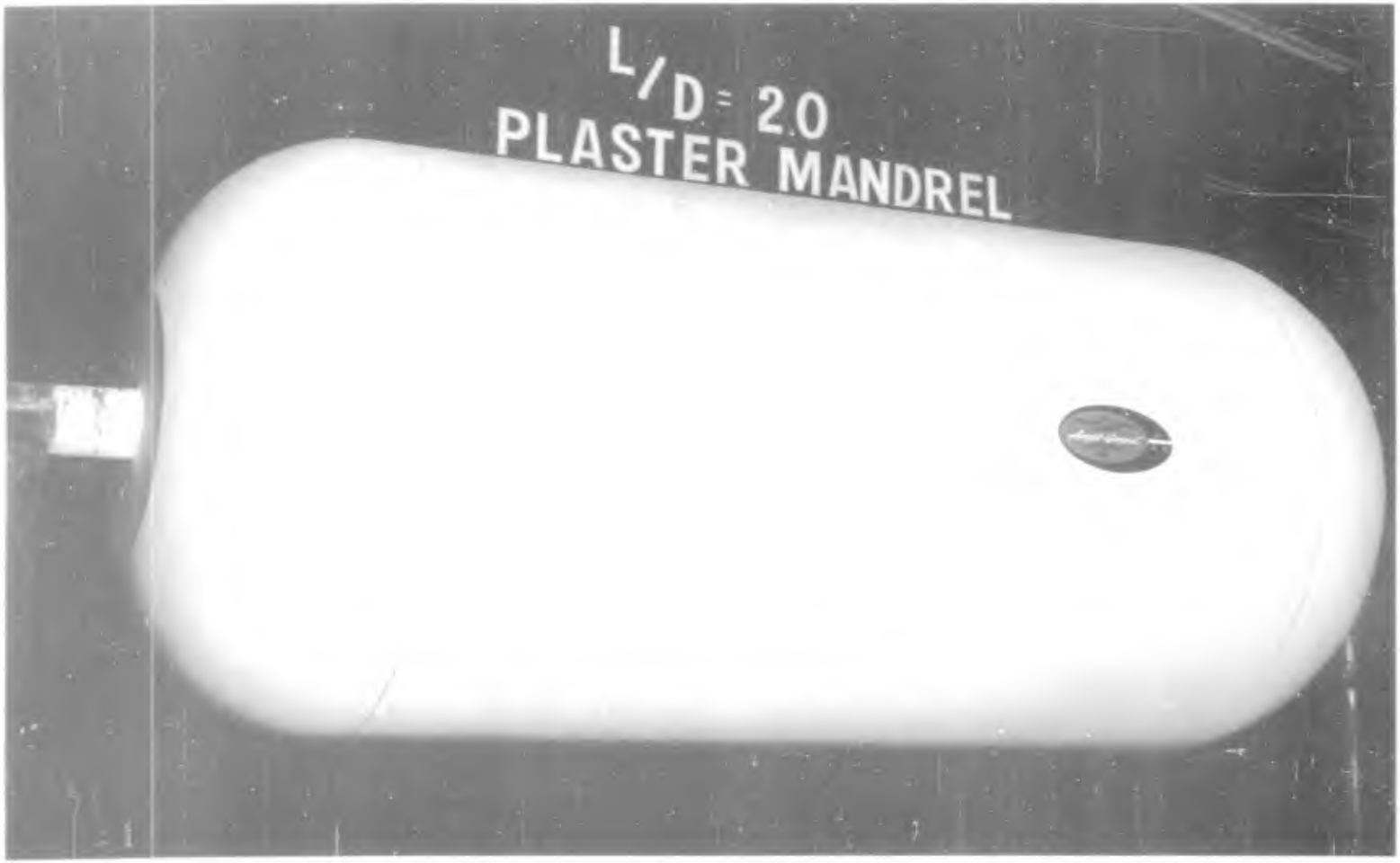

Figure 22. Plaster Mandrel for Model Chamber, $L/D_c = 2$

Figure 23. Lined Mandrel for Model Chamber, $L/D_c = 2$

Figure 24. Chamber 176439, Overall View

Figure 25. Chamber 176439, After Hydrotest

Figure 26. Chamber 176440, After Hydrotest

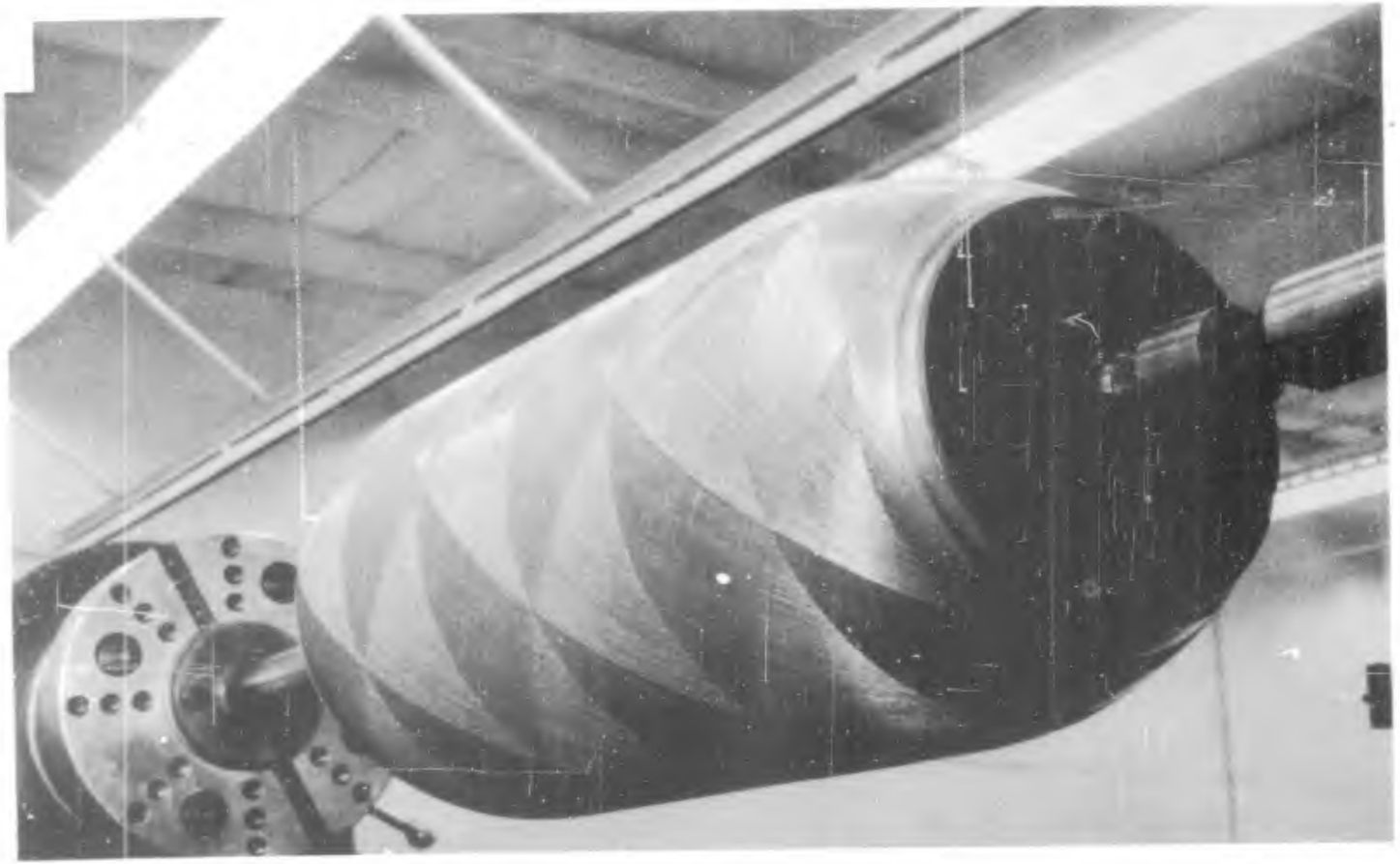

Figure 27. Chamber 176441, During Fabrication

Figure 28. Chamber 176441, Side View

Figure 29. Chamber 176441, After Hydrotest

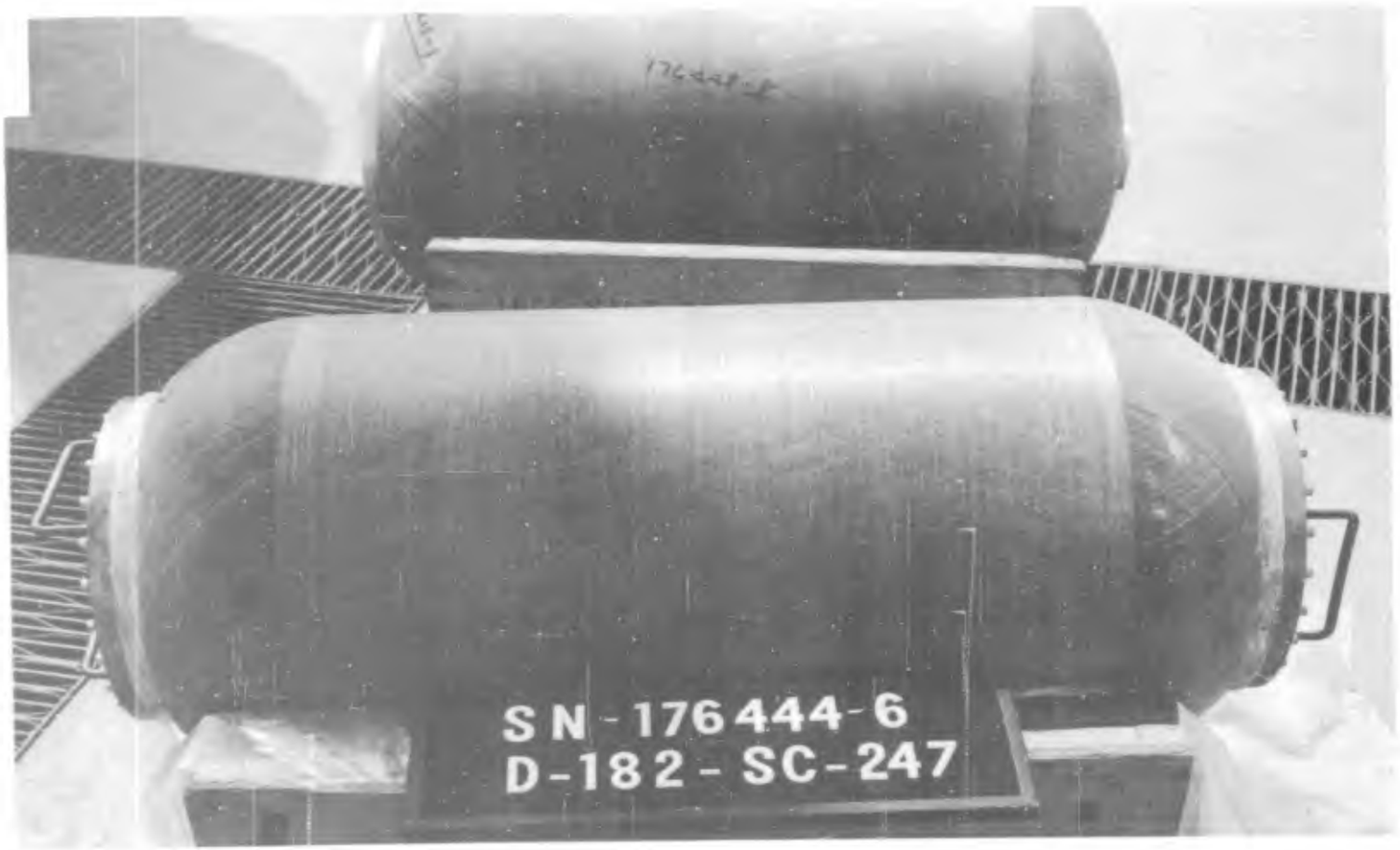

Figure 30. Chamber 176444, Prior to Hydrotest

Figure 31. Chamber 176444, After Hydroburst

Figure 32. Chamber 176445, Aft Head Prior to Cutting of Filaments

Figure 33. Chamber 176445, Aft Head After Cutting of Filaments

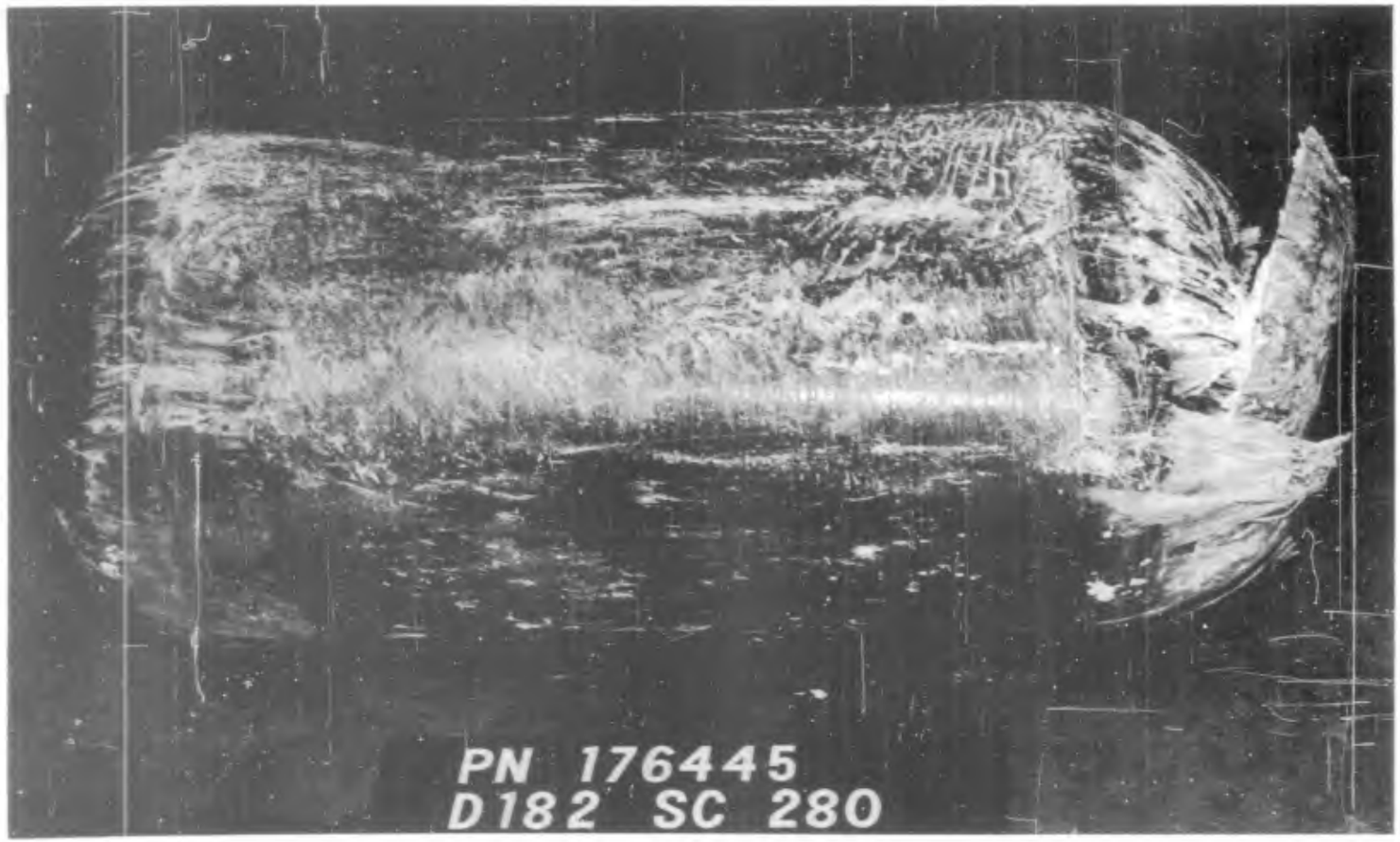

Figure 34. Chamber 176445, After Hydroburst

Figure 35. Chamber 176446, After Hydroburst

Figure 36. Chamber 176449, After Fabrication

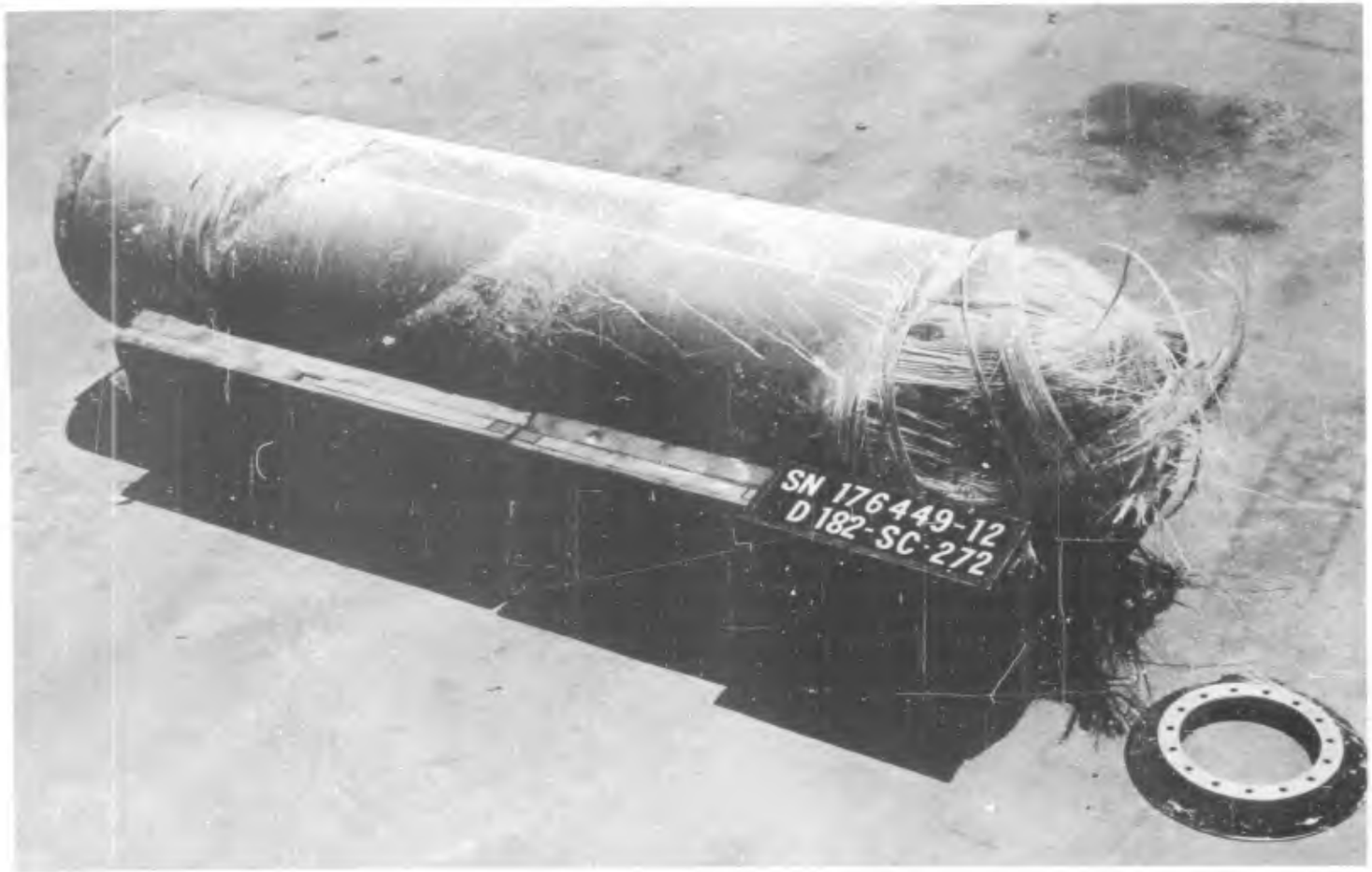

Figure 37. Chamber 176449, After Hydroburst

Figure 38. Chamber 176450, After Hydroburst

Figure 39. Chamber 176451, Overall View and Forward Head

Figure 40. Chamber 176451, After Hydroburst

Figure 41. Chamber 176452, After Hydroburst

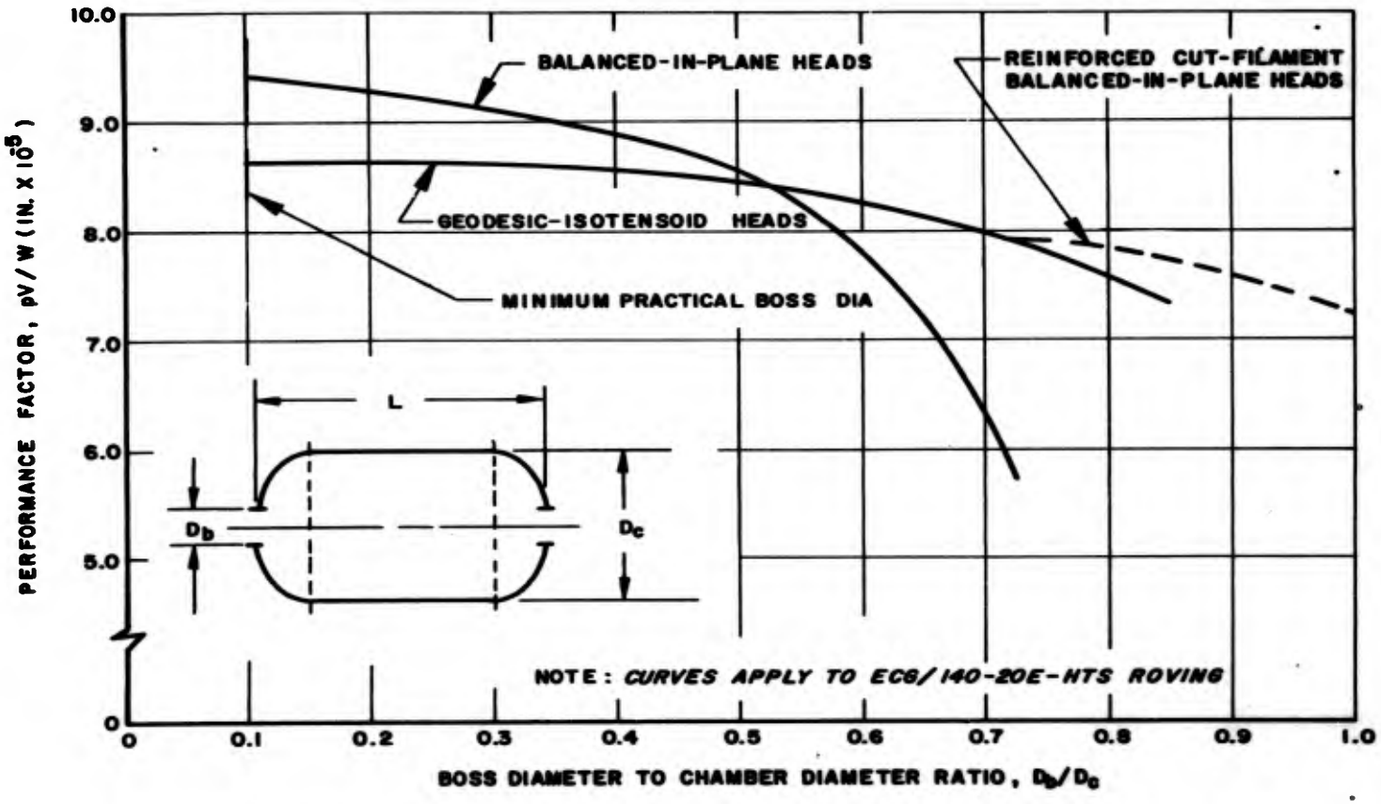

Figure 42. Actual Performance Factor vs Dimensional Parameters
Equal Boss Diameters Each End

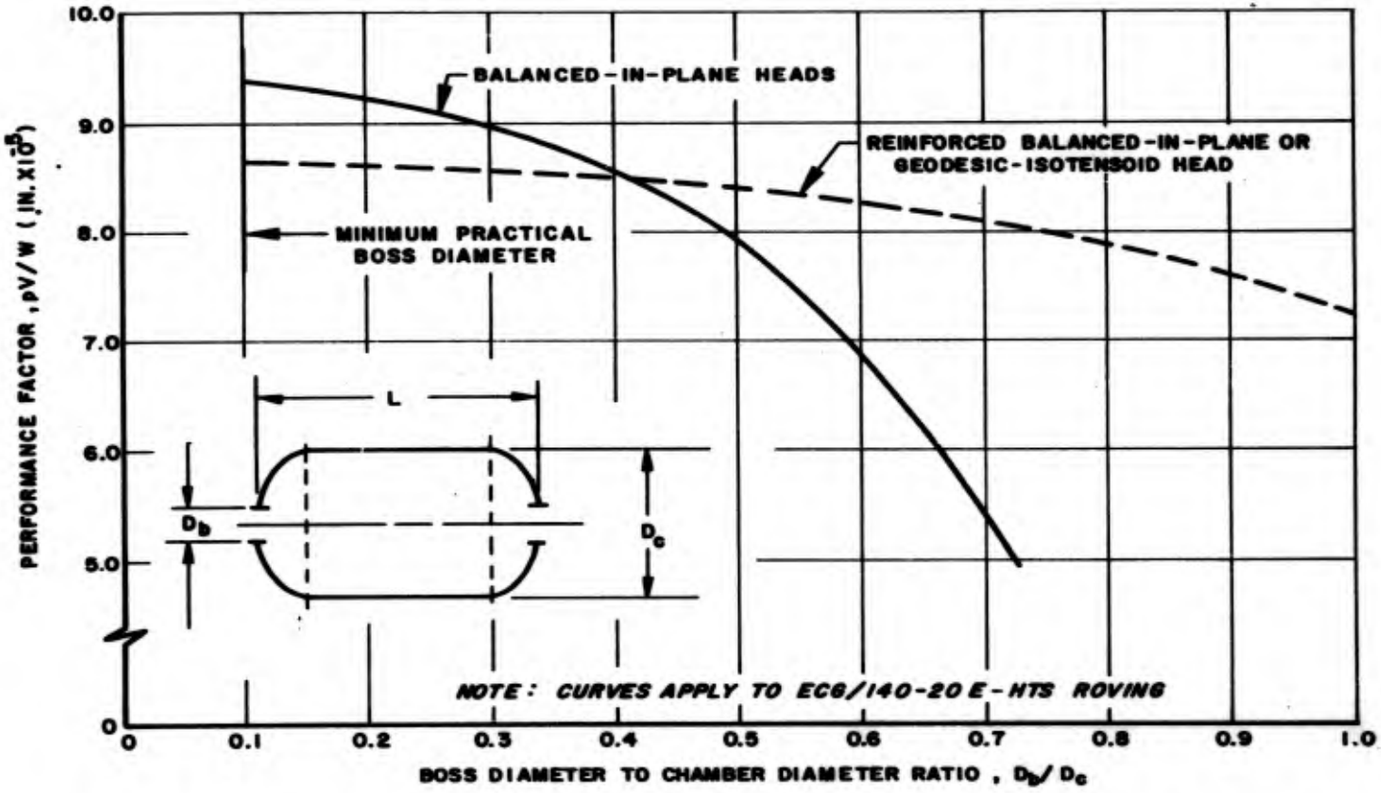

Figure 43. Actual Performance Factor vs Dimensional Parameters, D_b/D_c = 0.2 on One End

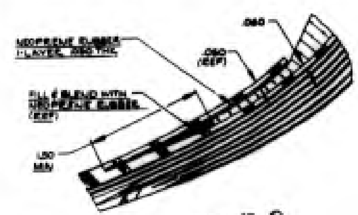

VIEW E

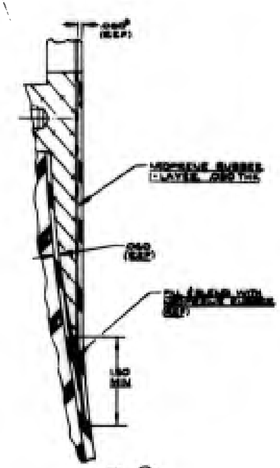

VIEW D

COORDINATES FWD & AFT OUTSIDE LINER	
X'_R	Y'
22.010	0
22.010	.270
22.005	.539
21.965	1.086
21.897	1.627
21.805	2.157
21.683	2.693
21.267	3.999
20.690	5.262
19.955	6.468
19.060	7.591
18.037	8.633
16.866	9.575
15.969	10.411
14.153	11.132
12.630	11.735
11.069	12.216
9.368	12.577
7.536	12.815
5.698	12.958

COORDINATES FWD LINER INNER	
X_L	Y
21.898	0
21.896	.268
21.885	.533
21.846	1.074
21.778	1.600
21.687	2.132
21.567	2.664
21.155	3.955
20.585	5.206
19.826	6.394
18.978	7.011
17.957	8.848
16.798	9.475
15.509	10.307
14.184	11.023
12.590	11.680
10.979	12.099
9.288	12.450
0	12.458

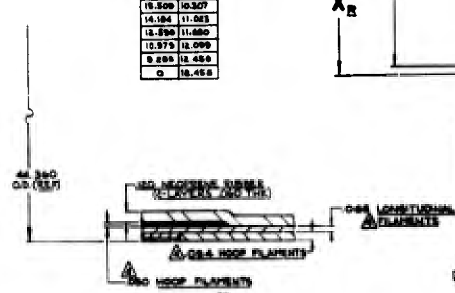

VIEW B

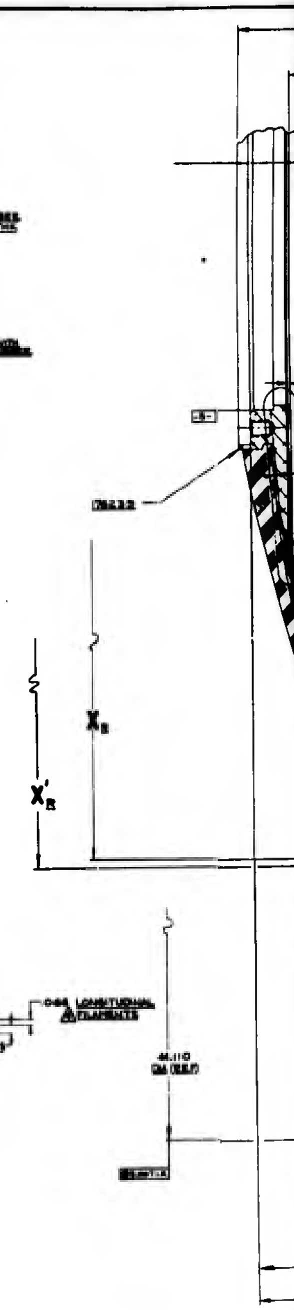

REMOVED

REMOVED

AXIS -A- IS DEFINED AS A STRAIGHT LINE CONNECTING THE CENTERS OF THE ENGINE CASE FWD SKIRT 44.110 DIA AND AFT SKIRT 48.010 DIA

4 FABRICATE PER AGC-13992

3 CONTOURED SURFACES OF LINER TO BE SMOOTH AND CONTINUOUS BETWEEN STATIONS

2 PRIOR TO RECEIVING INSULATION ALL METAL SURFACES WILL BE PREPARED PER AGC-13935 AND PRIMED WITH THIXON P-6 & THIXON AB PER AGC-137.5

NOTES: 1

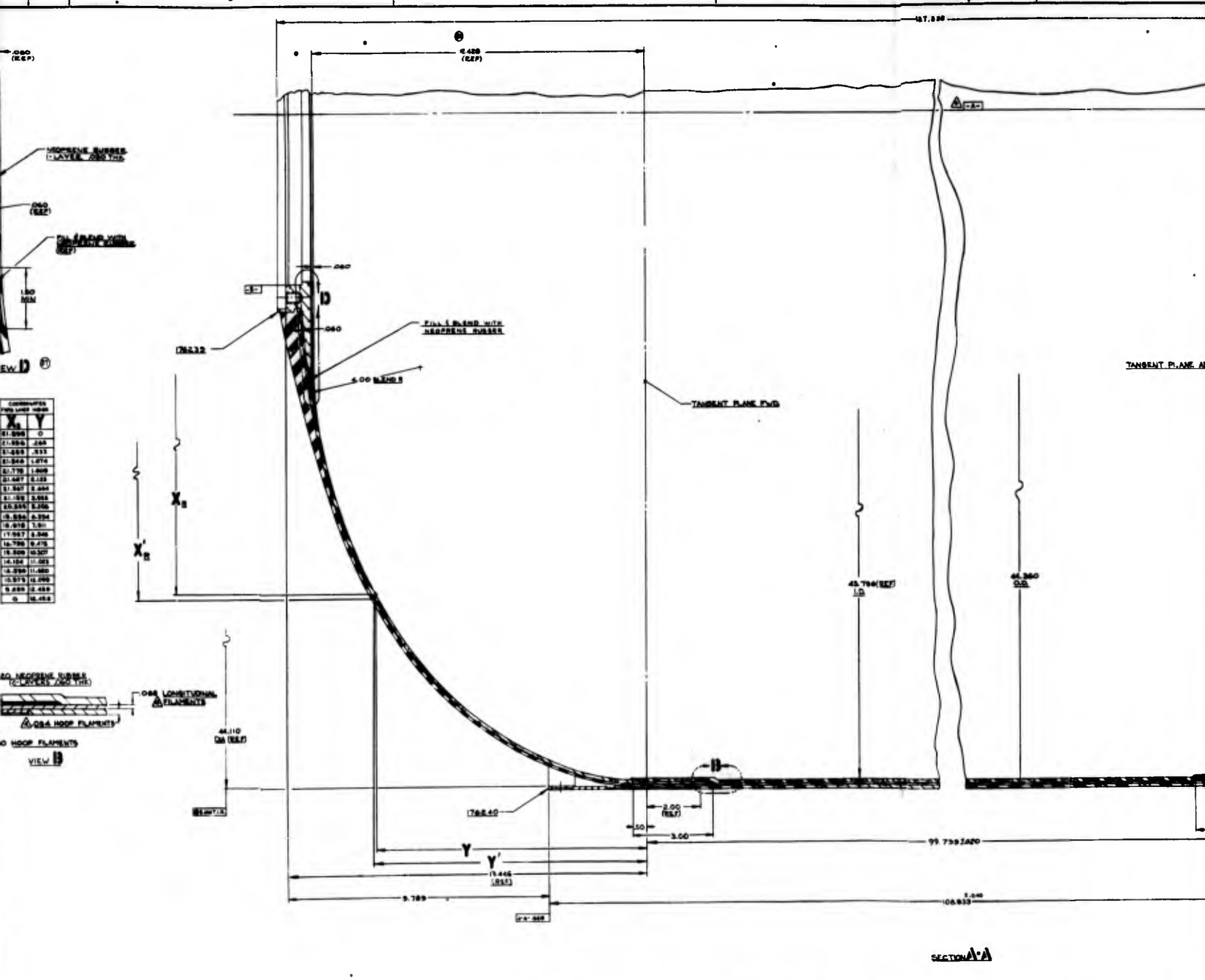

Figure 44. Serial No. 1, 44.3-Inch Cha

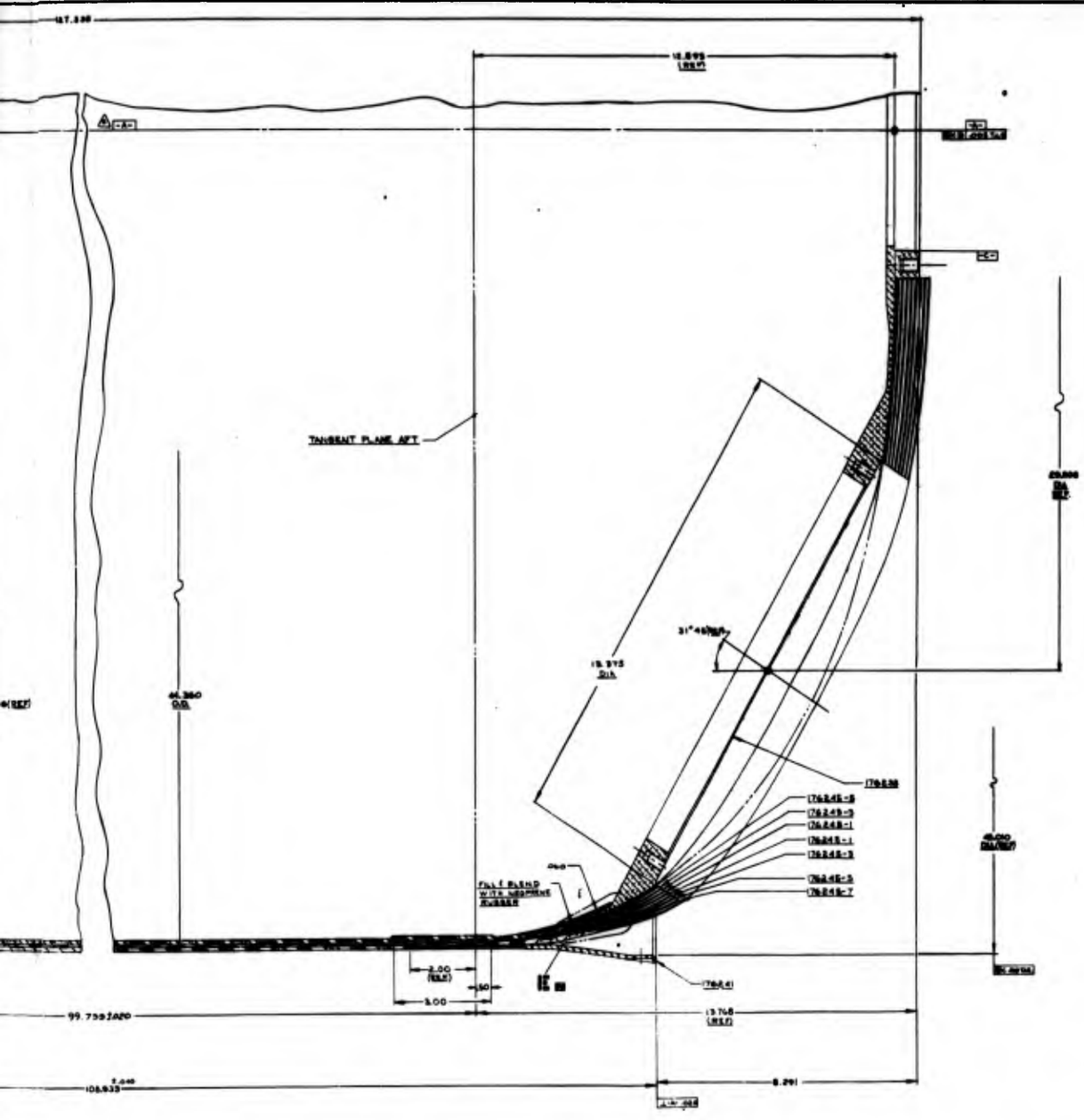

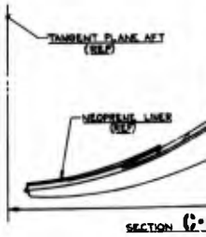

3

gure 44. Serial No. 1, 44.3-Inch Chamber

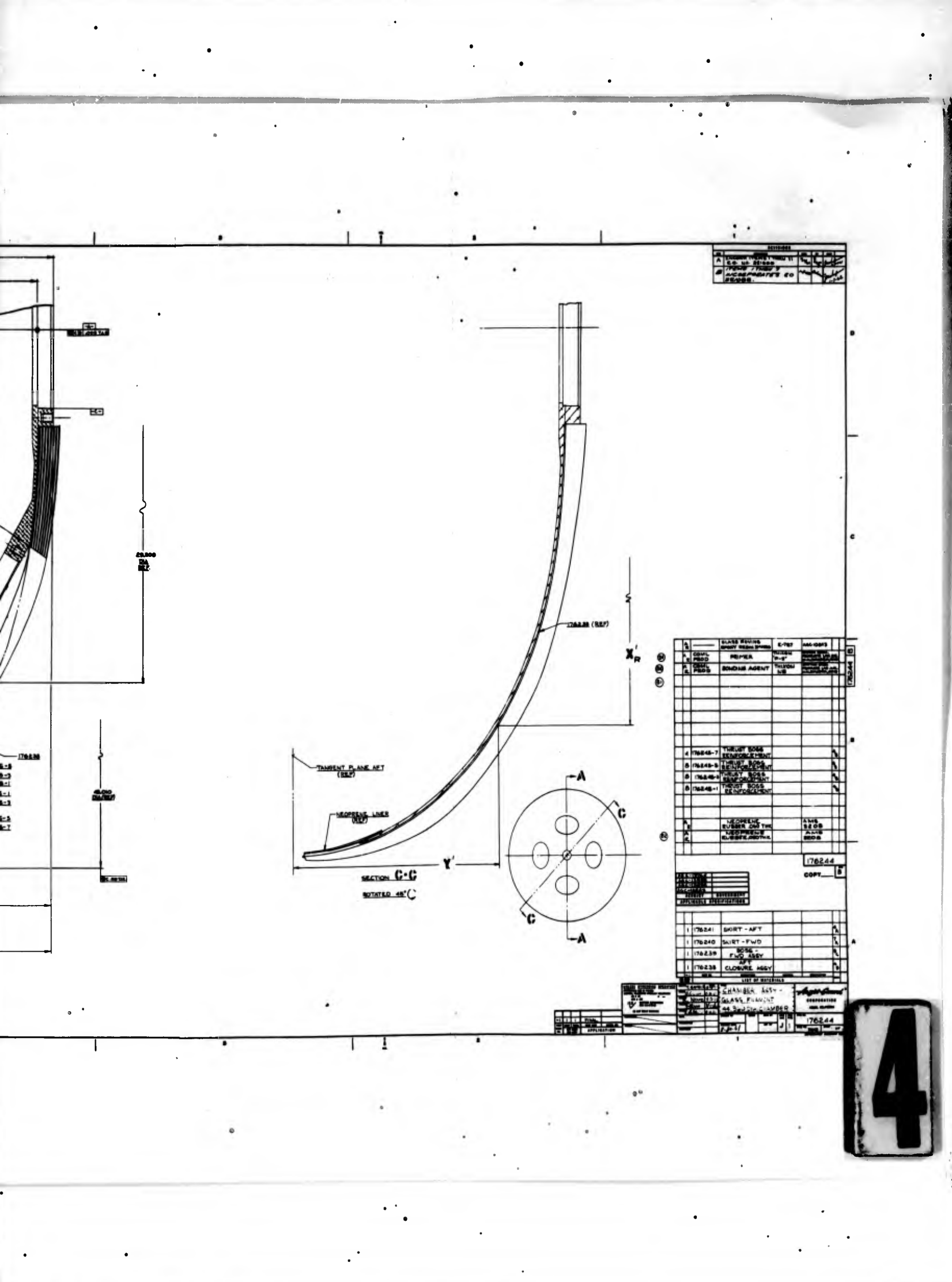
TANGENT PLANE AFT
NEOPRENE LINER
SECTION C-C
ROTATED 45°
A
C
C
A
4

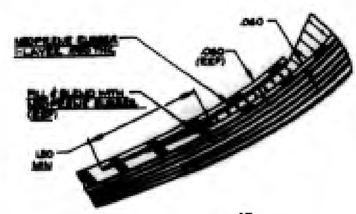

VIEW E

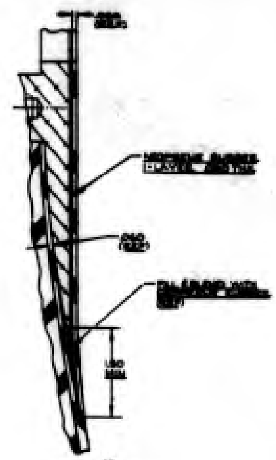

VIEW D

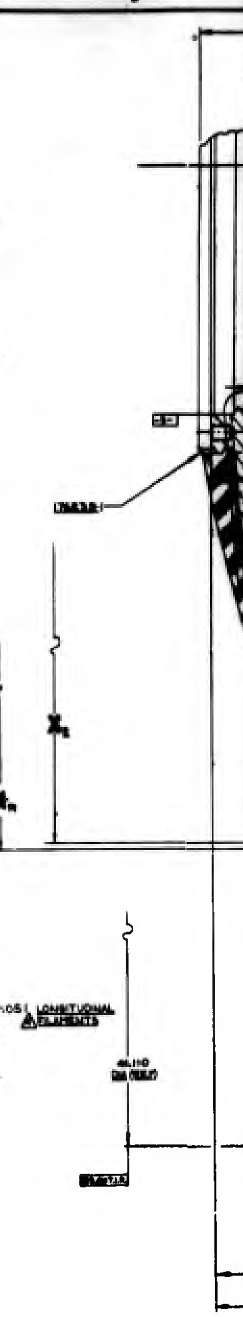

COORDINATES FWD OUTSIDE LINER X'_E	Y'
22.018	0
22.000	.440
21.963	1.099
21.877	1.759
21.760	2.418
21.589	3.078
21.371	3.737
21.114	4.396
20.809	5.056
20.464	5.715
20.063	6.374
19.571	7.033
19.031	7.691
18.414	8.350
17.706	9.008
16.906	9.665
15.945	10.322
14.828	10.977
13.478	11.629
11.788	12.276
10.788	12.594
9.563	12.908
8.380	13.150
7.386	13.259
0	13.259

COORDINATES FWD INSIDE LINER X_E	Y
21.898	0
21.889	.438
21.844	1.087
21.758	1.740
21.633	2.392
21.467	3.044
21.257	3.697
21.003	4.350
20.702	5.002
20.360	5.655
19.943	6.307
19.475	6.960
18.940	7.612
18.329	8.265
17.687	8.917
16.880	9.569
15.880	10.221
14.770	10.871
13.429	11.520
11.749	12.169
10.724	12.479
9.888	12.787
8.351	13.083
7.361	13.142
0	13.142

COORDINATES AFT OUTSIDE LINER S_R	R
22.018	0
22.010	.270
22.005	.539
21.965	1.086
21.897	1.627
21.808	2.187
21.663	2.693
21.547	[illegible]
20.690	5.342
19.955	6.466
19.068	7.591
18.037	8.633
16.866	9.575
15.964	10.411
14.183	11.136
12.630	11.735
[illegible]	12.215
9.305	12.577
7.530	12.815
5.698	12.953

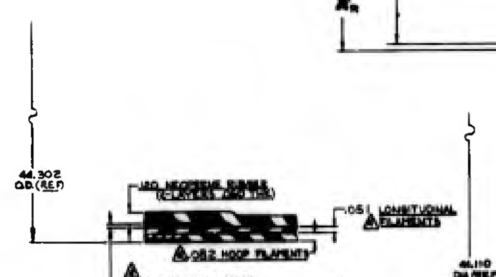

VIEW B

1. AXIS A IS DEFINED AS A STRAIGHT LINE CONNECTING THE CENTERS OF THE ENGINE CASE FWD SKIRT 44.110 DIA AND AFT SKIRT [illegible] DIA
2. FABRICATE PER AGC-[illegible]
3. CONTOURED SURFACES OF LINER TO BE SMOOTH AND CONTINUOUS BETWEEN STATIONS
4. PRIOR TO RECEIVING INSULATION ALL METAL SURFACES WILL BE [illegible]

1

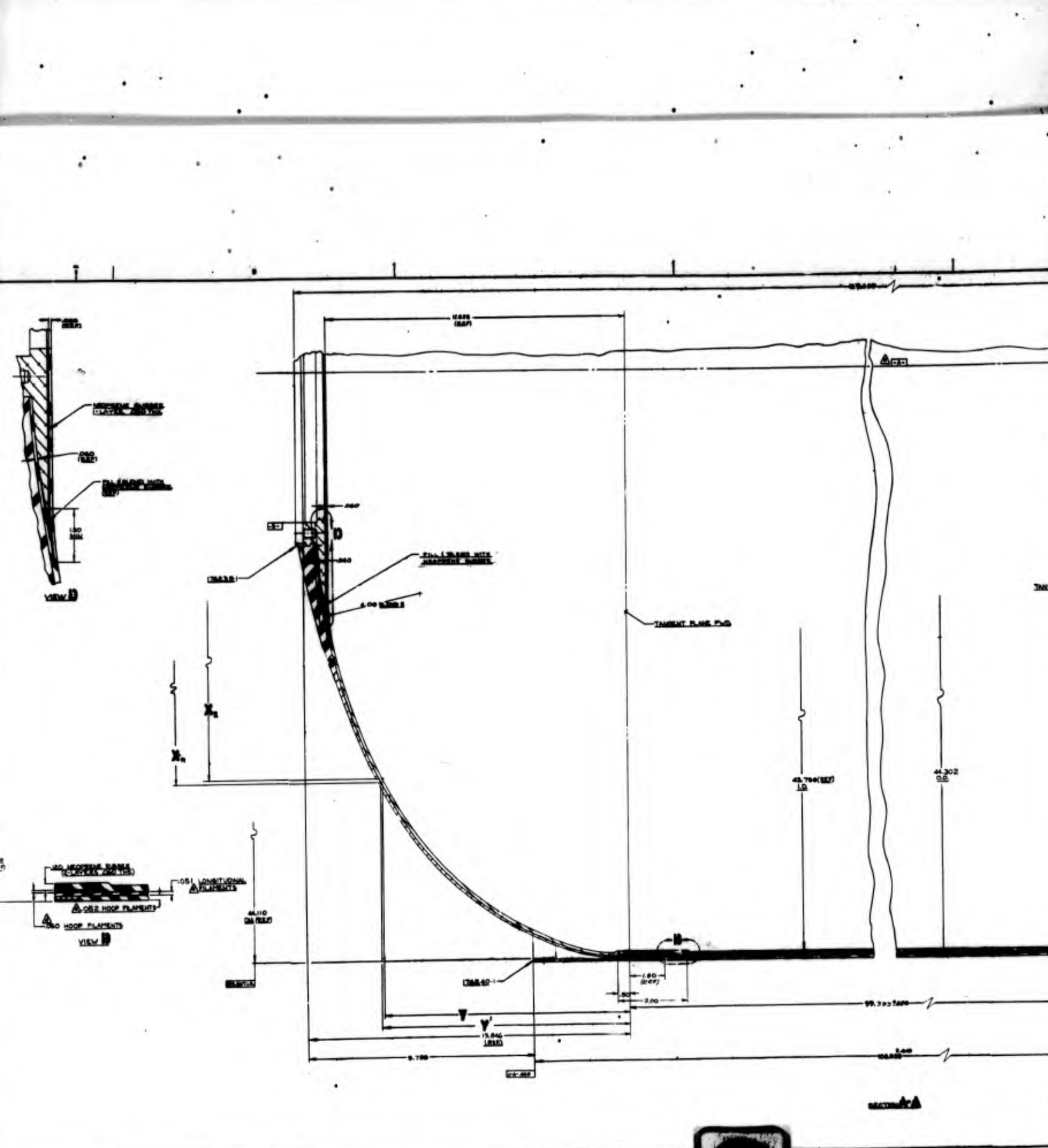

Figure 45. Serial No. 2, 44.3-

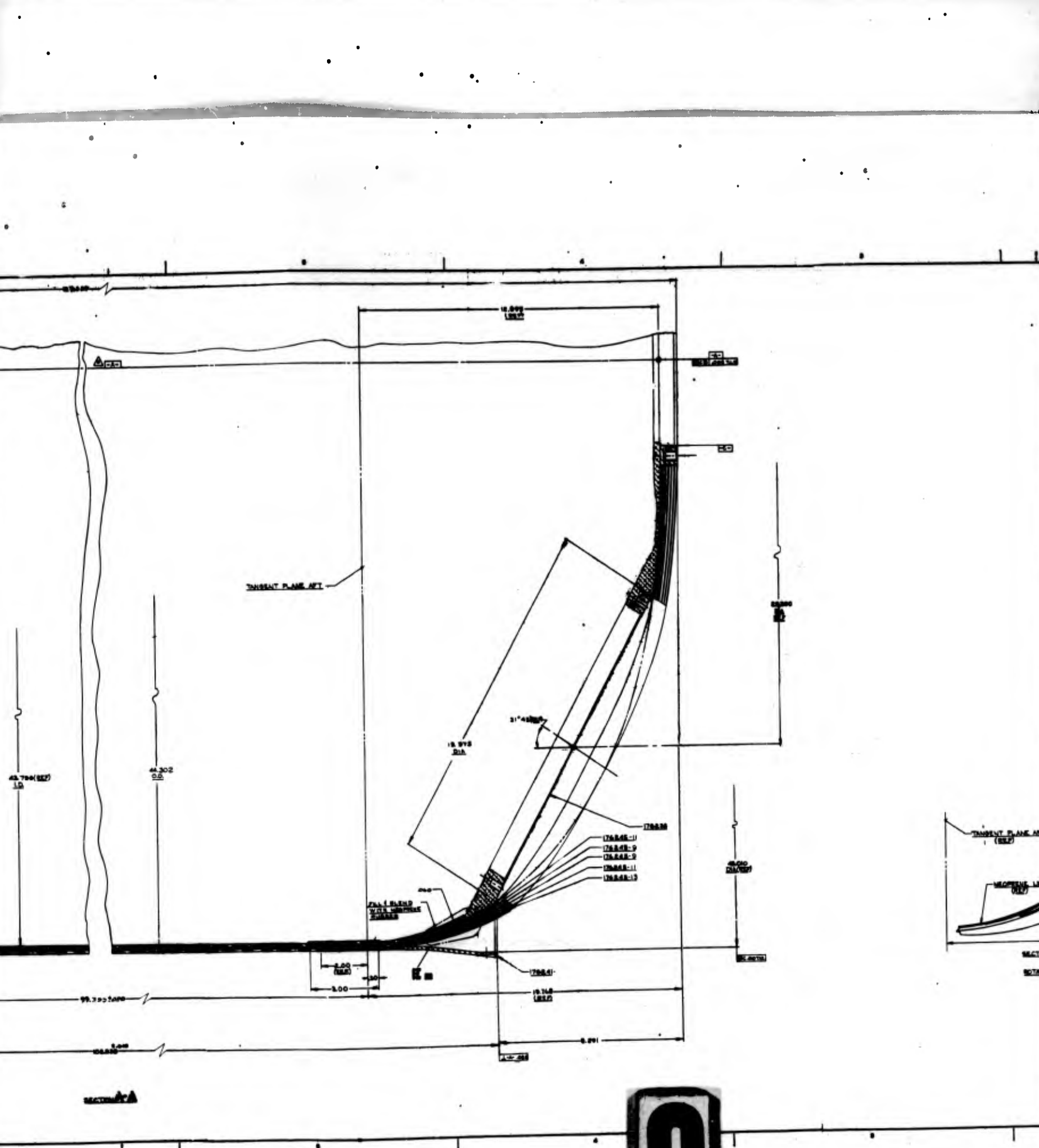

Figure 45. Serial No. 2, 44.3-Inch Chamber

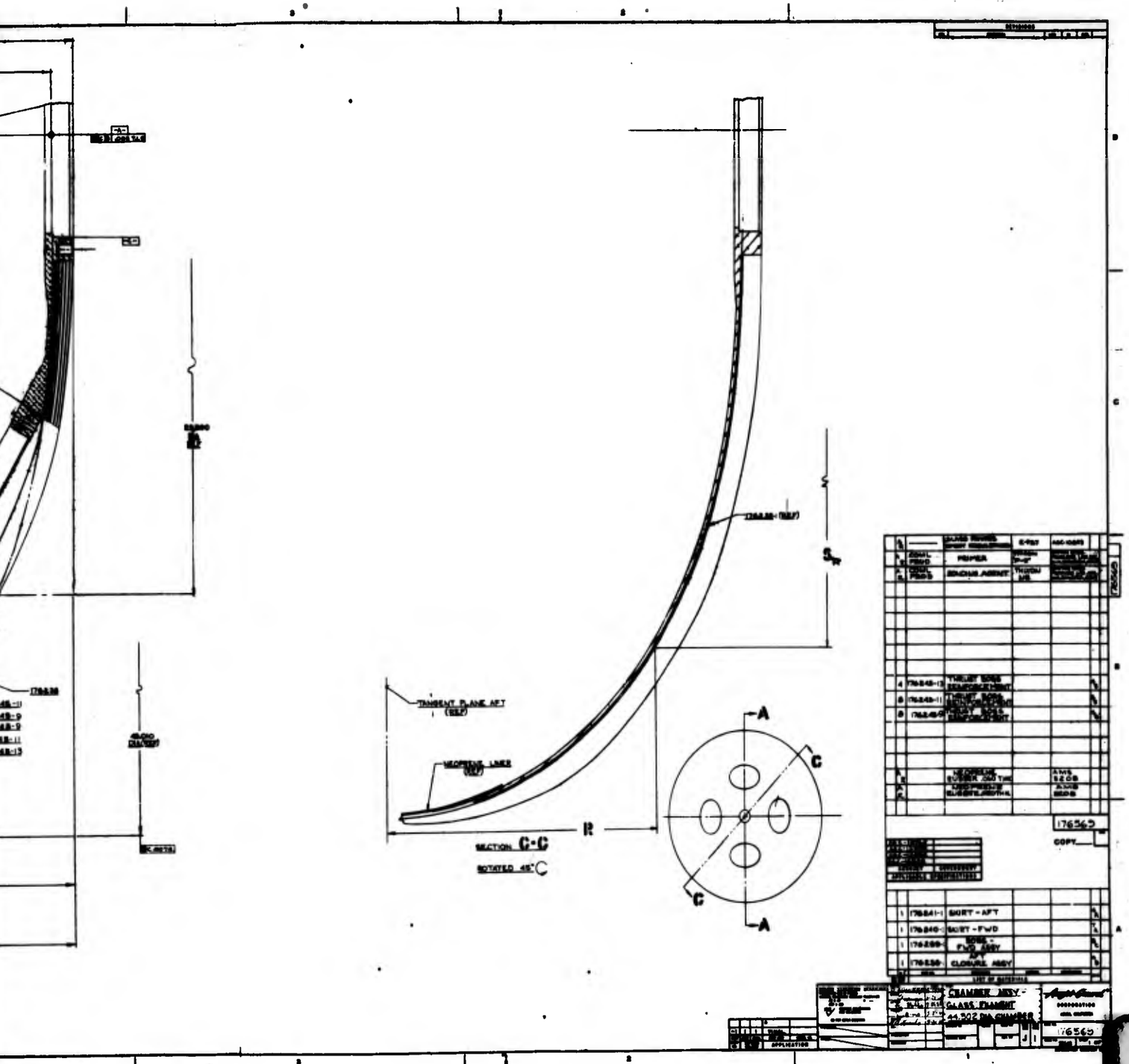
TANGENT PLANE AFT
NEOPRENE LINER
R
SECTION C-C
ROTATED 45°C
A
C
C
A

4

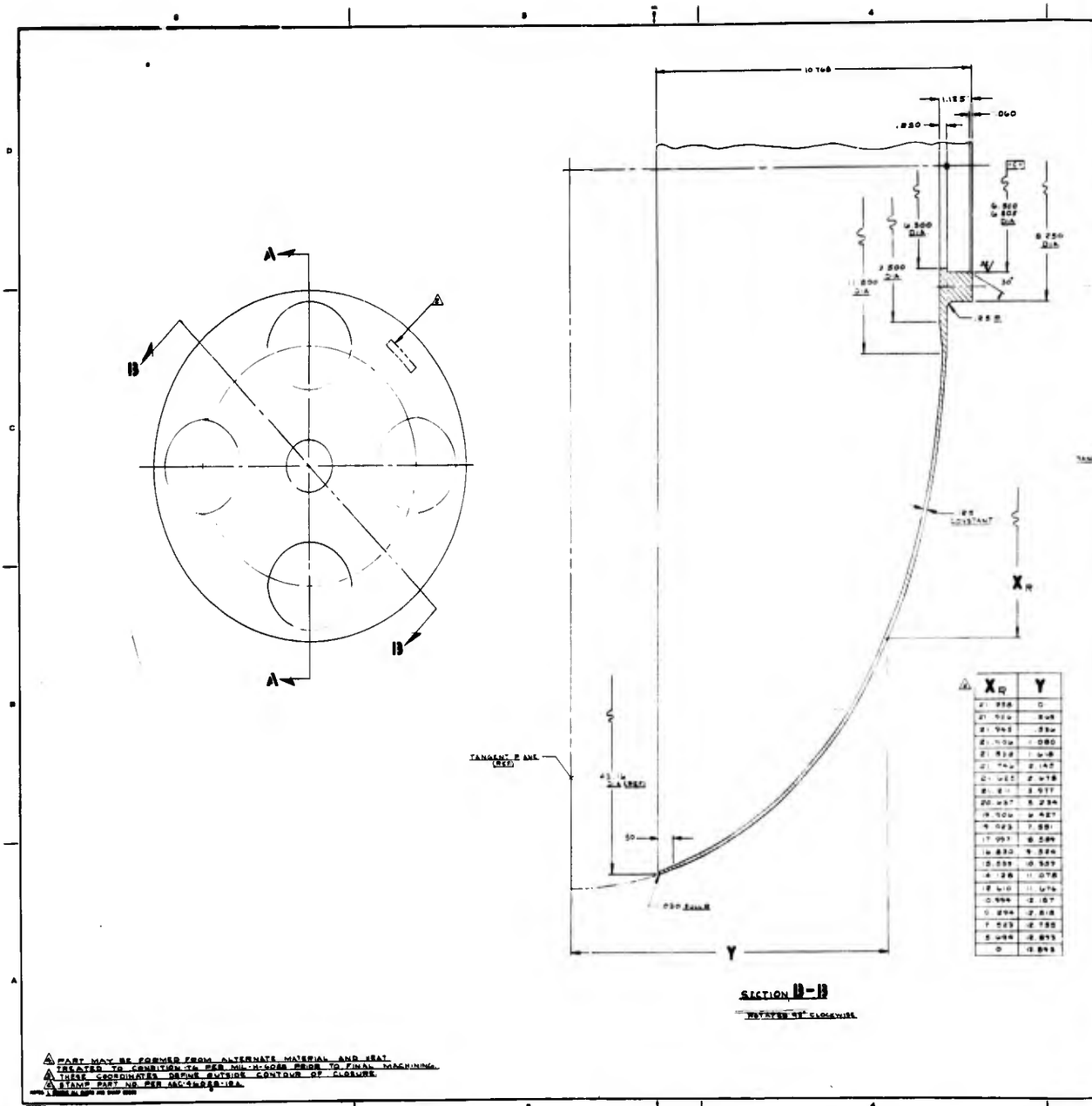

Figure 46. Aft-Closure Assembly

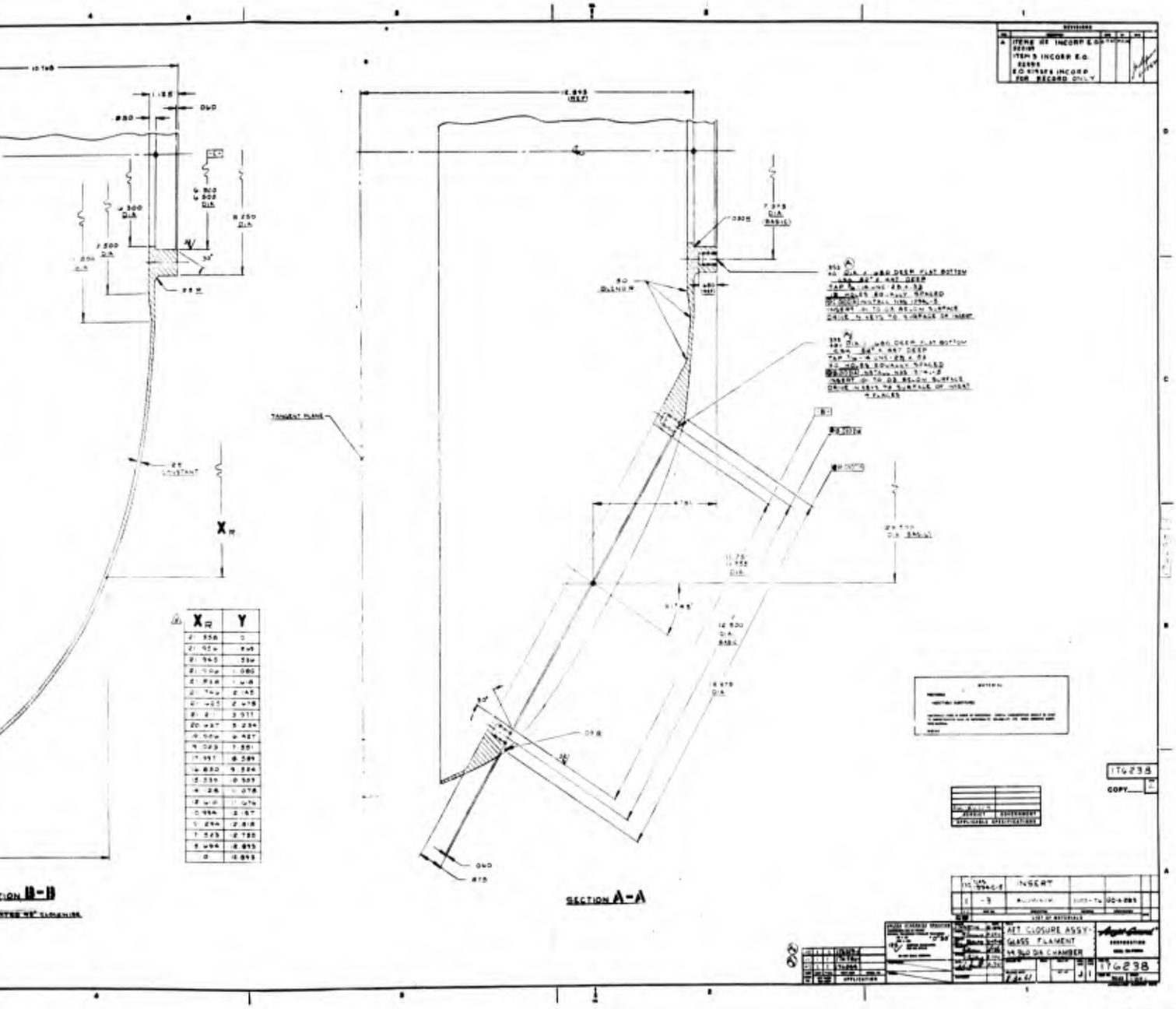

gure 46. Aft-Closure Assembly for 44.3-Inch Chambers

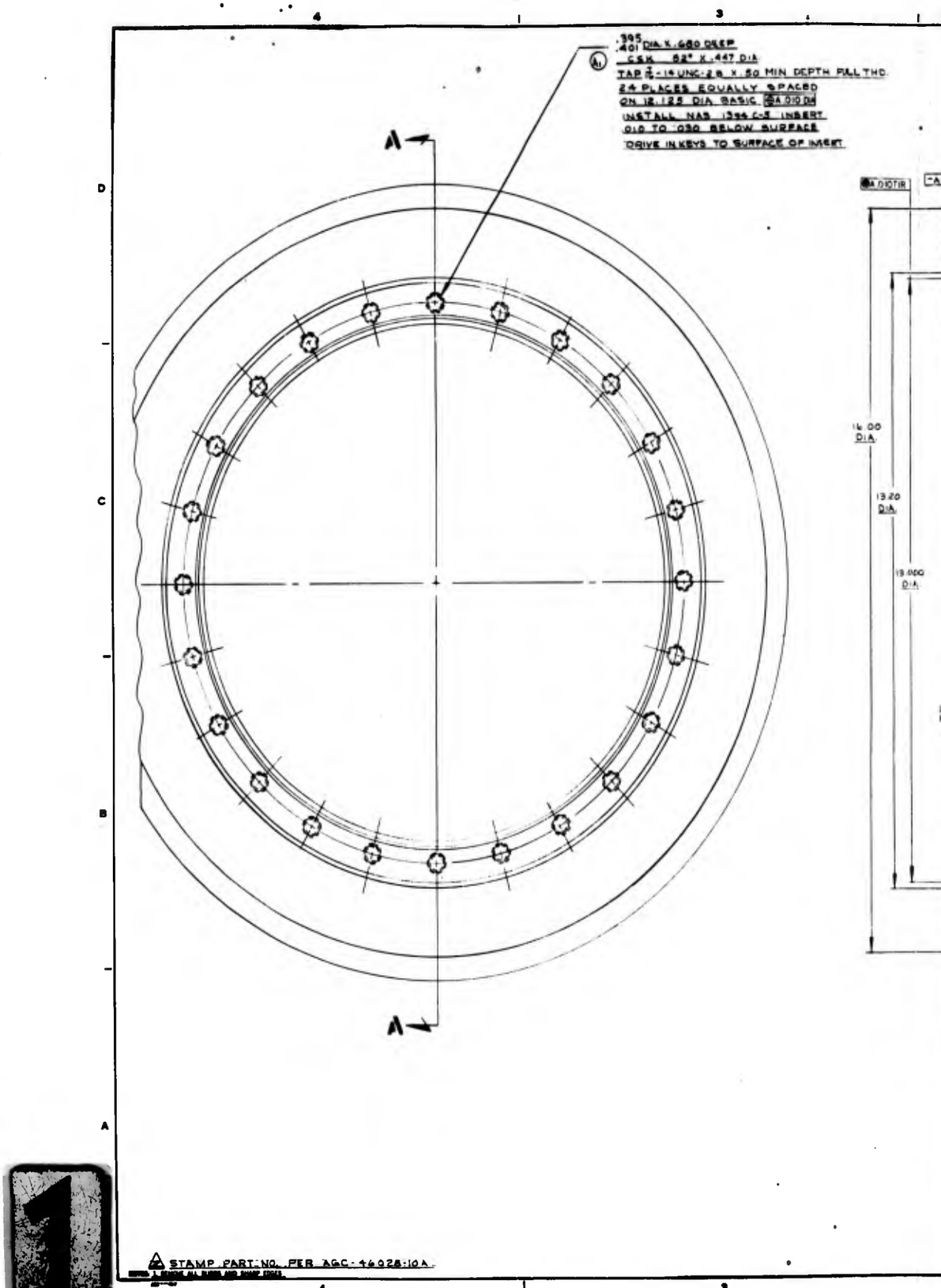

Figure 47. Forward-Boss Asse

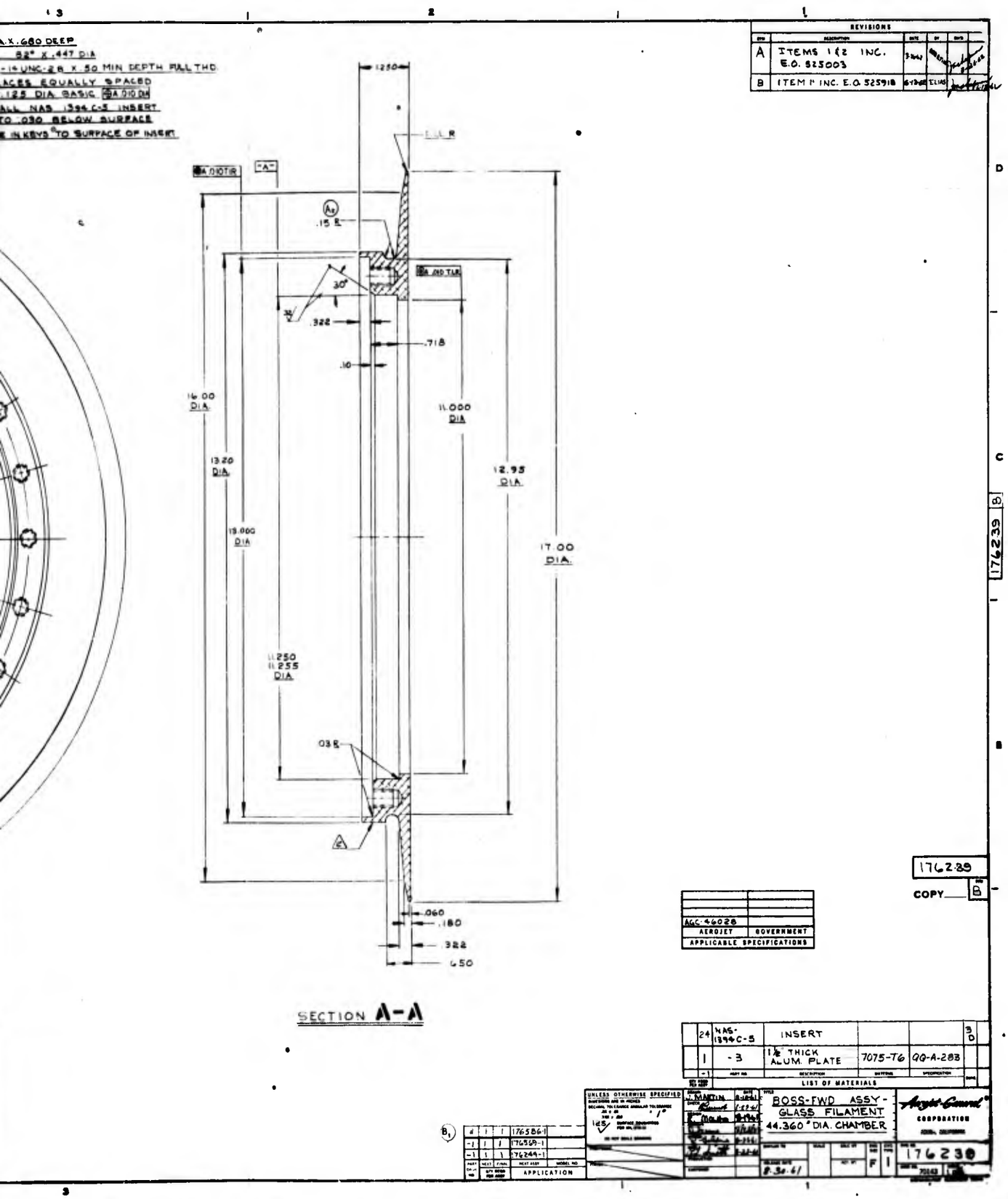

Figure 47. Forward-Boss Assembly for 44.3-Inch Chambers

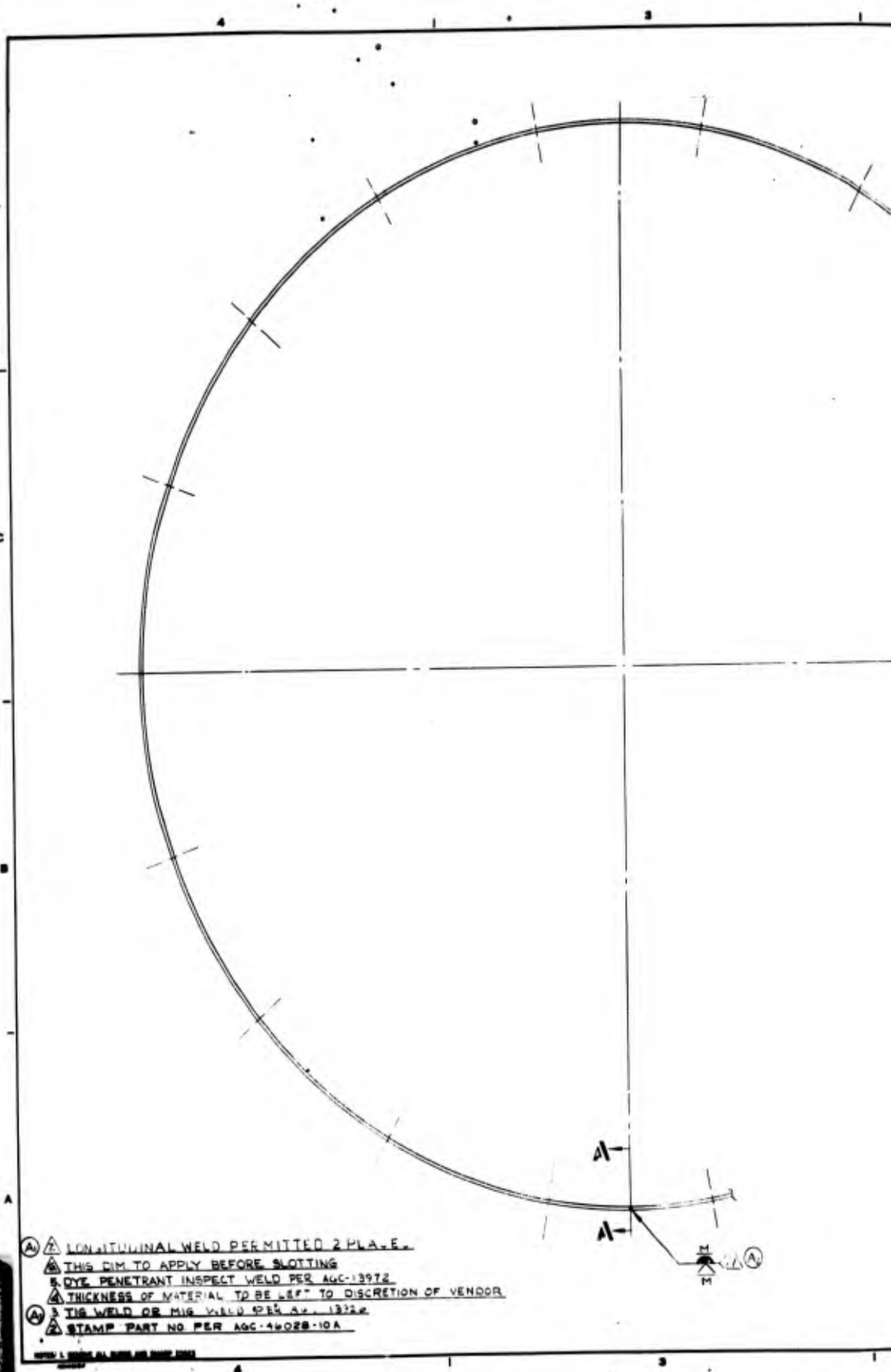

Figure 48. Forward Skirt

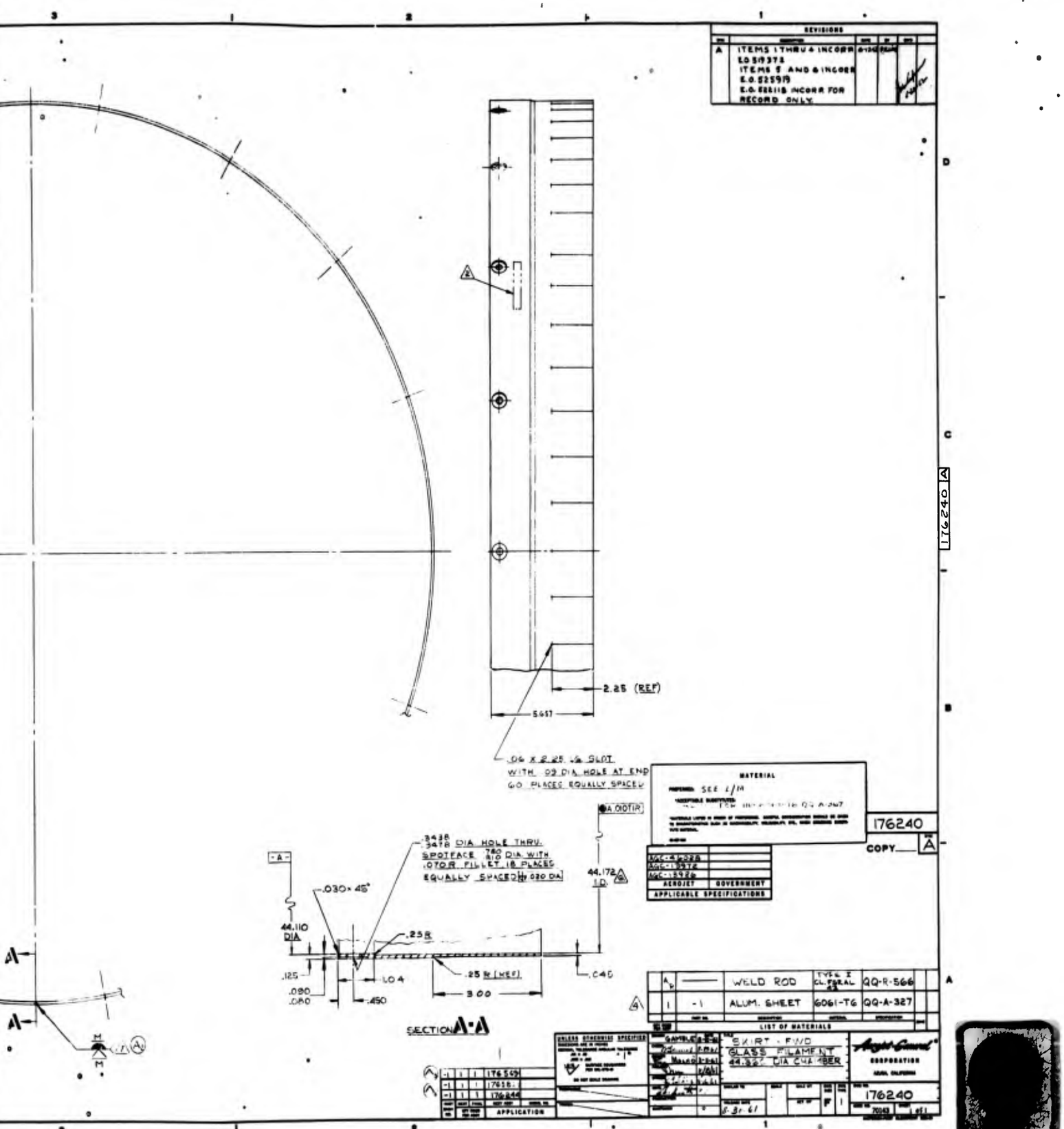

Figure 48. Forward Skirt for 44.3-Inch Chambers

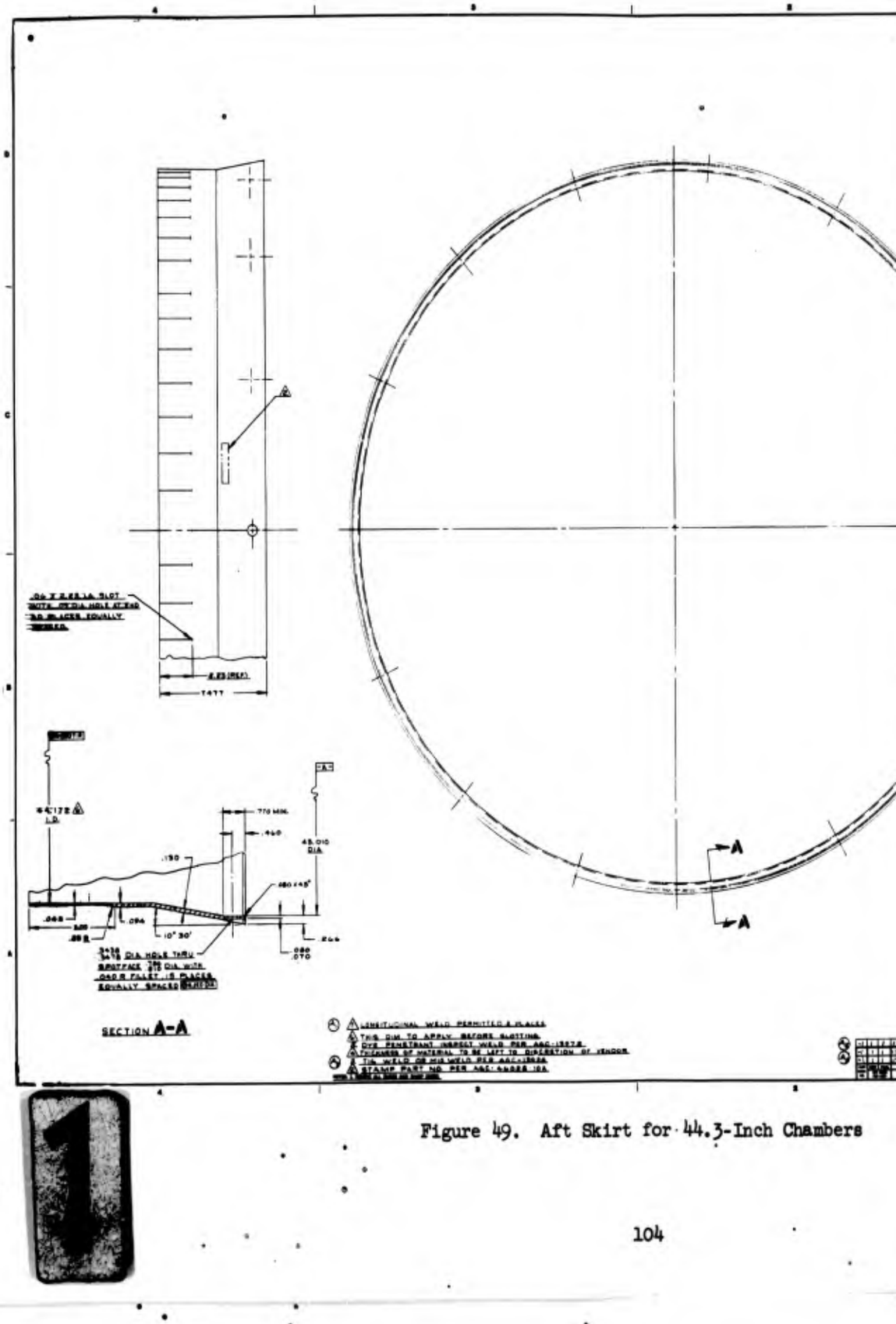

Figure 49. Aft Skirt for 44.3-Inch Chambers

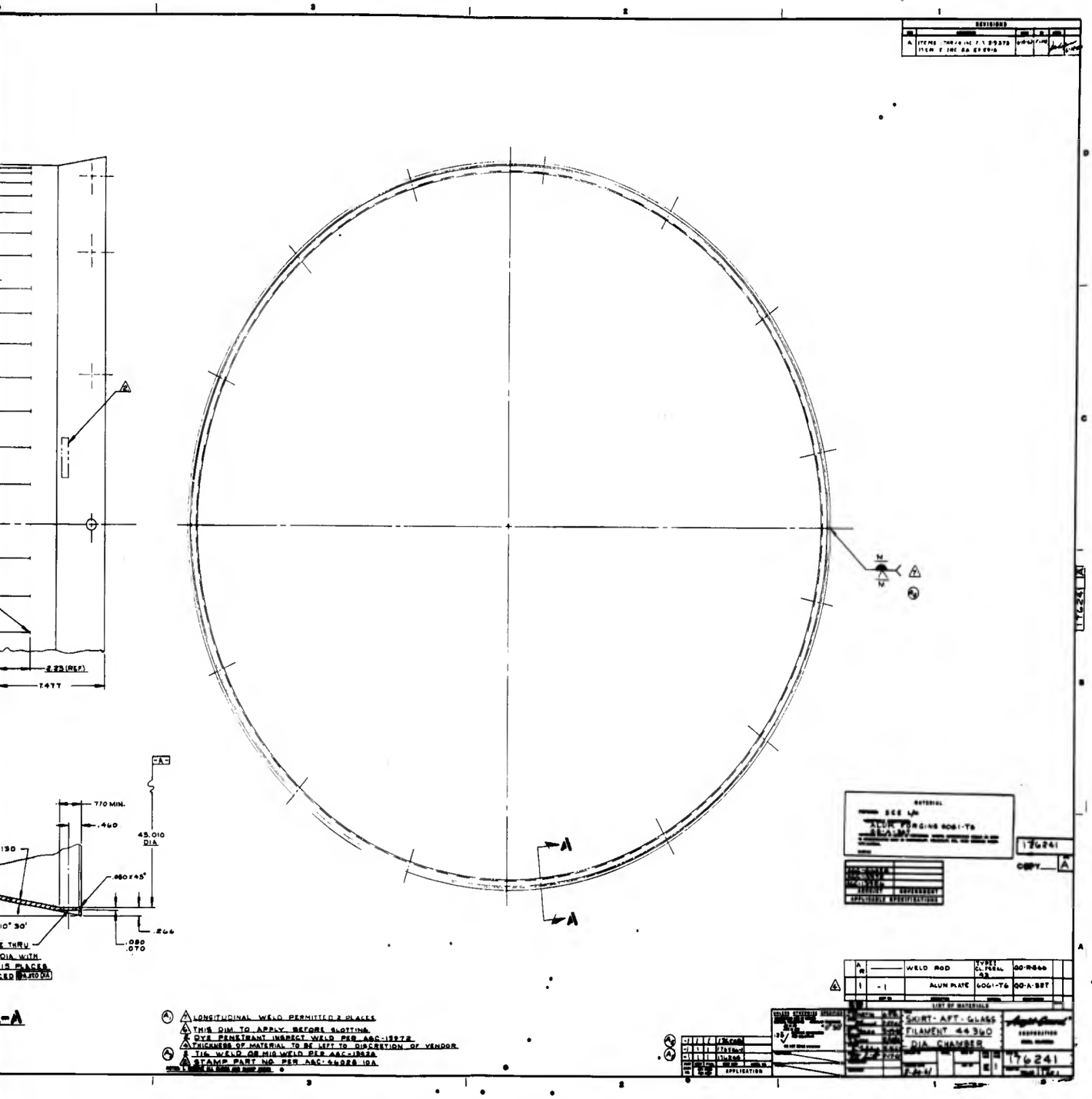

Figure 49. Aft Skirt for 44.3-Inch Chambers

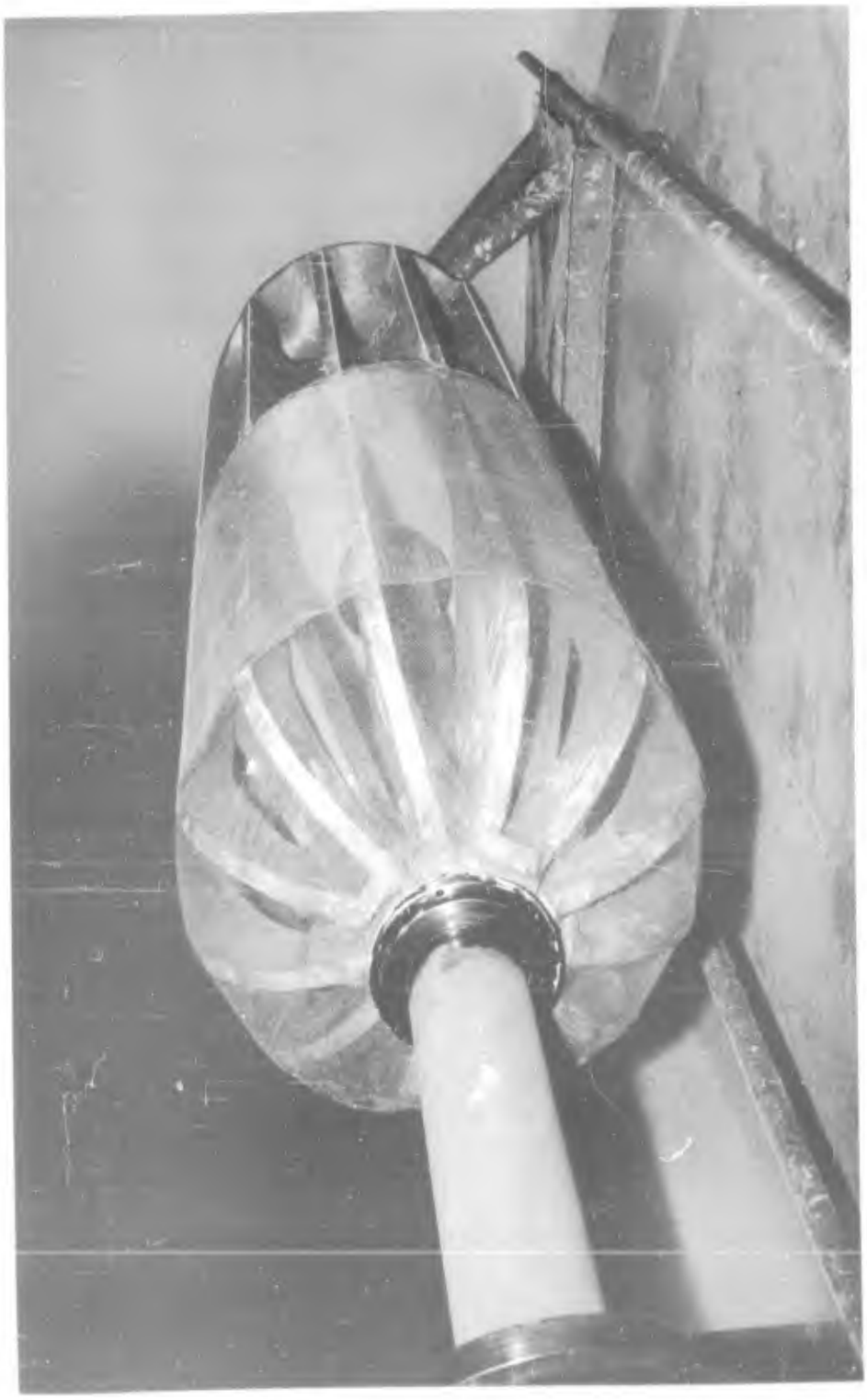

Figure 50. Mandrel Assembly, Ribbed and Disk Framework

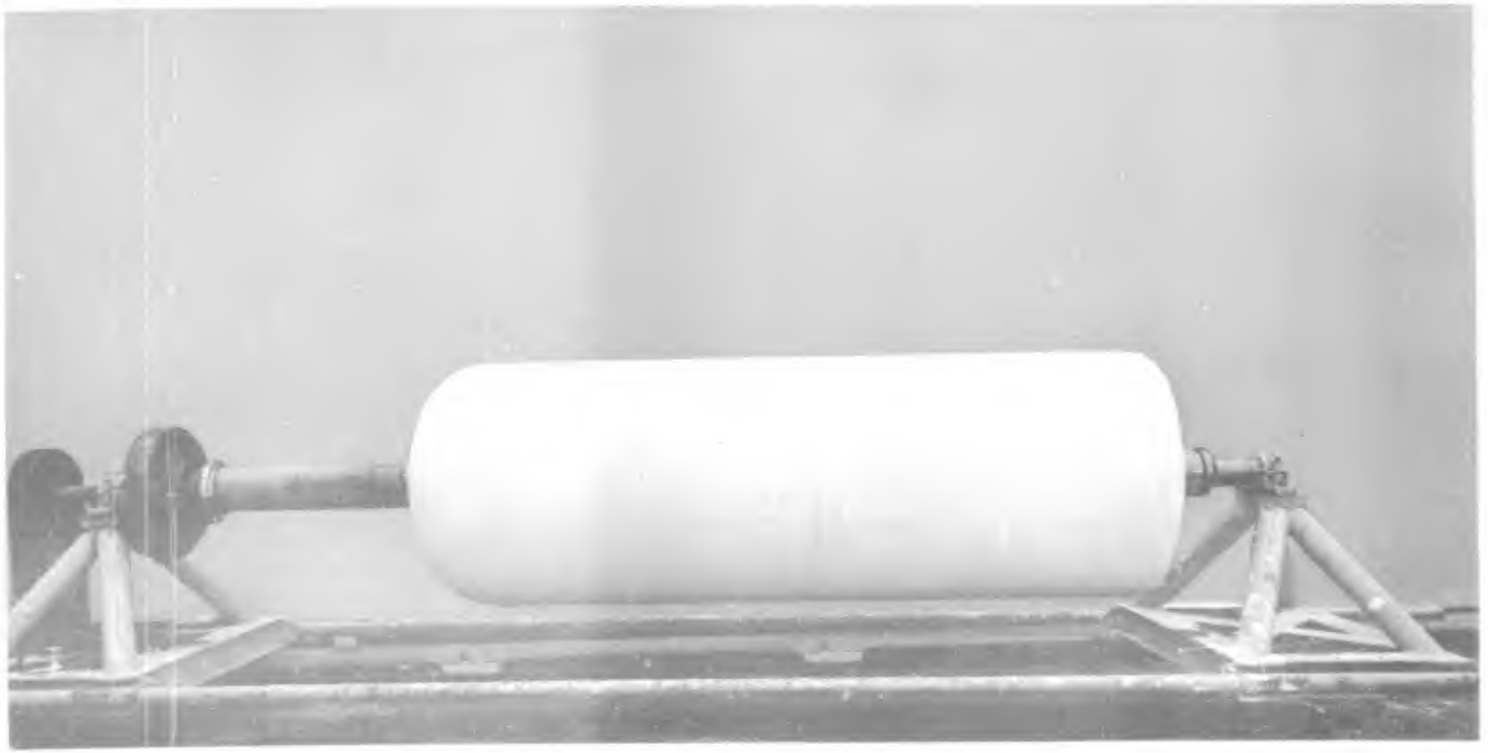

Figure 51. Mandrel Assembly, Final Swept Unit

Figure 52. Lined Mandrel Being Prepared for Vacuum Bagging

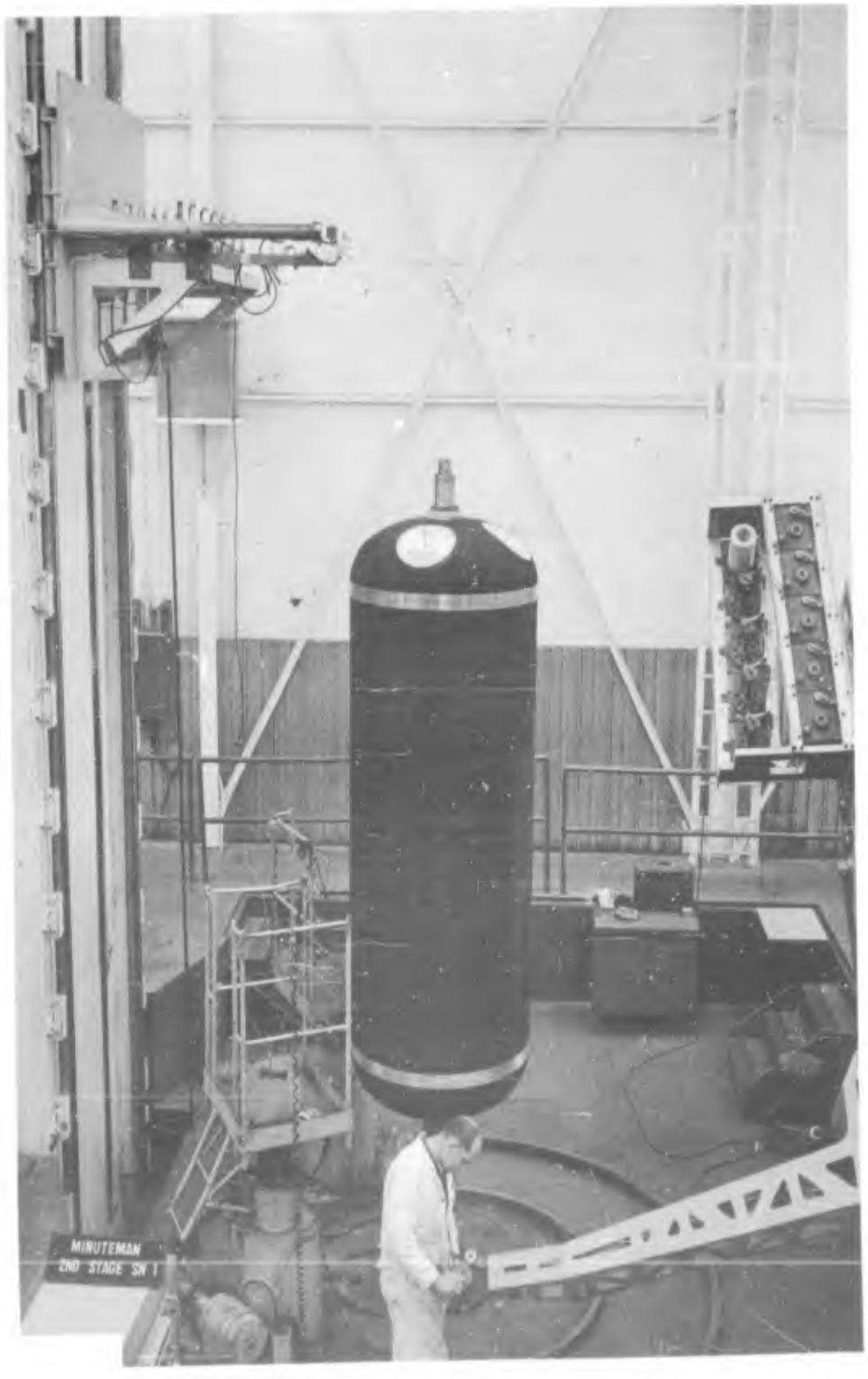

Figure 53. Application of Hoop-Filament Bands

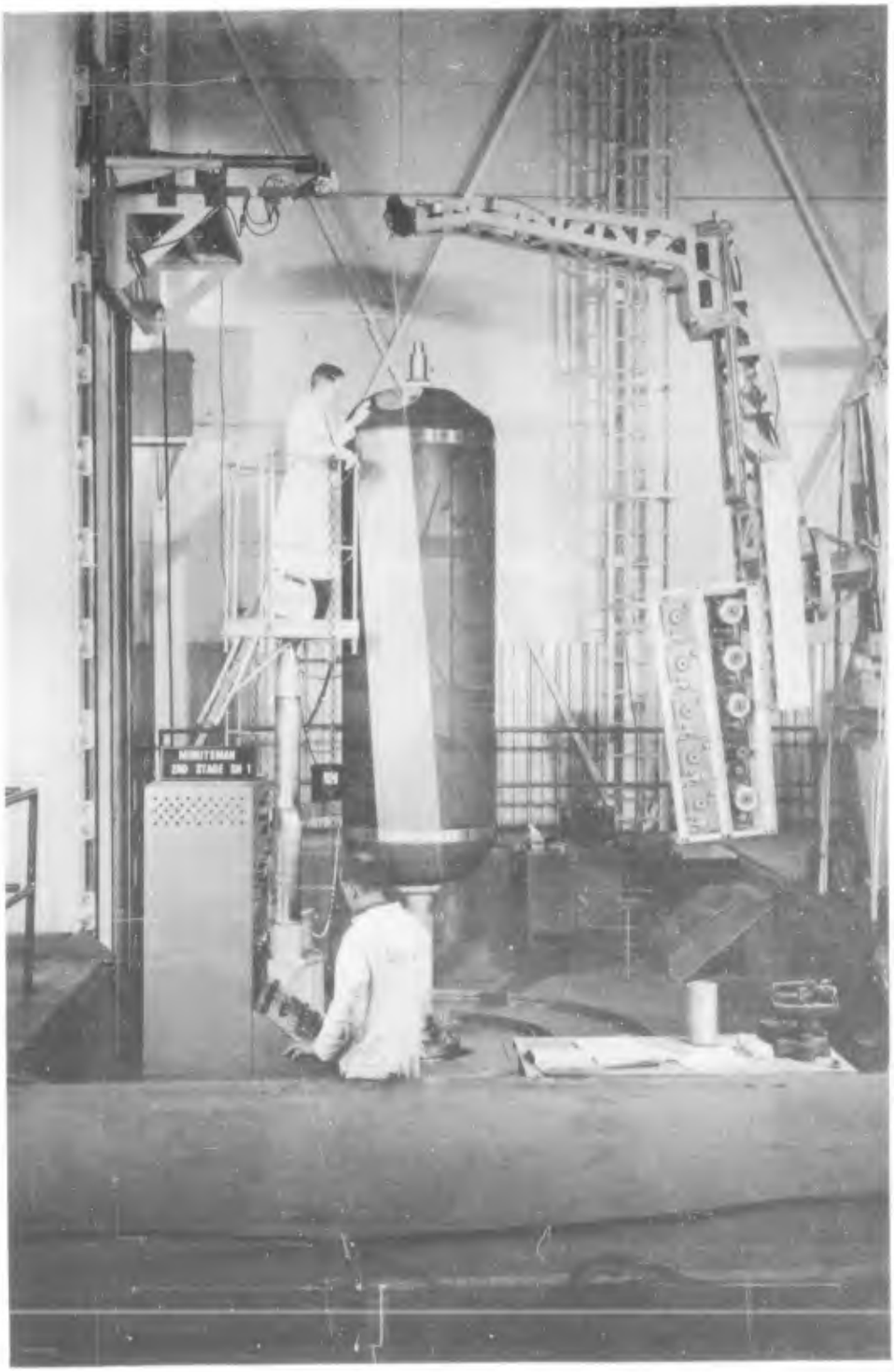

Figure 54. Application of Longitudinal Filaments

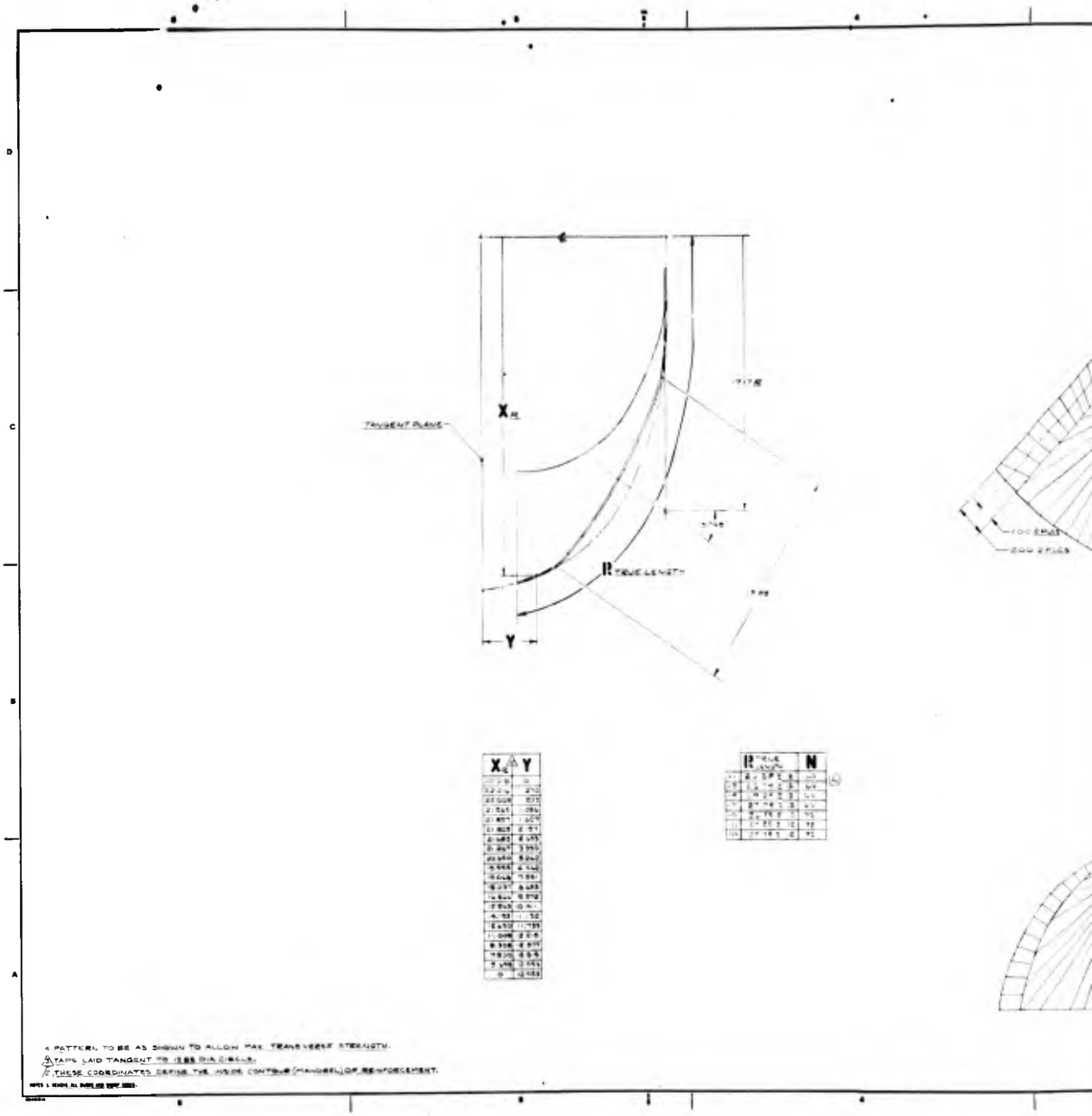

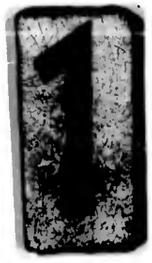

Figure 55. Thrust-Boss Reinforcemen

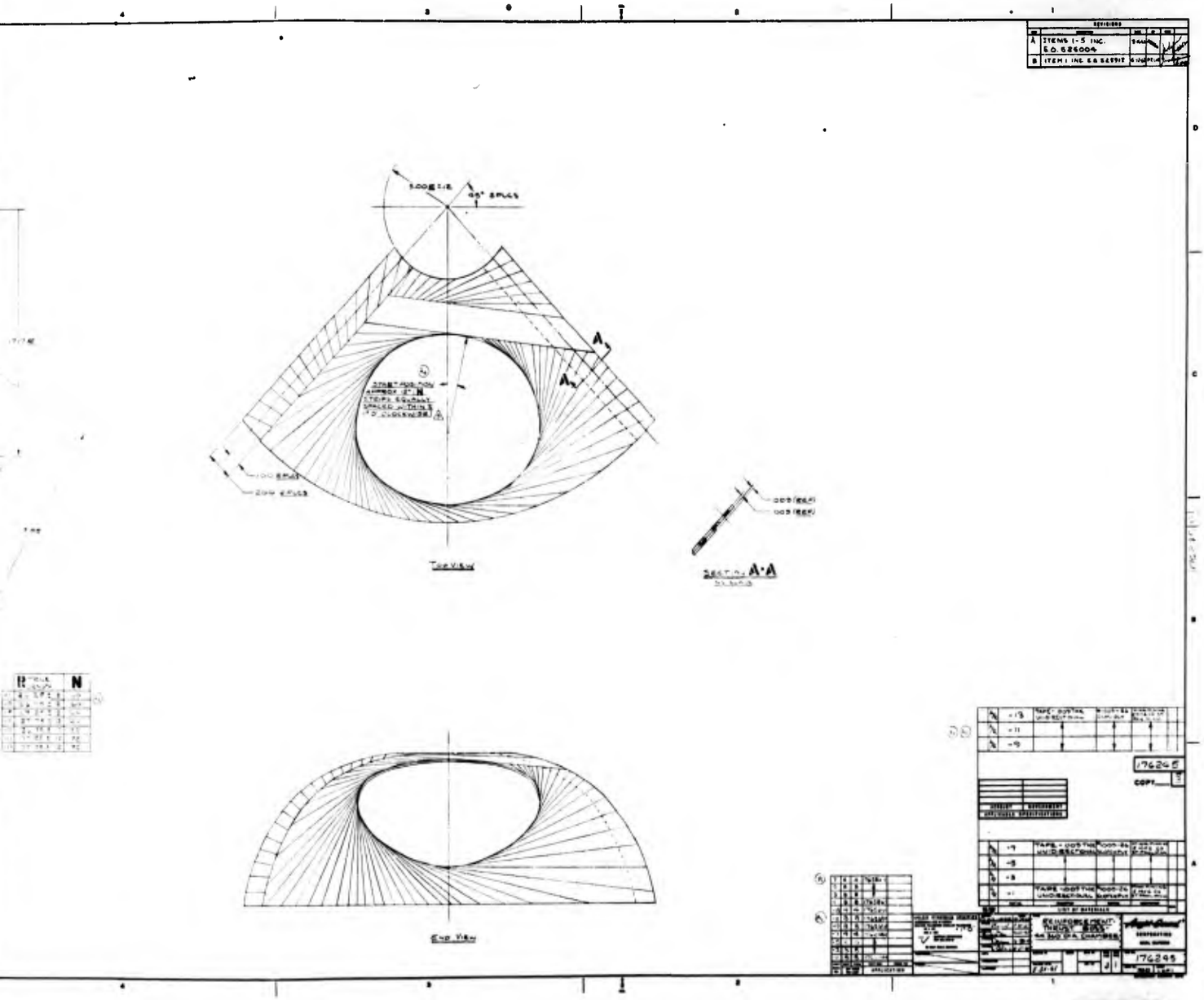

End View

ure 55. Thrust-Boss Reinforcement for 44.3-Inch Chambers

Figure 56. Positioning of Skirts Prior to Hoop-Filament Winding

Figure 57. Cutting of Filaments in Aft Nozzle Ports

Figure 58. Dimensional Checking of Chamber

Figure 59. Serial No. 1, 44.3-Inch Chamber in Stand Prior to Hydrotest

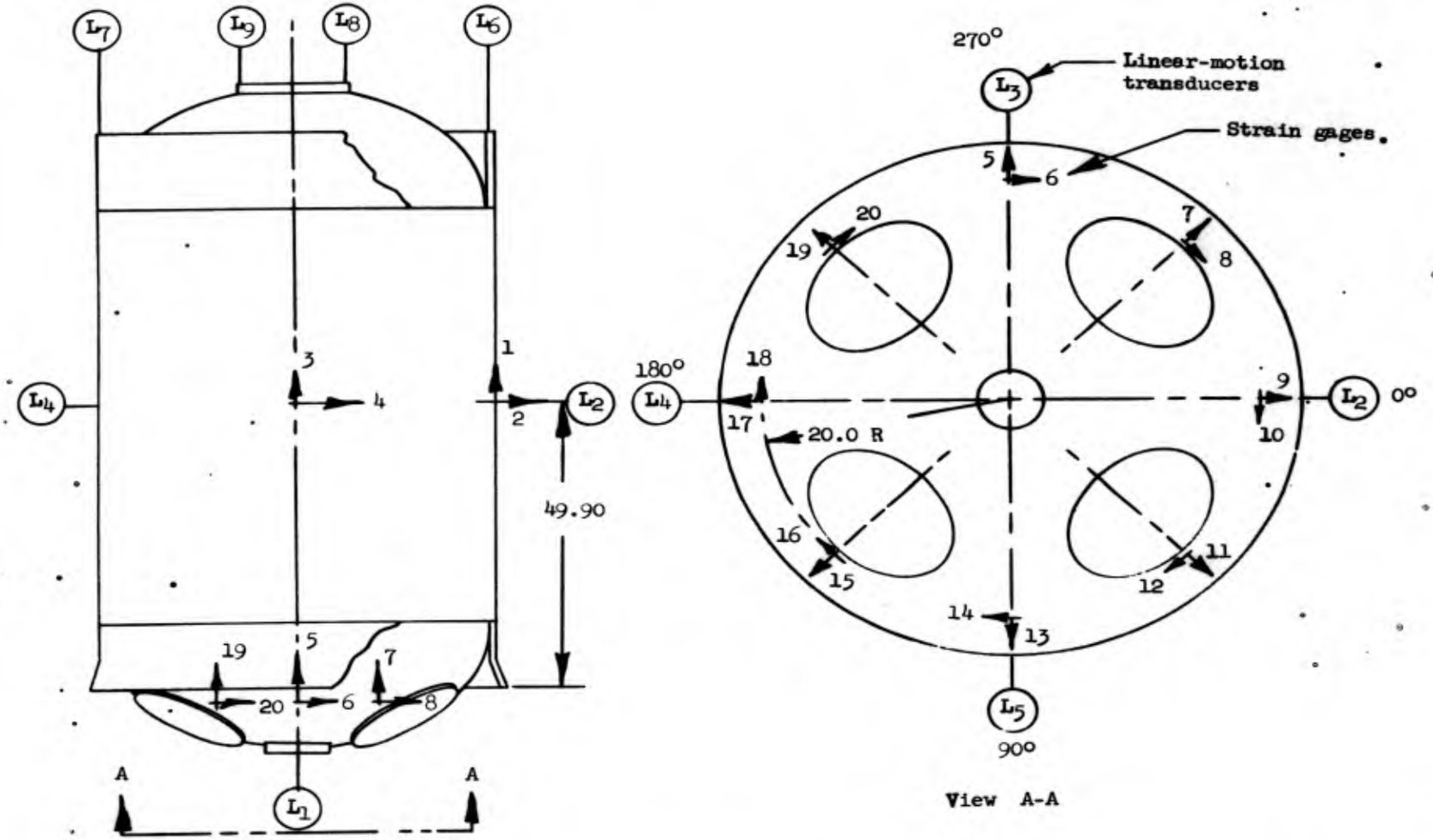

Figure 60. Location of Strain Gages and Linear-Motion Transducers for Proof-Pressure Testing - Serial No. 1,2, and 3, 44.3-Inch Chambers

Figure 61. Serial No.1, 44.3-Inch Chamber at Moment of Hydroburst

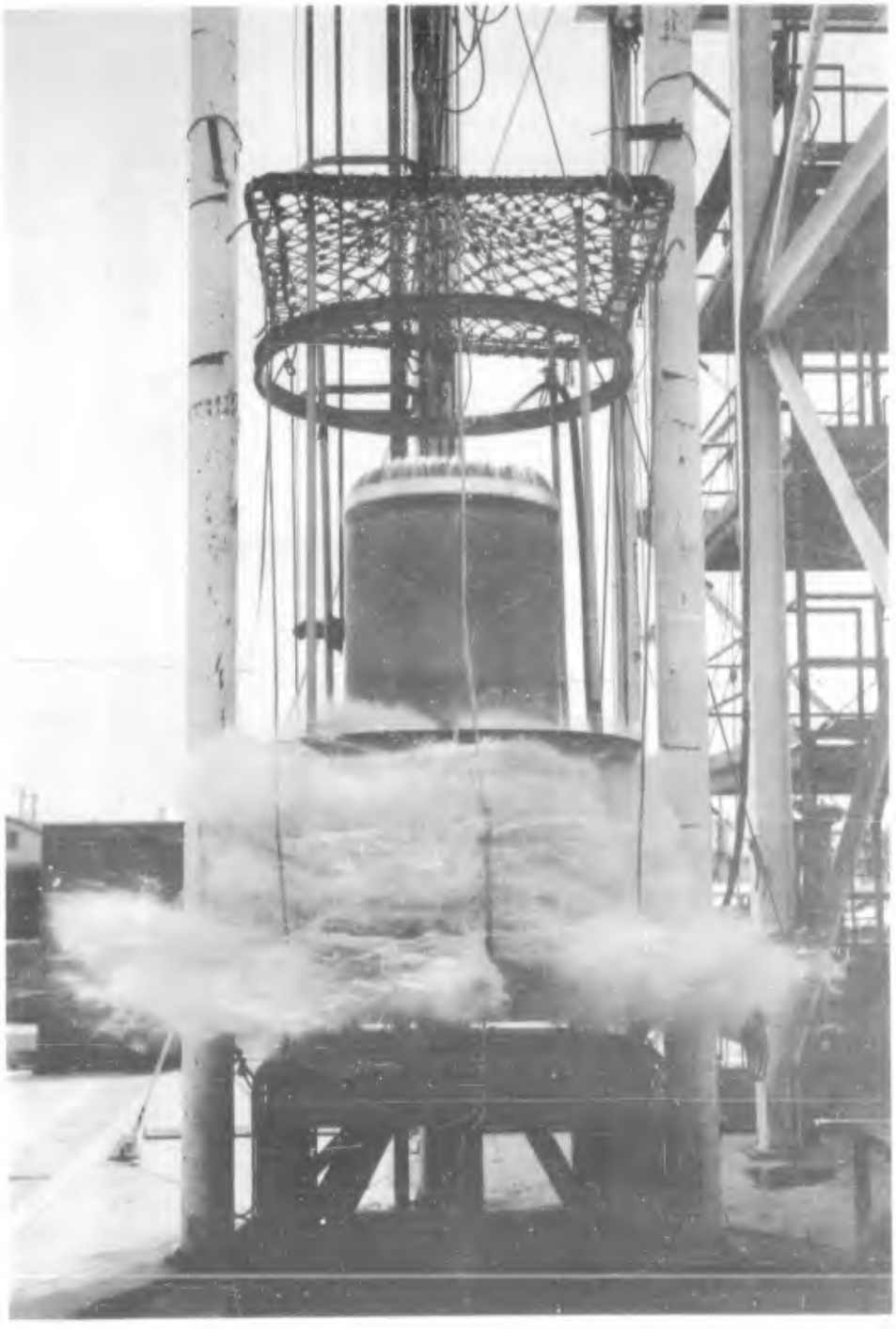

Figure 62. Serial No. 2, 44.3-Inch Chamber at Moment of Hydroburst

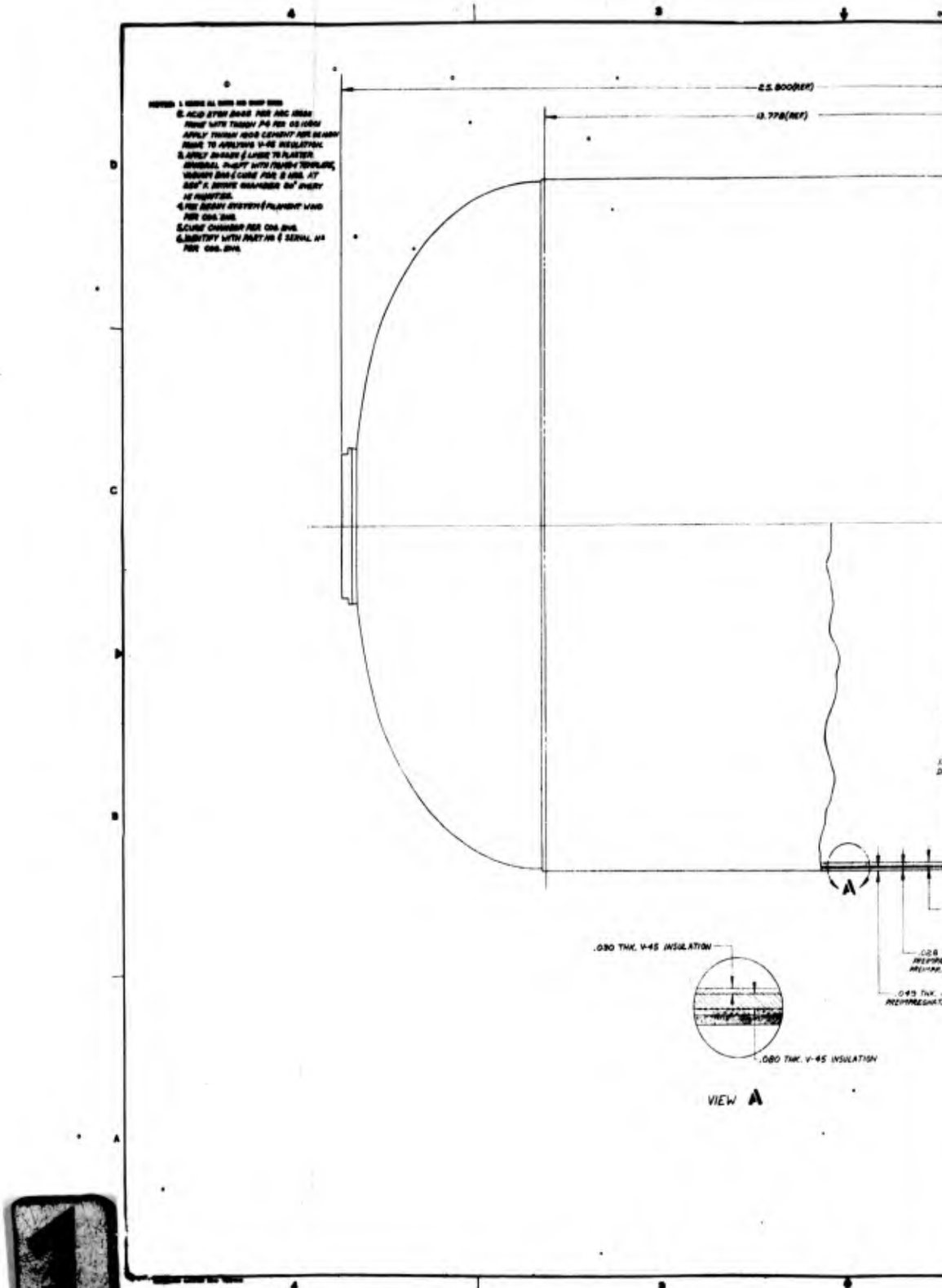

Figure 63. 18-Inch Chamber Assembly,

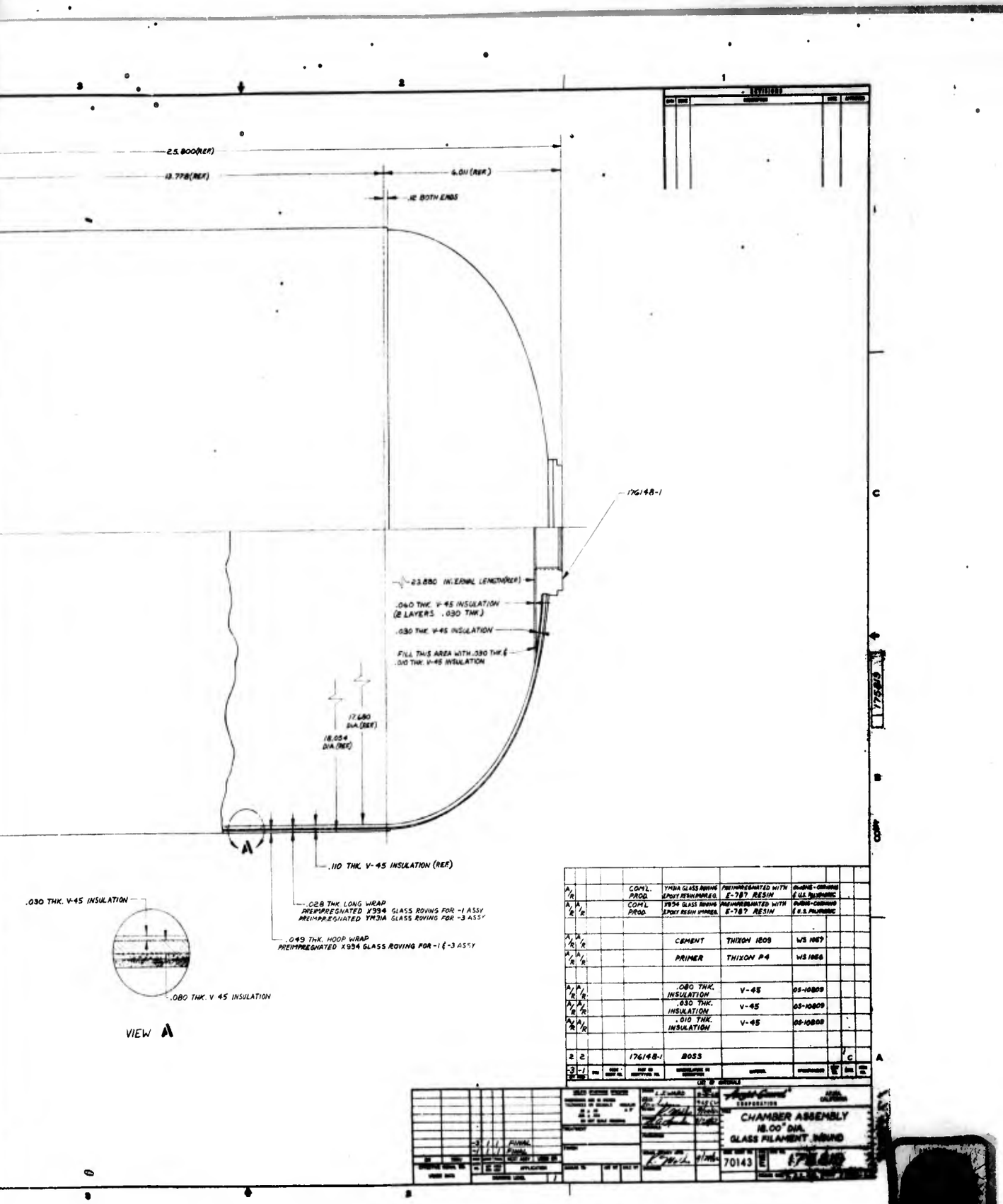

Figure 63. 18-Inch Chamber Assembly, Serial Nos. 3 and 4

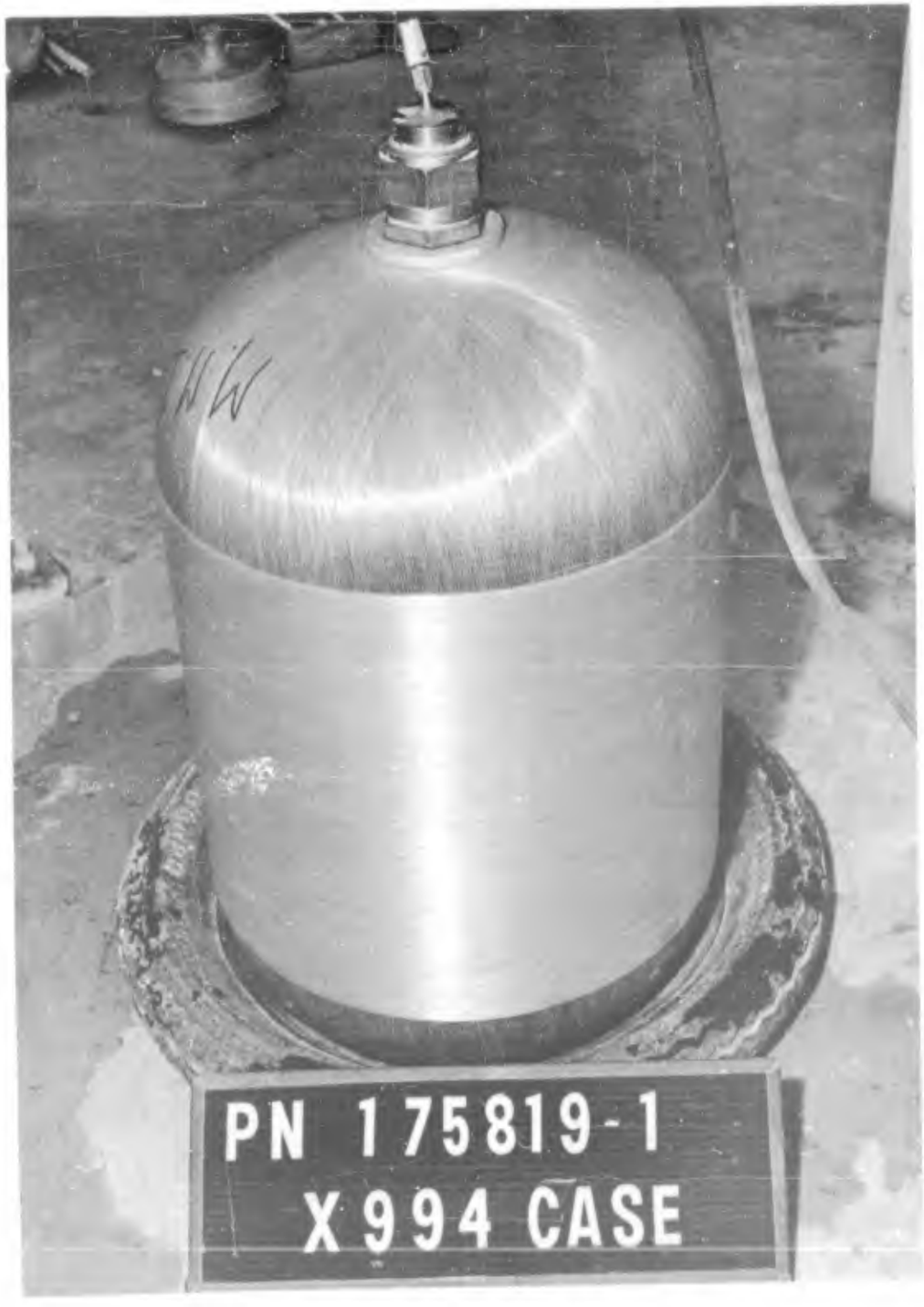

Figure 64. Serial No. 3, 18-Inch S994 Chamber Before Hydrotest

Figure 65. Serial No. 3, 18-Inch S994 Chamber After Hydrotest

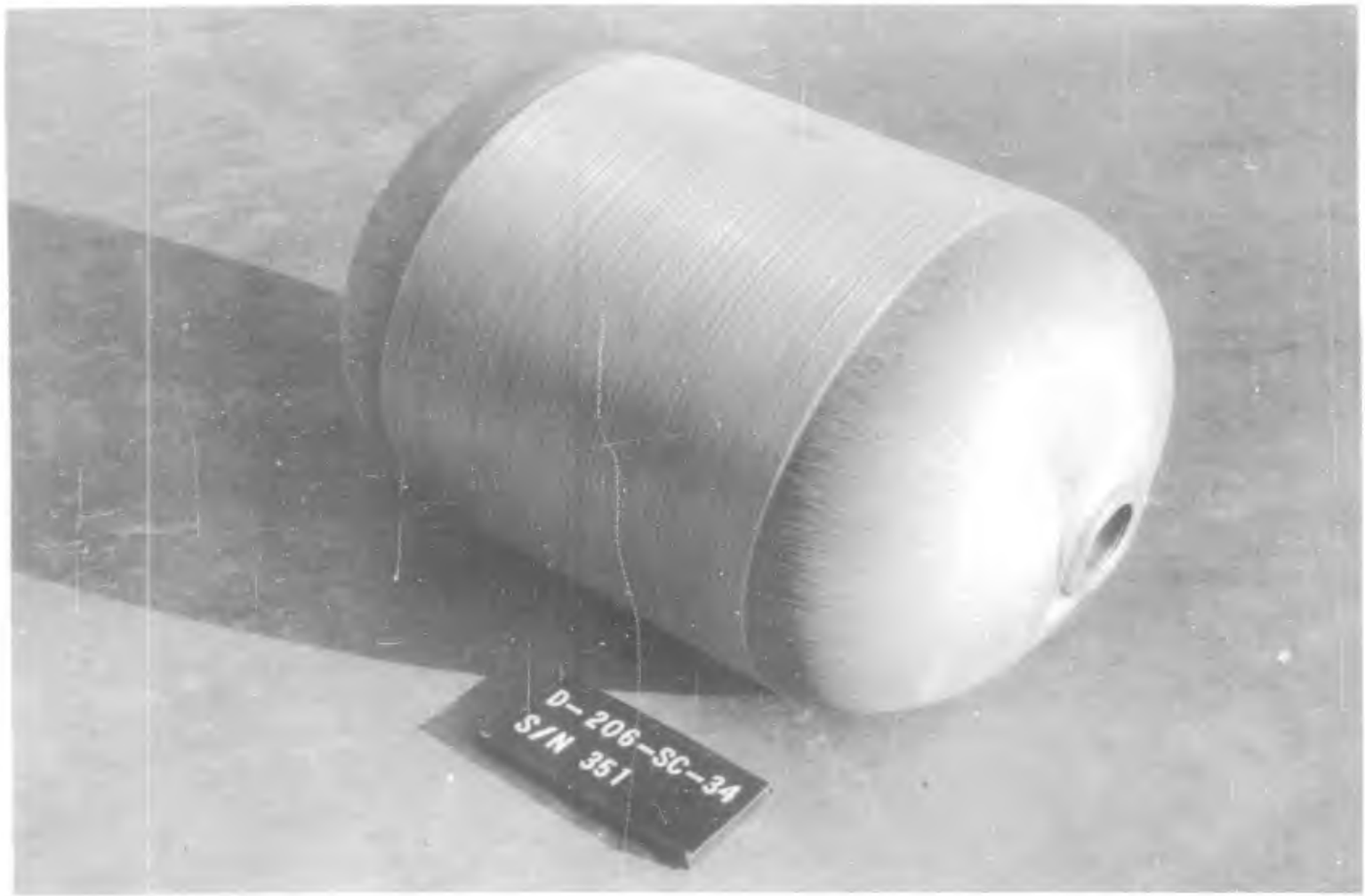

Figure 66. Serial No. 4, 18-Inch S994 Chamber Before Hydrotest

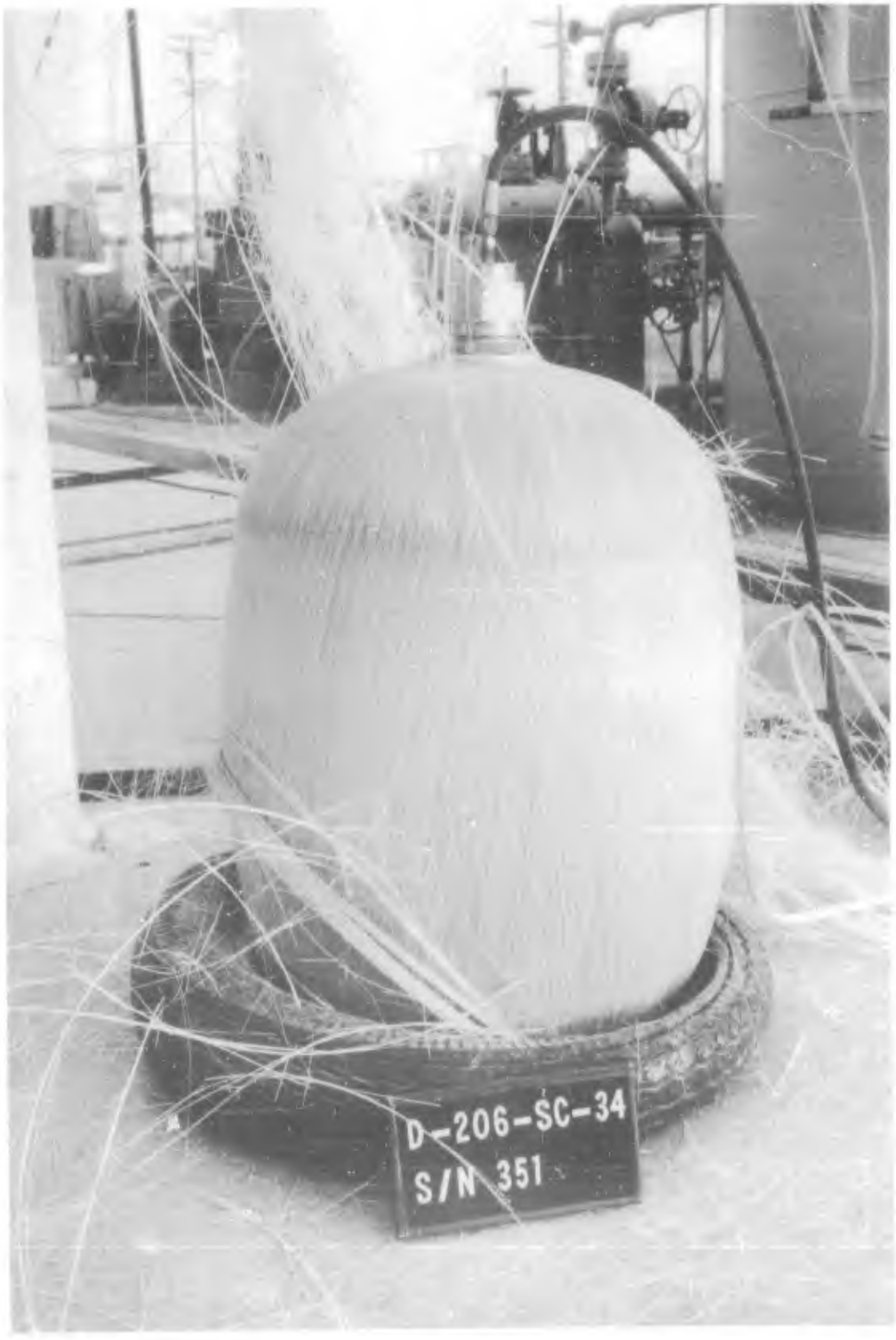

Figure 67. Serial No. 4, 18-Inch S994 Chamber After Hydrotest

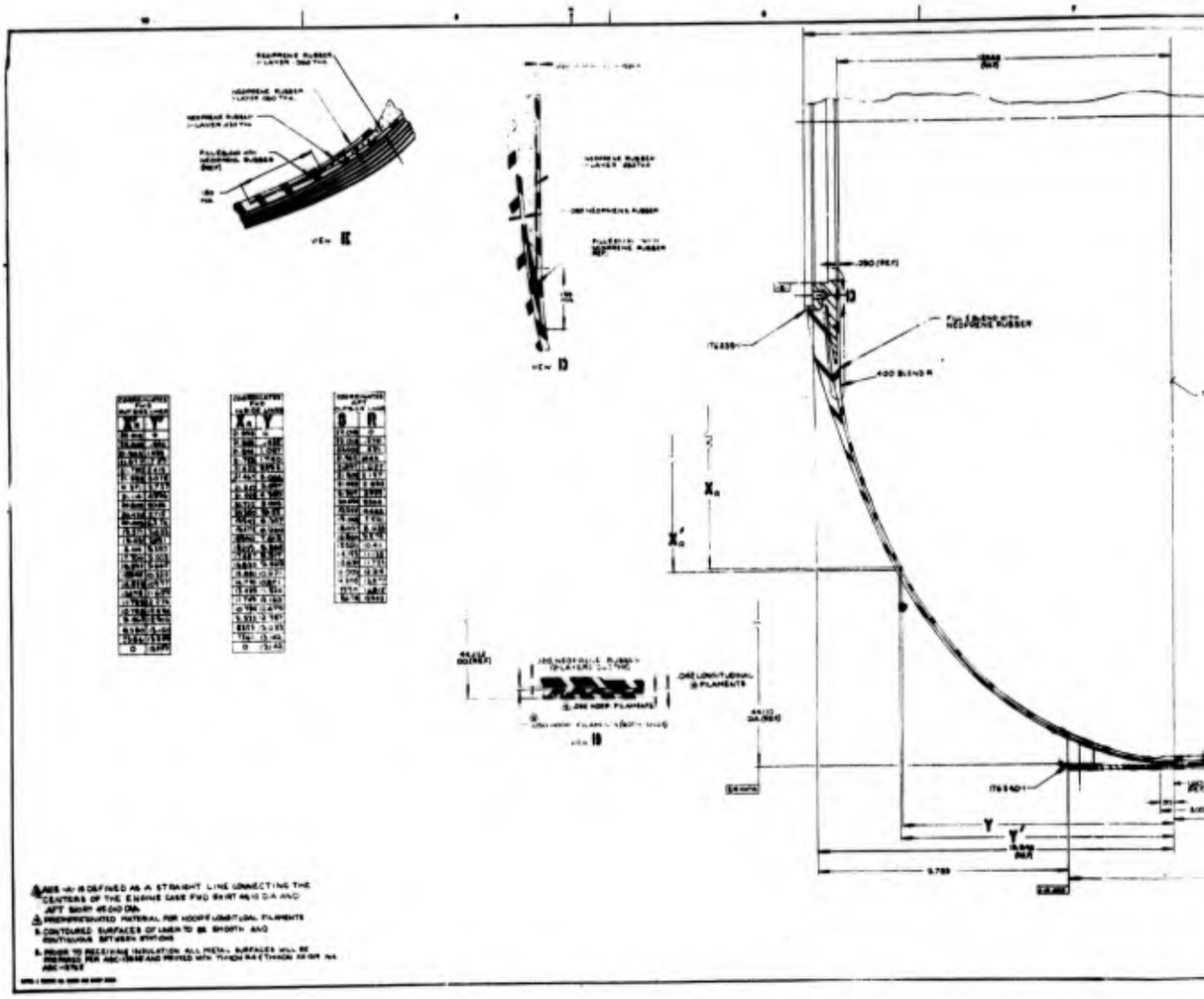

Figure

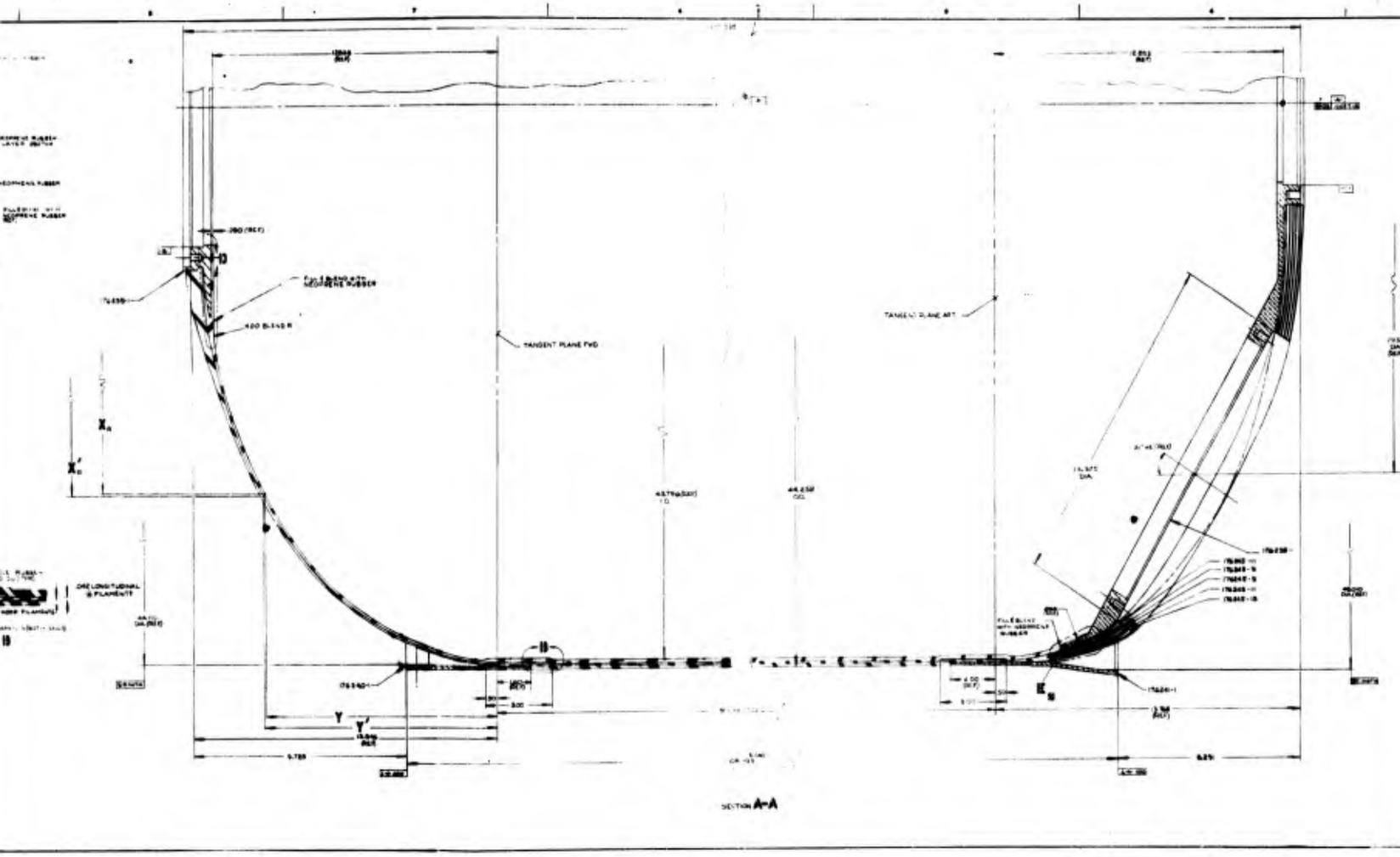

Figure 68. 44.3-Inch Chamber Assembly, Serial Nos. 3 and 4

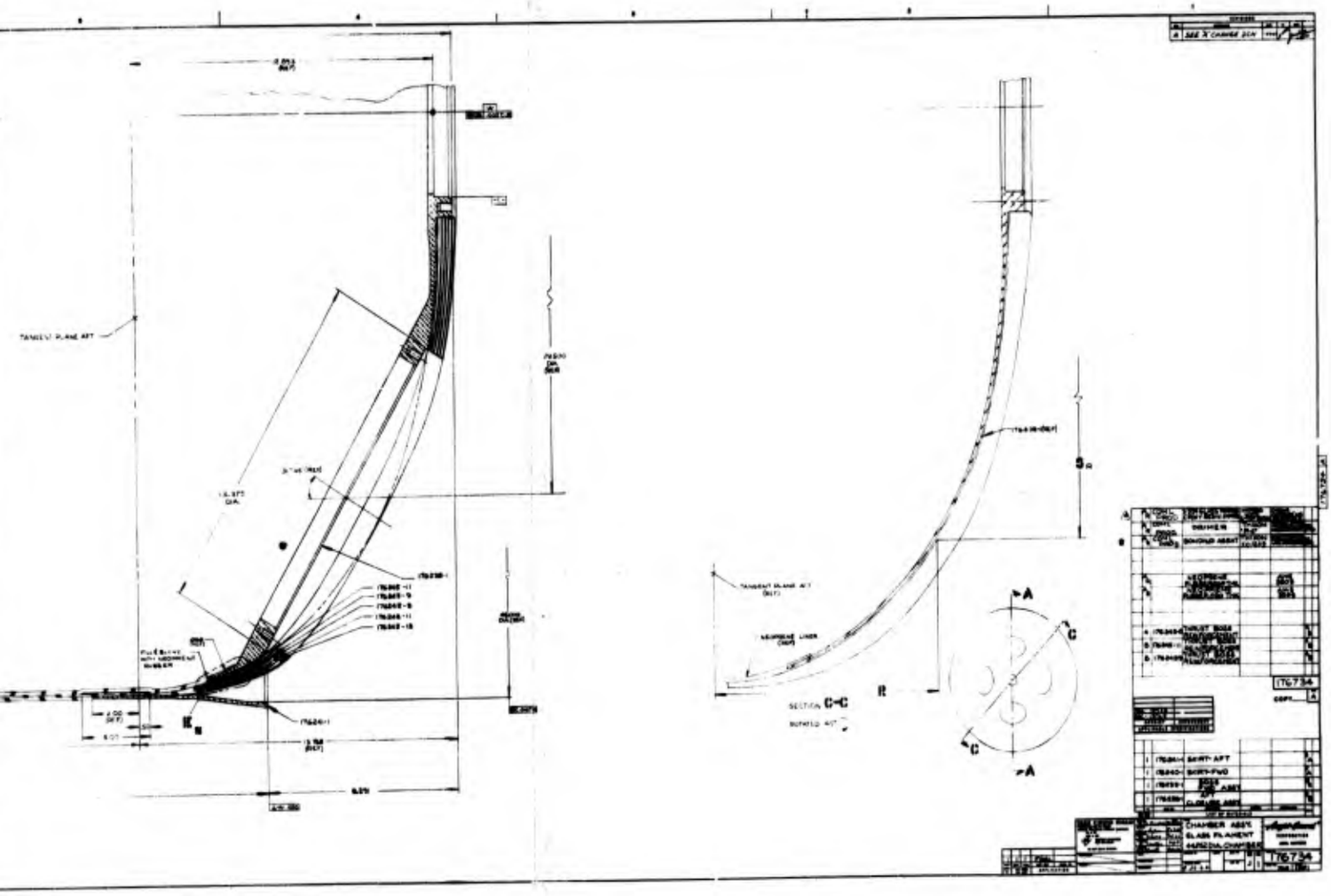

y, Serial Nos. 3 and 4

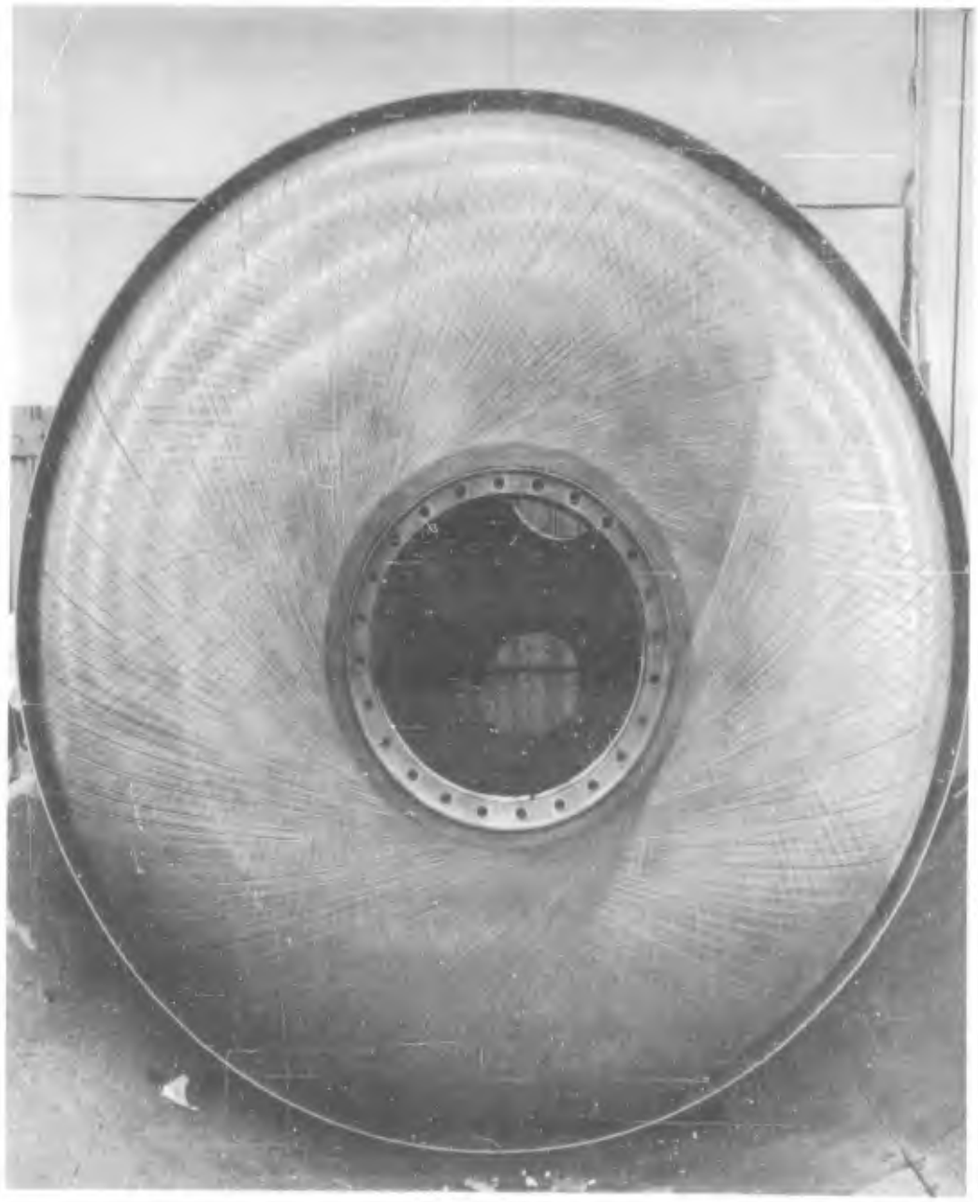

Figure 69. Serial No. 3, 44.3-Inch Chamber, Overall View of Forward Head

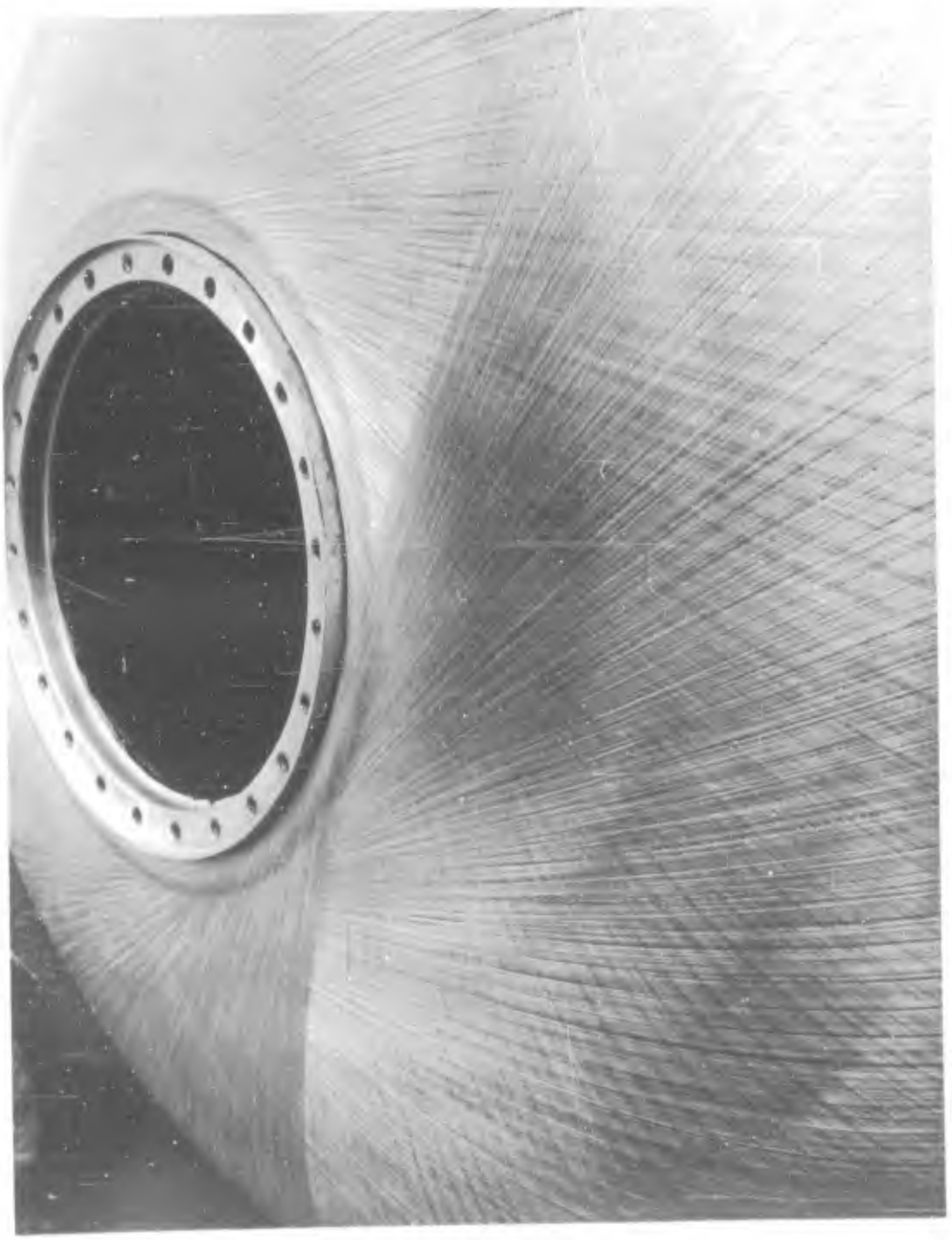

Figure 70. Serial No. 3, 44.3-Inch Chamber, Closeup View of Forward Boss

Figure 71. Serial No. 3, 44.3-Inch Chamber, Closeup View of Forward Head

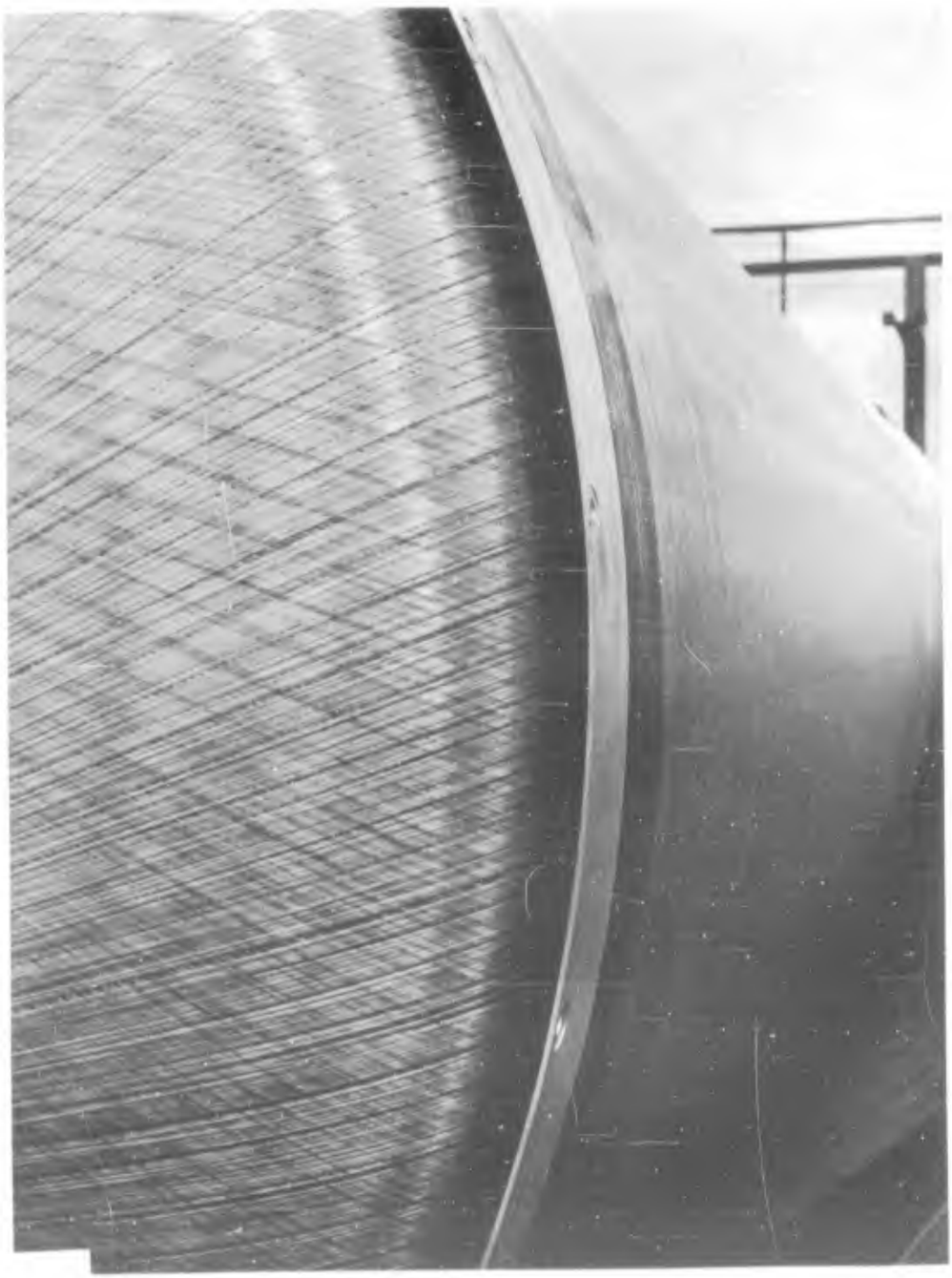

Figure 72. Serial No. 3, 44.3-Inch Chamber, Junction Between Forward Skirt and Forward Head

Figure 73. Serial No. 3, 44.3-Inch Chamber, Clcseup View of Cylindrical Section

Figure 74. Serial No. 3, 44.3-Inch Chamber, Overall View of Aft Head

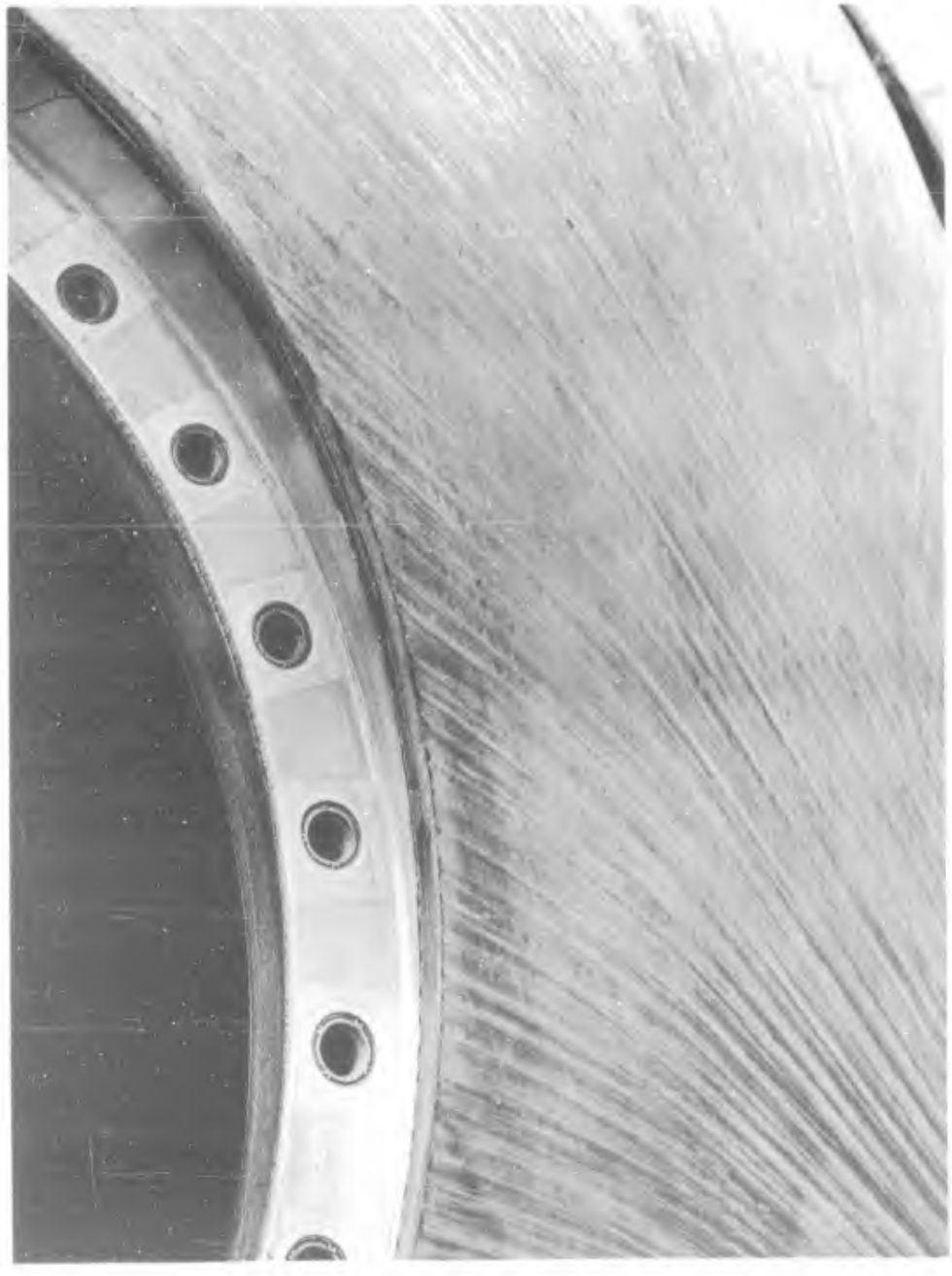

Figure 75. Serial No. 3, 44.3-Inch Chamber, Closeup View of Cut-Filament Aft-Port Area

Figure 76. Serial No. 3, 44.3-Inch Chamber, Junction Between Aft Skirt and Aft Head

Figure 77. Serial No. 3, 44.3-Inch Chamber, Forward Head Prior to Hydrotest

Figure 78. Serial No. 3, 44.3-Inch Chamber, Overall View Prior to Hydrotest

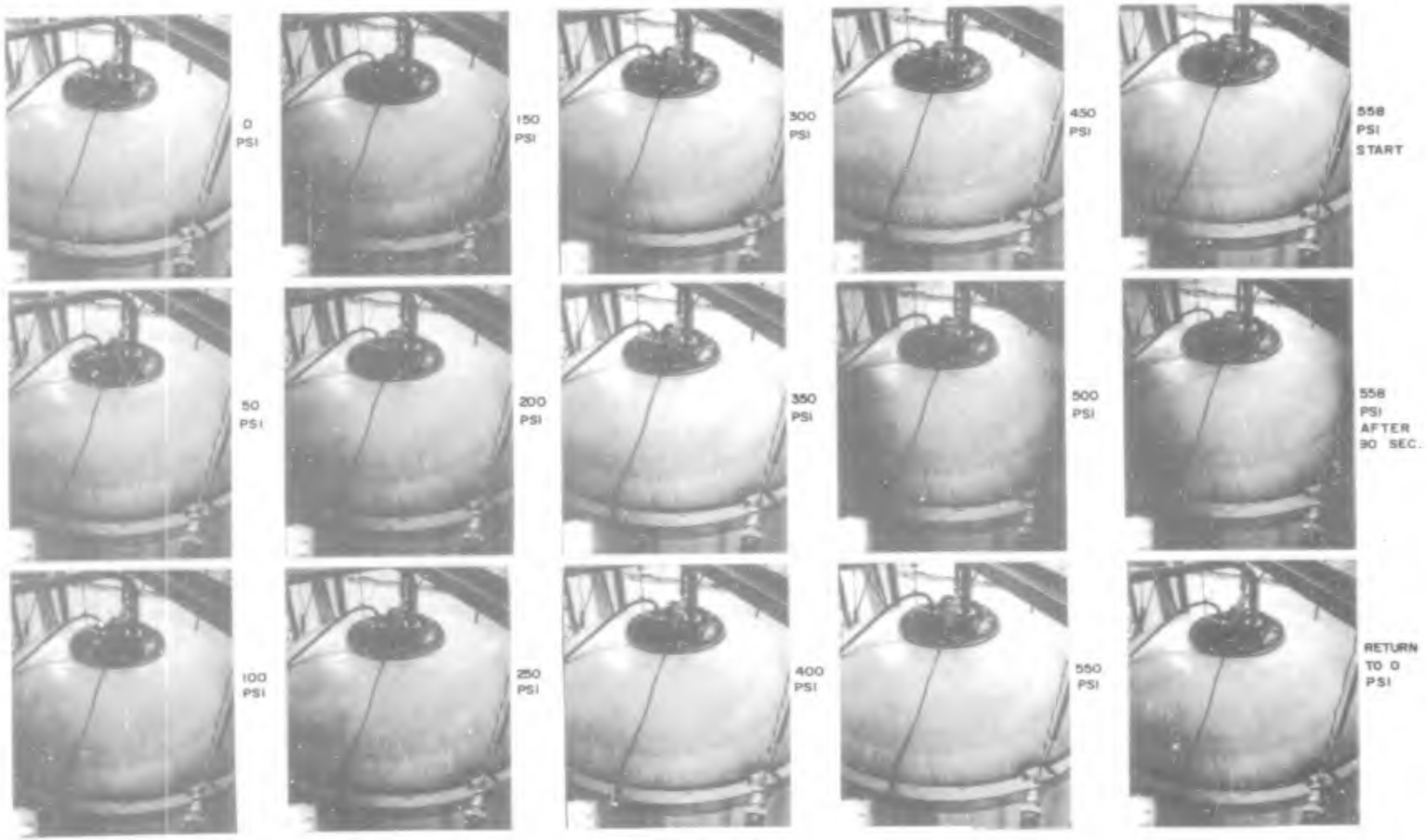

Figure 79. Serial No. 3, 44.3-Inch Chamber, Sequence Hydrotest Photos of Forward Head

Figure 80. Serial No. 3, 44.3-Inch Chamber at Moment of Hydroburst

Figure 81. Serial No. 3, 44.3-Inch Chamber After Hydroburst

Figure 82. Serial No. 4, 44.3-Inch Chamber, Structural Load Test Setup

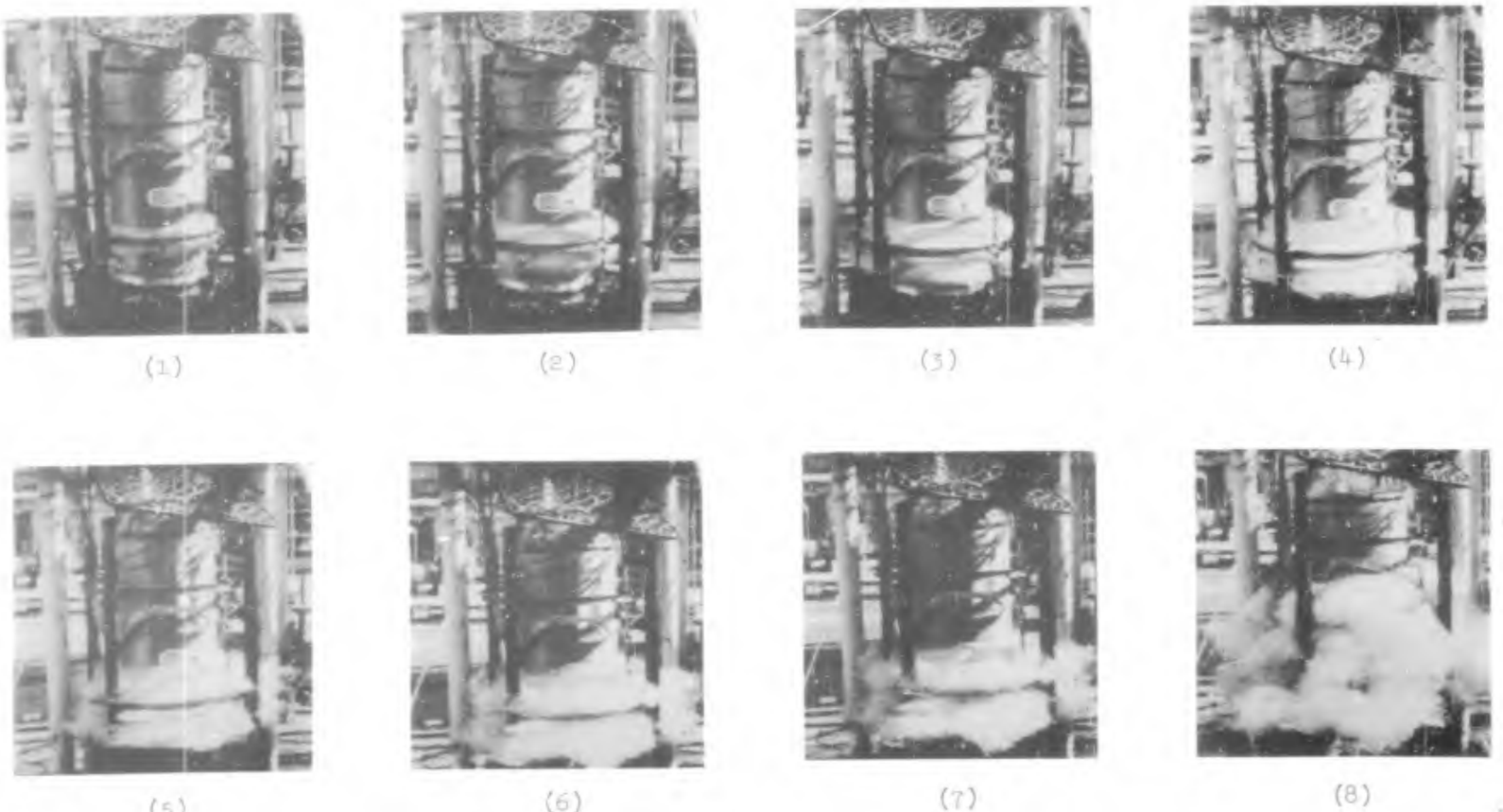

Figure 83. Serial No. 4, 44.3-Inch Chamber, Hydroburst Sequence

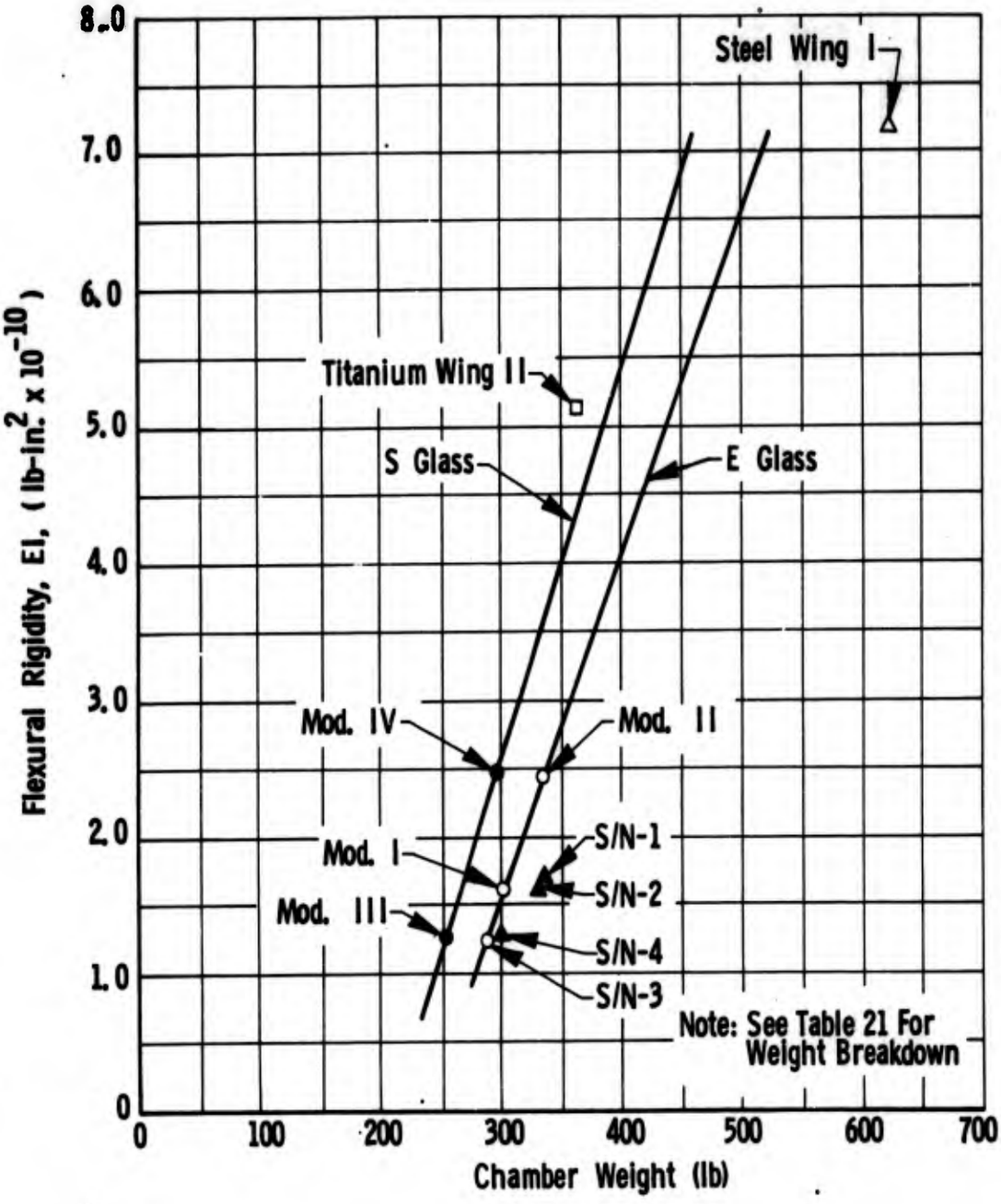

Figure 84. Flexural Rigidity vs Chamber Weight, Comparison of Various Materials, Second-Stage Minuteman Chambers

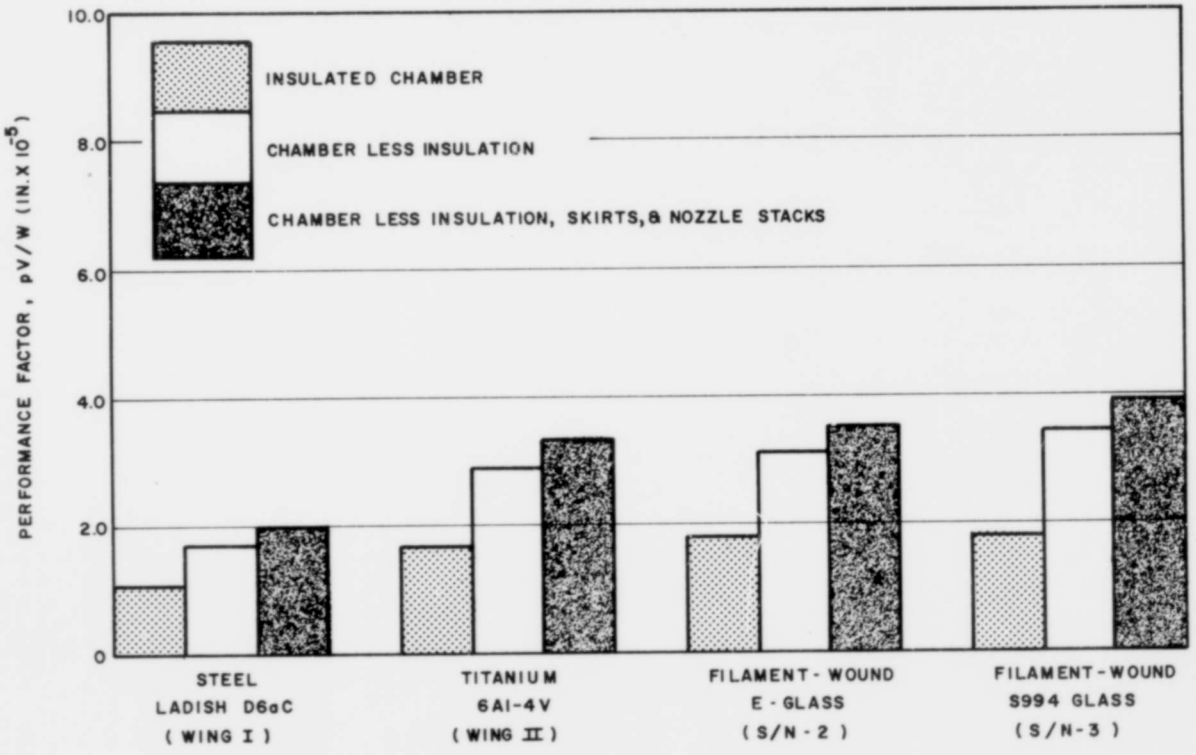

Figure 85. Performance at Proof Pressure, Second-Stage Minuteman Chambers

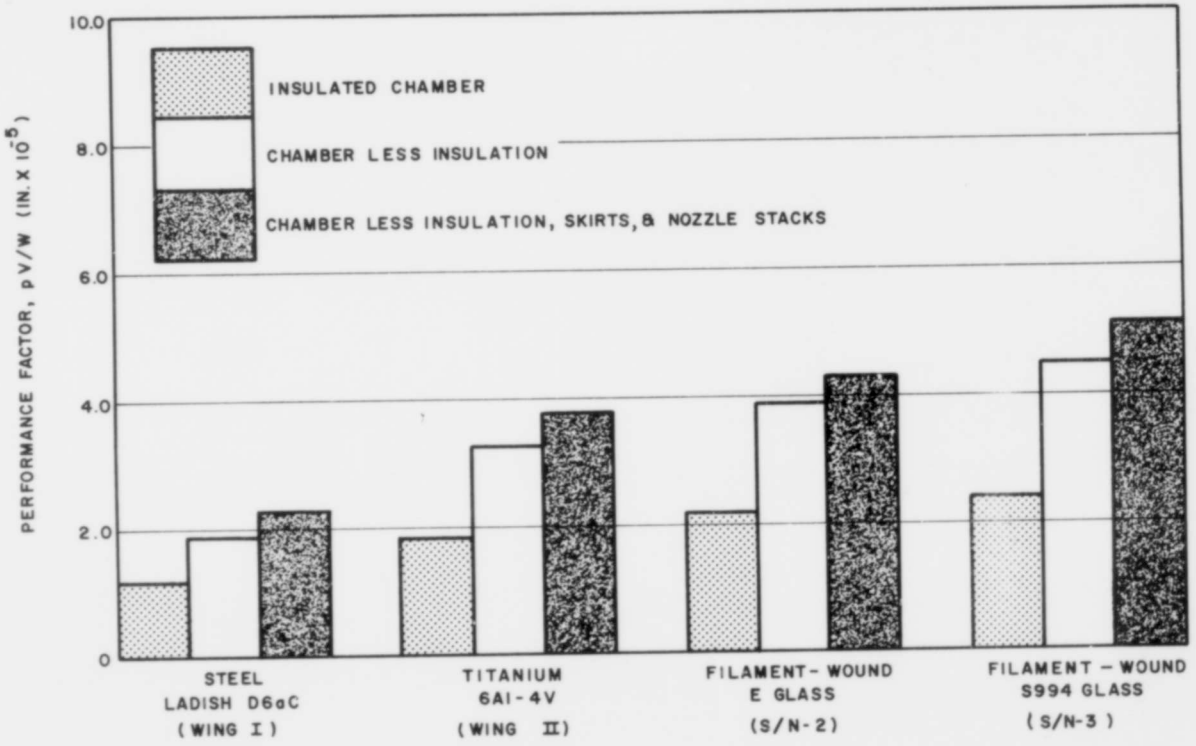

Figure 86. Performance at Burst Pressure, Second-Stage Minuteman Chambers

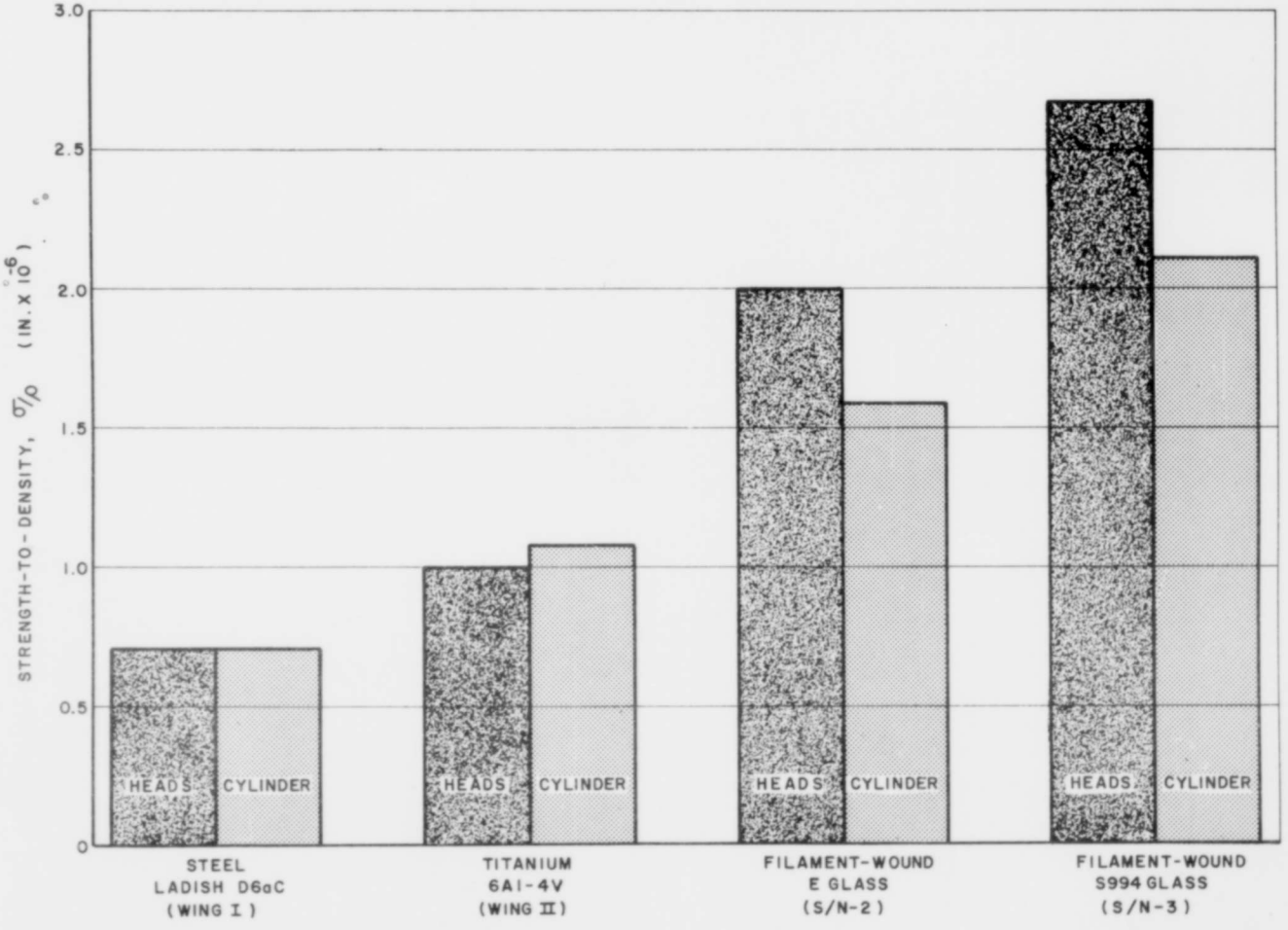

Figure 87. Ultimate Strength-to-Density Ratios, Second-Stage Minuteman Chambers

TABLE 1

DATA AND TEST RESULTS, 18-INCH-DIAME

Type of Head Contour	Part Number	D_{bf}/D_c	D_{ba}/D_c	L/D_c	Proof Pressure (psig)	Design Burst Pressure (psig)	Actual Burst Pressure (psig)	Filament Thick. Long. (in.)	Filament Thick. Hoop (in.)	Composite Thick. Long. (in.)	Composite Thick. Hoop (in.)	Area, & Dire of Fai
Geodesic Isotensoid	176435	0.2	0.2	0.6	480	600	530	0.0098	-	0.015	-	Boss, F Longitu
Balanced In-Plane	176436	0.2	0.2	0.6	600	750	893	0.0135	-	0.020	-	Knuckle Longitu
Balanced In-Plane	176437	0.5	0.5	0.6	600	750	943	0.0196	-	0.209	-	Knuckle Longitu
Balanced In-Plane	176438	0.2	0.5	0.6	600	750	690	0.0162	-	0.024	-	Knuckle Longitu
Geodesic Isotensoid	176439	0.2	0.2	2.0	480	600	580	0.0113	0.0190	0.017	0.029	Cyl., F Hoop
Geodesic Isotensoid	176440	0.5	0.5	2.0	680	850	1140	0.0247	0.0258	0.038	0.039	Cyl., F Hoop
Geodesic Isotensoid	176441	0.7	0.7	2.0	570	710	1080	0.0325	0.0143	0.051	0.022	Cyl., F Hoop
Balanced In-Plane	176442	0.2	0.2	2.0	600	750	700	0.0125	0.0239	0.019	0.036	Cyl., F Hoop
Balanced In-Plane	176443	0.5	0.5	2.0	600	750	830	0.0152	0.0233	0.023	0.035	Cyl., F Hoop
Balanced In-Plane	176444	0.7	0.7	2.0	300	375	360	0.0106	0.0113	0.015	0.016	Head, F Longit
Geodesic Isotensoid	176445	0.2	0.5	2.0	480	600	410	0.0104	0.2000	0.016	0.031	Lg. Bo Fila.t
Balanced In-Plane	176446	0.2	0.5	2.0	600	750	760	0.0144	0.0234	0.022	0.036	Lg. Bos Long.F
Geodesic Isotensoid	176447	0.2	0.7	2.0	480	600	395	0.0102	0.0205	0.016	0.033	Lg.Bos Film.t
Balanced In-Plane	176448	0.2	0.7	2.0	600	750	515	0.0155	0.0236	0.024	0.037	Lg. Bo Long.F
Balanced In-Plane	176449	0.5	0.5	4.0	600	750	830	0.0157	0.0237	0.024	0.036	Boss t Filam.
Balanced In-Plane	176450	0.7	0.7	4.0	600	750	610	0.0191	0.0222	0.029	0.034	Boss t Filam.
Balanced In-Plane	176451	0.2	0.5	4.0	600	750	125	0.0145	0.0239	0.022	0.036	Manuf in He
Balanced In-Plane	176452	0.2	0.7	4.0	600	750	540	0.0148	0.0239	0.023	0.037	Lg. F Long.F

TABLE 1

ND TEST RESULTS, 18-INCH-DIAMETER MODEL CHAMBERS, PHASE II

Filament Thick. Hoop (in.)	Composite Thick. Long. (in.)	Composite Thick. Hoop (in.)	Area, Type & Direction of Failure	Hoop Filament Stress in Cyl. (ksi)	Hoop Composite Stress in Cyl. (ksi)	Long. Filament Stress in Head (ksi)	Long. Composite Stress in Head (ksi)	Internal Volume (cu.in.)	Total Composite Weight (lb.)	Performance Factor (pV/W)	Strength to Density Head (σ/ρ)	Strength to Density Cyl. (σ/ρ)
-	0.015	-	Boss, Filam. Longitudinal	--	--	245.4	155.7	1990	1.49	0.71×10^6	2.07×10^6	--
-	0.020	-	Knuckle, Fila. Longitudinal	--	--	327.0	220.4	2030	1.96	0.92×10^6	2.93×10^6	--
-	0.209	-	Knuckle, Fila. Longitudinal	--	--	318.5	214.7	2373	2.70	0.83×10^6	2.86×10^6	--
-	0.024	-	Knuckle, Fila. Longitudinal	--	--	243.9	164.1	2180	2.26	0.67×10^6	2.19×10^6	--
0.0190	0.017	0.029	Cyl., Filam. Hoop	267.4	113.3	264.2	168.2	8218	6.24	0.76×10^6	2.10×10^6	1.49×10^6
0.0258	0.038	0.039	Cyl., Filam. Hoop	330.9	133.9	275.0	136.3	8191	11.24	0.83×10^6	1.82×10^6	1.79×10^6
0.0143	0.051	0.022	Cyl., Filam. Hoop	347.1	132.6	295.1	95.1	8338	9.00	0.79×10^6	1.27×10^6	1.77×10^6
0.0239	0.019	0.036	Cyl., Filam. Hoop	262.4	113.8	252.3	166.8	8226	7.69	0.75×10^6	2.22×10^6	1.51×10^6
0.0233	0.023	0.035	Cyl., Filam. Hoop	319.1	127.6	261.0	172.5	8265	8.14	0.86×10^6	2.30×10^6	1.70×10^6
0.0113	0.015	0.016	Head, Filam. Longitudinal	285.3	104.2	176.4	125.0	8516	4.90	0.63×10^6	1.67×10^6	1.39×10^6
0.2000	0.016	0.031	Lg. Boss, Long Fila.to Reinf	179.6	78.2	184.5	114.6	8203	7.33	0.46×10^6	1.53×10^6	1.04×10^6
0.0234	0.022	0.036	Lg. Boss to Long.Fil.Separ	296.8	119.2	248.2	161.4	8240	8.10	0.79×10^6	2.15×10^6	1.60×10^6
0.0205	0.016	0.033	Lg.Boss,Long Film.to Reinf	169.1	74.6	180.8	112.2	8113	7.62	0.42×10^6	1.50×10^6	0.99×10^6
0.0236	0.024	0.037	Lg. Boss to Long.Fil.Separ	192.3	73.6	152.7	97.0	8358	8.78	0.48×10^6	1.30×10^6	0.98×10^6
0.0237	0.024	0.036	Boss to Long. Filam.Separ.	315.7	128.8	242.7	158.8	17274	17.26	0.84×10^6	2.12×10^6	1.72×10^6
0.0222	0.029	0.034	Boss to Long. Filam.Separ.	247.9	85.9	150.8	97.4	17507	18.55	0.57×10^6	1.30×10^6	1.15×10^6
0.0239	0.022	0.036	Manuf.Damage in Head Area	--	--	--	--	17252	16.82	--	--	--
0.0239	0.023	0.037	Lg. Boss to Long.Fil.Separ.	202.7	81.7	166.5	108.5	17362	17.14	0.54×10^6	1.45×10^6	1.09×10^6

TABLE 2

CASE PARAMETERS, 44.3-INCH-DIAMETER FILAMENT-WOUND CHAMBERS

	Serial No. 1	Serial No. 2	Serial No. 3	Serial No. 4
	Aerojet-General Part Numbers			
Chamber	176244	176569	176734	176734
Hydrotest assembly	176284	176625	176370	176560
Components				
Forward boss	176239	176239	176239	176239
Aft closure	176238	176238	176238	176238
Forward skirt	176240	176240	176240	176240
Aft skirt	176241	176241	176241	176241
Reinforcement disks	176245	176245	176245	176245
	Materials			
Longitudinal glass roving	ECG 140-20E/HTS	ECG 140-20E/HTS	S994/HTS	S994/HTS
Hoop glass roving	ECG 140-20E/HTS	ECG 140-20E/HTS	S994/HTS	S994/HTS
Resin system	E-787 (prepreg)	E-787 (prepreg)	E-787 (prepreg)	E-787 (prepreg)
Reinforcement disks	1009-26 Scotchply	1009-26 Scotchply	1009-26 Scotchply	1009-26 Scotchply
Liner	Neoprene rubber	Neoprene rubber	Neoprene rubber	Neoprene rubber
Forward boss	7075-T6 aluminum	7075-T6 aluminum	7075-T6 aluminum	7075-T6 aluminum
Aft closure	7075-T6 aluminum	7075-T6 aluminum	7075-T6 aluminum	7075-T6 aluminum
Forward skirt	6061-T6 aluminum	6061-T6 aluminum	6061-T6 aluminum	6061-T6 aluminum
Aft skirt	6061-T6 aluminum	6061-T6 aluminum	6061-T6 aluminum	6061-T6 aluminum
	Boss to Case Diameter Ratios, %			
Forward boss/case	29.8	29.8	29.8	29.8
Aft boss/case	18.6	18.6	18.6	18.6
	Wrap-Pattern Criteria			
Longitudinal pattern (revolutions x turns)	4 x 174	3 x 201	3 x 172	3 x 172
Hoop pattern (layers x turns)	12 x 131	11 x 131	9 x 135	9 x 135

TABLE 2 (cont.)

	Serial No. 1	Serial No. 2	Serial No. 3	Serial No. 4
Wrap-Pattern Criteria (cont.)				
No. of strands x bandwidth, in. (longitudinal)	9 x 0.80	9 x 0.70	9 x 0.80	9 x 0.80
No. of strands x bandwidth, in. (hoop)	9 x 0.80	9 x 0.80	9 x 0.80	9 x 0.80
Head Contours				
Forward	Zero hoop stress	Balanced in plane	Balanced in plane	Balanced in plane
Aft	Zero hoop stress	Zero hoop stress	Zero hoop stress	Zero hoop stress
Mandrel Diameter, in.				
Desired	43.796	43.796	43.796	43.796
Actual	43.796	43.787	43.796	43.782
Liner OD, in.				
Desired	44.036	44.036	44.036	44.036
Actual	44.079	44.070	44.077	44.087
Chamber OD, in.				
Desired	44.360	44.302	44.252	44.252
Actual, before curing	44.385	44.255	44.286	44.310
Actual, after curing	44.264	44.212	44.199	44.223
Actual, after plaster removal	44.239	44.208	44.173	44.221
Longitudinal-Composite Thickness, in.				
Desired	0.068	0.051	0.042	0.042
Actual	0.061	0.054	0.040	0.043
Actual, per layer	0.0076	0.0090	0.0067	0.0072

TABLE 2 (cont.)

	Serial No. 1	Serial No. 2	Serial No. 3	Serial No. 4
	Hoop-Composite Thickness, in.			
Desired	0.094	0.082	0.066	0.066
Actual	0.089	0.083	0.063	0.068
Actual, per layer	0.0074	0.0075	0.0070	0.0077
	Chamber Length, Overall (Boss to Boss), in.			
Desired	127.335	127.335	127.335	127.335
Actual	126.960	126.825	127.500	127.250
	Length, Skirt to Skirt, in.			
Desired	108.933	108.933	108.933	108.933
Actual	108.615	108.750	108.950	109.00
	Length, Forward Boss to Skirt, in.			
Desired	9.789	9.789	9.789	9.789
Actual	9.429	9.650	9.325	10.000

TABLE 3

TEST RESULTS, 44.3-INCH-DIAMETER FILAMENT-WOUND CHAMBERS

	Serial No. 1	Serial No. 2	Serial No. 3	Serial No. 4
Chamber, AGC Part No.	176244	176569	176734	176734
Design Allowable Tensile Strength, ksi				
Ultimate, hoop filament	259.0	300.0	380.0	380.0
Ultimate, longitudinal filament	181.0	245.0	304.0	304.0
Ultimate, hoop composite (cylinder)	100.0	122.0	153.7	153.7
Ultimate, longitudinal composite (head)	120.0	160.0	200.0	200.0
Hoop composite (cylinder) at proof	80.0	97.5	124.5	124.5
Pressure, psi				
Proof	587	587	558	558
Design burst	734	734	734	734
Actual burst	855	730	728	696
Stress at Proof Pressure, ksi				
Hoop filament	222.6	231.8	281.8	278.9
Longitudinal filament	165.3	182.0	224.3	224.4
Hoop composite (cylinder)	86.7	94.9	119.3	111.8
Longitudinal composite (head)	106.0	119.9	153.7	143.6
Stress at Design Burst Pressure, ksi				
Hoop filament	278.3	289.7	370.6	362.0
Longitudinal filament	206.6	227.5	295.0	291.4
Hoop composite (cylinder)	108.0	118.6	157.0	145.1
Longitudinal composite (head)	133.0	150.0	202.0	186.5
Stress at Actual Burst Pressure, ksi				
Hoop filament	324.2	288.3	367.6	346.6
Longitudinal filament	240.8	226.3	292.7	278.9

TABLE 3 (cont.)

	Serial No. 1	Serial No. 2	Serial No. 3	Serial No. 4
Stress at Actual Burst Pressure, ksi (cont.)				
Hoop composite (cylinder)	126.3	118.0	155.7	138.9
Longitudinal composite (head)	154.4	149.1	200.4	178.5
Volume, cu ft				
Initial	101.60	101.21	101.90	99.7
Expansion at proof	5.09	5.83	6.20	7.2
Permanent expansion after proof cycle	0.12	0.22	0.16	-
Expansion at burst	7.76	-	7.90	-
Modulus of Elasticity (Cylinder), psi				
Tensile, hoop direction	4.52×10^6	5.40×10^6	5.81×10^6	4.92×10^6
Tensile, longitudinal	3.30×10^6	3.51×10^6	3.65×10^6	3.36×10^6
Compressive, longitudinal	-	-	-	3.22×10^6
Flexural, longitudinal	-	-	-	4.31×10^6
Rigidity, lb				
Tensile	6.85×10^7	6.65×10^7	5.20×10^7	5.17×10^7
Compressive	-	-	-	4.95×10^7
Flexural Rigidity,* lb-sq in.				
Bending	1.68×10^{10}	1.61×10^{10}	1.28×10^{10}	1.62×10^{10}
Strain at Proof Pressure, in./in.				
Hoop direction	0.0190	0.0176	0.0202	0.0203
Longitudinal direction	0.0130	0.0167	0.0164	0.0149

*The values for the Serial No. 1, 2, and 3 chambers are calculated on the basis of an assumption that the modulus of elasticity in bending (E_b) and the measured modulus of elasticity in tension (E_t) were equal. The value for the Serial No. 4 chamber is based on E_b as experimentally determined.

TABLE 3 (cont.)

	Serial No. 1	Serial No. 2	Serial No. 3	Serial No. 4
Performance Factor (pV/W), in.				
Composite structure				
Proof pressure	0.45×10^6	0.50×10^6	0.59×10^6	0.54×10^6
Burst pressure	0.66×10^6	0.63×10^6	0.76×10^6	0.66×10^6
Composite structure & metal components				
Proof pressure	0.32×10^6	0.33×10^6	0.37×10^6	0.35×10^6
Burst pressure	0.47×10^6	0.41×10^6	0.48×10^6	0.43×10^6
Ultimate Strength/Density Ratio (σ/ρ), in.				
Heads	2.12×10^6	2.00×10^6	2.68×10^6	2.38×10^6
Cylinder	1.67×10^6	1.58×10^6	2.10×10^6	1.85×10^6
Aerojet-Strand-Test Data, Ultimate Tensile Strength, ksi				
Longitudinal layers				
Average	326	330	424.1	408.2
High	347	347	488.2	443.1
Low	308	315	377.2	379.5
Hoop layers				
Average	324	335	433.5	433.8
High	341	352	470.1	454.9
Low	308	307	410.5	411.2
Burst-pressurization rate, psig/min	339	272	379	280

TABLE 4

WEIGHT COMPARISON, 44.3-INCH-DIAMETER FILAMENT-WOUND CHAMBERS

	Weight, lb			
	Serial No. 1 Chamber, AGC Part No. 176244	Serial No. 2 Chamber, AGC Part No. 176569	Serial No. 3 Chamber, AGC Part No. 176734	Serial No. 4 Chamber, AGC Part No. 176734
Total weight	440.0	417.0	370.6	380.0
Composite structures	227.0	203.5	167.8	179.9
Longitudinal filaments	98.5	83.5	59.8	74.1
Glass	79.8	67.7	49.4	59.0
Resin	18.7	15.8	10.4	15.1
Hoop filaments	91.0	88.9	71.7	70.4
Glass	74.6	71.8	59.1	56.2
Resin	16.4	17.1	12.6	14.2
Nozzle reinforcements	37.5	31.1	36.3	35.4
Glass	27.7	23.0	26.9	26.5
Resin	9.8	8.1	9.4	8.9
Metal hardware components	95.0	109.7	98.0	96.4
Forward boss	5.5	5.1	6.0	5.5
Aft closure	73.5	88.0	74.0	75.0
Forward skirt	6.0	6.5	7.0	5.9
Aft skirt	10.0	10.1	11.0	10.0
Liner	118.0	103.8	104.8	103.7

TABLE 5

MATERIAL TEST DATA, AS-RECEIVED S994 20-END HTS ROVING, LOT F-1053
(END USE: 44.3-INCH-DIAMETER CHAMBER, SERIAL NO. 3)

	Owens-Corning Tests				U.S. Polymeric Tests			
	High	Low	Average	Standard Deviation	High	Low	Average	Standard Deviation
Ultimate tensile strength, ksi	535.7	405.3	488.8	41.0	513.4	443.6	477.3	21.7
Weight per linear yard, g	0.595	0.574	0.588	0.006	0.601	0.575	0.589	0.006
Ignition loss, %	1.77	1.36	1.53	-	2.31	1.33	1.67	-

TABLE 6

MATERIAL TEST DATA, S994 20-END HTS ROVING PREIMPREGNATED WITH E-787 RESIN SYSTEM
LOT F-1053 (END USE: 44.3-INCH-DIAMETER CHAMBER, SERIAL NO. 3)

	U.S. Polymeric Tests				Aerojet-General Tests			
	High	Low	Average	Standard Deviation	High	Low	Average	Standard Deviation
Ultimate tensile strength, ksi	479.6	408.8	442.6	17.8	488.2	387.9	429.6	29.2
Weight per linear yard, g	0.603	0.578	0.591	0.007	0.593	0.575	0.588	0.009
Ignition loss, %	22.4	15.8	17.7	-	18.98	15.58	17.44	-
Volatiles, %	1.62	1.02	1.28	-	1.57	0.93	1.25	-
Resin flow, %	10.0	5.42	6.82	-	6.75	5.41	5.99	-
Horizontal shear, ksi								
After 2-hour boil	12.1	10.2	11.2	-	12.02	10.73	11.34	-
At 250°F	2.48	1.43	1.86	-	2.56	1.92	2.22	-

TABLE 7

S994 GLASS-ROVING EVALUATION, ROLL NO. 10, LOT F-1053
(END USE: SUBSCALE CHAMBER, SERIAL NO. 3)

	Weight per Linear Yard, g	Volatiles, %	Ignition Loss, %	Ultimate Tensile Strength, ksi
Owens-Corning Tests				
As-received roving	0.581	1.36	-	405.3
U.S. Polymeric Tests				
As-received roving	0.584	1.41	-	443.6
Preimpregnated roving	0.592	1.17	17.3	467.2
Aerojet-General Tests (Preimpregnated Roving)				
After receipt	0.590	1.00	17.23	420.0
Before longitudinal wrapping	0.580	1.03	16.86	433.4
After longitudinal wrapping	0.583	1.10	15.17	398.4
After hoop wrapping	0.582	-	16.79	432.9

TABLE 8

MATERIAL TEST DATA,* NOL-RING-SPECIMEN TESTS
S994 20-END HTS ROVING IMPREGNATED WITH E-787 RESIN SYSTEM, LOT F-1053
(END USE: 44.3-INCH-DIAMETER CHAMBER, SERIAL NO. 3)

	Aerojet-General Tests		
	Roll No. 10	Roll No. 11	Roll No. 31
Resin content, wt%	17.23	17.37	18.72
Ultimate tensile strength of composite, ksi			
Average	305.1	315.3	311.5
High	316.2	320.9	319.8
Low	296.1	305.0	302.4
Ultimate tensile strength of filaments, ksi			
Average	437.0	454.0	460.0
High	453.0	462.0	473.0
Low	424.0	439.0	447.0

*Specimen size: Approximately 0.250 in. wide by 0.060 in. thick.
Test equipment: Riehle Universal Testing Machine.
Head travel: 0.1 in./min.
Total number of specimens: Six from each roll.

TABLE 9

MATERIAL TEST DATA, AS-RECEIVED YM31A 20-END HTS ROVING
(END USE: 44.3-INCH-DIAMETER CHAMBER, SERIAL NO. 4)

Roll No.	Ultimate Tensile Strength, ksi*			Weight per Linear Yard, g**			Ignition Loss, %**		
	High	Low	Average	High	Low	Average	High	Low	Average
1	284.6	207.7	247.2	0.727	0.718	0.722	1.51	1.49	1.50
2	300.4	211.5	247.5	0.710	0.708	0.709	1.66	1.53	1.62
3	257.8	223.7	240.8	0.709	0.703	0.704	2.63	2.34	2.49
4	278.5	156.4	238.9	0.730	0.700	0.714	2.51	1.76	2.05
5	345.7	225.6	277.8	0.723	0.713	0.718	1.91	1.38	1.64
6	283.9	202.3	241.5	0.711	0.704	0.708	2.63	2.34	2.44
7	286.7	137.7	227.7	0.708	0.709	0.798	1.52	1.39	1.43
8	312.4	262.7	286.7	0.725	0.724	0.724	1.50	1.36	1.45
9	329.2	231.4	265.1	0.716	0.711	0.713	1.52	1.39	1.47
10	258.1	135.4	202.0	0.710	0.709	0.709	1.25	1.12	1.21
11	283.6	107.1	216.4	0.717	0.711	0.714	1.39	1.38	1.38
Av	-	-	244.7	-	-	0.712	-	-	1.70

*Average value on each roll represents four specimens per test.
**Average value on each roll represents three specimens per test.

TABLE 10

MATERIAL TEST DATA, AS-RECEIVED S994 20-END HTS ROVING, LOT F-1226
(END USE: 44.3-INCH-DIAMETER CHAMBER, SERIAL NO. 4)

	Owens-Corning Tests				U.S. Polymeric Tests			
	High	Low	Average	Standard Deviation	High	Low	Average	Standard Deviation
Ultimate tensile strength, ksi	474.0	407.0	440.1	17.9	452.4	400.3	425.5	11.8
Weight per linear yard, g	0.642	0.584	0.616	0.015	0.651	0.586	0.619	0.016
Ignition loss, %	1.87	1.54	1.69	-	1.85	1.34	1.68	-

TABLE 11

MATERIAL TEST DATA, S994 20-END HTS ROVING PREIMPREGNATED WITH E-787 RESIN SYSTEM
LOT F-1226 (END USE: 44.3-INCH-DIAMETER CHAMBER, SERIAL NO. 4)

	U.S. Polymeric Tests				Aerojet-General Tests			
	High	Low	Average	Standard Deviation	High	Low	Average	Standard Deviation
Ultimate tensile Strength, ksi	419.3	345.5	383.8	17.2	446.8	364.3	404.8	19.2
Weight per linear yard, g	0.690	0.580	0.628	0.027	0.664	0.582	0.629	0.026
Ignition loss, %	22.4	17.0	19.1	-	21.37	18.99	19.91	-
Volatiles, %	2.32	1.41	1.83	-	1.03	0.64	0.77	-
Resin flow, %	11.50	5.01	6.13	-	6.86	5.42	5.99	-
NOL-ring segments: horizontal shear, ksi								
After 2-hour boil	12.5	10.6	11.8	-	13.0	12.8	12.8	-
At 250°F	2.29	1.43	1.84	-	2.68	2.40	2.60	-

TABLE 12

MATERIAL TEST DATA,* NOL-RING-SPECIMEN TESTS
S994 20-END HTS ROVING IMPREGNATED WITH E-787 RESIN SYSTEM, LOT F-1226
(END USE: 44.3-INCH-DIAMETER CHAMBER, SERIAL NO. 4)

	Aerojet-General Tests				
	Roll No. 1	Roll No. 4	Roll No. 5	Roll No. 8	Roll No. 16
Resin content, wt%	19.51	19.02	19.67	19.61	20.16
Ultimate tensile strength of composite, ksi					
Average	266.2	269.2	264.6	279.1	279.4
High	282.5	285.4	266.7	292.3	292.4
Low	241.6	253.1	357.8	254.9	270.4
Ultimate tensile strength of filaments, ksi					
Average	400.8	401.2	399.7	421.6	426.5
High	425.4	425.3	402.9	441.5	446.4
Low	363.9	377.1	389.4	385.0	412.9

*Specimen size: Approximately 0.250 in. wide by 0.060 in. thick.
Test equipment: Riehle Universal Testing Machine.
Head travel: 0.1 in./min.
Total number of specimens: Five from each roll.

TABLE 11

MATERIAL TEST DATA, S994 20-END HTS ROVING PREIMPREGNATED WITH E-787 RESIN SYSTEM
LOT F-1226 (END USE: 44.3-INCH-DIAMETER CHAMBER, SERIAL NO. 4)

	U.S. Polymeric Tests				Aerojet-General Tests			
	High	Low	Average	Standard Deviation	High	Low	Average	Standard Deviation
Ultimate tensile Strength, ksi	419.3	345.5	383.8	17.2	446.8	364.3	404.8	19.2
Weight per linear yard, g	0.690	0.580	0.628	0.027	0.664	0.582	0.629	0.026
Ignition loss, %	22.4	17.0	19.1	-	21.37	18.99	19.91	-
Volatiles, %	2.32	1.41	1.83	-	1.03	0.64	0.77	-
Resin flow, %	11.50	5.01	6.13	-	6.86	5.42	5.99	-
NOL-ring segments: horizontal shear, ksi								
After 2-hour boil	12.5	10.6	11.8	-	13.0	12.8	12.8	-
At 250°F	2.29	1.43	1.84	-	2.68	2.40	2.60	-

TABLE 12

MATERIAL TEST DATA,* NOL-RING-SPECIMEN TESTS
S994 20-END HTS ROVING IMPREGNATED WITH E-787 RESIN SYSTEM, LOT F-1226
(END USE: 44.3-INCH-DIAMETER CHAMBER, SERIAL NO. 4)

	Aerojet-General Tests				
	Roll No. 1	Roll No. 4	Roll No. 5	Roll No. 8	Roll No. 16
Resin content, wt%	19.51	19.02	19.67	19.61	20.16
Ultimate tensile strength of composite, ksi					
Average	266.2	269.2	264.6	279.1	279.4
High	282.5	285.4	266.7	292.3	292.4
Low	241.6	253.1	357.8	254.9	270.4
Ultimate tensile strength of filaments, ksi					
Average	400.8	401.2	399.7	421.6	426.5
High	425.4	425.3	402.9	441.5	446.4
Low	363.9	377.1	389.4	385.0	412.9

*Specimen size: Approximately 0.250 in. wide by 0.060 in. thick.
Test equipment: Riehle Universal Testing Machine.
Head travel: 0.1 in./min.
Total number of specimens: Five from each roll.

TABLE 13

MATERIAL TEST DATA, AS-RECEIVED S994 20-END HTS ROVING, LOT F-1333*
(END USE: 44.3-INCH-DIAMETER CHAMBER, SERIAL NO. 4)

	Owens-Corning Tests			U.S. Polymeric Tests		
	High	Low	Average	High	Low	Average
Ultimate tensile strength, ksi	514.0	461.0	480.0	507.2	452.2	484.9
Weight per linear yard (gross), g	0.620	0.603	0.613	0.618	0.607	0.611
Ignition loss, %	1.77	1.49	1.62	2.25	1.64	2.15

*Thirteen rolls of material were rejected at U.S. Polymeric for excessive catenary. Replaced by Owens-Corning Fiberglas.

TABLE 14

MATERIAL TEST DATA, AS-RECEIVED S994 20-END HTS ROVING, LOT F-1379*
(END USE: 44.3-INCH-DIAMETER CHAMBER, SERIAL NO. 4)

	Owens-Corning Tests			U.S. Polymeric Tests		
	High	Low	Average	High	Low	Average
Ultimate tensile strength, ksi	489.0	454.0	467.0	468.2	403.6	436.0
Weight per linear yard, g	0.608	0.591	0.600	0.608	0.592	0.600
Ignition loss, %	1.55	1.23	1.38	1.54	0.93	1.17

*Replacement material for 13 rolls of Lot F-1333 rejected by U.S. Polymeric for excessive catenary.

TABLE 15

MATERIAL TEST DATA, S994 20-END HTS ROVING IMPREGNATED WITH E-787 RESIN SYSTEM
LOT F-1333* (END USE: 44.3-INCH-DIAMETER CHAMBER, SERIAL NO. 4)

	U.S. Polymeric Tests			Aerojet-General Tests		
	High	Low	Average	High	Low	Average
Ultimate tensile shear strength, ksi	382.9	302.2	334.0	411.5	324.4	377.8
Weight per linear yard, g	0.619	0.595	0.609	0.619	0.599	0.611
Ignition loss, %	22.2	19.6	20.6	23.0	21.4	22.1
Volatiles, %	-	-	-	1.74	0.85	1.25
Resin flow, %	7.35	5.35	6.31	9.07	7.16	8.20
Horizontal shear, ksi						
After 2-hour water boil	12.8	11.5	12.0	12.0	7.2	10.1
At 250°F	1.77	1.42	1.67	2.21	0.89	1.45

*Fifteen rolls of material only; 13 rolls previously rejected.

TABLE 16

MATERIAL TEST DATA, S994 20-END HTS ROVING IMPREGNATED WITH E-787 RESIN SYSTEM
LOT F-1379 (END USE: 44.3-INCH-DIAMETER CHAMBER, SERIAL NO. 4)

	U.S. Polymeric Tests			Aerojet-General Tests		
	High	Low	Average	High	Low	Average
Ultimate tensile strength, ksi	422.3	418.3	420.3	454.9	411.1	434.1
Weight per linear yard, g	0.603	0.590	0.598	0.605	0.588	0.595
Ignition loss, %	22.1	19.2	21.0	22.2	18.6	20.6
Volatiles, %	1.54	0.93	1.17	1.28	0.97	1.13
Resin flow, %	9.8	9.3	9.6	11.7	9.9	10.7
Horizontal shear, ksi						
After 2-hour water boil	12.5	10.9	11.9	12.4	8.7	10.5
At 250°F	2.62	2.31	2.50	3.57	2.95	3.30

TABLE 17

S994 GLASS ROVING PREIMPREGNATED WITH E-787 RESIN SYSTEM
SELECTED FOR USE ON 44.3-INCH-DIAMETER CHAMBER, SERIAL NO. 4

Lot No.	Roll No.	Weight per Linear Yard, g	Resin Content %	Ultimate Tensile Strength, ksi			
				Dry-Roving Test		Prepreg Test	
				Owens-Corning	U.S. Polymeric	U.S. Polymeric	Aerojet
F-1333	3	0.611	20.6	514.0	-	322.7	390.3
F-1333	5	0.603	19.9	492.0	-	349.3	401.3
F-1333	7	0.595	22.2	477.0	-	381.3	411.5
F-1333	8	0.619	19.5	496.0	-	382.9	389.0
F-1333	11	0.610	20.5	473.0	-	311.4	403.3
F-1333	14	0.595	20.5	466.0	-	302.2	379.5
F-1379	1	0.601	20.1	489.0	403.6	-	429.5
F-1379	2	0.593	20.5	478.0	416.1	-	440.1
F-1379	3	0.589	19.8	455.0	422.7	418.3	443.1
F-1379	4	0.596	20.6	478.0	420.8	-	454.9
F-1379	5	0.605	20.4	456.0	444.7	-	433.8
F-1379	6	0.598	19.8	458.0	437.4	-	431.6
F-1379	7	0.591	19.1	454.0	431.5	-	436.7
F-1379	8	0.590	19.2	469.0	444.3	-	437.5
F-1379	9	0.596	19.8	452.0	443.5	420.2	411.2
F-1379	10	0.599	19.6	467.0	448.7	422.3	445.4
F-1379	11	0.588	22.1	459.0	443.3	-	429.1
F-1379	12	0.598	21.4	489.0	448.9	-	424.3
Average	-	0.599	21.3	473.4	-	-	441.8
				Alternate Rolls			
F-1333	13	0.613	20.5	475.0	-	340.6	371.8
F-1333	15	0.611	20.6	461.0	495.0	338.1	372.2

TABLE 18

S994 GLASS-ROVING EVALUATION, ROLL NO. 4, LOT F-1333
(END USE: SUBSCALE CHAMBER, SERIAL No. 4)

	Weight per Linear Yard g	Volatiles %	Ignition Loss %	Ultimate Tensile Strength, ksi
		Owens-Corning Tests		
As-received roving	0.617	-	1.57	487.0
		U.S. Polymeric Tests		
As-received roving	0.618	-	1.64	452.2
Preimpregnated roving	0.611	1.73	20.40	352.9
		Aerojet-General Tests		
After receipt	0.610	1.74	21.43	392.2
Before longitudinal wrap	0.608	1.05	22.14	391.1
After longitudinal wrap	0.610	1.18	23.45	380.3
After hoop wrap	0.617	1.44	24.52	418.3

TABLE 19

S994 GLASS-ROVING EVALUATION - SUBSCALE, 18-INCH-DIAMETER CHAMBER, SERIAL NO. 3

	Present Program*	Polaris Program**
Glass roving	S994 HTS, Roll No. 10, Lot F-1053	"E" HTS
Resin system	E-787 preimpregnation	E-787 preimpregnation
Test temperature	Ambient	Ambient
Wrap pattern	Standard, balanced in plane	Standard, balanced in plane
Burst pressure, psig	1313	1080
Glass weight, lb		
Longitudinal composite	3.65	3.96
Hoop composite	2.47	2.83
Stress (burst), ksi		
Longitudinal filament	375.0	295.0
Hoop filament	388.0	307.0
Longitudinal composite	251.0	195.0
Hoop composite	177.0	134.0
Mode of failure	Hoop	Hoop
Pressurization rate, psig/min	148	150

*Composite structure of subscale, 18-in.-dia chamber fabricated entirely from Roll No. 10.

**To date of Serial No. 3 testing, latest standard control unit (Serial No. 277) fabricated and tested in the Polaris subscale program.

TABLE 20

S994 GLASS-ROVING EVALUATION - SUBSCALE, 18-INCH-DIAMETER CHAMBER, SERIAL NO. 4

	Present Program*	Polaris Program**
Glass roving	S994 HTS, Roll No. 4, Lot F-1333	S994 HTS, Roll No. 57, Lot F-1351
Resin system	E-787 preimpregnation	58-68R
Test temperature	Ambient	Ambient
Wrap pattern	Standard, balanced in plane	Standard, balanced in plane
Burst pressure, psig	1385	1390
Glass weight, lb		
Longitudinal composite	4.09	3.87
Hoop composite	2.85	2.69
Stress (burst), ksi		
Longitudinal filament	376.7	377.4
Hoop filament	403.6	404.4
Longitudinal composite	241.8	257.8
Hoop composite	170.4	180.1
Mode of failure	Hoop	Hoop
Pressurization rate, psig/min	142	350

*Composite structure of subscale, 18-in.-dia chamber fabricated entirely from Roll No. 4, Lot F-1333.

**To date of Serial No. 4 testing, latest standard control unit (Serial No. 359) fabricated and tested in the Polaris subscale program.

TABLE 21

WEIGHT COMPARISON
HOMOGENEOUS AND FILAMENT-WOUND CASE DESIGNS FOR SECOND-STAGE MINUTEMAN

	Weight, lb									
	Steel (Wing I)	Titanium (Wing II)	Filament-Wound Chambers*							
			S/N 1	S/N 2	Mod I	Mod II	S/N 3	Mod III	Mod IV	S/N 4
Insulated chamber, total	956.3	621.6	599.0	590.2	560.2	594.2	542.8	512.3	547.8	553.5
Chamber, total	627.8	364.6	342.0	333.2	303.2	337.2	285.8	255.3	290.8	296.5
Case	536.1	321.0	306.0	296.6	266.6	300.6	248.8	218.8	254.3	260.6
Skirts	59.1	25.6	16.0	16.6	16.6	16.6	17.0	17.0	17.0	15.9
Nozzle stacks**	32.6	18.0	20.0	20.0	20.0	20.0	20.0	20.0	20.0	20.0
Insulation**	328.5	257.0	257.0	257.0	257.0	257.0	257.0	257.0	257.0	257.0

*The Mod I and Mod III chambers were respectively the Serial No. (S/N) 2 and 3 test chambers minus excess weight (30 lb) removed from the aft boss plate. The Mod II and Mod IV chambers were respectively equivalent to the Mod I and Mod II chambers with the additional composite structure necessary to meet flight conditions (see tabulation in Section IV,G of text).

**The nozzle-stack and insulation weights shown for the filament-wound chambers are estimated values.

APPENDIX I

STRUCTURAL ANALYSIS – SERIAL NO. 1, 44.3-INCH, "E" GLASS CHAMBER

The fabricated Serial No. 1, 44.3-in.-dia, "E" glass, filament-wound chamber is analyzed below on the basis of actual winding data and laboratory tests of the glass roving.

A. AREA OF SINGLE END*

$$A_{end} = \frac{W}{\rho L N_1}$$

where

W = weight of glass roving, lb

L = specimen length, in.

ρ = glass density = 0.092 lb/cu in.

N_1 = number of ends

W/L = 0.6535 g/yard

Therefore,

$$A_{end} = \frac{0.6535 \text{ g/yard}}{(0.092 \text{ lb/cu in.})\ (36 \text{ in./yard})\ (453.6 \text{ g/lb})\ (20 \text{ ends})}$$

$$= 21.76 \times 10^{-6} \text{ sq in./end}$$

B. FILAMENT THICKNESS

1. Longitudinal

$$\text{Cross-sectional area} = \pi D_c t_f = A_{end} N_1 N_2 N_3 N_4 N_5 \frac{1}{\cos \alpha}$$

where

D_c = chamber diameter, in.

$t_{f,1}$ = longitudinal-filament thickness, in.

N_2 = number of strands per tape

N_3 = number of tapes per turn

N_4 = number of turns per revolution

---

*See Appendix V of Volume II.

N_5 = number of revolutions

α = angle between filament and meridional direction, degrees

Therefore,

$$t_{f,l} = \frac{A_{end}\ N_1\ N_2\ N_3\ N_4\ N_5}{\pi\ D_c \cos \alpha}$$

$$= \frac{(21.76 \times 10^{-6})\ (20)\ (9)\ (2)\ (174)\ (4)}{\pi\ (44.000)\ (0.996)}$$

$$= 0.0394 \text{ in.}$$

The longitudinal-composite thickness (t_l, in.) is determined as follows:

$$t_l = \frac{t_{f,l}}{P_{vg}}$$

where

P_{vg} = amount of glass filament in composite, vol%

= 0.67 (based on resin content of 18.83 wt%)

Therefore,

$$t_l = \frac{0.0394}{0.67}$$

$$= 0.061 \text{ in.}$$

2. Hoop

Cross-sectional area = $t_{f,h}\ L_c = A_{end}\ N_1\ N_2\ N_6\ N_7$

where

$t_{f,h}$ = hoop-filament thickness, in.

L_c = cylinder length, in.

N_6 = number of tapes per layer

N_7 = number of layers

Therefore,

$$t_{f,h} = \frac{A_{end}\ N_1\ N_2\ N_6\ N_7}{L_c}$$

$$= \frac{(21.76 \times 10^{-6})\ (20)\ (9)\ (131)\ (12)}{102.899}$$

$$= 0.0576 \text{ in.}$$

The hoop-composite thickness (t_h, in.) is determined as follows:

$$t_h = \frac{t_{f,h}}{P_{vg}}$$

$$= \frac{0.05758}{0.671}$$

$$= 0.089 \text{ in.}$$

C. THEORETICAL HOOP-COMPOSITE STRESS AT PROOF

$$\sigma_h = \frac{(p_p)\ (a)}{t_l + t_h}$$

$$= \frac{(587)\ (22.15)}{0.061 + 0.089}$$

$$= 86{,}700 \text{ psi}$$

D. ACTUAL STRESSES AT PROOF PRESSURE

1. Longitudinal Filament

$$\sigma_{f,l} = \frac{(p_p)\ (D_l)}{4\ (t_{f,l})\ (\cos^2 \alpha)}$$

$$= \frac{(587)\ (44.000)}{(4)\ (0.03938)\ (0.996)^2}$$

$$= 165{,}300 \text{ psi}$$

2. Hoop Filament

$$\sigma_{f,h} = \frac{(p_p)(D_h)}{2\ (t_{f,h})} \left(1 - \frac{\tan^2 \alpha}{2}\right)$$

$$= \frac{(587)\ (44.150)}{(2)\ (0.0576)} \left(1 - \frac{0.00724}{2}\right)$$

$$= 222{,}600 \text{ psi}$$

3. Longitudinal Composite (Head)

$$\sigma_l = \frac{(p_p)\ (D_l)}{4\ t_l}$$

$$\sigma_l = \frac{(587)\ (44.000)}{(4)\ (0.061)}$$

$$= 105{,}900 \text{ psi}$$

E. PREDICTED BURST PRESSURE

1. Longitudinal

$$p = p_p \left(\frac{F_{tu,f,l}}{\sigma_{f,l}}\right) \left(\frac{\sigma_{f,a}}{\sigma_{f,d}}\right)$$

where

p = predicted burst pressure, psi

$F_{tu,f,l}$ = design allowable longitudinal-filament stress, psi

$\sigma_{f,a}$ = actual average filament stress from strand-test data, psi

$\sigma_{f,d}$ = design filament stress, psi

Therefore,

$$p = 587 \left(\frac{245{,}000}{165{,}300}\right) \left(\frac{326{,}000}{350{,}000}\right)$$

$$= 811 \text{ psi}$$

Hoop

$$p_h = p_p \left(\frac{F_{tu,f,h}}{\sigma_{f,h}}\right) \left(\frac{\sigma_{f,a}}{\sigma_{f,d}}\right)$$

where

p_h = predicted burst pressure, psi

$F_{tu,f,h}$ = design allowable hoop-filament stress, psi

Therefore,

$$p_h = 587 \left(\frac{300{,}000}{222{,}600}\right) \left(\frac{324{,}000}{350{,}000}\right)$$

$$= 732 \text{ psi}$$

APPENDIX II

DESIGN ANALYSIS - SERIAL NO. 2, 44.3-INCH, "E" GLASS CHAMBER

The design of this chamber was based on the internal pressure requirements of the Minuteman second stage because it was primarily intended for use in evaluating the filament-wound structure from the standpoint of its performance as a pressure vessel. The internal pressure requirements were as follows:

Estimated operating pressure	534 psi
Proof pressure at 80°F = 1.10 x 534	587 psi
Design ultimate pressure = 1.25 x 587	734 psi

The symbols used are defined below.

A_e	effective area
A_f	area of filament
D_b	boss diameter
D_h	mean diameter of hoop composite
D_l	mean diameter of longitudinal composite
D_m	mean diameter of cylinder
F_{tu}	allowable ultimate tensile strength
$F_{tu,f,h}$	allowable ultimate tensile strength in hoop filaments
$F_{tu,f,l}$	allowable ultimate tensile strength in longitudinal filaments
M.S.	margin of safety
P_{vg}	volume of glass filament in composite
p_b	design burst pressure
p_p	design proof pressure
r	radius
$t_{f,h}$	equivalent hoop-filament thickness
$t_{f,l}$	equivalent longitudinal-filament thickness
t_h	total hoop-composite thickness

t_l total longitudinal-composite thickness

α angle between line in axial direction and filament path

$\sigma_{f,h}$ hoop-filament stress

$\sigma_{f,l}$ longitudinal-filament stress

σ_h hoop stress (total cylinder composite thickness)

σ_l longitudinal stress (total cylinder composite thickness)

A. CYLINDER

1. Longitudinal Filament

$$\sigma_{f,l} = \frac{p_b D_l}{4 t_{f,l} \cos^2\alpha}$$

where

$p_b = 734$ psi

$D_l = 44.087$ in.

$t_{f,l} = P_{vg} t_l$

$= 0.661 \times 0.051$

$= 0.0337$ in.

and

$\alpha = 4^o50'$

Therefore,

$$\sigma_{f,l} = \frac{(734)(44.087)}{(4)(0.0337)\left[\cos^2(4^o50')\right]}$$

$= 242{,}000$ psi

$$\text{M.S.} = \frac{F_{tu,f,l}}{\sigma_{f,l}} - 1$$

where

$F_{tu,f,l} = 245{,}000$ psi

Therefore,

$$\text{M.S.} = \frac{245{,}000}{242{,}000} - 1 = +0.01$$

2. Hoop Filament

Neglecting the small strength contribution of the longitudinal filaments,

$$\sigma_{f,h} = \frac{p_b D_h}{2 t_{f,h}}$$

where

$D_h = 44.220$ in.

$t_{f,h} = P_{vg} t_h$

$= 0.661 \times 0.082$

$= 0.0542$ in.

Therefore,

$$\sigma_{f,h} = \frac{(734)(44.220)}{(2)(0.0542)}$$

$= 299{,}000$ psi

$$\text{M.S.} = \frac{F_{tu,f,h}}{\sigma_{f,h}} - 1$$

$F_{tu,f,h} = 300{,}000$ psi

Therefore,

$$\text{M.S.} = \frac{300{,}000}{299{,}000} - 1 = +0.003$$

3. Composite Longitudinal (Cylinder)

$$\sigma_l = \frac{p_b D_m}{4(t_l + t_h)}$$

$D_m = 44.169$ in.

$$\sigma_l = \frac{(734)(44.169)}{4(0.051 + 0.082)}$$

$= 61{,}000$ psi

4. Composite Hoop (Cylinder)

$$\sigma_h = \frac{p_b D_m}{2(t_l + t_h)}$$

$$= \frac{(734)(44.169)}{2(0.051 + 0.082)}$$

$= 122{,}000$ psi

5. Composite Hoop at Proof Pressure (Cylinder)

$$\sigma_h = \frac{p_p D_m}{2(t_l + t_h)}$$

$$= \frac{(587)(44.169)}{2(0.051 + 0.082)}$$

$$= 97{,}500 \text{ psi}$$

B. HEADS

1. Filament at Equator (Forward and Aft)

$$\sigma_{f,l} = \frac{p_b D_l}{4\, t_{f,l} \cos^2 \alpha}$$

$$= \frac{(734)(44.087)}{4\,(0.0337)\left[\cos^2 (4^\circ 5')\right]}$$

$$= 242{,}000 \text{ psi}$$

$$\text{M.S.} = \frac{245{,}000}{242{,}000} - 1 = +0.01$$

2. Longitudinal Composite (Forward and Aft)

$$\sigma_l = \frac{p_b D_l}{4\, t_l}$$

$$= \frac{(734)(44.087)}{(4)(0.051)}$$

$$= 158{,}800 \text{ psi}$$

3. Nozzle-Port Reinforcement

$$A_e = N K A_f \sum_{n\psi = -90^\circ}^{n\psi = +90^\circ} \cos n\psi$$

where

N = number of reinforcement layers = 5

K = strength-reduction factor = 0.5 (see Appendix V of Volume II)

A_f = cross-sectional area of glass per tape = 0.0096 in.^{2}

ψ = angle between adjacent tapes = 5°

n = all integers between limits of $-\frac{90}{\psi}$ and $+\frac{90}{\psi}$

Therefore,

$$A_e = (5)(0.5)(0.0096)(22.5)$$

$$= 0.5400 \text{ in.}^2$$

$$P = \frac{p_b r_2}{2}\left|\frac{D_b}{2}\right|$$

where

r_2 = radius of curvature at center of port = 32.719 in.

D_b = 13.88 in.

Therefore,

$$P = \frac{(734)(32.719)(13.88)}{4}$$

$$= 83,400 \text{ lb}$$

$$\sigma_f = \frac{P}{A_e}$$

$$= \frac{83,400}{0.5400} = 154,400 \text{ psi}$$

$$\text{M.S.} = \frac{F_{tu}}{\sigma_f} - 1$$

F_{tu} = 180,000 psi

Therefore,

$$\text{M.S.} = \frac{180,000}{154,400} - 1 = +0.16$$

C. FORWARD BOSS

1. Flange

The forward boss is assumed to act as a circular plate with a fixed inner edge. The end-for-end wrap pattern of the longitudinal filament produces a rigid band approximately 0.70 in. wide around the boss, which supports the flange. Outside of this band, the filaments are bridged and therefore offer no additional support. The basic load (W) on the flange is shown below. Bending stress at the juncture of the flange and boss is calculated by the use of formulas for loading on a flat plate (reference: Roark, Formulas for Stress and Strain, Case 22, p. 201).

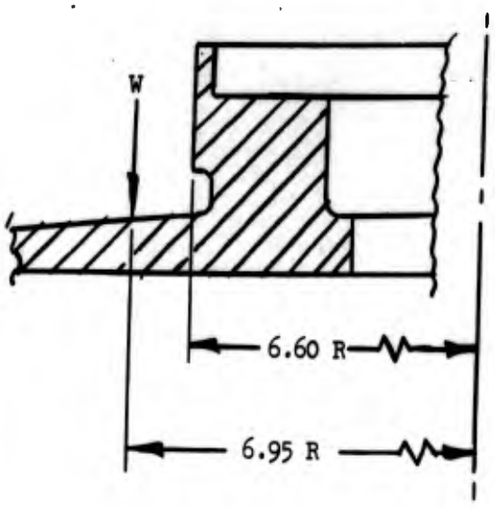

$$\sigma = \frac{\beta_{22} W}{t^2}$$

where

$$W = \pi p_b a^2$$

$$= (\pi)(734)(6.95)^2$$

$$= 111{,}300 \text{ lb}$$

$$\beta_{22} = 0.06 \text{ (for a/b = 1.053)}$$

Therefore,

$$\sigma = \frac{(0.06)(111{,}300)}{(0.312)^2}$$

$$= 68{,}600 \text{ psi}$$

$$F_{tu} = 77{,}000 \text{ psi (Mil Handbook 5)}$$

$$\text{M.S.} = \frac{77{,}000}{68{,}600} - 1 = +0.12$$

2. Threads

$$\sigma_3 = \frac{p_b a^2 \pi}{N \pi d \, l \, (0.5)}$$

$$= \frac{(734)(6.013)^2 (\pi)}{(24)(\pi)(0.368)(0.5)(0.5)}$$

$$= 12{,}000 \text{ psi}$$

$$F_{su} = 46{,}000 \text{ (Mil Handbook 5)}$$

$$= \frac{46{,}000}{12{,}000} - 1 = +2.83$$

3. Bolts

$$\text{Load per bolt} = \frac{p_b \pi r^2}{N}$$

$$= \frac{(734)(\pi)(6.060)^2}{24}$$

$$= 3530 \text{ lb}$$

F_{tu} = 11,050 lb

M.S. $= \frac{11,050}{3,530} - 1 = +2.13$

D. AFT CLOSURE

1. Off-Center Ports

a. Plate Adjacent to Ports

The stresses in this area are negligible.

b. Boss Threads

$$\sigma_s = \frac{p_b \pi a^2}{N \pi d l (0.5)}$$

$$= \frac{(734)(6.25)^2(\pi)}{(30)(\pi)(0.368)(0.5)(0.5)}$$

$$= 10,400 \text{ psi}$$

$$\text{M.S.} = \frac{46,000}{10,400} - 1 = +3.42$$

c. Bolts

$$\text{Load per bolt} = \frac{p_b \pi r^2}{N}$$

$$= \frac{(734)(\pi)(6.25)^2}{30}$$

$$= 3000 \text{ lb}$$

$$\text{M.S.} = \frac{11,050}{3000} - 1 = +2.68$$

2. Center Boss

a. Plate Adjacent to Boss

$$\sigma = \frac{\beta_{22} W}{t^2}$$

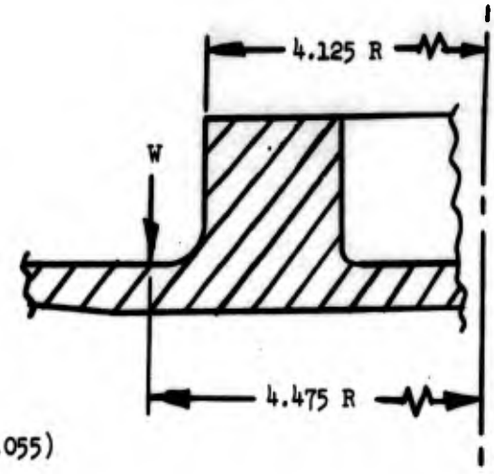

where

$W = \pi p_b a^2$

$= \pi (734)(4.475)^2$

$= 46,300$ lb

$\beta_{22} = 0.06$ (for a/b = 1.055)

Therefore,

$\sigma = \frac{(0.06)(46,300)}{(0.240)^2}$

$= 48,400$ psi

$F_{tu} = 77,000$ psi (Mil Handbook 5)

M.S. $= \frac{77,000}{48,400} - 1 = +0.59$

b. Threads

$\sigma_s = \frac{p_b \pi a^2}{N \pi d l (0.5)}$

$= \frac{(734)(\pi)(3.688)^2}{(12)(\pi)(0.368)(0.5)(0.5)}$

$= 9040$ psi

M.S. $= \frac{46,000}{9,040} - 1 = +4.09$

c. Bolts

Load per bolt $= \frac{p_b \pi r^2}{N} = \frac{(734)(\pi)(3.688)^2}{12} = 2620$ lb

$F_{tu} = 11,050$ lb

M.S. $= \frac{11,050}{2,620} - 1 = +3.22$

APPENDIX III

STRUCTURAL ANALYSIS – SERIAL NO. 2, 44.3-INCH, "E" GLASS CHAMBER

The fabricated Serial No. 2, 44.3-in.-dia, "E" glass, filament-wound chamber is analyzed below on the basis of actual winding data and laboratory tests of the glass roving.

A. AREA OF SINGLE END*

$$A_{end} = \frac{W}{\rho L N_1}$$

where

W = weight of glass roving, lb

L = specimen length, in.

ρ = glass density = 0.092 lb/cu in.

N_1 = number of ends

W/L = 0.647 g/yard

Therefore,

$$A_{end} = \frac{0.647 \text{ g/yard}}{(0.092 \text{ lb/cu in.})\ (36 \text{ in./yard})\ (453.6 \text{ g/lb})\ (20 \text{ ends})}$$

$$= 21.53 \times 10^{-6} \text{ sq in./end}$$

B. FILAMENT THICKNESS

1. Longitudinal

$$\text{Cross-sectional area} = \pi D_c t_f = A_{end} N_1 N_2 N_3 N_4 N_5 \frac{1}{\cos \alpha}$$

where

D_c = chamber diameter, in.

$t_{f,1}$ = longitudinal-filament thickness, in.

N_2 = number of strands per tape

N_3 = number of tapes per turn

N_4 = number of turns per revolution

*See Appendix V of Volume II.

N_5 = number of revolutions

α = angle between filament and meridional direction, degrees

Therefore,

$$t_{f,l} = \frac{A_{end}\, N_1\, N_2\, N_3\, N_4\, N_5}{\pi\, D_c \cos \alpha}$$

$$= \frac{(21.53 \times 10^{-6})\,(20)\,(9)\,(2)\,(201)\,(3)}{\pi\,(44.125)\,(0.996)}$$

$$= 0.0359 \text{ in.}$$

The longitudinal-composite thickness (t_l, in.) is determined as follows:

$$t_l = \frac{t_{f,l}}{P_{vg}}$$

where

P_{vg} = amount of glass filament in composite, vol%

= 0.67 (based on resin content of 19.0 wt%)

Therefore,

$$t_l = \frac{0.0359}{0.67}$$

$$= 0.054 \text{ in.}$$

2. Hoop

Cross-sectional area = $t_{f,h}\, L_c = A_{end}\, N_1\, N_2\, N_6\, N_7$

where

$t_{f,h}$ = hoop-filament thickness, in.

L_c = cylinder length, in.

N_6 = number of tapes per layer

N_7 = number of layers

Therefore,

$$t_{f,h} = \frac{A_{end}\, N_1\, N_2\, N_6\, N_7}{L_c}$$

$$= \frac{(21.53 \times 10^{-6})\,(20)\,(9)\,(131)\,(11)}{102.899}$$

$$= 0.05558 \text{ in.}$$

The hoop-composite thickness (t_h, in.) is determined as follows:

$$t_h = \frac{t_{f,h}}{P_{vg}}$$

$$= \frac{0.0555}{0.67}$$

$$= 0.083 \text{ in.}$$

C. THEORETICAL HOOP-COMPOSITE STRESS AT PROOF

$$\sigma_h = \frac{(p_p)\ (a)}{t_l + t_h}$$

$$= \frac{(587)\ (22.15)}{0.054 + 0.083}$$

$$= 94{,}900 \text{ psi}$$

D. ACTUAL STRESSES AT PROOF PRESSURE

1. Longitudinal Filament

$$\sigma_{f,l} = \frac{(p_p)\ (D_l)}{4\ (t_{f,l})\ (\cos^2 \alpha)}$$

$$= \frac{(587)\ (44.125)}{(4)\ (0.0359)\ (0.996)^2}$$

$$= 182{,}000 \text{ psi}$$

2. Hoop Filament

$$\sigma_{f,h} = \frac{(p_p)(D_h)}{2\ (t_{f,h})} \left(1 - \frac{\tan^2 \alpha}{2}\right)$$

$$= \frac{(587)\ (43.988)}{(2)\ (0.05558)} \left(1 - \frac{0.00724}{2}\right)$$

$$= 231{,}800 \text{ psi}$$

3. Longitudinal Composite (Head)

$$\sigma_l = \frac{(p_p)\ (D_l)}{4\ t_l}$$

$$\sigma_1 = \frac{(587)\ (44.125)}{(4)\ (0.054)}$$

$$= 119{,}900 \text{ psi}$$

E. PREDICTED BURST PRESSURE

1. Longitudinal

$$p = p_p \left(\frac{F_{tu,f,l}}{\sigma_{f,l}}\right) \left(\frac{\sigma_{f,a}}{\sigma_{f,d}}\right)$$

where

p = predicted burst pressure, psi

$F_{tu,f,l}$ = design allowable longitudinal-filament stress, psi

$\sigma_{f,a}$ = actual average filament stress from strand-test data, psi

$\sigma_{f,d}$ = design filament stress, psi

Therefore,

$$p = 587 \left(\frac{245{,}000}{182{,}000}\right) \left(\frac{330{,}000}{350{,}000}\right)$$

$$= 745 \text{ psi}$$

2. Hoop

$$p_h = p_p \left(\frac{F_{tu,f,h}}{\sigma_{f,h}}\right) \left(\frac{\sigma_{f,a}}{\sigma_{f,d}}\right)$$

where

p_h = predicted burst pressure, psi

$F_{tu,f,h}$ = design allowable hoop-filament stress, psi

Therefore,

$$p_h = 587 \left(\frac{300{,}000}{231{,}800}\right) \left(\frac{335{,}000}{350{,}000}\right)$$

$$= 730 \text{ psi}$$

APPENDIX IV

DESIGN ANALYSIS - SERIAL NO. 3, 44.3-INCH, S994 CHAMBER

This appendix presents the design analysis for the Serial No. 3, 44.3-in.-dia, S994, filament-wound chamber. In general, the design approach was that discussed in Appendix V of Volume II. The illustrations referred to are in Volume II, as noted. The design parameters employed are tabulated below.

Chamber diameter, D_c	44.3 in.
Chamber length, L	127.3 in.
Cylinder length, L_c	99.299 in.
Forward-boss diameter, D_{bf}	13.20 in.
Aft-boss diameter, D_{ba}	8.25 in.
Type of head contour and wrap	Balanced-in-plane
Material	S994/HTS,20 end
Design burst pressure, p	734 psi
Proof pressure, p_p	587 psi
Resin content	20 wt%
Off-center ports	Four included in aft head
Other pertinent parameters	See Table 2 (Volume I)

A. ALLOWABLE FILAMENT STRENGTH

1. Pure Strand

Laboratory tests indicate that the average ultimate strength for S994/HTS, 20-end, glass roving is 25% above the strength of ECG-140-20E-HTS glass. Therefore,

$$F_{tu,s} = (1.25)(350,000) = 437,000 \text{ psi}$$

2. Effects of Geometry*

a. Boss Diameter

$$\frac{D_b}{D_c} = \frac{D_{ba} + D_{bf}}{2D_c} = \frac{13.20 + 8.25}{(2)\ (44.3)}$$

$$= 0.242$$

$K_1 = 0.99$ (from Figure 4, Volume II)

b. Chamber Length

$$\frac{L}{D_c} = \frac{127.3}{44.3} = 2.87$$

$K_2 = 1.01$ (from Figure 5, Volume II)

*See Appendix V of Volume II.

3. Effects of Thickness*

a. Longitudinal

$$\frac{t_{f,l}}{D_c} = (0.935 \times 10^{-6})(p)(\frac{350,000}{437,000})$$

$$= (0.750 \times 10^{-6})(734)$$

$$= 550 \times 10^{-6}$$

$K_3 = 1.03$ (from Figure 6, Volume II)

b. Hoop

$$\frac{t_{f,h}}{D_c} = (1.75 \times 10^{-6})(p)(\frac{350,000}{437,000})$$

$$= (1.40 \times 10^{-6})(734)$$

$$= 1030 \times 10^{-6}$$

$K_3 = 1.04$ (from Figure 6, Volume II)

4. Effects of Chamber Diameter*

$D_c = 44.3$ in.

a. Longitudinal

$K_4 = 0.868$ (from Figure 7, Volume II)

b. Hoop

$K_4 = 0.937$ (from Figure 7, Volume II)

5. Effects of Off-Center Ports*

$K_p = 0.88$ (four off-center ports)

6. Design Allowables*

a. Longitudinal

$$F_{tu,f,l} = 0.89\, K_1\, K_2\, K_3\, K_4\, K_p\, K_{tu,s}$$

$$= (0.89)(0.99)(1.01)(1.03)(0.868)(0.88)(437,000)$$

$$= 304,000 \text{ psi}$$

*Ibid.

b. Hoop

$$F_{tu,f,h} = 0.89\ K_3 K_4\ F_{tu,s}$$

$$= (0.89)(1.04)(0.937)(437,000)$$

$$= 380,000 \text{ psi}$$

B. EQUIVALENT FILAMENT THICKNESS

1. Longitudinal

$$t_{f,l} = \frac{p\ a}{(2F_{tu,f,l})(\cos^2 \alpha)}$$

$$\tan \alpha = \frac{D_{ba} + D_{bf}}{2L} = \frac{13.20 + 8.25}{(2)(127.3)}$$

$$= 0.0842$$

$$= 4^o 49'$$

$$\cos \alpha = 0.996$$

$$t_{f,l} = \frac{(734)\ (22.15)}{(2)(304,000)(0.996)^2}$$

$$= 0.0267 \text{ in.}$$

2. Hoop

$$t_{f,h} = \frac{p\ a}{F_{tu,f,h}} \left[1 - \frac{\tan^2 \alpha}{2}\right]$$

$$= \frac{(734)\ (22.15)}{380,000} \left[1 - \frac{(0.0842)^2}{2}\right]$$

$$= 0.0425 \text{ in.}$$

C. COMPOSITE THICKNESS

$P_{vg} = 0.661$ (see Figure 2, Volume II)

1. Longitudinal

$$t_l = \frac{t_{f,l}}{P_{vg}} = \frac{0.0267}{0.661}$$

$$= 0.0404 \text{ in.}$$

2. Hoop

$$t_h = \frac{t_{f,h}}{P_{vg}} = \frac{0.0425}{0.661}$$

$$= 0.0643 \text{ in.}$$

3. Cylinder

$$t_c = t_h + t_l = 0.0643 + 0.0404$$

$$= 0.1047 \text{ in.}$$

D. COMPOSITE STRESSES (PROOF PRESSURE)

1. Longitudinal (Head)

$$\sigma_l = \frac{p_p\, a}{2\, t_l}$$

$$= \frac{(587)\ (22.15)}{(2)\ (0.0404)}$$

$$= 160{,}500 \text{ psi}$$

2. Hoop (Cylinder)

$$\sigma_h = \frac{p_p\, a}{t_l + t_h}$$

$$= \frac{(587)\ (22.15)}{0.1047}$$

$$= 124{,}500 \text{ psi}$$

In a discussion with Air Force representatives it was decided to pressurize the case to a hoop-composite stress in the cylinder of 119,000 psi (or 25% above the stress level reached at proof pressure for the Serial No. 2 chamber), rather than 124,500 psi as designed. This decision was made because of unknown resin-crazing characteristics at this pressure and because of the desire to minimize detrimental effects that might have jeopardized achievement of the required burst pressure. To permit pressurization to 587 psi while meeting the 119,000-psi stress level, the cylinder composite thickness would have to be increased as follows:

$$t_l + t_h = \frac{p_p\, a}{\sigma_h}$$

$$= \frac{(587)\ (22.15)}{119{,}000} = 0.108 \text{ in.}$$

It was therefore assumed that $t_l = 0.042$ in. and $t_h = 0.066$ in.

APPENDIX V

STRUCTURAL ANALYSIS - SERIAL NO. 3, 44.3-INCH, S994 CHAMBER

The fabricated Serial No. 3, 44.3-in.-dia, S994, filament-wound chamber is analyzed below on the basis of actual winding data and laboratory tests of the glass roving.

A. AREA OF SINGLE END*

$$A_{end} = \frac{W}{\rho L N_1}$$

where

W = weight of glass roving, lb

L = specimen length, in.

ρ = glass density = 0.088 lb/cu in.

N_1 = number of ends

W/L = 0.588 g/yard

Therefore,

$$A_{end} = \frac{0.588 \text{ g/yard}}{(0.088 \text{ lb/cu in.})\ (36 \text{ in./yard})\ (453.6 \text{ g/lb})\ (20 \text{ ends})}$$

$$= 20.5 \times 10^{-6} \text{ sq in./end}$$

B. FILAMENT THICKNESS

1. Longitudinal

$$\text{Cross-sectional area} = \pi D_c t_{f,l} = A_{end} N_1 N_2 N_3 N_4 N_5 \frac{1}{\cos \alpha}$$

where

D_c = chamber diameter, in.

$t_{f,l}$ = longitudinal-filament thickness, in.

N_2 = number of strands per tape

N_3 = number of tapes per turn

N_4 = number of turns per revolution

*See Appendix V of Volume II.

N_5 = number of revolutions

α = angle between filament and meridional direction, degrees

Therefore,

$$t_{f,l} = \frac{A_{end}\, N_1\, N_2\, N_3\, N_4\, N_5}{\pi\, D_c \cos \alpha}$$

$$= \frac{(20.5 \times 10^{-6})\ (20)\ (9)\ (2)\ (172)\ (3)}{\pi\ (44.078)\ (0.996)}$$

$$= 0.0276 \text{ in.}$$

The longitudinal-composite thickness (t_l, in.) is determined as follows:

$$t_l = \frac{t_{f,l}}{P_{vg}}$$

where

P_{vg} = amount of glass filament in composite, vol%

= 0.69 (based on resin content of 17.44 wt%)

Therefore,

$$t_l = \frac{0.0276}{0.69}$$

$$= 0.040 \text{ in.}$$

2. Hoop

Cross-sectional area = $t_{f,h}\, L_c = A_{end}\, N_1\, N_2\, N_6\, N_7$

where

$t_{f,h}$ = hoop-filament thickness, in.

L_c = cylinder length, in.

N_6 = number of tapes per layer

N_7 = number of layers

Therefore,

$$t_{f,h} = \frac{A_{end}\, N_1\, N_2\, N_6\, N_7}{L_c}$$

$$= \frac{(20.5 \times 10^{-6})\ (20)\ (9)\ (135)\ (9)}{102.899}$$

$$= 0.0436 \text{ in.}$$

The hoop-composite thickness (t_h, in.) is determined as follows:

$$t_h = \frac{t_{f,h}}{P_{vg}}$$

$$= \frac{0.0436}{0.69}$$

$$= 0.063 \text{ in.}$$

C. THEORETICAL HOOP-COMPOSITE STRESS AT PROOF

$$\sigma_h = \frac{(p_p)\ (a)}{t_l + t_h}$$

$$= \frac{(587)\ (22.15)}{0.040 + 0.063}$$

$$= 126{,}200 \text{ psi}$$

To permit the required hoop-composite stress of 119,000 psi to be attained as requested by the Air Force, the proof pressure had to be lowered to

$$p_p = \frac{(119{,}000)\ (0.103)}{22.15} = 558 \text{ psi}$$

D. ACTUAL STRESSES AT PROOF PRESSURE

1. Longitudinal Filament

$$\sigma_{f,l} = \frac{(p_p)\ (D_l)}{4\ (t_{f,l})\ (\cos^2 \alpha)}$$

$$= \frac{(558)\ (44.078)}{(4)(0.0276)(0.996)^2}$$

$$= 224{,}300 \text{ psi}$$

2. Hoop Filament

$$\sigma_{f,h} = \frac{(p_p)(D_h)}{2(t_{f,h})} \cdot \left| 1 - \frac{\tan^2 \alpha}{2} \right|$$

$$= \frac{(558)\ (44.186)}{(2)\ (0.0436)} \left| 1 - \frac{0.00724}{2} \right|$$

$$= 281{,}800 \text{ psi}$$

3. Longitudinal Composite (Head)

$$\sigma_l = \frac{(p_p)(D_l)}{4\ t_l}$$

$$\sigma_l = \frac{(558)(44.078)}{(4)(0.040)}$$

$$= 153{,}700 \text{ psi}$$

E. PREDICTED BURST PRESSURE

1. Longitudinal

$$p_l = p_p \left(\frac{F_{tu,f,l}}{\sigma_{f,l}} \right) \left(\frac{\sigma_{f,a}}{\sigma_{f,d}} \right)$$

where

p_l = predicted burst pressure, psi

$F_{tu,f,l}$ = design allowable longitudinal-filament stress, psi

$\sigma_{f,a}$ = actual average filament stress from strand-test data, psi

$\sigma_{f,d}$ = design filament stress = 437,000 psi

Therefore,

$$p_l = 558 \left(\frac{304{,}000}{224{,}300} \right) \left(\frac{424{,}100}{437{,}000} \right)$$

$$= 734 \text{ psi}$$

2. Hoop

$$p_h = p_p \left(\frac{F_{tu,f,h}}{\sigma_{f,h}} \right) \left(\frac{\sigma_{f,a}}{\sigma_{f,d}} \right)$$

where

p_h = predicted burst pressure, psi

$F_{tu,f,h}$ = design allowable hoop-filament stress, psi

Therefore,

$$p_h = 558 \left(\frac{380{,}000}{281{,}800} \right) \left(\frac{433{,}500}{437{,}000} \right)$$

$$= 745 \text{ psi}$$

APPENDIX VI

DESIGN ANALYSIS - SERIAL NO. 4, 44.3-INCH, S994 CHAMBER

This appendix presents the design analysis for the Serial No. 4, 44.3-in.-dia, S994, filament-wound chamber. In general, the design approach was that discussed in Appendix V of Volume II. The illustrations referred to are in Volume II, as noted. The design parameters employed are tabulated below.

Chamber diameter, D_c	44.3 in.
Chamber length, L	127.3 in.
Cylinder length, L_c	99.299 in.
Forward-boss diameter, D_{bf}	13.20 in.
Aft-boss diameter, D_{ba}	8.25 in.
Type of head contour and wrap	Balanced-in-plane
Material	S994/HTS, 20-end
Design burst pressure, p	734 psi
Proof pressure, p_p	560 psi
Resin content	20 wt%
Off-center ports	Four included in aft head
Other pertinent parameters	See Table 2 (Volume I)

A. ALLOWABLE FILAMENT STRENGTH

1. Pure Strand

Laboratory tests indicate that the average ultimate strength for S994/HTS, 20-end, glass roving is 25% above the strength of ECG-140-20E-HTS glass. Therefore,

$$F_{tu,s} = (1.25)(350{,}000 \text{ psi}) = 437{,}000 \text{ psi}$$

2. Effects of Geometry*

a. Boss Diameter

$$\frac{D_b}{D_c} = \frac{D_{ba} + D_{bf}}{2D_c} = \frac{13.20 + 8.25}{(2)\ (44.3)}$$

$$= 0.242$$

$K_1 = 0.99$ (from Figure 4, Volume II)

b. Chamber Length

$$\frac{L}{D_c} = \frac{127.3}{44.3}$$

$$= 2.87$$

$K_2 = 1.01$ (from Figure 5, Volume II)

*See Appendix V of Volume II.

3. Effects of Thickness*

a. Longitudinal

$$\frac{t_{f,l}}{D_c} = (0.935 \times 10^{-6})\ (p)\ (\frac{350,000}{437,000})$$

$$= (0.750 \times 10^{-6})\ (734)$$

$$= 550 \times 10^{-6}$$

$K_3 = 1.03$ (from Figure 6, Volume II)

b. Hoop

$$\frac{t_{f,h}}{D_c} = (1.75 \times 10^{-6})\ (p)\ (\frac{350,000}{437,000})$$

$$= (1.40 \times 10^{-6})\ (734)$$

$$= 1030 \times 10^{-6}$$

$K_3 = 1.04$ (from Figure 6, Volume II)

4. Effects of Chamber Diameter*

$D_c = 44.3$ in.

a. Longitudinal

$K_4 = 0.868$ (from Figure 7, Volume II)

b. Hoop

$K_4 = 0.937$ (from Figure 7, Volume II)

5. Effects of Off-Center Ports*

$K_p = 0.88$ (four off-center ports)

6. Design Allowables*

a. Longitudinal

$$F_{tu,f,l} = 0.89\ K_1\ K_2\ K_3\ K_4\ K_p\ K_{tu,s}$$

$$= (0.89)(0.99)(1.01)(1.03)(0.868)(0.88)(437,000)$$

$$= 304,000 \text{ psi}$$

*Ibid.

b. Hoop

$$F_{tu,f,h} = 0.89\ K_3\ K_4\ F_{tu,s}$$
$$= (0.89)(1.04)(0.937)(437,000)$$
$$= 380,000 \text{ psi}$$

B. EQUIVALENT FILAMENT THICKNESS

1. Longitudinal

$$t_{f,l} = \frac{p\ a}{(2F_{tu,f,l})(\cos^2 \alpha)}$$

$$\tan \alpha = \frac{D_{ba} + D_{bf}}{2L} = \frac{13.20 + 8.25}{(2)(127.3)}$$

$$= 0.0842$$

$$= 4^{\circ}49'$$

$$\cos \alpha = 0.996$$

$$t_{f,l} = \frac{(734)\ (22.15)}{(2)(304,000)(0.996)^2}$$

$$= 0.0267 \text{ in.}$$

2. Hoop

$$t_{f,h} = \left(\frac{p\ a}{F_{tu,f,h}}\right)\left(1 - \frac{\tan^2 \alpha}{2}\right)$$

$$= \left[\frac{(734)(22.15)}{380,000}\right]\left[1 - \frac{(0.0842)^2}{2}\right]$$

$$= 0.0425 \text{ in.}$$

C. COMPOSITE THICKNESS

$P_{vg} = 0.661$ (see Figure 2, Volume II)

1. Longitudinal

$$t_l = \frac{t_{f,l}}{P_{vg}} = \frac{0.0267}{0.661}$$

$$= 0.0404 \text{ in.}$$

2. Hoop

$$t_h = \frac{t_{f,h}}{P_{vg}} = \frac{0.0425}{0.661}$$

$$= 0.0643 \text{ in.}$$

3. Cylinder

$$t_c = t_h + t_l = 0.0643 + 0.0404$$

$$= 0.1047 \text{ in.}$$

D. COMPOSITE STRESSES (PROOF PRESSURE)

1. Longitudinal (Head)

$$\sigma_l = \frac{p_p a}{2 t_l}$$

$$= \frac{(587)(22.15)}{(2)(0.0404)}$$

$$= 160{,}500 \text{ psi}$$

2. Hoop (Cylinder)

$$\sigma_h = \frac{p_p a}{t_l + t_h}$$

$$= \frac{(587)(22.15)}{0.1047}$$

$$= 124{,}500 \text{ psi}$$

It was determined that, within practical limits, the Serial No. 4, 44.3-in. chamber was to be identical to the Serial No. 3 chamber. The longitudinal and hoop thicknesses were therefore made equal to those of the Serial No. 3 chamber (Appendix IV, Volume I): $t_l = 0.042$ in. and $t_h = 0.066$ in.

APPENDIX VII

STRUCTURAL ANALYSIS - SERIAL NO. 4, 44.3-INCH, S994 CHAMBER

The fabricated Serial No. 4, 44.3-in.-dia, S994, filament-wound chamber is analyzed below on the basis of actual winding data and laboratory tests of the glass roving.

A. AREA OF SINGLE END*

$$A_{end} = \frac{W}{\rho L N_1}$$

where

W = weight of glass roving, lb

L = specimen length, in.

ρ = glass density = 0.088 lb/cu in.

N_1 = number of ends

W/L = 0.559 g/yard

Therefore,

$$A_{end} = \frac{0.599 \text{ g/yard}}{(0.088 \text{ lb/cu in.})(36 \text{ in./yard})(453.6 \text{ g/lb})(20 \text{ ends})}$$

$$= 20.8 \times 10^{-6} \text{ sq in./end}$$

B. FILAMENT THICKNESS

1. Longitudinal

$$\text{Cross-sectional area} = \pi D_c t_{f,l} = A_{end} N_1 N_2 N_3 N_4 N_5 \frac{1}{\cos \alpha}$$

where

D_c = chamber diameter, in.

$t_{f,l}$ = longitudinal-filament thickness, in.

N_2 = number of strands per tape

N_3 = number of tapes per turn

N_4 = number of turns per revolution

*See Appendix V of Volume II.

N_5 = number of revolutions

α = angle between filament and meridional direction, degrees

Therefore,

$$t_{f,l} = \frac{A_{end}\, N_1\, N_2\, N_3\, N_4\, N_5}{\pi\, D_c \cos \alpha}$$

$$= \frac{(20.8 \times 10^{-6})\,(20)\,(9)\,(2)\,(170)\,(3)}{\pi\,(44.117)\,(0.996)}$$

$$= 0.0279 \text{ in.}$$

The longitudinal-composite thickness (t_l, in.) is determined as follows:

$$t_l = \frac{t_{f,l}}{P_{vg}}$$

where

P_{vg} = amount of glass filament in composite, vol%

= 0.652 (based on resin content of 20.4 wt%)

Therefore,

$$t_l = \frac{0.0279}{0.652}$$

$$= 0.043 \text{ in.}$$

2. Hoop

Cross-sectional area = $t_{f,h}\, L_c = A_{end}\, N_1\, N_2\, N_6\, N_7$

where

$t_{f,h}$ = hoop-filament thickness, in.

L_c = cylinder length, in.

N_6 = number of tapes per layer

N_7 = number of layers

Therefore,

$$t_{f,h} = \frac{A_{end}\, N_1\, N_2\, N_6\, N_7}{L_c}$$

$$= \frac{(20.8 \times 10^{-6})\ (20)\ (9)\ (126)\ (9)}{99.799}$$

$$= 0.0442 \text{ in.}$$

The hoop-composite-thickness (t_h, in.) is determined as follows:

$$t_h = \frac{t_{f,h}}{P_{vg}}$$

$$= \frac{0.0442}{0.655}$$

$$= 0.068 \text{ in.}$$

C. THEORETICAL HOOP-COMPOSITE STRESS AT PROOF

$$\sigma_h = \frac{(p_p)(a)}{t_l + t_h}$$

$$= \frac{(587)\ (22.15)}{0.043 + 0.068}$$

$$= 117{,}140 \text{ psi}$$

Aerojet and Air Force personnel had previously determined that this chamber was to be as nearly identical as possible to the Serial No. 3, 44.3-in. chamber prior to the application of structural loads, in order to determine as accurately as possible what effect (if any) the loading had upon this chamber. On this basis it was decided to proof test this chamber at 558 psig instead of 587 psig. This decision was made because

1. Actual fabrication data and Aerojet-strand-test data indicated that failure would occur at 730 psig in the longitudinal filaments, due to the low strength of the glass available for use on this chamber. A pressure of 558 psig preloaded the longitudinal filaments to a stress level of 224,000 psi, identical to that induced in the Serial No. 3 chamber at the proof pressure.

2. The Serial No. 3 chamber had also been tested at 558 psi.

D. ACTUAL STRESSES AT PROOF PRESSURE

1. Longitudinal Filament

$$\sigma_{f,l} = \frac{(p_p)\ (D_l)}{4(t_{f,l})(\cos^2 \alpha)}$$

$$\sigma_{f,l} = \frac{(558)(44.117)}{(4)(0.0279)(0.996)^2}$$

$$= 224{,}350 \text{ psi}$$

2. Hoop Filament

$$\sigma_{f,h} = \frac{(p_p)(D_h)}{2(t_{f,h})} \left(1 - \frac{\tan^2 \alpha}{2}\right)$$

$$= \frac{(558)\ (44.185)}{(2)\ (0.0430)} \left(1 - \frac{0.00724}{2}\right)$$

$$= 278{,}891 \text{ psi}$$

3. Longitudinal Composite (Head)

$$\sigma_l = \frac{(p_p)(D_l)}{4\ t_l}$$

$$= \frac{(558)(44.117)}{(4)\ (0.043)}$$

$$= 143{,}650 \text{ psi}$$

E. PREDICTED BURST PRESSURE

1. Longitudinal

$$p_l = p_p \left(\frac{F_{tu,f,l}}{\sigma_{f,l}}\right) \left(\frac{\sigma_{f,a}}{\sigma_{f,d}}\right)$$

where

p_l = predicted burst pressure, psi

$F_{tu,f,l}$ = design allowable longitudinal-filament stress, psi

$\sigma_{f,a}$ = average filament stress from strand-test data, psi

$\sigma_{f,d}$ = design filament stress = 437,000 psi

Therefore,

$$p_l = 558 \left(\frac{304{,}000}{224{,}350}\right) \left(\frac{422{,}737}{437{,}000}\right)$$

$$= 730 \text{ psi}$$

2. Hoop

$$P_h = P_p \left(\frac{F_{tu,f,h}}{\sigma_{f,h}}\right) \left(\frac{\sigma_{f,a}}{\sigma_{f,d}}\right)$$

where

P_h = predicted burst pressure, psi

$F_{tu,f,h}$ = design allowable hoop-filament stress, psi

Therefore,

$$P_h = 558 \left(\frac{380,000}{278,891}\right) \left(\frac{433,800}{437,000}\right)$$

$$= 754 \text{ psi}$$

UNCLASSIFIED